THE UNIVERSITY OF MICHIGAN

7260-1-F

Technical Report ECOM-01263-F October 1967

Broadband Antenna Techniques Study

Final Report
April 1965 through May 1967

Report No. 8

Contract No. DA-28-043 AMC-01263(E)
DA Project No. 5A6-79191-D902-02-11

Prepared by
J.E. Ferris, J.A.M. Lyon, G.C. Rassweiler,
C.C. Chen, J.C. Parker, D.L. Smith, J.B. Rao
and W.E. Zimmerman

The University of Michigan
Department of Electrical Engineering
Radiation Laboratory
Ann Arbor, Michigan 48108

For

United States Army Electronics Command, Fort Monmouth, J.J.

Distribution Statement

Each transmittal of this document outside the Department of Defense must have prior approval of CG, USAECOM, Ft. Monmouth, N.J. Attn: AMSEL-WL-S

Engn
UMR
1429
10.8

ABSTRACT

Many of the possibilities of a size-reduced planar log-periodic antenna have been investigated. Studies on elements included shortening by various methods. Shortening of the boom length was studied. Influences on radiation pattern and VSWR and influence of different phasing lengths of feed line between adjacent elements for a given boom spacing were considered. Experimental array work was done on an adjustable model. Experimental work was then extended to a one-fourth size model of the projected exploratory development design. Later an exploratory development model was built. It showed good radiation performance with adherence to contract specifications except for minor deviations.

Basic studies were made on size-reduced log conical helix antennas. These studies included an investigation of techniques to develop a light weight slow wave winding for a conical helix antenna. The final exploratory development model of the antenna was of square pyramidal shape and utilized coiled windings on air-filled fiber cylinders. No useful size reduction of a log conical helix antenna was realized using this technique. Considerable success was obtained with a cylindrical helix wound with a coiled wire over a plastic tube filled with a ferrite material (see contract AF 33(615)3609). A four-to-one reduction in diameter of a log conical helix can be obtained at the cost of additional weight with this construction.

An extensive study of the exponentially tapered reactive antenna (EXTRA) has been conducted. Typical impedance, pattern and surface current data have been obtained for two EXTRA antenna configurations. These data have shown that this particular antenna configuration satisfied the initial requirements suggested by Hallén. The surface current data demonstrates that the reactive elements caused the current to be attenuated as it propagates toward the tip of the antenna. The impedance data show the antenna to be a broadband device (10:1 frequency band). The pattern data are not as encouraging since there is a tendency for the antenna to radiate toward end fire at the higher frequencies. Data are presented for the EXTRA antenna mounted over three ground plane configurations. The deliverable antenna consists of the EXTRA element and the 9 inch rodded ground plane.

FOREWORD

This report was prepared by The University of Michigan Radiation Laboratory of the Department of Electrical Engineering. The work was performed under United States Army Electronics Command Contract No. DA 28-043 AMC-01263(E). The contract was initiated under United States Army Project No. 5A6-79191-D902-02-11, "Broadband Antenna Techniques Study". Work was administered under the direction of the Electronics Warfare Laboratory, Supporting Developments Technical Area at Fort Monmouth, New Jersey. Mr. Anthony Digiacomo is the Project Manager and Mr. George Haber is the Contract Monitor.

The material reported herein represents the results of the investigation into techniques applicable to the design and development of broadband antennas.

The authors wish to acknowledge the contributions of E. C. Bublitz, R. J. Carducci, P. W. Eng, U. E. Gilreath, J. B. Hutt, K. M. Jagdmann, A. J. Loudon, D. R. Marble, K. A. Pitcher and B. C. Vrieland in the experimental measurements performed and reported.

TABLE OF CONTENTS

TABLE OF CONTENTS
(Continued)

LIST OF ILLUSTRATIONS

LIST OF ILLUSTRATIONS
(Continued)

LIST OF ILLUSTRATIONS
(Continued)

LIST OF ILLUSTRATIONS
(Continued)

LIST OF ILLUSTRATIONS
(Continued)

LIST OF ILLUSTRATIONS
(Continued)

LIST OF ILLUSTRATIONS
(Continued)

LIST OF ILLUSTRATIONS
(Continued)

I

INTRODUCTION

Under Task 1 (Chapter II) a design study has been made of the possibilities of a foreshortened planar log periodic antenna. Experimental data have been accumulated on the effectiveness of various types of shortened elements. Studies were made on the possibilities of shortening the boom. A one-fourth size model was made, suitable for operating at four times the specified frequency range. Later, an exploratory development model was produced. The dimensions of this model are: Boom length 13.5' ; length of longest element, 13.8'.

Radiation patterns were taken in the E-plane and the VSWR was measured. The pattern data covered the entire range from 20 MHz to 230 MHz. The experimental data obtained on VSWR and radiation patterns conformed largely to the requirements of the specifications. The observed VSWR above 24 MHz is within the limitations set except for two points, each with a width approximately 2 MHz wide. The radiation patterns are generally within specifications except for some departure of the back-lobe level requirements between 20 and 28 MHz. The directivity observed exceeds that required by the specifications.

Under Task 2 (Chapter III) an exploratory development model based on extensive studies of the log conical helix antenna has been produced. It was not possible to make an intermediate scale model such as was done in Task 1 in the time allocated. Much of the time was spent in development of windings that could result in a reduced size antenna. Some of the techniques studied were unacceptable due to the weight involved. Therefore, the development of windings was finally focused on the light-weight possibilities. In order to meet the weight restrictions of the specifications the type of winding finally chosen for this log-conical antenna was a cylindrical helical winding.

As a reasonable approximation to a conical structure a pyramidal form was selected; the base of this pyramid is a square. Using this pyramidal cone a coiled winding was placed on this general framework. Although a bifilar continuous winding is used for this antenna, each of the two windings is composed of a number of solenoids wound on cylinders, and connected together at the joined ends of the cylinders. They are arranged on each face of the pyramid according to the selected pitch angle, forming a slant array of cylindrical tubes running at a slight angle with the bottom edge of the triangular face. These cylinders have a maximum diameter of 6-1/8" for the bottom most cylinder. The successive cylinders going from the bottom base to the top apex are smaller in diameter. All cylinders are wound with a solenoidal winding of No. 20 wire with enamel insulation and a given pitch angle on

each segment of the cylinder. The dimensions of the final development model are: altitude from apex to base, 4', and each side of the square base, 4'6". The length of each diagonal of the base is 6'3". The total weight of the assembled antenna is 46 lbs.

This developmental model has been subjected to VSWR and impedance tests as well as radiation pattern tests. A departure from the specifications in the matter of VSWR on the basis of a 50Ω feed have been observed at one frequency. Likewise, the radiation pattern tests indicate a backlobe level in excess of that allowed by the specifications over most of the 50 to 1100 MHz frequency range.

Under Task 3 (Chapter IV) an extensive study of both capacitive and inductive loaded antenna configurations have been conducted. A major portion of this chapter is concerned with the exponentially tapered reactive antenna (EXTRA) that has been constructed employing capacitive reactance. In addition, there is some final data that has been collected for the inductive concept. A recommended approach is presented in the event there is interest in a continuation of the broadband omnidirectional study employing the inductive concepts. Many of the disadvantages associated with capacitive loading are discussed along with the problems that are associated with designing and constructing a broadband omnidirectional antenna employing inductive elements. Included are typical impedance, pattern and surface current data that have been collected for some of the antennas that have been considered during the contractual period of this study.

II

FORESHORTENED PLANAR LOG-PERIODIC ANTENNA

The purpose of this study is to develop the design of a foreshortened planar log-periodic antenna which satisfies the following requirements:

1) The size is to be one-half the length and one-half the width of a normal sized log-periodic antenna with a height of less than 6" and weight less than 50 lbs.

2) The half power beamwidth is to be less than 70^{o} in the E-plane, 135^{o} in the H-plane, beam tilt is to be less than $\pm 5^{o}$, and the side and back lobe levels are to be at least 10 db down from the main lobe.

3) The antenna gain is to be greater than 3 db over an isotropic source for a frequency range of 20 - 230 MHz.

4) The VSWR is to be less than 2.5:1 with respect of a 50 Ω load.

5) The field is to have linear polarization.

2.1 Design and Testing of Exploratory Development Model

The assembled exploratory development model is pictured in Fig. 2-1 in its testing configuration 40' above rooftop level. The structure has an overall boom length of 411.5 cm, (13.5 ft), which includes the inductance terminating the twin channel construction. The width of the largest elements are 422.0 cm (13.8 ft). The fore-shortening techniques employed would potentially allow greater element length reductions at the expense of an increased boom length. Lightweight aluminum and fiberglass materials were used in the construction throughout. The mechanical and electrical design follows closely that established in the one-fourth size scale models. Further information on the design is presented in the following subsections. In addition, the testing results are presented and discussed along with some recommendations for exploring potentialities of these design techniques.

2.1.1 Mechanical Design

The contract specifications contained no environmental requirements for the mechanical design. Consequently, the exploratory development model was built with sufficient sturdiness to withstand reasonable handling and testing loads. A detailed consideration of stress loadings could conceivably lead to a design of less weight. The present antenna withstood winds of 30 mph during certain portions of the testing procedure. The total antenna weight is 54.4 lbs. excluding a fiberglass mounting

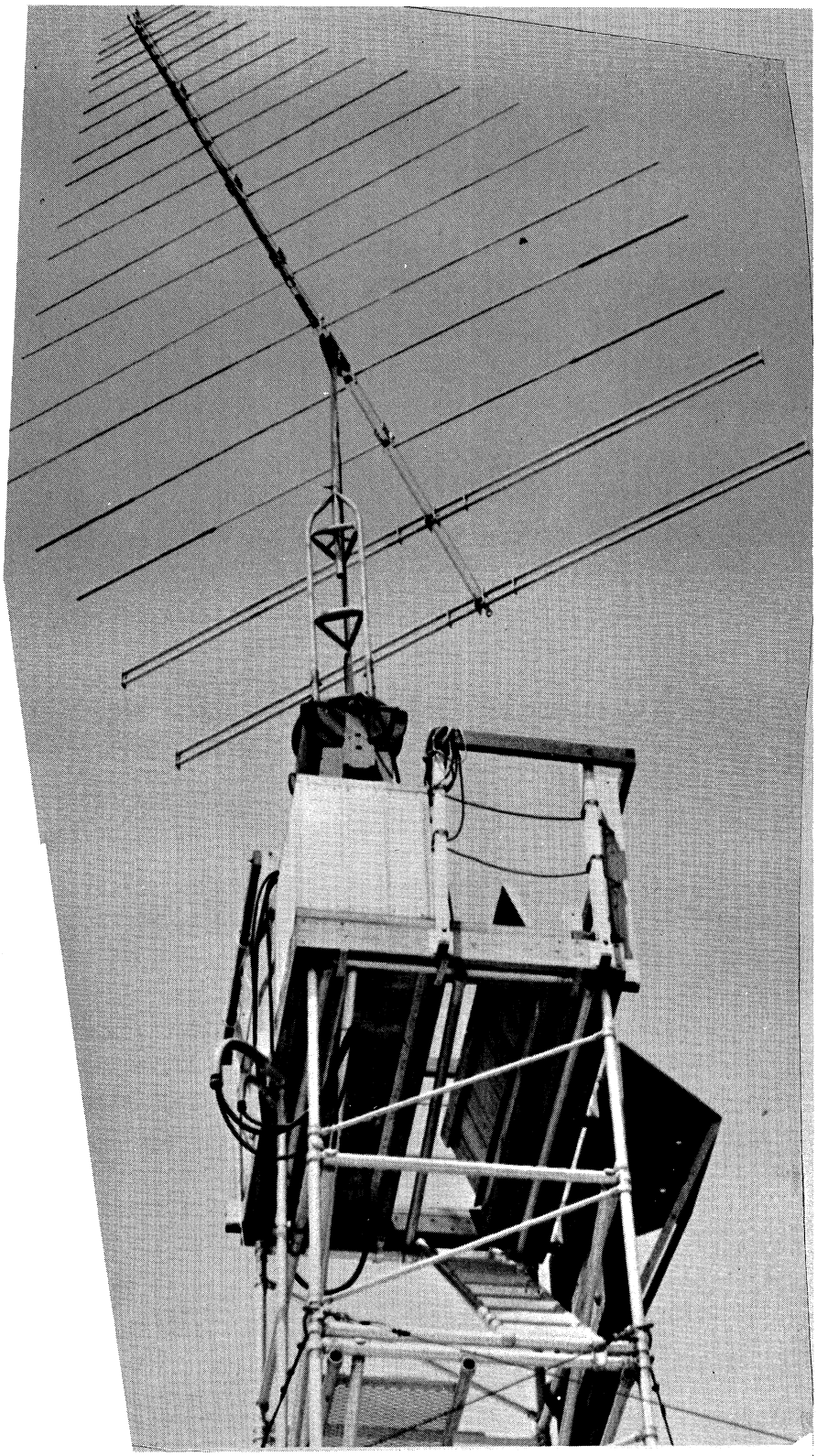

FIG. 2-1: LOG PERIODIC PLANAR ARRAY MOUNTED IN TESTING CONFIGURATION.

pole supplied with the exploratory development model.

This disassembled antenna is pictured in Fig. 2-2 in a configuration which emphasized the mechanical design considerations. The upper left region of the picture shows the 14 aluminum elements associated with the high frequency section of the array. The short elements are constructed entirely of 1/2" O.D. tube. The element bases are threaded, as is the aluminum channel forming the boom, to facilitate rapid assembly. The upper right region of the picture shows the 5 elements associated with the lower octave section of the array. Element No. 5 is constructed of 3/4" O.D. tube. Elements 4 and 3 contain successively larger portions of helical slow wave structure near the element tips. These helices are constructed of No. 8 solid aluminum "TV ground" wire, wound around a 1" O.D. fiberglass form. Elements 2 and 1 are constructed entirely of type G-10 fiberglass material. The helical structure is identical with that of elements 4 and 3, and represents a 1:4 frequency scaling of those used in the scale model investigations. The lower left region of Fig. 2-2 illustrates the boom construction for the high frequency section of the array. The boom consists of two aluminum channels measuring 1" high by 2" wide by 1/8" thick and aligned with the wide sides facing each other so as to form a balanced transmission line of low characteristic impedance. Channel separation is maintained by 1/4" thick fiberglass plates appropriately spaced along the boom. A length of RG-8/U cable runs along the bottom of one channel to the antenna tip. At the bottom tip, the center conductor of the coaxial cable connects to the opposite aluminum channel. Mechanical symmetry is preserved in this tip construction. The total length of the high frequency section of boom is 185.2 cm. (6.03 ft). The boom for the low frequency section measures 223.2 cm (7.26 ft), and is shown in the lower right of Fig. 2-2, with its inductive termination attached. The general construction techniques are similar for both sections of the boom. The threaded mounting brackets which accept aluminum elements No. 5, 4, and 3 have a greater vertical displacement between the sockets. This serves as a transition into the thicker folded helical elements, attached at the rear of this boom section. The mounting brackets for elements No. 2 and 1 are fashioned solely out of G-10 fiberglass material. Short pieces of aluminum wire are incorporated in the bracket design so that the element is electrically fed as a folded helical dipole. Between elements No. 5 and 4 is a sturdy mounting plate for attaching the fiberglass pole to the boom.

The assembly procedure is straight forward and uncritical. First, the two sections of the central boom are attached, making certain that the tops of each coincide. Next, the elements are attached as indicated in the foregoing pictures. The two folded helical dipole elements are labeled corresponding to the mounting brackets to which they are attached; e.g., 1-R, 1-L, for element No. 1, right hand, and left

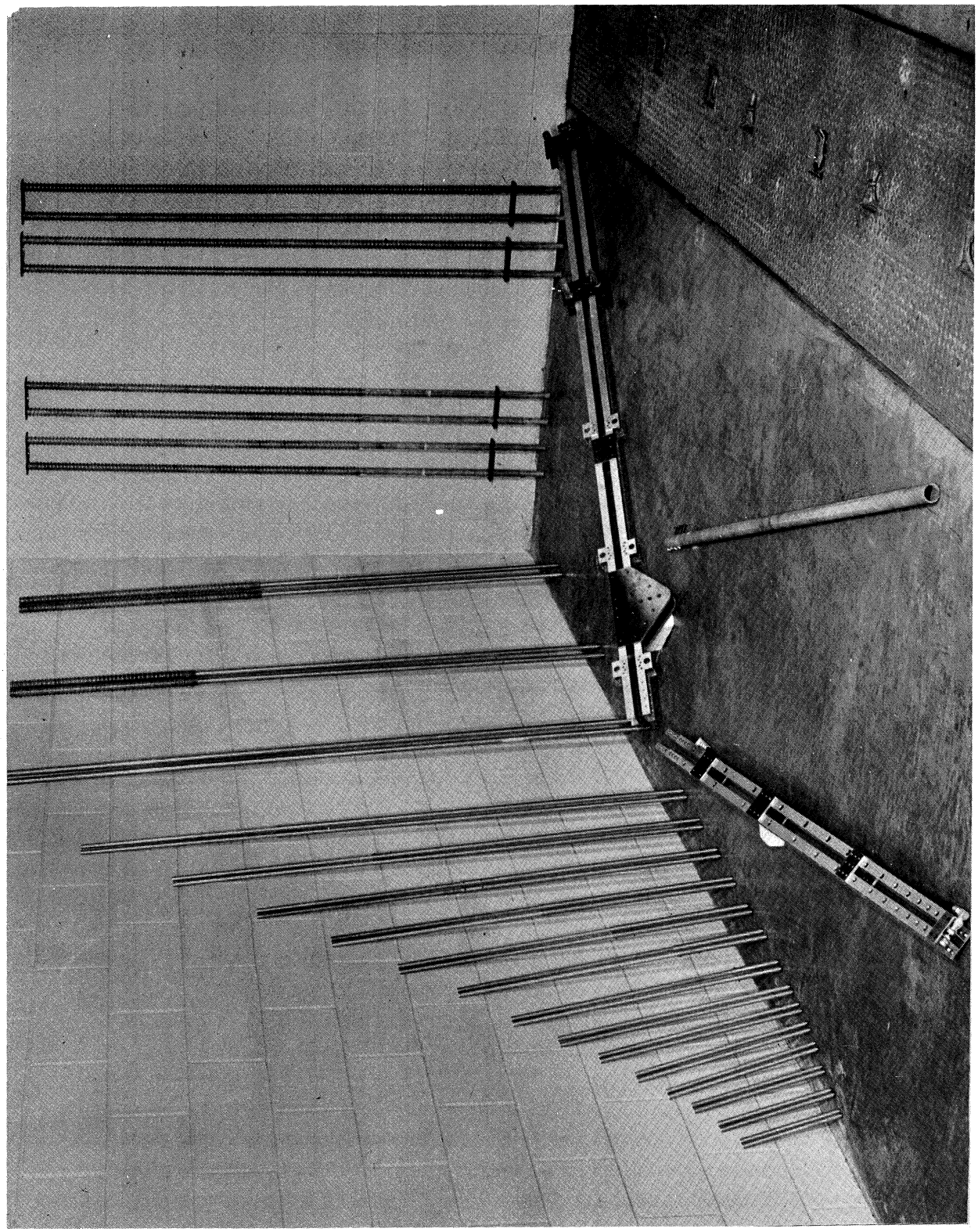

FIG. 2-2: DISASSEMBLED LOG PERIODIC PLANAR ARRAY.

hand half-element, respectively, as viewed facing toward the apex. The mounting mast is then attached and lastly, so as to prevent damage, the inductive termination is fastened in place.

2.1.2 Electrical Design

The primary electrical design utilizes the findings of the scale model investigations. Except for minor mechanical considerations, the exploratory development model is a full scale version of the antenna discussed in Section 2.2.2, having the design parameters, $\alpha = 45^{o}$, $\tau = 0.85$, and $\sigma = 0.0375$. The basic steps in the design procedure are outlined below. Little emphasis is placed upon the conventional aspects, which have been thoroughly described elsewhere (Smith, 1966).

Once the electrical parameters α, τ and σ are specified, the usual design procedure is to specify the resonant frequency of the longest element in the array. Although the elements in the lower frequency octave of operation are fore-shortened, the positioning along the boom corresponds to the normal design procedure. The resonant frequency of element No. 1 was specified at 18.0 MHz, a somewhat conservative value corresponding to a normal low frequency truncation constant, $K_1 = 0.55$. The high frequency truncation constant is $K_2 = 0.30$. The foregoing information is sufficient to completely define the positioning and electrical length of each element. The antennas impedance properties are controlled independent of the pattern performance by adjusting the spacing between the two channels which form the antenna boom. This spacing was determined experimentally on the one-fourth size scale replica for best impedance matching to a 50 Ω coax transmission line.

The special design considerations for the fore-shortened elements in the lower octave of operation are discussed in Section 2.2.2. This design entailed obtaining elements which possess both a good impedance match to the twin channel feed line and which also have a reasonable impedance bandwidth. As with the one-fourth size scale replica, the resonant frequencies were altered from their nominal values in order to improve VSWR and front-to-back ratio performance. Table II-1 compares the nominal resonant frequency of elements No. 1 - 5 as given by the design parameters to measured values obtained when the elements were removed from the array.

Only those foreshortening techniques which were applicable to an array operating at power levels of 2000 watts were employed in this exploratory development model. Consequently, the array structure itself is considered operable at the power level of 2000 watts. Operation at this power level would require only one relatively simple modification of the coax feed line to the array. Since normal operation of the

array entails VSWR values considerably larger than unity, the power handling capability of the coax feedline must be 2000 watts times the VSWR at the particular operating frequency. This would normally entail a coax feed line capable of handling 5000 watts assuming a VSWR of 2.5 to 1. To ensure this capability, 1-5/8" diameter rigid coax would be required. The RG-8/U coax supplied with the exploratory development model will safely handle 180 watts at 230 MHz, 280 watts at 100 MHz, and 600 watts at 20 MHz, assuming a VSWR of 2.5 to 1.

TABLE II-1

Element No.	Nominal Frequency MHz	Actual Frequency MHz
1	18.0	18.0
2	21.2	21.0
3	24.9	24.2
4	29.9	27.5
5	34.5	32.0

2.1.3 Testing Results

All testing was performed with the exploratory development model positioned 40 feet above rooftop level and 14 feet above the aluminum scaffolding, as pictured in Fig. 2-1. In addition, the radiation pattern and comparison gain measurements utilized a ground reflection range located at a distance of 625 ft. from the test antenna. Fig. 2-3 is a photograph of the wire trapezoidal tooth ground reflection antenna installation as viewed facing the exploratory development model test antenna. Measurements were made at the nominal frequencies listed in Table II-2. The measurement frequencies are sufficiently close together to allow at least two measurements, and generally three measurements, per log-period of the test antenna. The nominal frequencies below 50.0 MHz are accurate to within about $\pm$ 0.5 MHz. Above 50.0 MHz, the nominal frequency values may be as much as 4 per cent higher than the actual frequency.

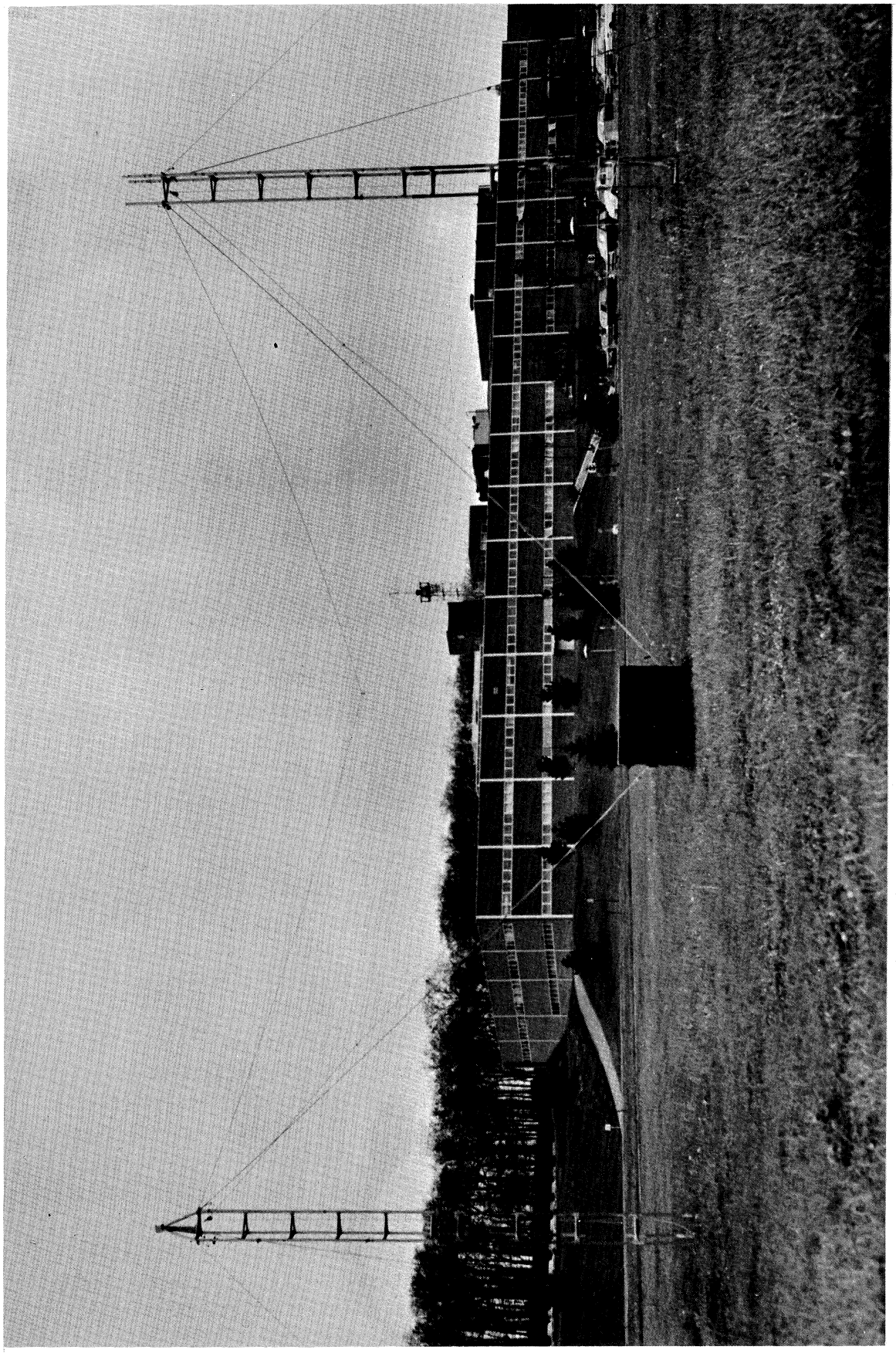

FIG. 2-3: GROUND REFLECTION RANGE VIEWED FROM REFERENCE ANTENNA IN FIELD.

TABLE II-2

f [MHz]	Δf_* [MHz]
17 through 26	1
28 through 42	2
45 through 60	3
64 through 80	4
85 through 100	5
108 through 140	8
150 through 240	10

2.1.3a Patterns

Radiation patterns were obtained by illuminating the exploratory development model with a plane wave incident from the ground reflection antenna installation. The output of the Scientific Atlanta Series 1300 receiver attached to the test antenna was used to drive a polar plotter which responded linearly to power. The frequencies at which the patterns were recorded deviate occasionally from those in Table II-2 in order to avoid pattern interference with local CB, FM, and TV transmitting facilities Selected E-plane linear power radiation patterns which are representative of all those taken are presented in Fig. 2-4. The characteristics of all the radiation patterns are summarized in Figs. 2-5 and 2-6. The 3 db E-plane beamwidth measured in degrees, and the front-to-sidelobe ratio measured in db, are plotted as a function of frequency in Fig. 2-5. It is interesting to note that the 3 db beamwidth tends to decrease at the higher frequencies. This may be attributed to a partial excitation of the $3\lambda/2$ mode which interacts with the $\lambda/2$ mode as an array within an array to narrow the beamwidth. This explanation is supported by observing the radiation patterns at 112 MHz and 230 MHz where distortion due to excitation of the $3\lambda/2$ mode is in evidence. The current probing experiments on the one-fourth size scale model, reported in Section 2.2.1, established the partial excitation of this higher order mode. The front-to-sidelobe level plotted in Fig. 2-5 indicates that extraneous lobes are lower than about -10db for frequencies greater than about 28.5 MHz. The higher backlobe at lower frequencies is associated with element foreshortenings of near 2:1. It is quite conceivable that further experimentation with the resonant frequencies of elements No. 1 and 2 could yield improved performance. It is interesting to note that the backlobe remains relatively constant from 26 MHz down to 20 MHz, and then increases abruptly. This would indicate the existance of an alternate trade-off between backlobe level and the lowest acceptable operating frequency.

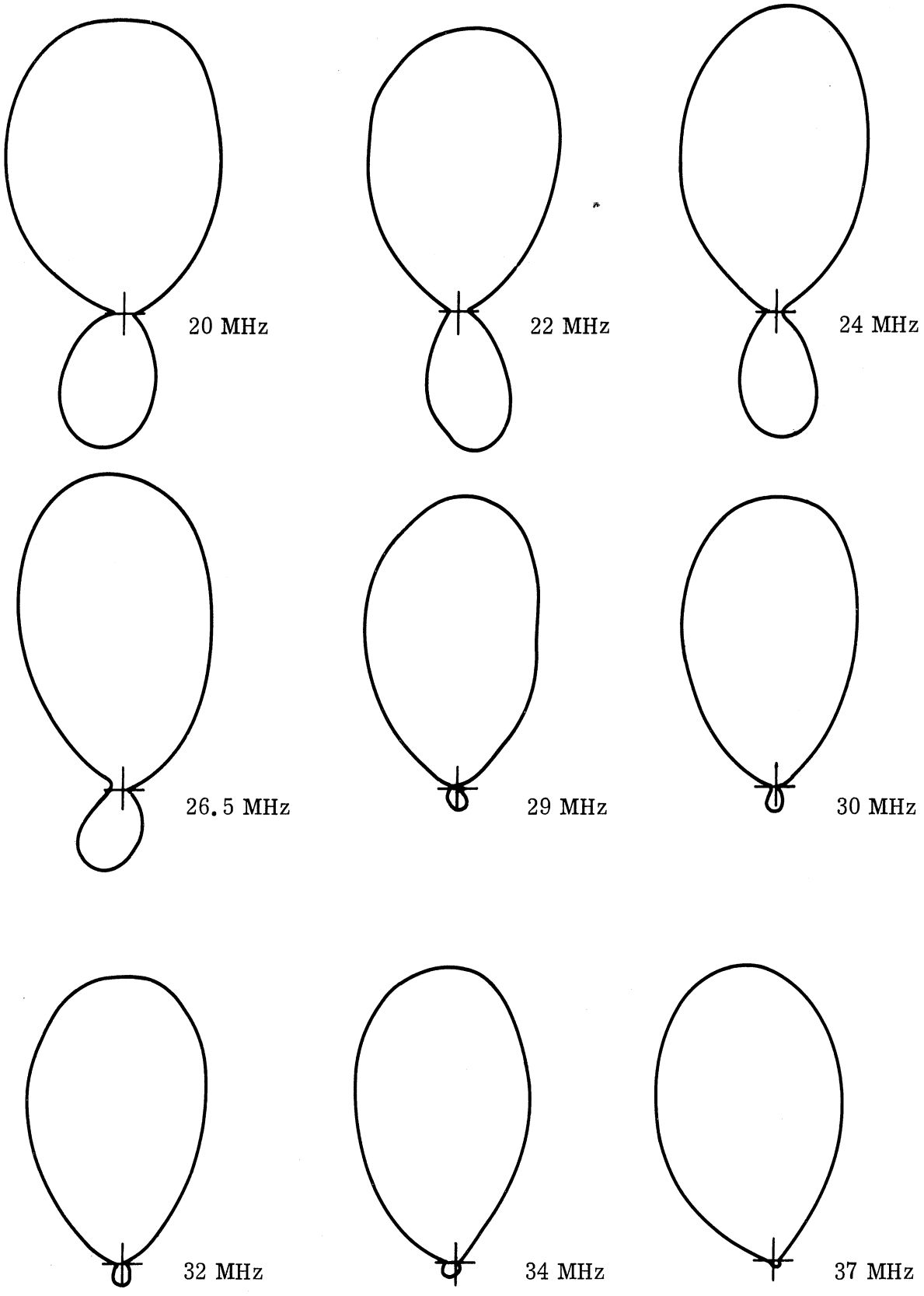

FIG. 2-4a: LOG PERIODIC PLANAR ARRAY E-PLANE RADIATION PATTERNS (20 MHz through 37 MHz).

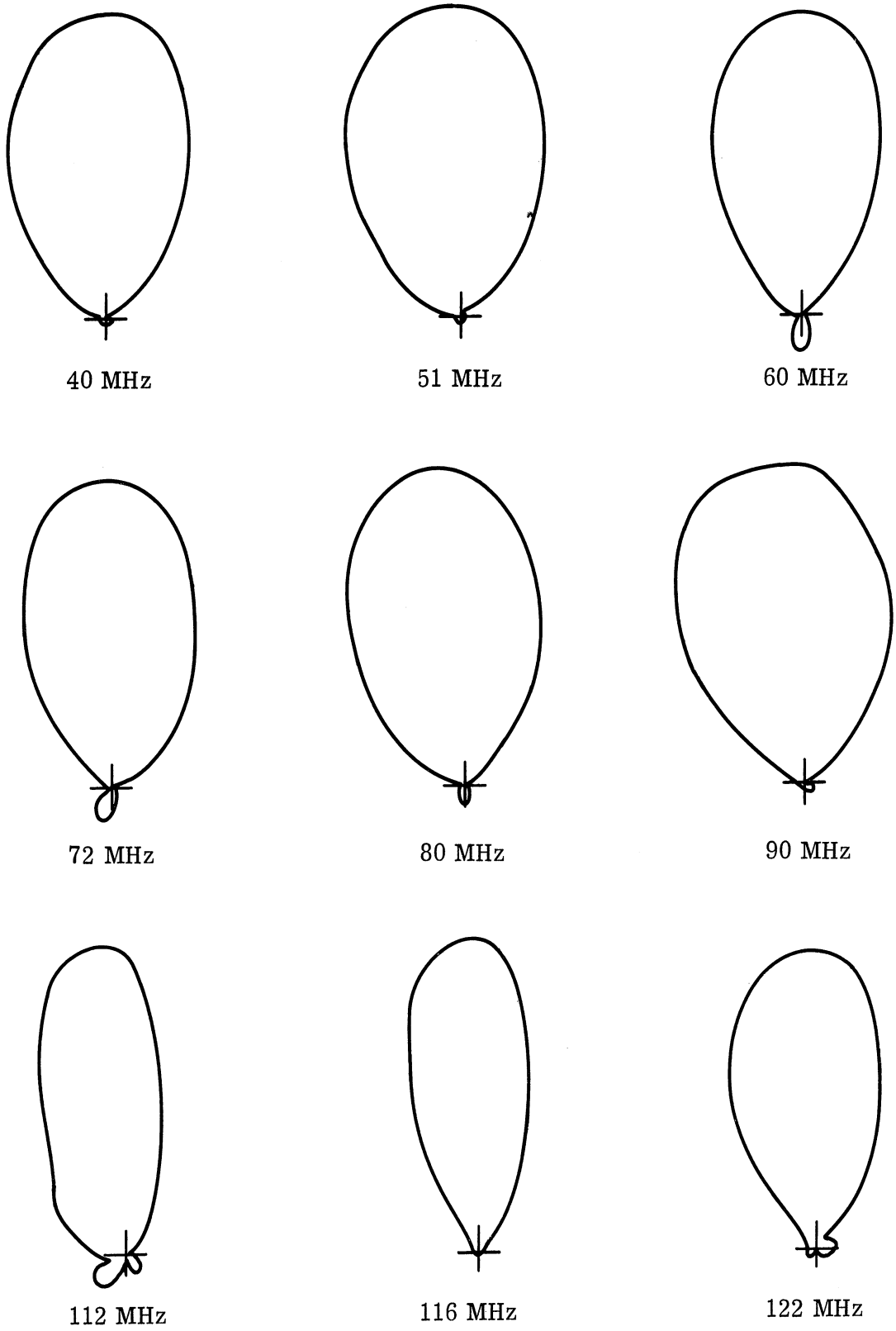

FIG. 2-4b: LOG PERIODIC PLANAR ARRAY E-PLANE RADIATION PATTERNS (40 MHz through 122 MHz).

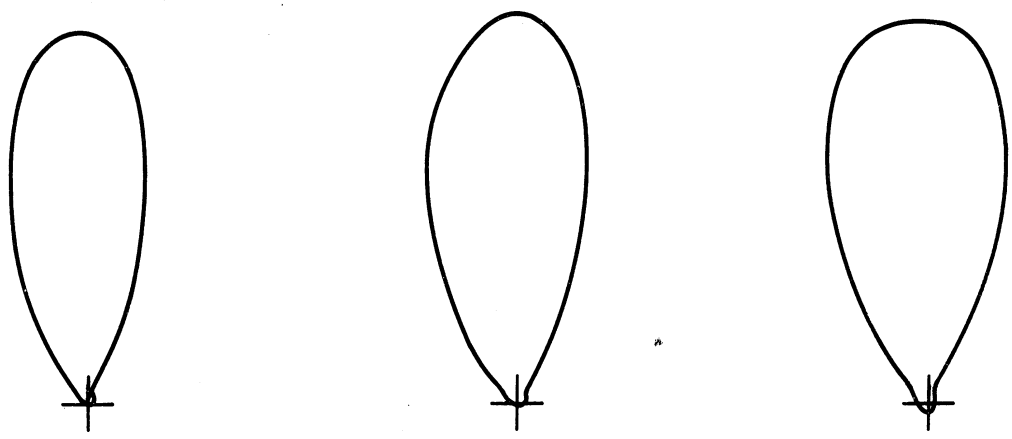

132 MHz 140 MHz 150 MHz

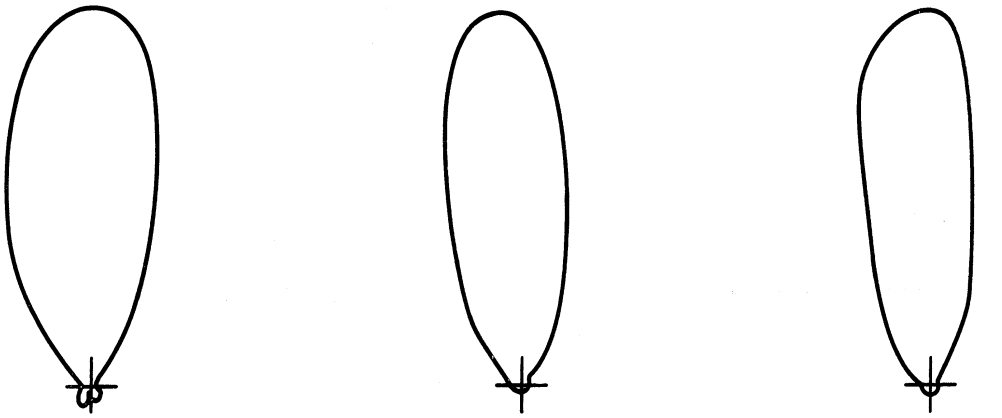

170 MHz 200.5 MHz 211 MHz

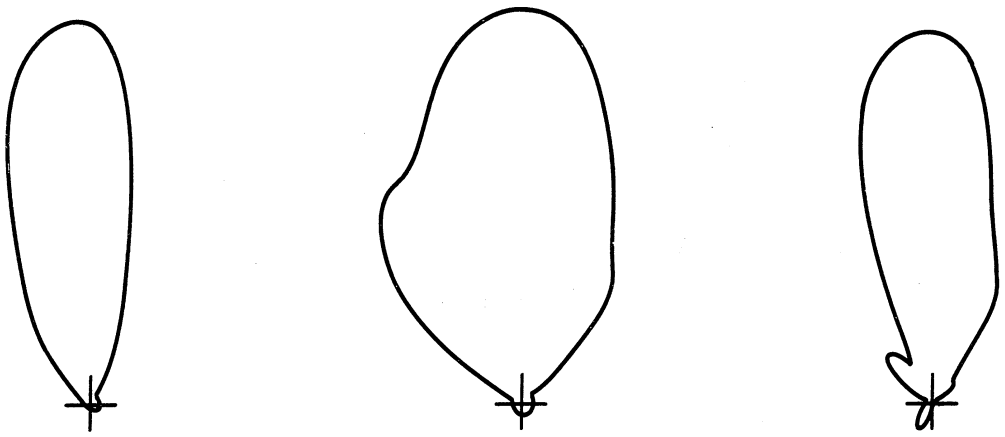

220 MHz 230 MHz 240 MHz

FIG. 2-4c: LOG PERIODIC PLANAR ARRAY E-PLANE RADIATION PATTERNS (132 MHz through 240 MHz).

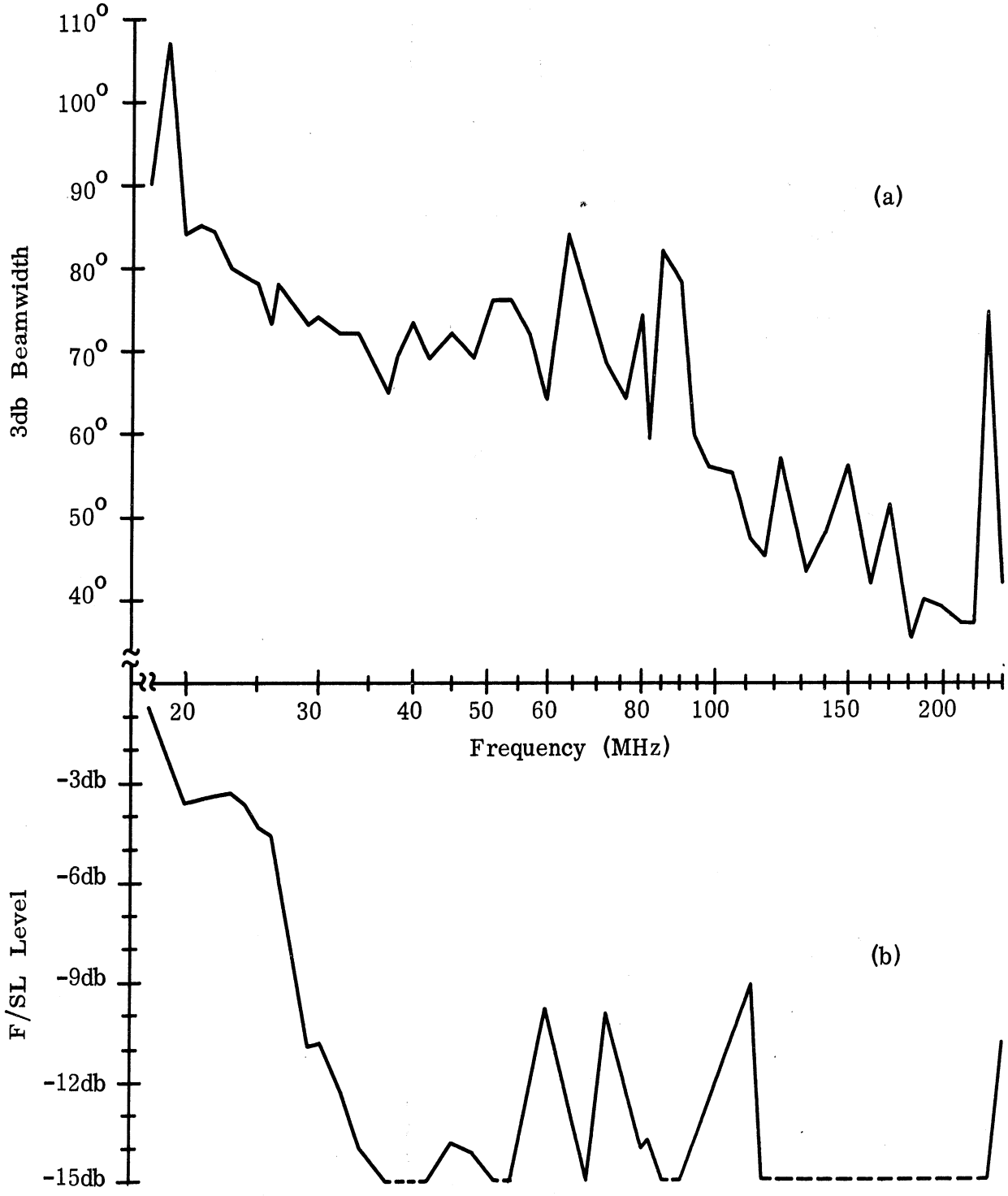

FIG. 2-5: LOG-PERIODIC PLANAR ARRAY, (a) 3-db Beamwidth vs Frequency, and (b) Front-to-sidelobe Ratio vs Frequency.

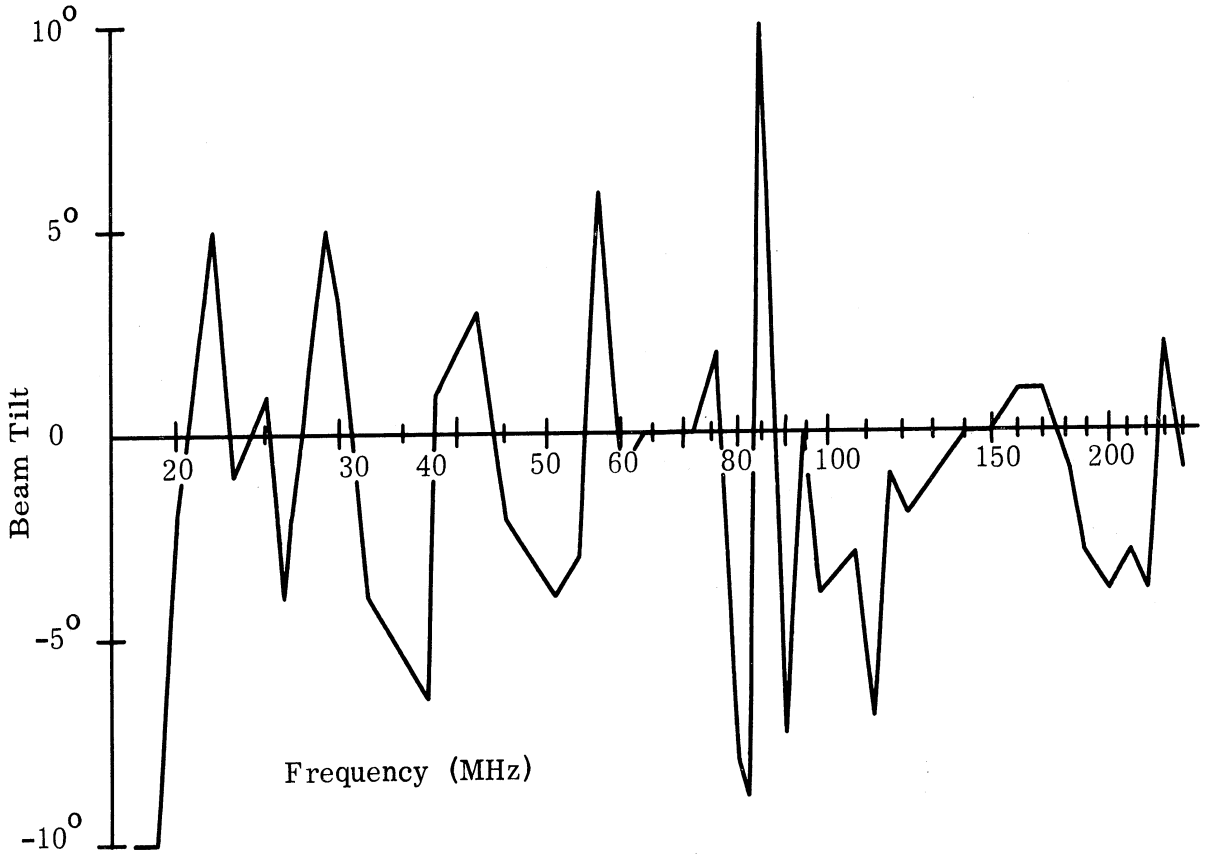

FIG. 2-6: LOG-PERIODIC PLANAR ARRAY, BEAM TILT FROM FORESIGHT VS FREQUENCY.

Figure 2-6 indicates the beam tilt on either side of the antenna boresight as a function of frequency. As can be seen, the beam tilt is generally within $\pm 5^{o}$, and approaches $\pm 10^{o}$ only over a narrow frequency interval.

2.1.3b Gain

Gain measurements were made on the finished exploratory development model while in the same testing configuration as subsection 2.1.3a, and as pictured in Fig. 2-1 and 2-3. The measurement technique used was that of comparing the signal strength of the exploratory development model with that of a resonant half wave dipole for two different frequencies. The chosen frequencies were 30.0 MHz, which typifies performance in the higher frequency portion of the foreshortened element region, and 112.5 MHz, which typifies performance in the region without element foreshortening. The comparison was made using a precision attenuator in the I. F. portion of a Scientific Atlanta Series 1300 receiver. This procedure minimizes the error introduced by receiver nonlinearity. In addition, care was taken to account for all cable losses in both the exploratory development model and resonant dipole, the effect of the hybrid used to feed the resonant dipole, as well as corrections due to slight mismatches of the antennas with the coaxial transmission line. The resulting measured gains with respect to an isotropic radiator, and including the above corrections are as follows: 4.4 ± 0.6db at 30 MHz, and 6.9 ± 0.6db at 112.5 MHz. This latter figure is representative of the gain throughout the unforeshortened element portion of the array, and agrees quite favorably with the results reported by Isbell (1960). The ± 0.6 db accuracy estimate results primarily from possible equipment drift over the time interval necessary for performing the measurement.

2.1.3c VSWR

The measurement of VSWR was obtained while the exploratory development model was atop the tower as pictured in Fig. 2-1. The technique used in obtaining the data was that of exciting the antenna at the frequencies listed in Table II-2, and measuring the magnitude of the reflection coefficient at each frequency. An Anzac model H-9 hybrid was used to serve as a directional coupler, and a Hewlett-Packard model 8405 A vector voltmeter was used to measure the reflection coefficient. All data are referenced to the input connector of the 15.5 ft length of RG-8/U coaxial cable furnished with the exploratory development model. The reflection coefficient data as well as the equivalent VSWR data are plotted in Fig. 2-7 as a function of frequency. Aside from the high VSWR values below 24 MHz, the VSWR is less than 2.5:1 except for approximately a 2 MHz region about 42.5 MHz and 79.5 MHz. Experience with the one-fourth size scale replica indicates that the two regions of high

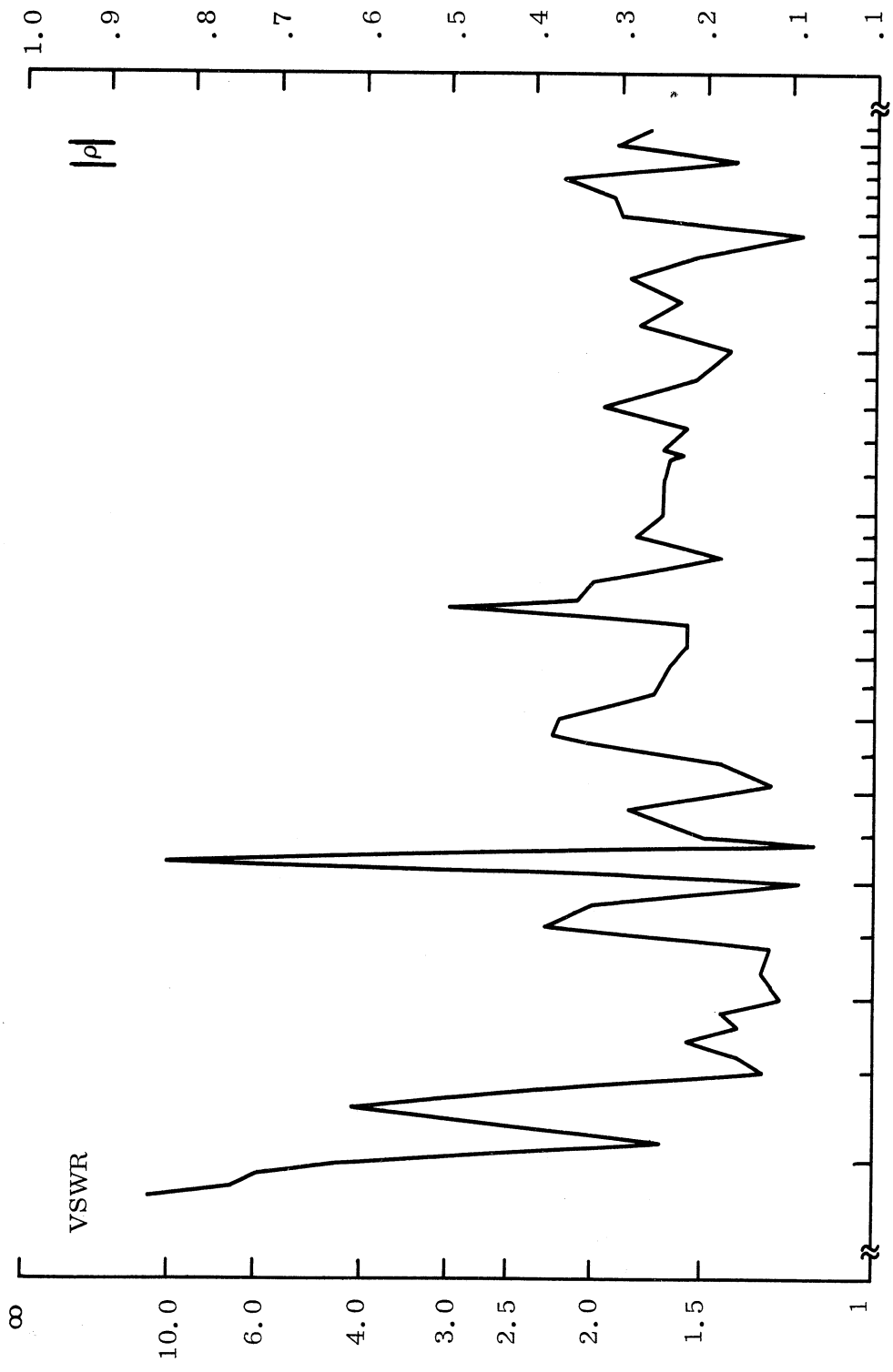

FIG. 2-7: LOG-PERIODIC PLANAR ARRAY, VSWR VS FREQUENCY.

VSWR are a result of terminating the twin channel transmission line with a lumped inductance. As pointed out in section 2.2.2, substantial improvement in VSWR is obtained by using this termination. Further experimentation should allow the elimination of these two narrow frequency regions of high VSWR. Improvement of the VSWR below 24 MHz should be possible by altering the resonant frequencies of elements No. 1 and 2.

2.2 Scale Model Investigations

Frequency scaled models were constructed in order to further investigate the more promising fore-shortening techniques discussed in section 2.3. The antenna boom length was minimized by employing the largest possible apex angle α (half-angle) which permitted compliance with the pattern and VSWR requirements. This angle was obtained experimentally by testing a versatile model and adjusting σ and τ in order to optimize α. The resulting design parameters were applied to a carefully scaled one-fourth size replica of the high frequency portion of the proposed exploratory development model. This scale model featured a boom construction utilizing two sections of brass channel stock in order to allow adjustments which determined an optimum impedance design. The boom so formed constitutes a transmission line with the same characteristic impedance as that in the final full-size exploratory development model. The results of this investigation are reported in section 2.2.1. After the one-fourth size scale replica of the high-frequency section of the antenna had been fabricated and tested, the same structure was expanded to include modeling of the low-frequency section. The two sections representing the entire array were then tested together. This complete one-fourth size model was tested to verify the compatibility of the design parameters of the high frequency section with conclusions reached in the fore-shortened element studies. The results of the experimentation with this complete one-fourth scale model are reported in section 2.2.2.

2.2.1 High-Frequency Section

As mentioned, in order to minimize the antenna boom length, it was decided to design the extreme high-frequency portion of the LPDA to correspond to as large an apex angle as possible. When the apex angle α is increased, two fundamental limitations arise. First, for a given τ, there is an increase in the separation of resonant frequency for adjacent elements. If this separation becomes too large, the energy is not completely radiated in the $\lambda/2$ active region, and pattern degradation results. Secondly, for a given bandwidth as τ is increased, thereby preventing pattern degradation, the VSWR with respect to the mean radiation resistance, R_o, rises sharply. Thus, there exists only a restricted range of values for τ in which both good patterns and tolerable VSWR may be simultaneously maintained. As α is

increased, the range of acceptable values for τ decreases until either the pattern deteriorates by breaking up, or the VSWR requirements can no longer be met. The experiments reported in this section were designed to determine the optimum values of the design parameters, α, τ and σ suitable for an antenna required to meet the contract specifications.

Results reported by Isbell (1960) were consulted to determine reasonable values for the design parameters with which to begin the experimental studies on optimization. Very little published information was available on experimental data for antenna performance with an apex half-angle greater than 45^{o}. An angle $\alpha = 45^{o}$ was selected as a starting point. The reference by Isbell indicates that with $\alpha = 45^{o}$, one should expect acceptable VSWR only if τ is less than approximately 0.90. The lowest value of τ for which data were presented with $\alpha = 45^{o}$ was $\tau = 0.81$, where the measured directivity was 5.2 db over an isotropic source. For $\tau = 0.89$, the measured directivity was 6.2db over the isotropic value. Since $\tau = 0.81$ results in a relatively low VSWR and a relatively small number of elements, this value was selected for initial testing. The adjustable model (1/4 size) shown in Fig. 2-8 was used for obtaining radiation patterns and input impedances for these and additional values of design parameters.

Using the design values, $\alpha = 45^{o}$, $\tau = 0.81$, and correspondingly $\sigma = 0.0475$, radiation patterns were obtained over the frequency range 160 MHz to 900 MHz in increments of 20 MHz. The patterns revealed objectionable distortion, breakup, or backlobes in three distinct frequency regions, each region being 80 to 100 MHz wide. By applying current probing techniques to the model, it was conslusively established that the pattern deformation was caused by the excitation of the $3\lambda/2$ mode on elements behind the $\lambda/2$ active region. The influence of this $3\lambda/2$ mode was also observable in the impedance measurements. The smooth clockwise rotation of impedance values when represented on the Smith Chart was disrupted within the frequency ranges corresponding to pattern deformation. However, it was encouraging to find the VSWR within about 2.3:1. Since the VSWR was better than necessary, it was decided to increase τ to 0.85 while maintaining $\alpha = 45^{o}$ in an attempt to radiate all the energy within the $\lambda/2$ active region.

Using the design values just established, $\alpha = 45^{o}$, $\tau = 0.85$, and $\sigma = 0.0375$ on the readjusted one-fourth size versatile model shown in Fig. 2-8, radiation patterns were taken over the frequency range 200 MHz to 1100 MHz at 20 MHz intervals. These patterns revealed substantial improvement over the $\tau = 0.81$ design. Pattern breakup was eliminated and backlobes were reduced by about 5.0db within the one objectionable 40 MHz wide frequency band centered around 420 MHz. Pattern distortion was noticable around the frequencies where breakup had previously occurred,

FIG. 2-8: ADJUSTABLE SCALE MODEL USED TO OPTIMIZE THE DESIGN PARAMETERS.

but was slight enough to be considered acceptable. Impedance measurements indicated that the VSWR with respect to R_o, the mean input resistance, was still about 2.3:1. However, R_o had decreased from 50 to 35Ω, a situation which was subsequently compensated by increasing the central boom characteristic impedance, Z_o.

Based upon the foregoing experimentation, it was decided to incorporate the design parameters $\alpha = 45^o$, $\tau = 0.85$, and $\sigma = 0.0375$ into a one-fourth size scale replica of the proposed exploratory development model. Among the various reasons motivating this decision are the following: a) an attempt to further improve the patterns by increasing τ above 0.85 raised concern about rapidly increasing VSWR, b) a further increase in τ would add significantly to the required number of elements and, consequently to antenna weight. Moreover, it was deemed desirable to incorporate these design parameters into an array utilizing the twin channel boom construction. This latter geometry allowed a more realistic optimization of the boom characteristic impedance Z_o for the full size exploratory development model.

Using these design parameters, the high frequency portion of the one-fourth size scale replica was constructed and tested. This model consisted of the upper portion of the completed scale replica pictured in Fig. 2-9. Radiation patterns were taken over the frequency range of 300 MHz to 900 MHz. The results of these measurements are summarized in Fig. 2-10a and 2-10b. The ratio of front-to-side-lobe level measured in db is plotted in Fig. 2-10b as a function of frequency. The relatively narrow frequency region in which a high front to sidelobe level occurs around 620 MHz was not present in the previous scale model measurements. Examination of the patterns indicated that the $3\lambda/2$ mode had been too strongly excited at this frequency. With such large values of α, the excitation of this mode is apparently quite sensitive to slight mechanical perturbations. It was felt that such pattern deficiencies could be corrected in the full sized model by slight adjustments in the element lengths should it be necessary. As shown in section 2.1.3a, the need for such an adjustment procedure was not necessary in the full size model. Figure 2-10a presents the 3db beamwidth in the E-plane as a function of frequency. All the data points are within the 70^o specification in the contract requirements. Impedance measurements were also taken on this particular model and are presented in Fig. 2-11a and 2-11b. The longest element in the high frequency portion of the one-fourth size scale replica was nominally resonant at 162 MHz. Figure 2-11a indicates that above 165 MHz the impedance enters the 2.5:1 VSWR circle, and rotates smoothly around the Smith Chart origin which was normalized to 50 Ω. The locus of impedance values was centered about the Smith Chart origin by experimentally varying the characteristic impedance Z_o of the twin channel transmission line. The Smith Chart impedance plot for frequencies between 660 MHz and 920 MHz is shown in

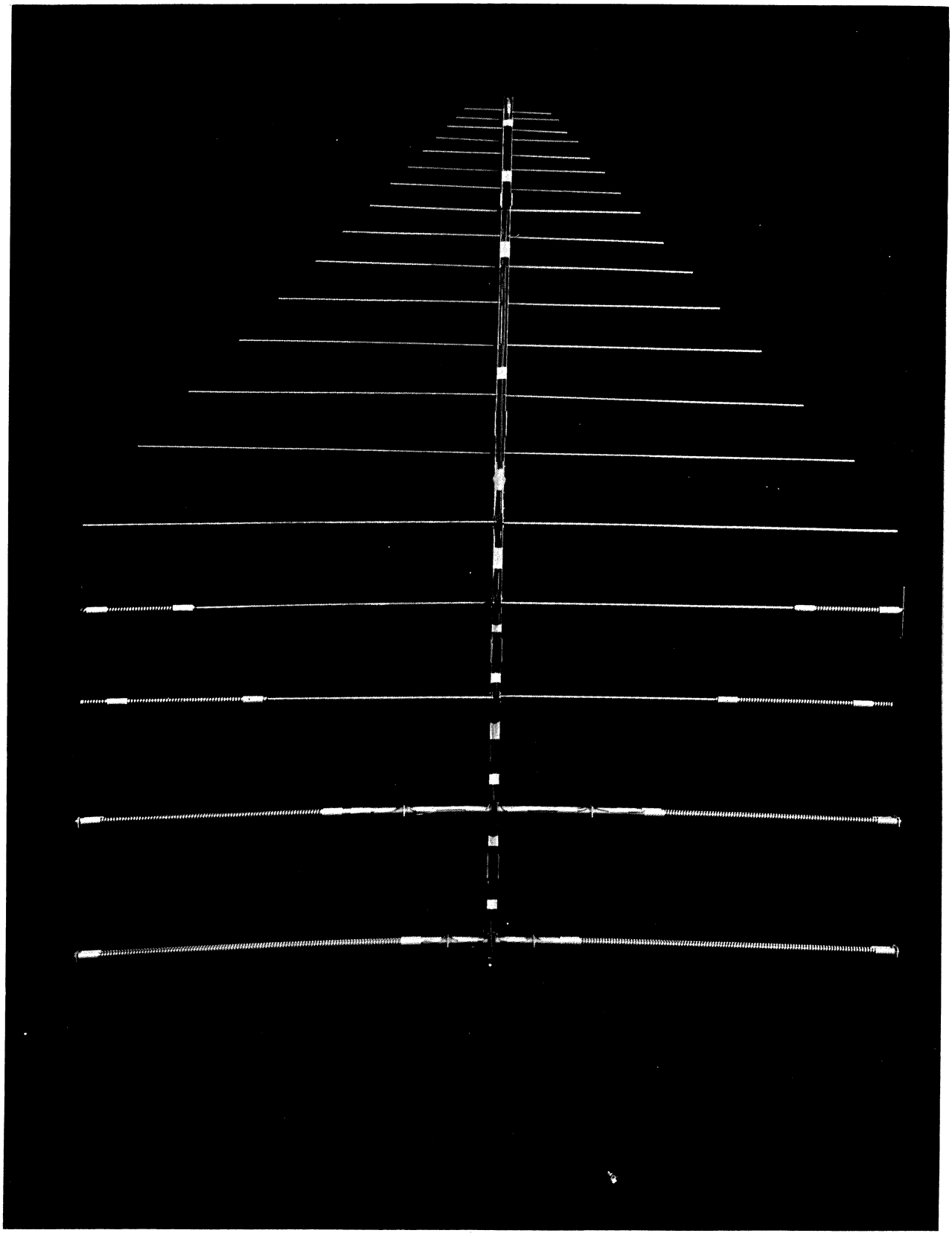

FIG. 2-9: ONE-FOURTH SIZE SCALE REPLICA OF EXPLORATORY DEVELOPMENT MODEL.

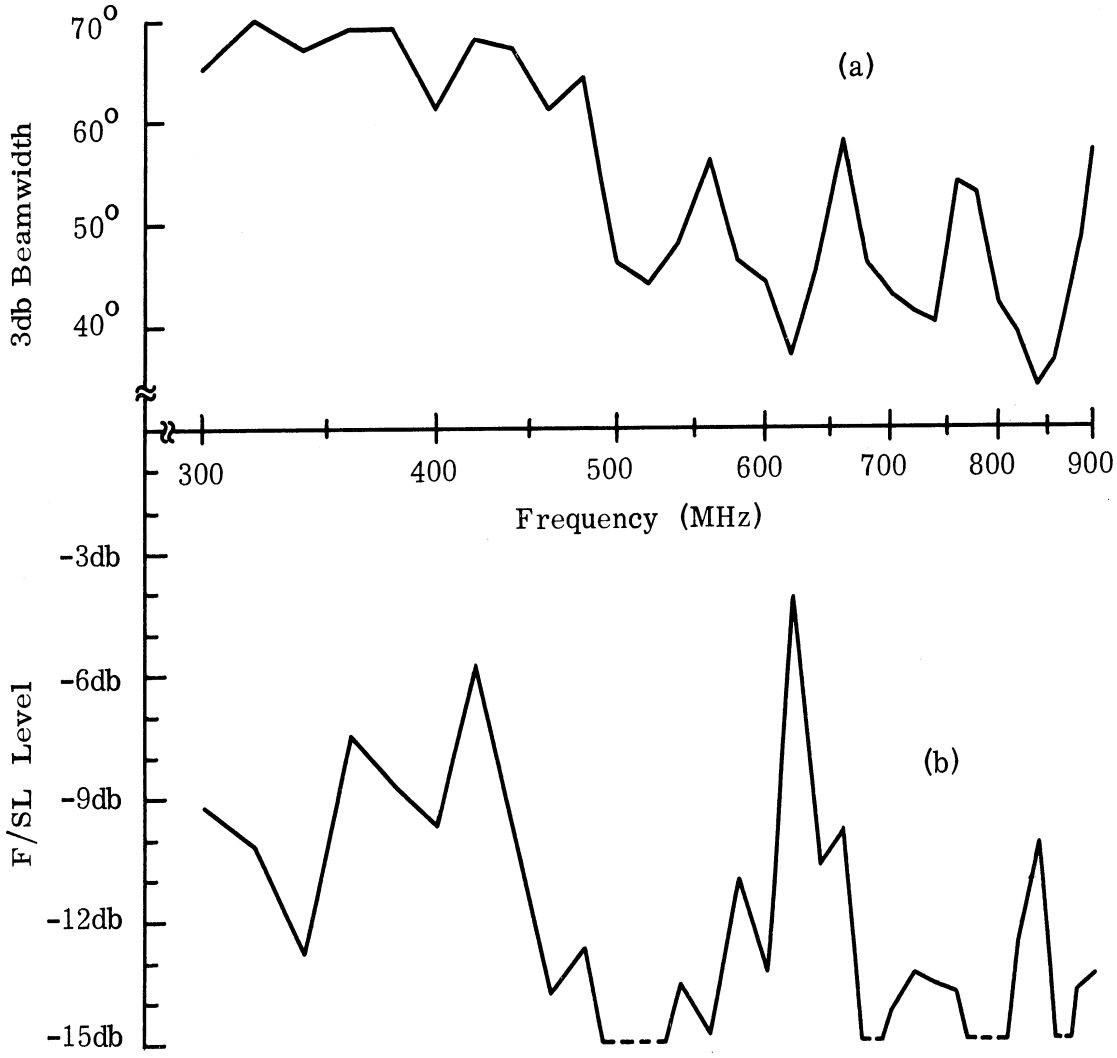

FIG. 2-10: HIGH FREQUENCY PORTION OF ONE-FOURTH SIZE SCALE REPLICA, (a) 3-db Beamwidth vs Frequency, and (b) Front-to-sidelobe Ratio vs Frequency.

Fig. 2-11b. The slight shift of impedance loci to the right results from an effective series inductance caused by asymmetry in the transition from the coax to twin channel transmission lines at the tip of the array. The feed symmetry was improved on the full size exploratory development model. Also noticeable in Fig. 2-11b is a decrease in mean radiation resistance R_o, below the previous 50 Ω value in Fig. 2-11a. This results from a combined effect of having elements which are electrically thicker at this high frequency end, and the presence of a partial excitation of the $3\lambda/2$ mode. Since the impedance values are referenced to the antenna tip, and contain no effect due to transmission line losses, the impedance measured on the full size exploratory development model should have somewhat reduced VSWR when measured at the end of a reasonable length of coaxial feed line.

2.2.2 Low Frequency Section

After the high frequency section of the one-fourth size scale replica had been tested as described in Section 2.2.1, the five elements which constitute the low frequency section were added to the model. The basic studies and experiments leading to the use of these foreshortened elements are discussed in detail in Section 2.3.1. The elements are attached to the central boom at the positions specified by the design parameters used in the high frequency section. Elements No. 1 and 2 each utilize a folded dipole arrangement which results in a 4:1 step-up of the impedance level. Elements No. 3 and 4 are not folded, but utilize the same principle of distributed end loading. Further details are presented in Section 2.3.1.

Considerable experimental effort was expanded in optimizing the performance in this lower frequency octave of operation. The principle effort was directed toward: a) experiments with various terminations on the twin channel transmission line, and b) experimental adjustment of the resonant frequencies of various elements. Since these experiments were fairly detailed, only the significant results will be summarized below. The optimization was based upon the simultaneous achievement of an acceptably low VSWR and good radiation patterns. As an aid to monitoring VSWR while adjustments were being made on the scale replica, swept frequency measurements of the magnitude of the reflection coefficient were obtained with the replica placed inside of a small anechoic chamber so as to simulate free space conditions. In addition, impedance measurements were obtained at spot frequencies by measuring the complex reflection coefficient and plotting it on the Smith Chart. These techniques greatly facilitated the rapidity with which various experiments could be performed. Experiments were performed on the complete scale replica for terminations of the twin channel transmission line consisting of an open circuit, a short circuit, and various arbitrary impedances. The simple open circuit

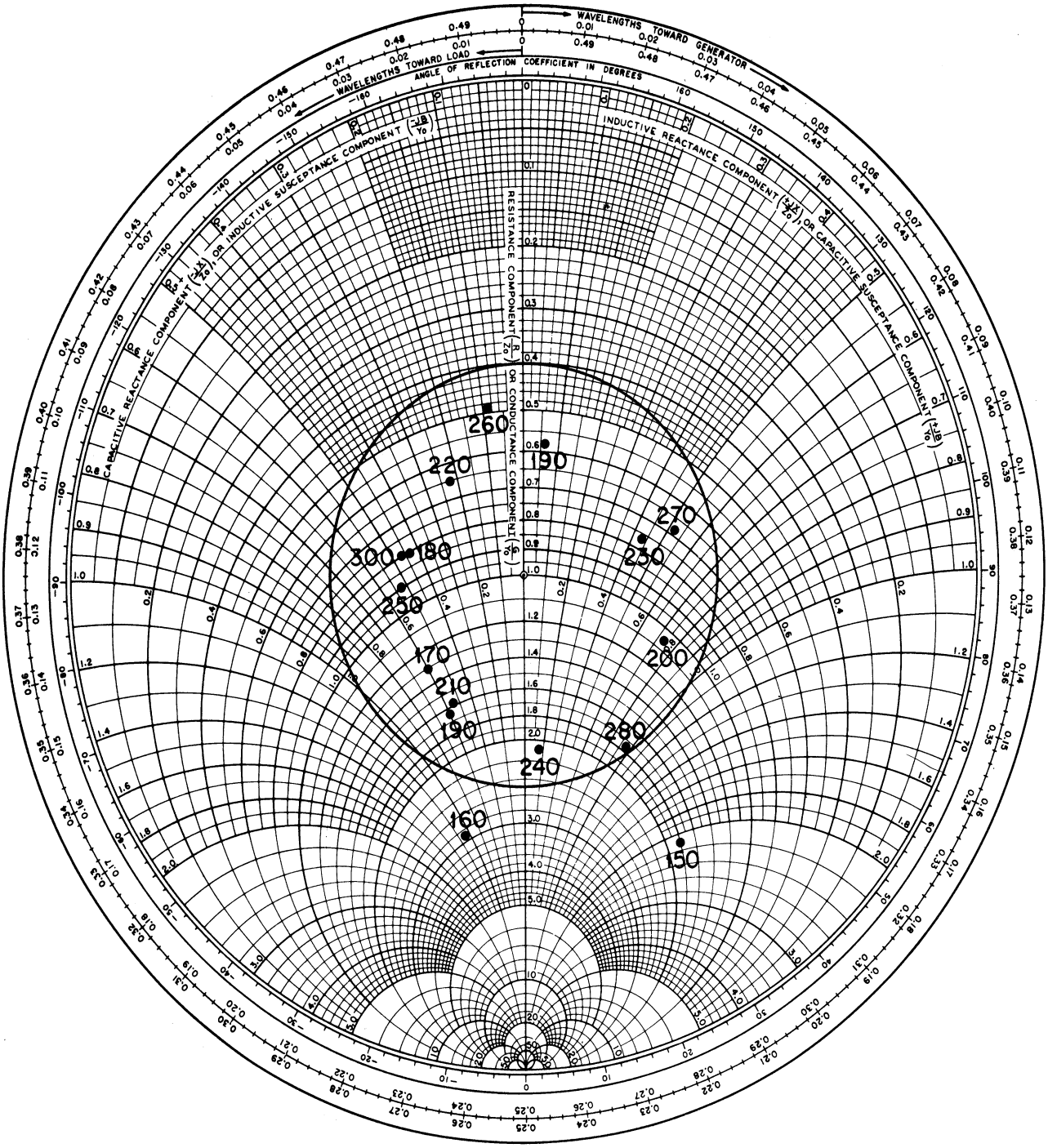

FIG. 2-11a: HIGH FREQUENCY PORTION OF ONE-FOURTH SIZE SCALE REPLICA INPUT IMPEDANCE (150 MHz through 300 MHz).

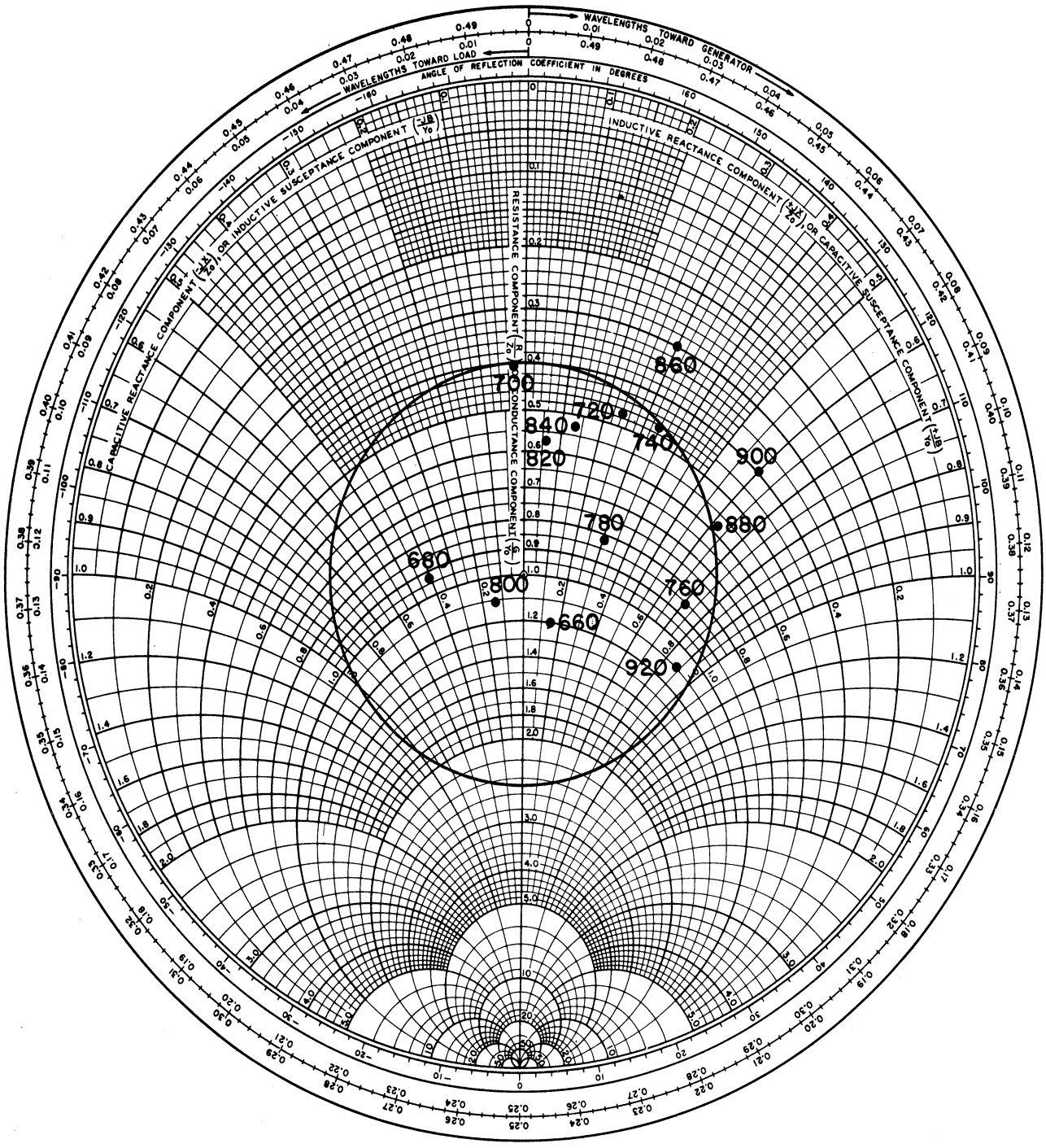

FIG. 2-11b: HIGH FREQUENCY PORTION OF A ONE-FOURTH SIZE SCALE REPLICA INPUT IMPEDANCE (660 MHz through 920 MHz).

termination was investigated first in the hope that the array would function satisfactorily. However, swept frequency measurements of the magnitude of reflection coefficient, and Smith Chart impedance plots, indicated the existance of highly accentuated impedance variations within the lower octave of array operation. The rapid fluctuations in impedance ranged from a near match condition of 50 Ω, to impedance values both five times higher and lower than 50 Ω, as referenced to the tip of the array. It was experimentally determined that replacing the open circuit by a short circuit termination substantially suppressed the eccentric impedance excursions, to the extent that a VSWR of 2.5:1 was maintained nearly throughout the lower frequency octave of operation. The consequences of this short circuit termination were the following: 1) since element No. 1 now functioned only as a parasitic, the low frequency limit for VSWR less than 2.5:1 was increased from 70 MHz to 85 MHz, and 2) a narrow region of high peak VSWR appeared at a frequency substantially higher than that of operation in the lower frequency octave. Since the zero impedance termination exhibited a substantial improvement in VSWR characteristics, other low impedance reactance terminations were investigated. It was found that a lumped inductive termination of relatively low impedance resulted in essentially the same benefits as the short circuit termination, but in addition allowed sufficient excitation of the lowest frequency element so as to decrease the minimum frequency at which a VSWR of 2.5:1 could exist. The narrow VSWR spike still existed above the lower frequency octave, and shifted lower in frequency with increasing inductive reactance. Efforts to eliminate this spike while maintaining a low impedance termination on the transmission line proved futile. An effective inductive termination normally exists when the balanced transmission line is short circuited at a distance of $\lambda/16$ behind the last element, as used by Isbell (1960). Apparently the effect of the inductive termination is somehow adversely influenced due to the presence of the foreshortened elements. The optimum inductive termination on this scale replica was found to be a three turn coil of No. 18 AWG wire wound on a 3/16" diameter from1/8 inch separation between turns. Concurrent with the optimization of VSWR characteristics, radiation patterns were also observed for the various transmission line terminations. Fortunately, and somewhat surprisingly, little difference in radiation patterns was observed for the various terminations, although the coil termination provided slightly improved backlobe suppression.

Although the inductive termination on the twin channel transmission line substantially improved the VSWR characteristics, some further improvement was possible by a slight adjustment of resonant frequencies of the foreshortened elements. In particular, a region of relatively higher VSWR existed slightly above 100 MHz. The radiation patterns also indicated a relatively higher backlobe in this feequency region. Consequently, the resonant frequencies of the two foreshortened

elements on either side of this frequency were moved slightly closer together. This resulted in both a reduction in VSWR and radiation pattern backlobe throughout this frequency region. The final resonant frequencies of the foreshortened elements after optimization are recorded in Table II-3. Figure 2-12 pictures the low frequency portion of the scale replica after the optimization procedure was complete. The resonant frequency of element No. 4 was lowered by means of the wire extensions as pictured.

TABLE II-3

Element No.	Resonant Frequency MHz
1	72.0
2	83.0
3	96.0
4	107.0
5	136.0

This technique was used simply as a convenience in place of adding an additional length of helix. A longer portion of helical slow wave structure was used in the exploratory development model to lower the resonant frequency. Figure 2-12 indicates that the coaxial feed cable is removed from the antenna at the low frequency end. The full size exploratory development model is designed to have the coaxial feed cable leave the array at the location of the mounting mast. Experimentation has confirmed that the impedance is affected negligibly by the particular location at which the feed cable is removed.

The results of the radiation patterns of the scale replica after the optimization procedure was complete are presented in Figs. 2-13a and 2-13b. The 3db beamwidth plotted in Fig. 2-13a indicates that pattern degradation occurred below about 87.5 MHz. Also, the ratio of front-to-sidelobe level, as plotted in Fig. 2-13b, is still somewhat higher than desirable near 105 MHz. The low frequency cut-off behavior is somewhat better than indicated in Fig. 2-13 since the actual generator frequency was about 2.5 per cent lower than the indicated nominal values. The low frequency impedance behavior of the scale replica is presented in Fig. 2-14. These impedance values are referenced to the tip of the model. With the exception of a slight departure at the low frequency end, the impedance values are within the 2.5:1 VSWR circle measured relative to 50 Ω.

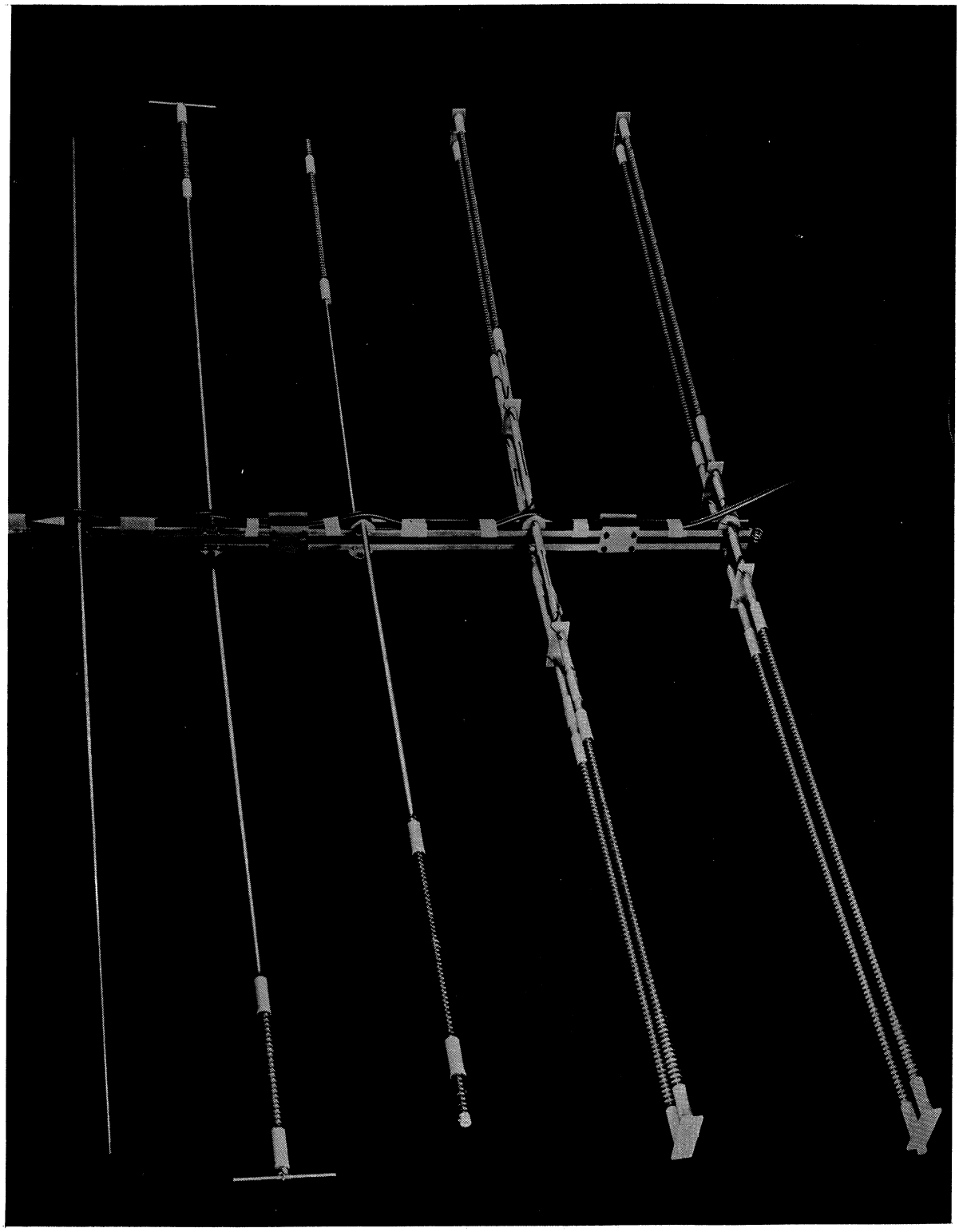

FIG. 2-12: LOW FREQUENCY PORTION OF ONE-FOURTH SIZE SCALE REPLICA OF EXPLORATORY DEVELOPMENT MODEL.

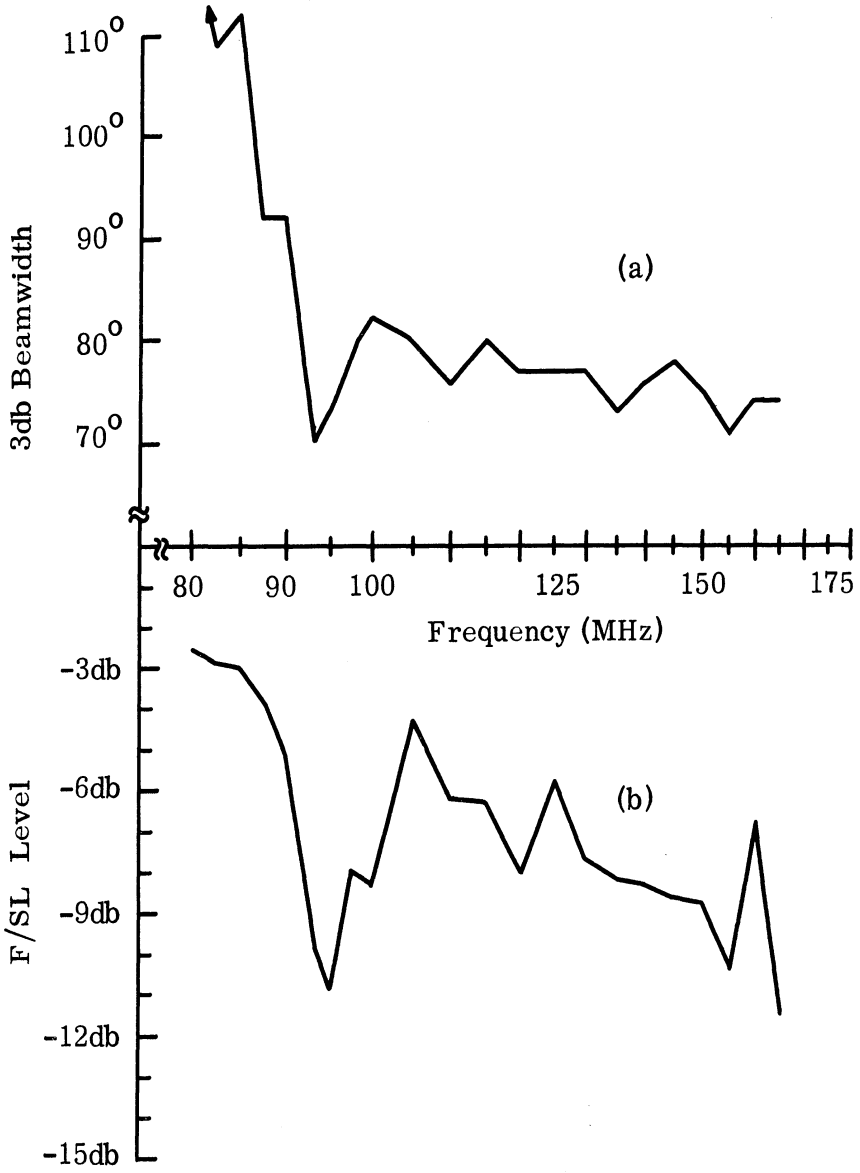

FIG. 2-13: ONE-FOURTH SIZE SCALE REPLICA, (a) 3-db Beamwidth vs Frequency, and (b) Front-to-sidelobe Level vs Frequency.

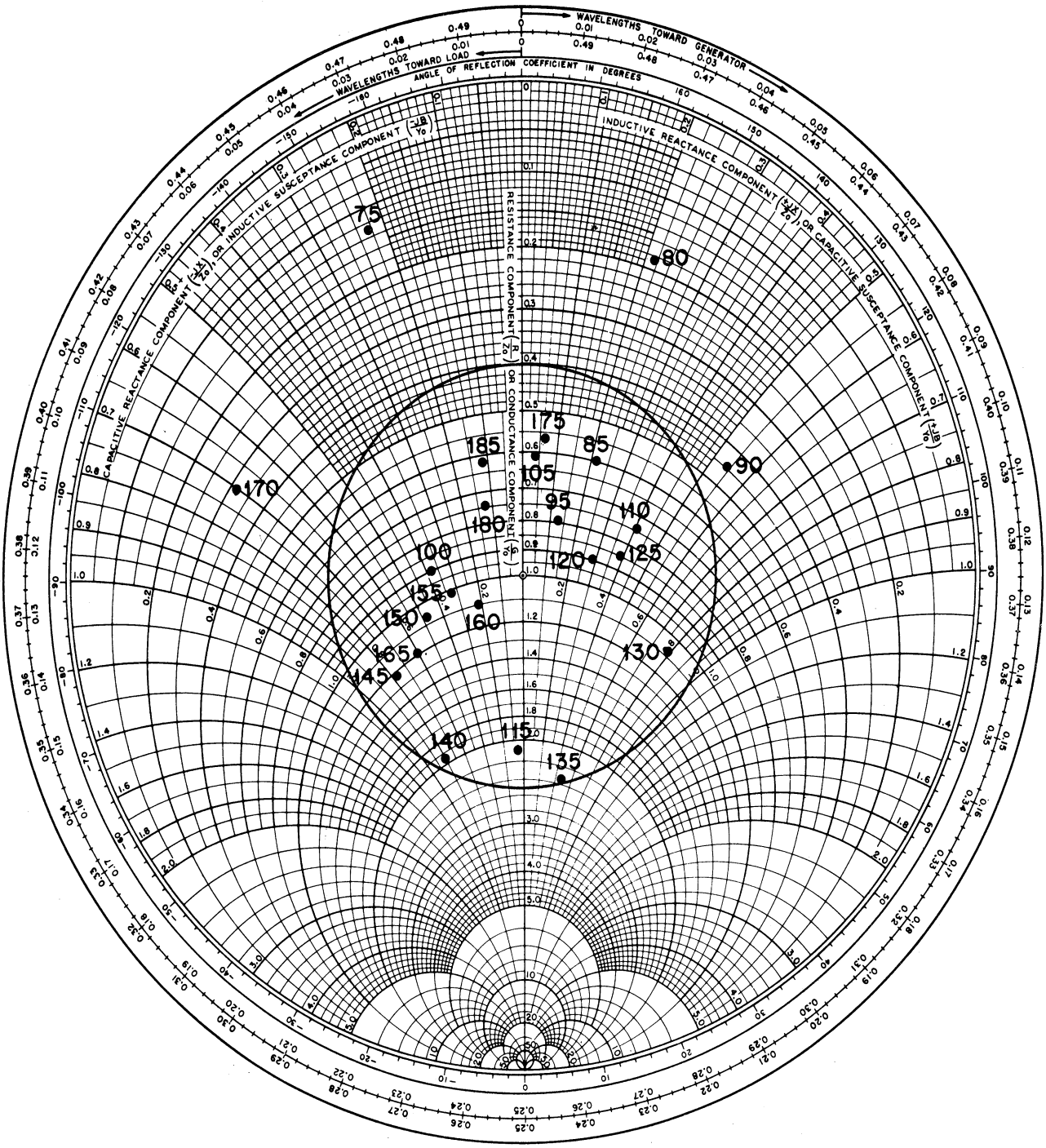

FIG. 2-14: ONE-FOURTH SIZE SCALE REPLICA INPUT IMPEDANCE (75 MHz through 185 MHz).

2.3 Foreshortened Element Studies

There is a definite orderly approach that can be applied to produce the best foreshortened element. First, loading should produce as close to a uniform current distribution along the element as possible. This will result in the highest input resistance. Second, any single lumped reactance used as a broadbanding scheme with the antenna element should form a shunt network since this produces the optimum bandwidth. Third, the element should have as large an effective diameter as possible to produce the smallest inherent Q. Section 2.3.1 discusses this in more detail.

With these ideas in mind, several types of foreshortened elements were investigated. These included helical, zig-zag, and bent dipoles of various configurations. Folded versions of several of these elements were also investigated. The lightest weight, most rugged element that has the best electircal properties is the folded helical dipole. The development of this element is discussed in Section 2.3.2, while other element investigations are covered in Section 2.3.3.

2.3.1 Principles of Bandwidth Optimization

It is generally realized that the impedance bandwidth of the individual elements in a planar log-periodic dipole array is a limiting factor in the permissible size reduction for this type of antenna. Some of the known facts relating to the optimization of impedance bandwidth in foreshortened linear elements have been gathered below. The intent of this section is to identify some fundamental principles which should be followed in order to achieve optimum impedance bandwidth. Impedance bandwidth, as used here, is defined as the frequency interval about resonance for which the input reactance does not exceed the resonant input resistance.

The input impedance of a linear element can be represented for small frequency deviation about any frequency, except for anti-resonance, by a series resistance and reactance. Moreover, the derivative with respect to frequency of this reactance will always be positive, unless some impedance compensation network is acting upon the element terminals. When a linear element is operated at a frequency away from self-resonance, a pure reactance is sometimes placed in series with the element at its terminals to make the total impedance series resonant. This of course leaves the input resistance unaltered. Since the frequency derivative of impedance for any passive purely reactive single element is positive, the frequency sensitivity of the resulting series resonant circuit will be increased. Hence, for the situation where input resistance is unaltered, it may be concluded that any element loading which has the effect of adding series reactance at the element terminals will increase the

frequency sensitivity, and hence decreas the element impedance bandwidth. The above conclusion indicates that any loading which introduces a specified amount of series terminal reactance should be applied so as to maximize the input resistance, and hence the impedance bandwidth. Resonating a symmetrically fed linear element of length less than 0.5λ requires the introduction of inductive series terminal reactance. Moreover, since the maximum point of the standing wave current distribution occurs at the terminals, the input resistance equals the element radiation resistance. It is well known that the maximum radiation resistance for a given element of total length $2h \leq 0.5\lambda$ occurs when the standing wave current distribution is uniform; this corresponds to $I(z) = I_o$ (constant amplitude), over the entire length.

To a fair approximation the current distribution for an unloaded thin element is: $I(z) = I_m \sin k(h - |z|)$. For a short element, this distribution is essentially triangular. A frequently used technique for optimizing the short element current distribution is to end load the element. This tends to create the desired uniform current distribution; hence, it increases the radiation resistance for a given length h. Another effective technique sometimes used is to uniformly load the element, so as to decrease the phase velocity of the current. This results in a current distribution approximated by:

$$I(z) = I_m \sin \beta (h - |z|), \quad \text{where} \quad \beta = \omega/v_p > k = \omega/c.$$

The element of half length h can be made self-resonant by proper adjustment of the uniform loading. Resonance occurs when v_p is such that $\beta h = \pi/2$. This distribution has a larger current moment, and hence a larger radiation resistance, than that of an unloaded element of the same length. This technique of improving the impedance bandwidth is often implemented through the use of small diameter coiled elements.

One might further increase the element input resistance, and hence impedance bandwidth, by adding some ohmic resistance in series with the already optimized radiation resistance. For example, adding an ohmic resistance at the element terminals equal in magnitude to the radiation resistance would approximately double the impedance bandwidth. The resultant decrease in efficiency may be justified in certain receiving applications. However, for high power transmitting applications the heat generated in the loading or compensating resistance may be excessive.

An alternative approach which also tends to further increase the impedance bandwidth without adding significantly to ohmic dissipation is the insertion of a parallel resonant circuit across the element terminals. The susceptances of the

element and the parallel resonant circuit tend to cancel over some frequency band. A parallel resonant circuit of optimum configuration has been treated by Shnitkin and Levy (1962). Such an approach performs well at VHF-UHF frequencies where stubby dipoles having low Q may conveniently be constructed. At lower frequencies its usefulness tends to decrease since elements are generally of higher Q.

2.3.2 Helical Elements

The discussion of element foreshortening principles in Section 2.3.1 indicated that a self resonant slow wave structure represents an improved foreshortening technique for attempting to retain impedance bandwidth. Such a slow wave structure is easily constructed using a small diameter helix as discussed by Li and Beam (1957). The helix acts as a uniform loading by slowing the phase velocity of a signal propagating on the structure. Owing to the small diameter of the helix, the radiation remains essentially linearly polarized. Several lengths of helical slow wave structure were constructed so as to represent a one-fourth size scale model of a structure with a phase velocity reduction of 0.5 at 20 MHz. This construction was then used in experiments to obtain an optimum design of elements for the one-fourth size scale replica of the exploratory development model.

The slow wave structure was designed with a phase velocity reduction of 0.5 in order to accomodate a 2 to 1 size reduction in the lowest frequency element. In addition, portions of the slow wave structure were used as end loading on elements which required a less than 2 to 1 reduction in length. A meaningful appreciation for the first order effect of such loading is obtained by considering the transmission line approximation for a linear radiating element. Oftentimes one approximates the impedance behavior of a resonant $\lambda/2$ dipole by comparing it to a radiation resistance in series with a $\lambda/4$ length of transmission line open circuited at the far end and possessing a characteristic impedance given by an average of that associated with the dipole. Analogously, when a slow wave structure is present at the dipole ends, the model becomes a cascade of two transmission line sections, with differing phase velocities and characteristic impedances. Dipole resonance is obtained when the infinite impedance existing at the open circuit end of the analogous transmission line is transformed through the two cascaded transmission line sections into an apparent short circuit at the driving point terminals. The required overall length of the cascaded transmission line sections is to remain a constant, and the resonant frequency lowered by adding successively longer portions of slow wave structure. However, the exact length of each portion depends not only on the phase velocity in each, but also upon the characteristic impedance of each. In particular, signals originating at the feed terminals are reflected not only at the open circuited end, but also at the

transition between the two transmission line sections when the characteristic impedances are not identical. This results in a somewhat complicated phenomenon with the characteristic impedance of the helical slow wave structure not readily defined. As a result, the required length of slow wave structure necessary to resonant a linear element at a desired frequency was determined experimentally. An interesting consequence of reflections taking place at the discontinuity in characteristic impedance is that the elements are self resonant in a lowest order mode at two distince frequencies. Care must be taken that the higher resonant frequency resulting from such reflection does not disrupt normal log perioic array action. Successful designs for elements No. 3 and 4 in the scale replica model were obtained using such techniques.

When element foreshortening approaching 2 to 1 is obtained using these techniques, the resonant input resistance becomes substantially lower than that corresponding to the unforeshortened element. This low value of resonant resistance may be transformed by a factor of 4 by employing a folded dipole type of construction. By utilizing this technique, an element foreshortened by a factor of 2 to 1, which for uniformly distributed loading has a resonant resistance of approximately 20Ω, is transformed to approximately the value of a full size element. In addition, the impedance bandwidth is improved due to an increase in effective radius for the combined linear elements. This folded configuration also possesses multiple resonant frequencies, and care must be taken to ensure that they do not affect normal log-periodic array operation. Moreover, when two helical slow wave structures are brought within close proximity of each other, the interaction of the structures causes a decrease in phase velocity reduction. Experiments performed with two $\lambda/2$ resonant slow wave helical structures indicated that the resonant frequency increases approximately 13 per cent when the structures were brought to 1 inch separation. Each such structure was 1/4 inch in diameter and 52.5 cm long. An experimental effort was also undertaken to account for these effects in designing elements No. 1 and 2 to be resonant at the desired frequencies.

Initial experiments on the foreshortened helical elements were made on a monopole version fed against an aluminum ground plane. The ground plane, which was 4' square, was inserted in one wall of 5' cubical anechoic chamber. Absorber material was placed around the periphery of the ground plane, thereby minimizing the excitation of edge currents. The net effect of the ground plane inserted in the chamber was that of simulating free space performance over a somewhat larger ground plane. Since the experiments consisted of entirely comparative measurements, the slight inaccuracies due to this size of ground plane were insignificant. Experimentation consisted primarily of determining the element's resonant frequency impedance, and bandwidth. Swept frequency measurements of the magnitude of reflection coefficient, as well as actual impedance measurements, were obtained for

many element configurations. A right-hand helix images in a ground plane as a left-hand helix. Since only right-hand helices were used for the complete dipole configuration, the monopole versions were observed to resonant about 2 per cent higher in frequency than the corresponding dipole configurations.

2.3.3 Partially Folded Monopole and Zig-Zag Monopole

In order to shorten the individual elements, the feasibility of partially folded dipoles including zig-zag dipoles has been investigated. Figure 2-15 illustrates the VSWR data of a 15 cm monopole constructed of No. 18 enameled wire erected above a ground plane. The VSWR was taken with, 1) the monopole being straight, 2) bent at a 90^{o} angle, 5 cm from the end, and 3) bent twice in the shape of the Greek letter Γ. Minimum VSWR increased from 1.18 to 1.28 and 1.42 respectively, while the resonance frequency shifted from 460 to 480 MHz. Figure 2-16 illustrates the VSWR data of a 15 cm high zig-zag monopole with a conductor constructed of a 30 cm length of No. 18 enameled copper wire. Again it is interesting to note that bending the end of the zig-zag monopole has little effect on resonance frequency and input impedance. Apparently there is little interaction between the monopole and its end. However, the resonance frequency of the zig-zag monopole occurs at 380 MHz. A shortening of 18 per cent in height is obtained when compared to the straight monopole.

2.4 Foreshortened Arrays

In addition to the work on helical dipole arrays reported in Section 2.2, log periodic dipole array studies were made to test additional methods of foreshortening dipole elements and techniques for reducing the boom length. From the experiments performed, it appears that the values of the spacing factor, σ, can be made smaller than the 0.08 value that is commonly used. Experiments also indicate that making the section of transmission line connecting adjacent dipoles electrically longer than the free space distance between the dipoles has little, if any, effect on the radiation patterns of log-periodic dipole arrays.

Other experiments verify that under special conditions, bent dipole elements can be used to reduce the width of log-periodic dipole arrays. Both the width and length can be reduced if a smaller spacing factor as described earlier is used, along with bent dipoles that are bent towards the tip of the array. Mixing zig-zag elements with bent dipoles did not improve performance of an array over that obtained entirely with bent dipole elements.

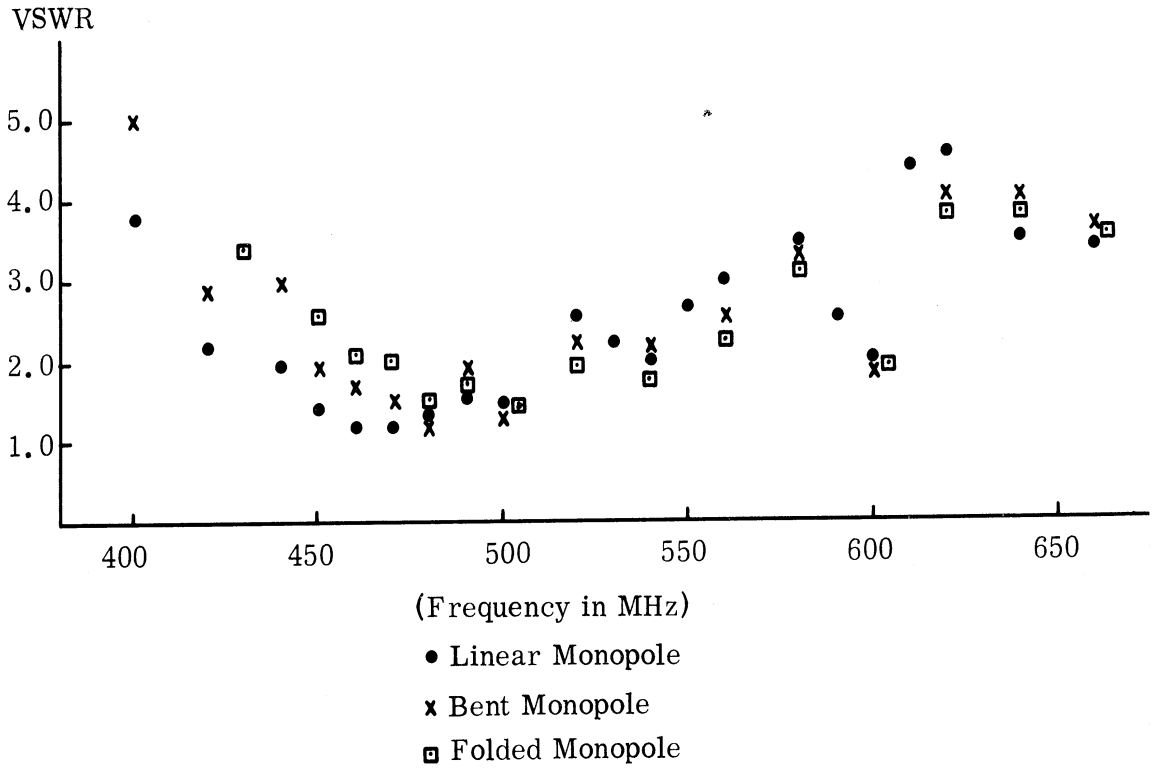

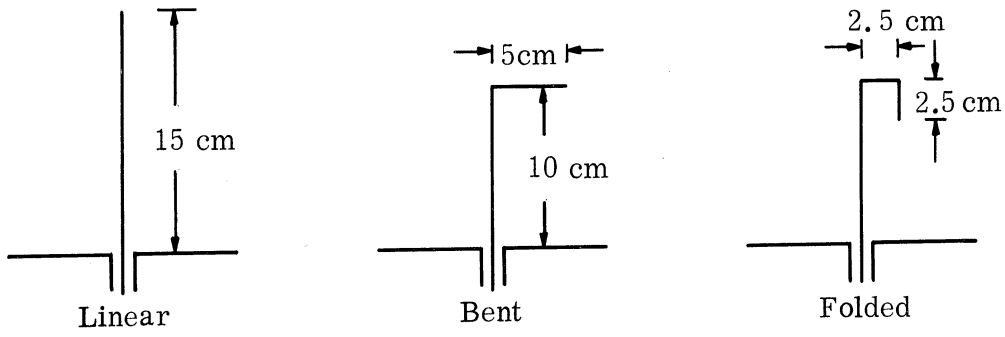

FIG. 2-15: VSWR FOR LINEAR, BENT AND FOLDED MONOPOLE MADE OF NO. 18 ENAMELED COPPER WIRE.

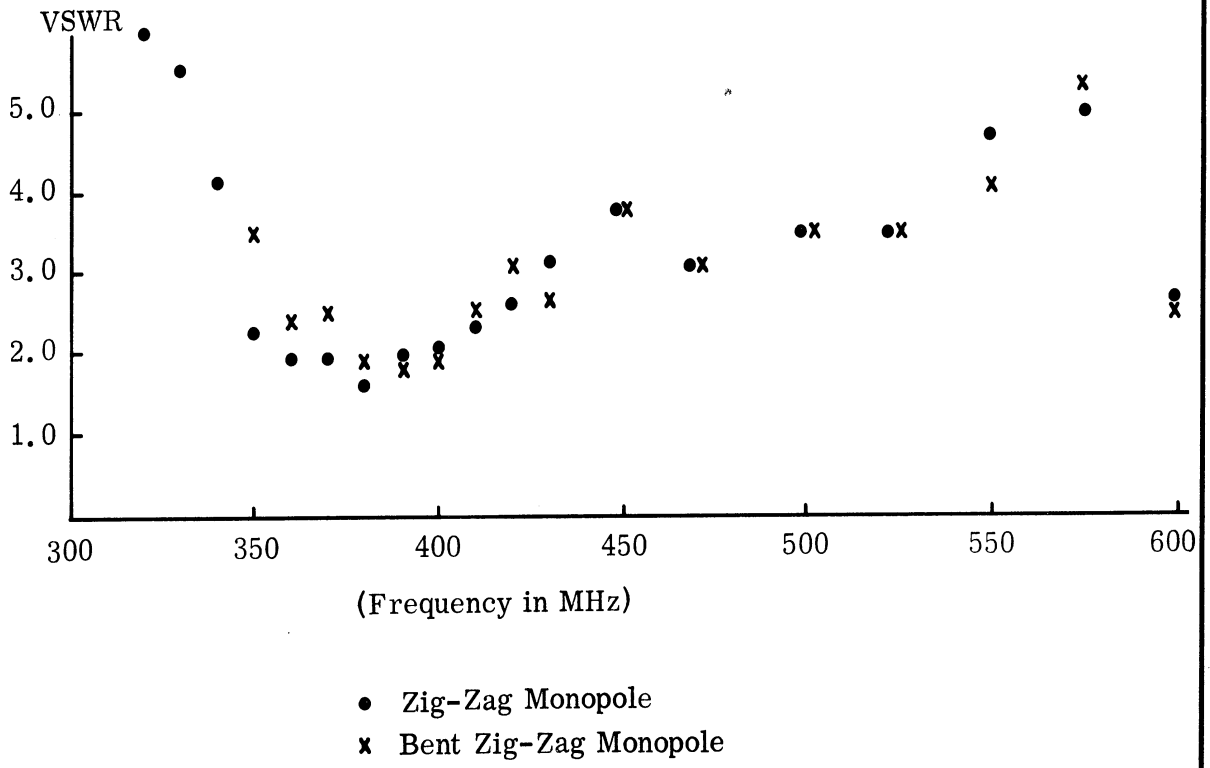

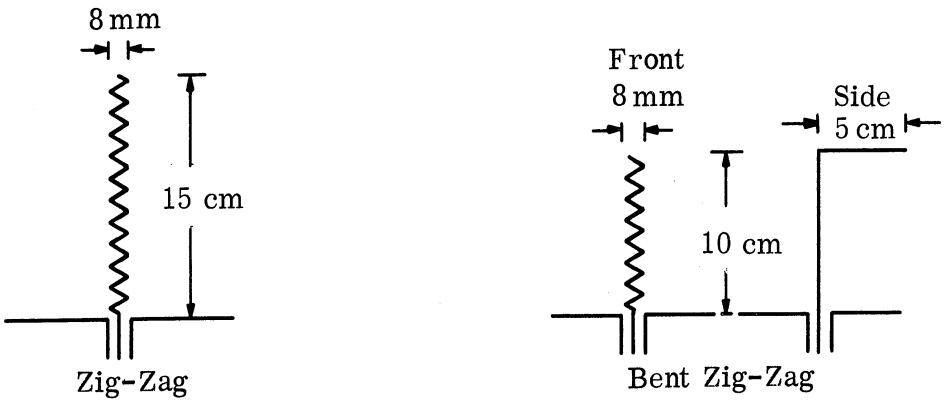

FIG. 2-16: VSWR FOR ZIG-ZAG AND BENT ZIG-ZAG MONOPOLE CONSTRUCTED OF NO. 18 ENAMELED COPPER WIRE. (Total length of conductor = 30 cm).

2.4.1 Boom Spacing Studies

An early attempt was made to establish the feasibility of using smaller than normal design spacings of the elements along the beam. For this purpose, an antenna design, LPDA-1, was made. The dimensions of the antenna appear in Fig. 2-17. This design has a feed structure consisting of two hollow copper tubes, through one of which a coaxial cable is used as an infinite balun. The feed is at the front end and the center conductor of the coaxial feed is attached to the opposite hollow tube in a symmetrical fashion. Considerable attention was given to making the feed at the front as symmetrical as possible.

This design has also been built using a simple transmission line of two wires crossing in the horizontal plane. This configuration uses a balanced feed at the front end which is excited through an Anzac hybrid. The experimental results achieved are almost exactly the same for either type of feed structure.

The design of antenna LPDA-1 uses a tapering factor, τ, of 0.88. This is a common design value. A spacing of 0.04λ (free-space wavelength) was utilized; this value of the σ factor is approximately half the value normally used under common design procedures. On the basis of the two design factors τ and σ, the half angle subtended by the apex of the antenna is $\alpha = 37^{\circ}$. Twenty dipole elements were used in this design. The antenna has the following dimensions: 9.5 cm across the smallest tip of the antenna; 103 cm across the bottom corresponding to the length of the longest dipole element, 66 cm corresponding to the overall length of the boom.

A series of E-plane radiation patterns were taken from 100 MHz to 1500 MHz. The radiation patterns are shown in Figs. 2-18a and 2-18b. The E-plane half power beamwidth at any frequency does not vary much from that of an antenna having the usual boom spacing (σ) of approximately twice the value used for this experimental antenna. Decreasing the boom length, by decreasing the spacing of elements, does seem to result in some decrease in gain.

The standing wave ratio was below 2.0 for the antenna that was fed with the hybrid. The measurements were made at the end of a 1.5 meter piece of RG-8/U coaxial cable.

2.4.2 Foreshortened Array with a Long Transmission Line

The boom length of a log-periodic antenna for a given tapering factor can be shortened by using a small spacing factor, and the radiation patterns still remain in

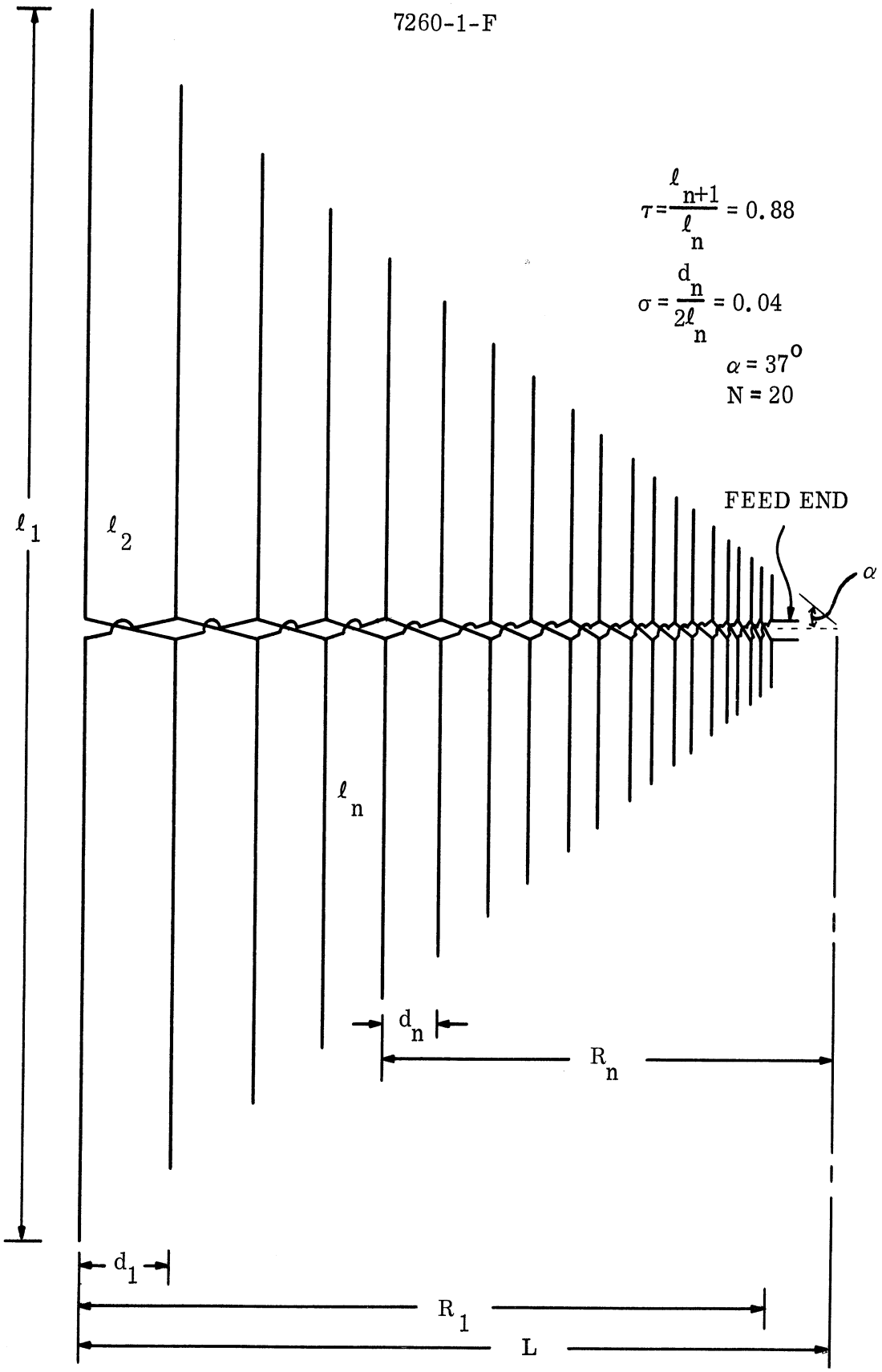

FIG. 2-17: ANTENNA LPDA-1. LONGEST DIPOLE 100 cm ($\lambda/2$ at 150 MHz)
SHORTEST DIPOLE 8.8 cm ($\lambda/2$ at 1700 MHz)
SIZE: 103 cm x 66 cm

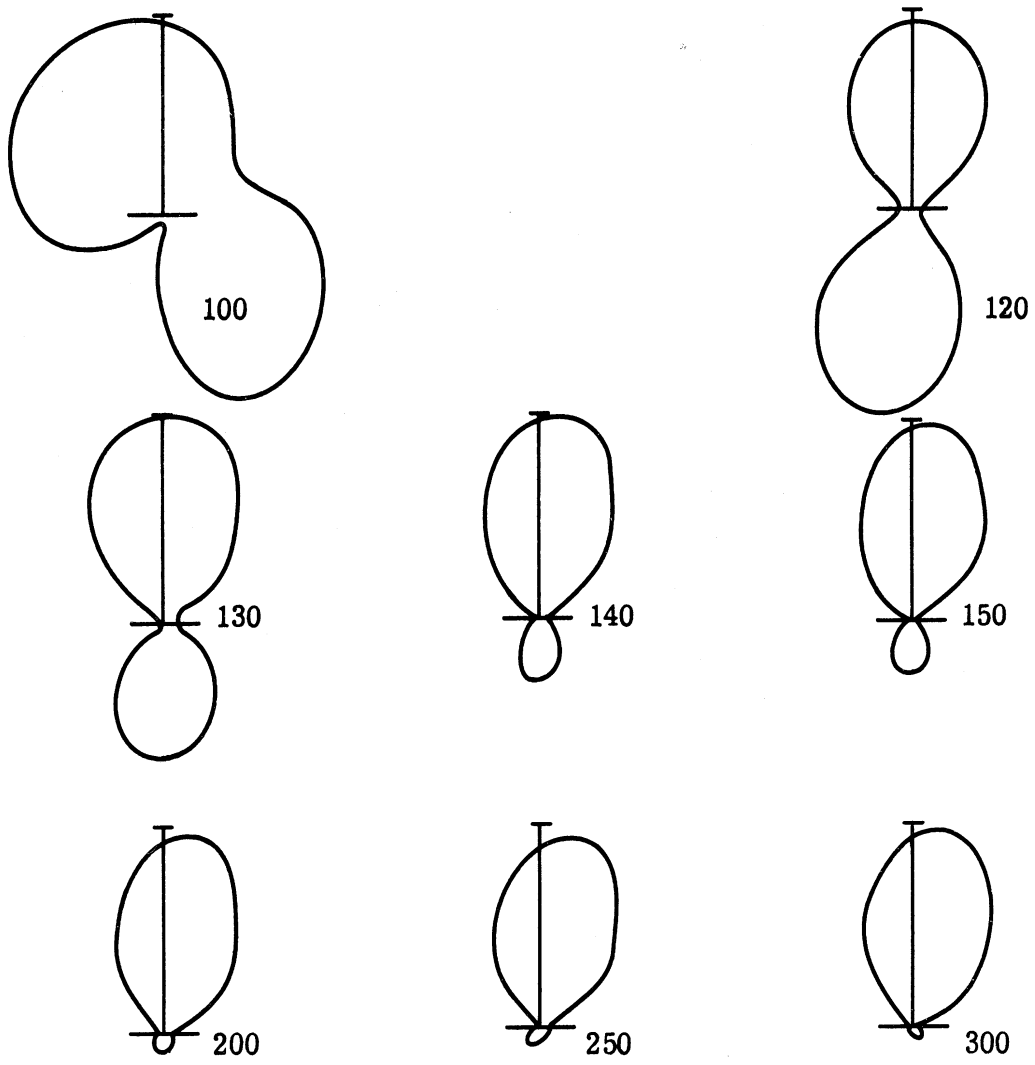

FIG. 2-18a: LPDA-1 100 - 300 MHz E-PLANE LINEAR POWER PATTERNS.

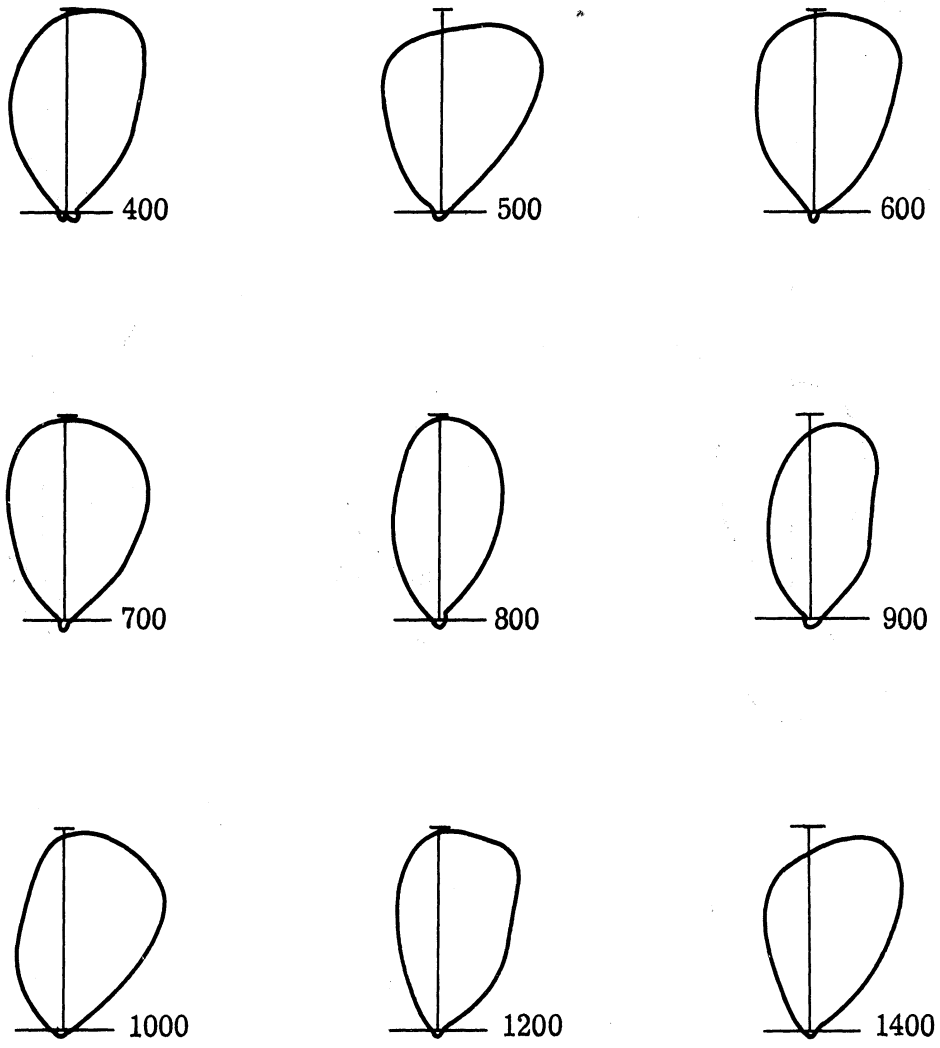

FIG. 2-18b: LPDA-1 400 - 1400 MHz E-PLANE LINEAR POWER PATTERNS.

the backfire direction. However, smaller spacing will result in lower directivity and higher VSWR. As an attempt to study the possibility of using a small spacing factor (less than 0.04) without deteriorating the directivity and VSWR characteristics, a longer transmission line connecting one element to the next was used to vary the phase of the exciting field along the axis of the antenna structure.

Figure 2-17 shows the structure used in this experiment. The parameters are as follows: tapering factor, $\tau = 0.88$, spacing factor, $\sigma = 0.04$, and the half angle subtended by the apex of the antenna, $\alpha = 37^{\circ}$. The antenna consists of 20 dipole elements and has an overall dimension of 9.5 cm across the smallest tip, 103 cm across the bottom corresponding to the length of the longest dipole, 66 cm corresponding to the overall length of the boom. Instead of using two rigid hollow copper tubes as feeder lines, the dipoles are fed by a flexible 72 Ω "twin-lead" transmission line. The tip of the antenna was connected to a pair of RG-58/U coaxial cables coming from a balanced Anzac hybrid. In this configuration, the phase delay from the feed point of one element to the feed point of the next element can be adjusted by varying the length of the transmission line.

Various lengths of transmission line were used. Figure 2-19 shows the radiation patterns with a straight length of transmission line fed between adjacent elements and with a transmission line that is twice the length of the straight distance between adjacent dipole elements.

Figure 2-20 shows the radiation patterns of an antenna with a smaller spacing ($\sigma = 0.02$, $\tau = 0.88$, $\alpha = 56^{\circ}$). The elements of this antenna are the same as the former one while the axial length is squeezed to half of its original spacing ($\sigma = 0.04$). The length of the transmission line corresponds to a straight length at the $\sigma = 0.04$ spacing.

Figure 2-21 shows the magnitude of the VSWR vs frequency measured at the tip of the antenna with straight and lengthened transmission lines between elements. It is observed from both radiation patterns and reflection coefficient measurements that no substantial changes occur when a longer transmission line is used between adjacent dipole elements. This agrees with the results obtained by R. L. Carrel (1961), which indicated that the transmission line is a mechanism to transfer energy from the feed point to the resonant dipoles. Within the active region near the resonant dipoles, apparently the effect of element coupling predominates over the effect of variations in transmission line length. The transmission field vanished in the vicinity of the active region, while radiation field originates in the active region, and propagates in the direction of the smaller dipoles.

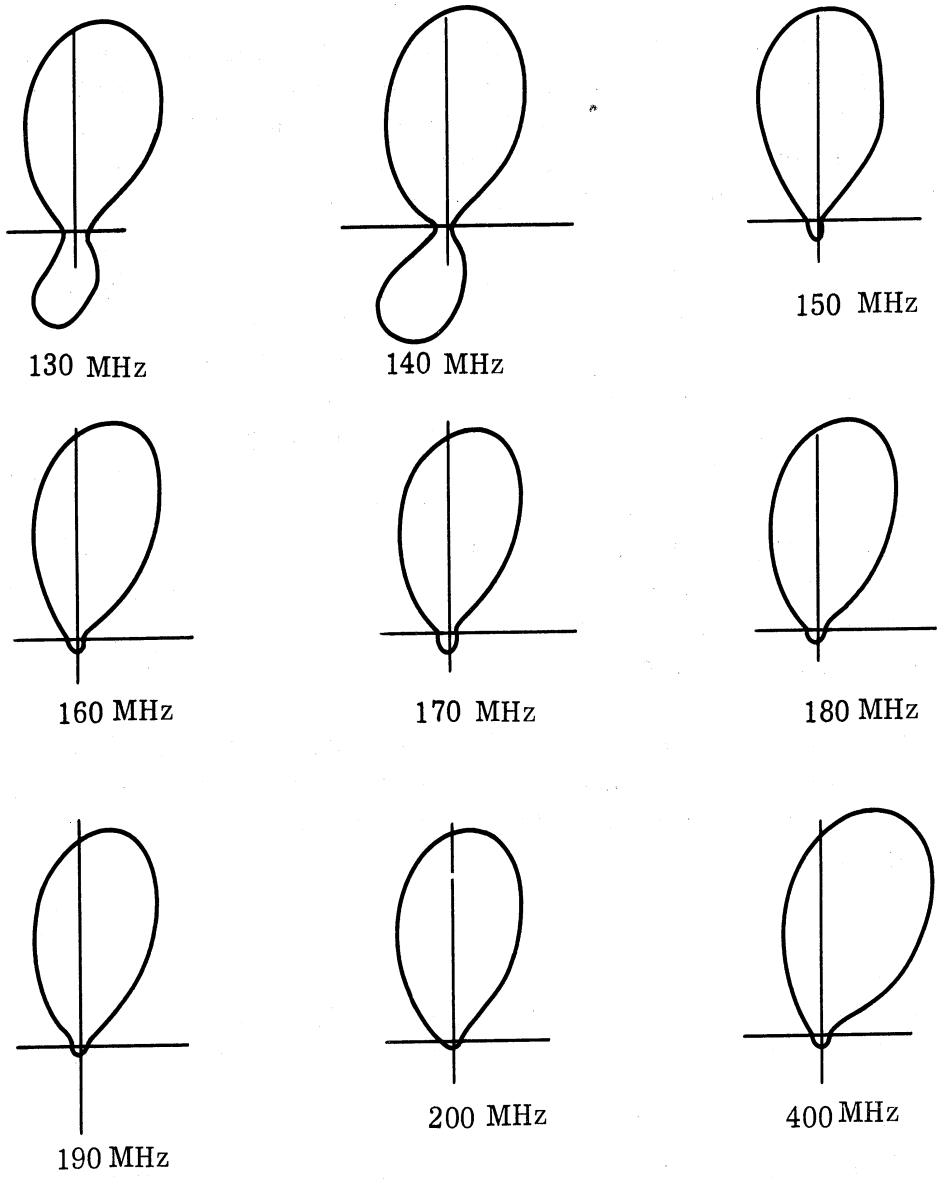

FIG. 2-19a: $\tau = 0.88$, $\sigma = 0.04$, $\alpha = 37^{o}$ TRANSMISSION LINE BETWEEN DIPOLE ELEMENTS IS STRAIGHT.

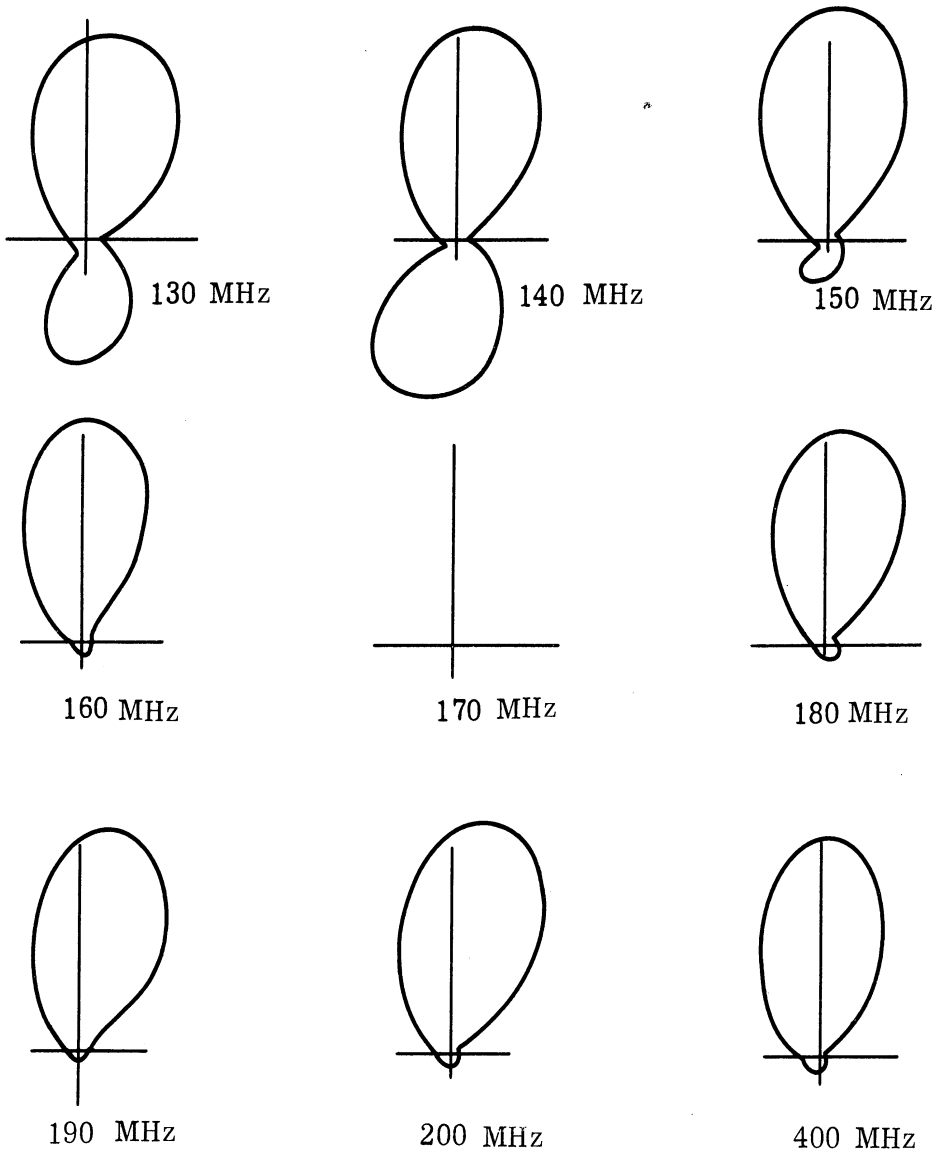

FIG. 2-19b: $\tau = 0.88$, $\sigma = 0.04$, $\alpha = 37^{o}$ TRANSMISSION LINE BETWEEN ELEMENTS IS LOOPED AND TWICE ITS STRAIGHT LENGTHS.

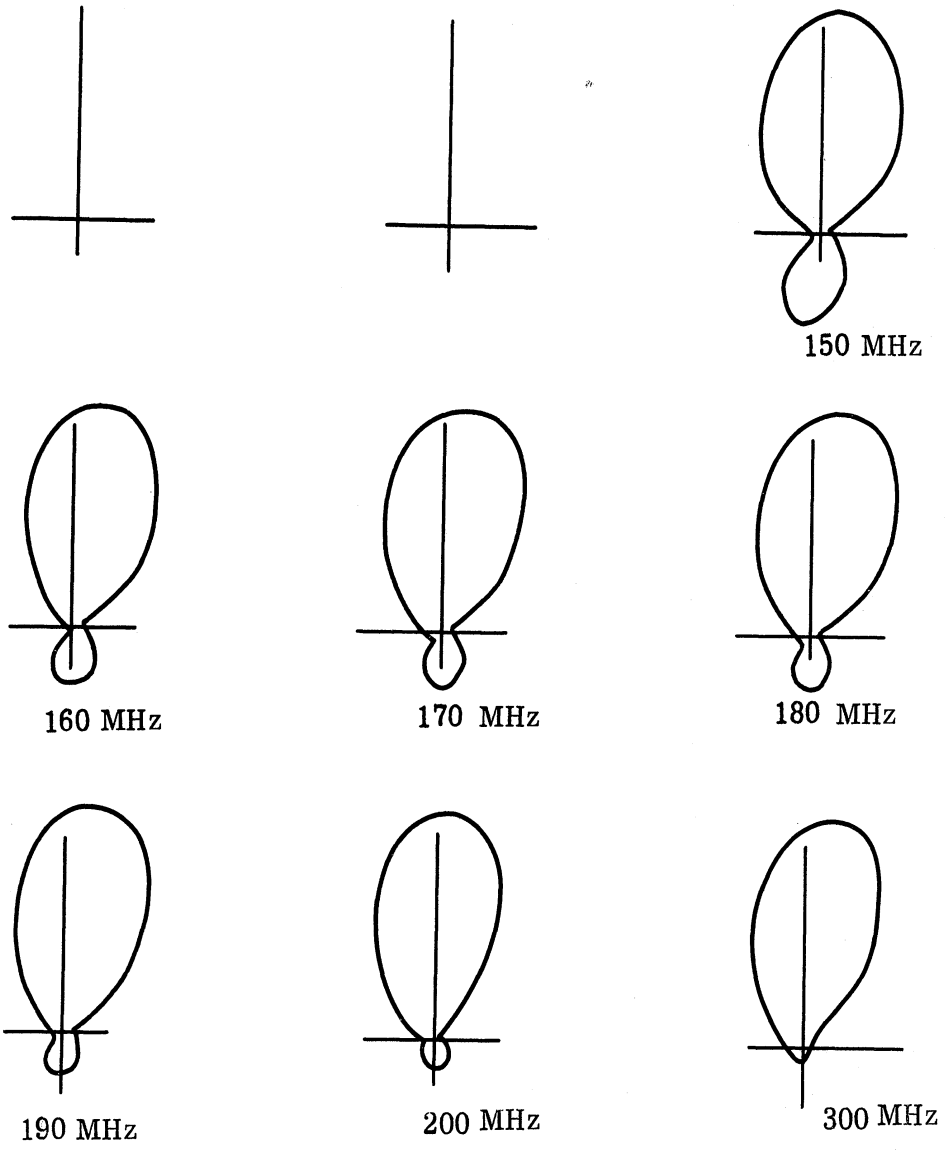

FIG. 2-20: $\tau = 0.88$, $\sigma = 0.02$, $\alpha = 56^{\circ}$ TRANSMISSION LINE IS LOOPED UP AND TWICE ITS STRAIGHT LENGTH.

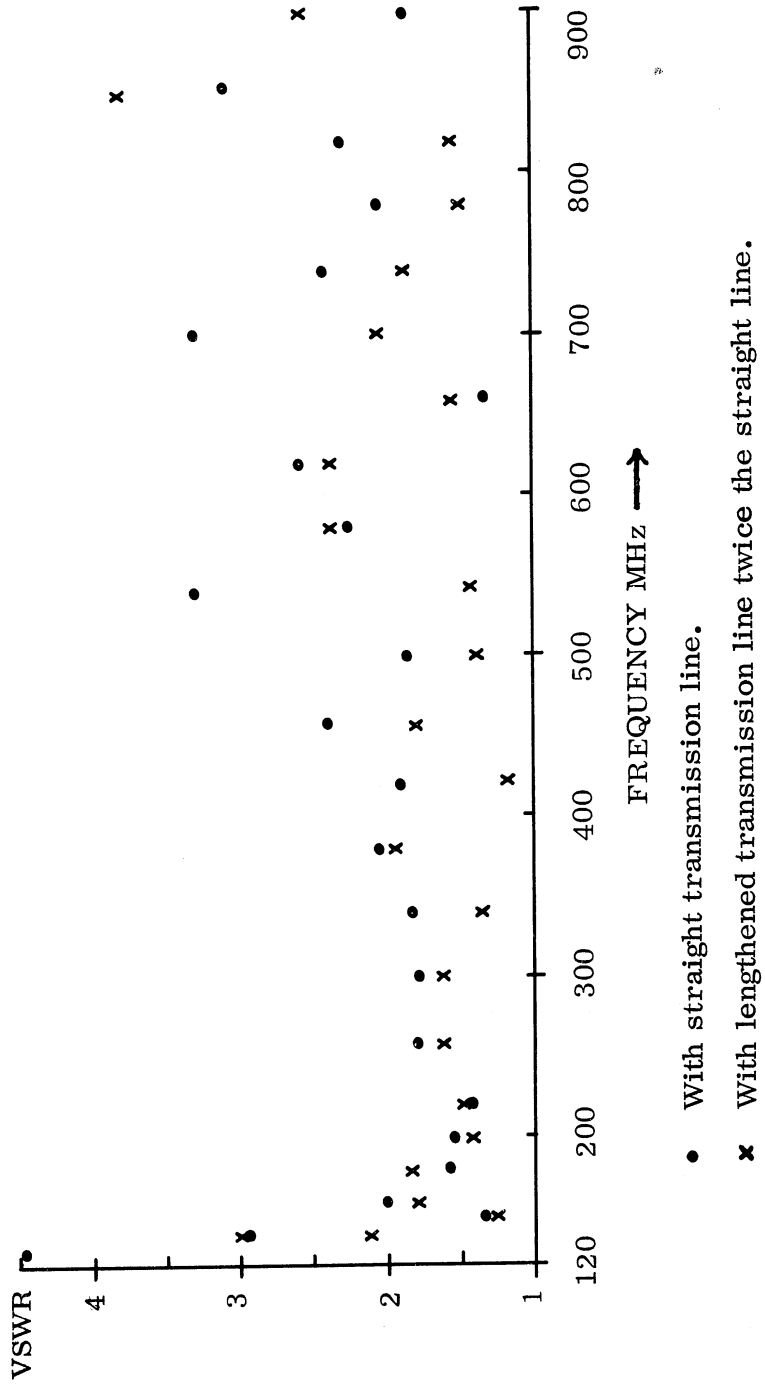

FIG. 2-21: VSWR VS. FREQUENCY FOR CONFIGURATIONS FOR THE FAR FIELD PATTERNS OF WHICH ARE SHOWN IN FIG. 2-19.

2.4.3 Bent Element Arrays

In this study an attempt was made to evaluate the effectiveness of right angle bends or folds on each of the electric dipole elements in the lower frequency range. The antenna with bends shortening the individual elements is designated LPDA-2. The dimensions of the antenna appear in Fig. 2-22. The design utilized the reduced spacing of the elements along the boom as indicated in Section 2.4.1 where σ is equal to 0.04. Other design parameters used were similar to antenna LPDA-1 discussed in that section. The final overall physical size of this antenna is: 9.5 cm across the apex end, 55 cm across the bottom corresponding to the longest element, 75 cm measured from the shortest element to the longest element (along boom).

E-plane linear power patterns were obtained for the frequency range 130 MHz to 1500 MHz. There are indications from design considerations that this antenna would operate well above 1500 MHz, perhaps up to 1700 MHz. However, the antenna was not tested above 1500 MHz due to the lack of suitable signal generator at the time of testing.

An examination of the patterns shown in Fig. 2-23 indicates that suitable radiation patterns have been obtained down to 150 MHz. This indicates that a good radiation pattern for an element that is 55 cm long has been achieved through the use of the folds at each end of this element. If the 55 cm length represented one-half wave length, this would corrsepond to a frequency of about 280 MHz. This indicates that a reduction in the lowest frequency of operation from approximately 280 to 150 MHz, has been achieved.

Impedance measurements have been made and are presented in Fig. 2-24a and 2-24b. The type of feed has been changed from the previous crossed line type, for which patterns were taken, to an infinite balun type. This latter feed consists of 5.4 feet of RG-58/U cable fed through one of two central tubes running to the apex of the antenna. This type of feed has been found to provide lower VSWR values. The data appearing in Fig. 2-24 were obtained by measuring the magnitude and phase of the reflection coefficient at the source end of the feed cable. The figures indicate that the VSWR values are lower than 2.5 to 1 over the frequency range of 270 to 600 MHz. The increase in VSWR above 600 MHz has been traced to imperfections in the element construction. The increased VSWR below 270 MHz is associated with the active regions entering the foreshortened element region of the array.

In order to further investigate the increase in VSWR in that portion of the antenna structure incorporating 90° bends, to achieve element foreshortening,

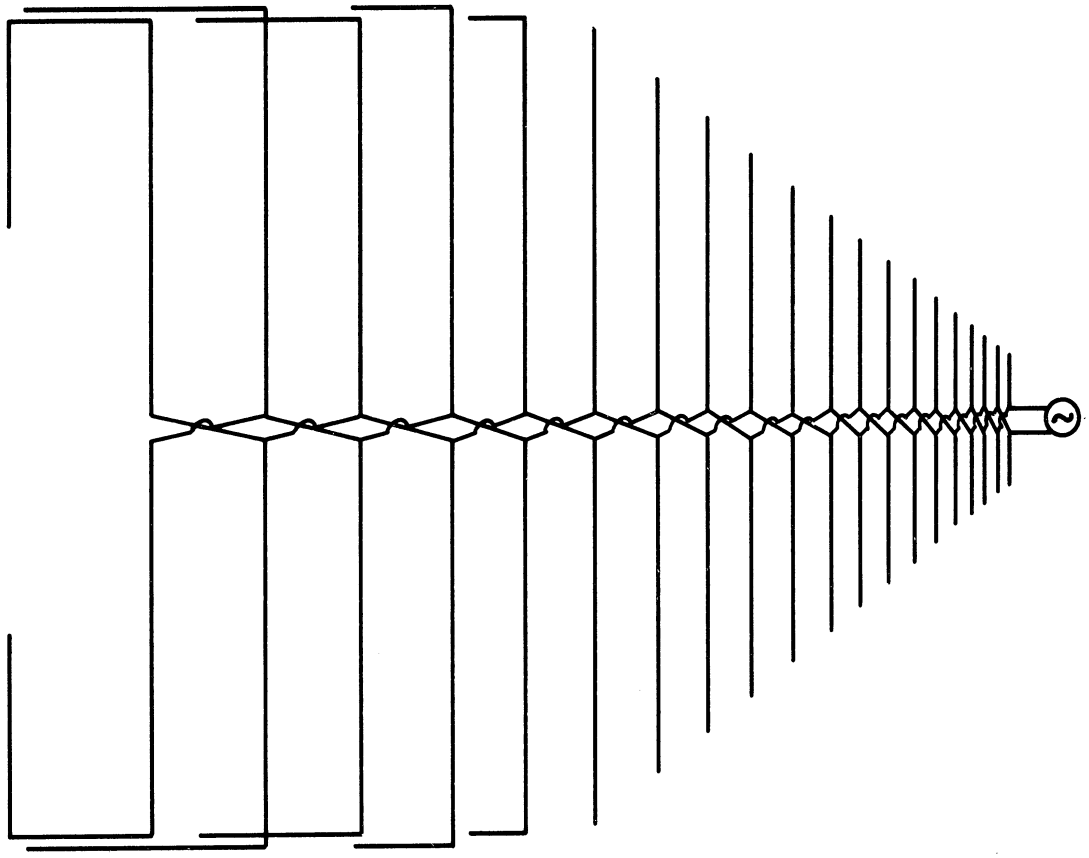

FIG. 2-22: ANTENNA LPDA-2: LONGEST DIPOLE 100 cm ($\lambda/2$ at 150 MHz)
SHORTEST DIPOLE 8.8 cm ($\lambda/2$ at 1700 MHz)
SIZE: 55 cm x 75 cm

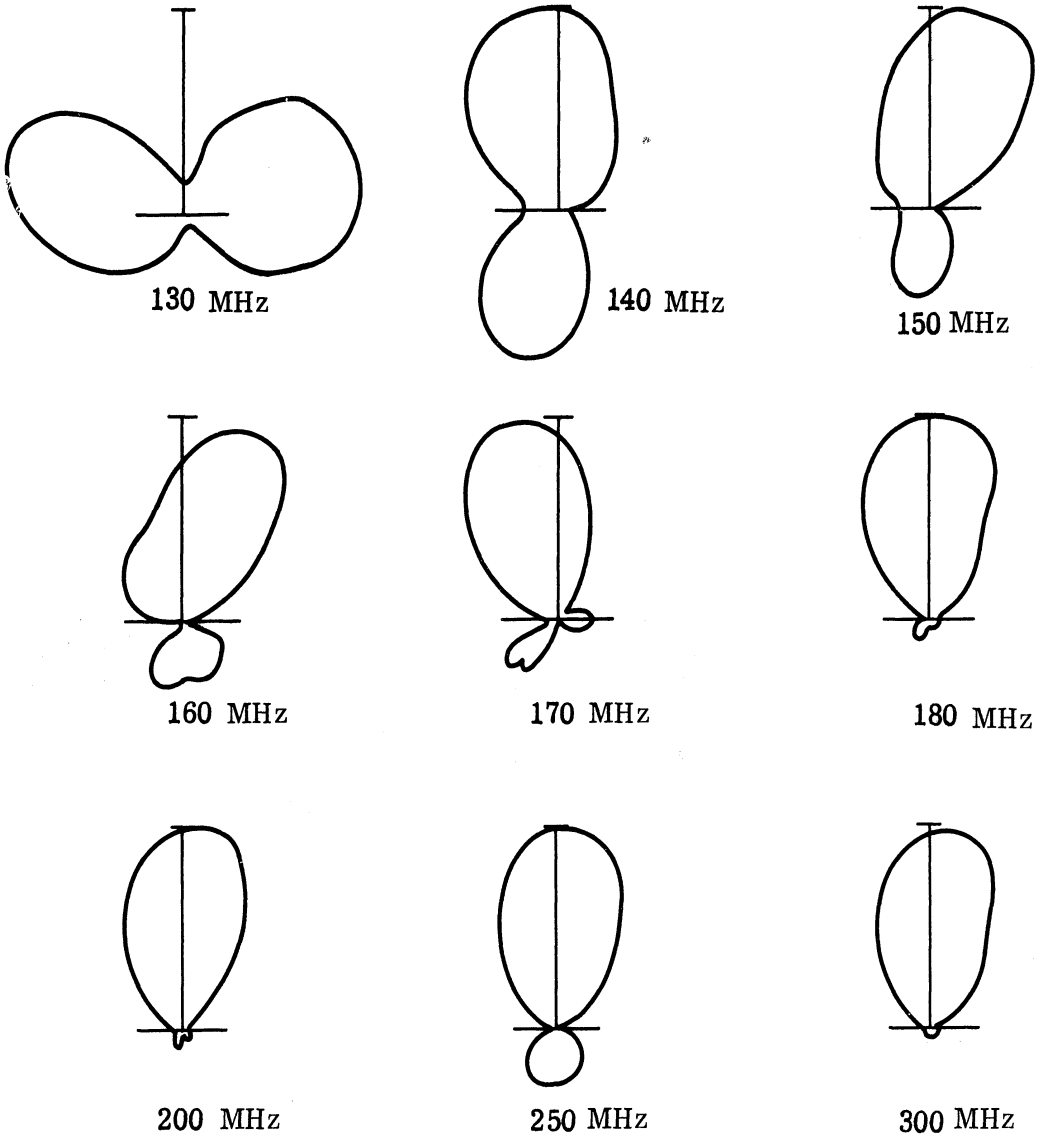

FIG. 2-23: LPDA-2 130 - 300 MHz E-PLANE LINEAR POWER PATTERNS.

Note: Patterns above 300 MHz are nearly identical to those of LPDA-1 shown in Fig. 2-18b.

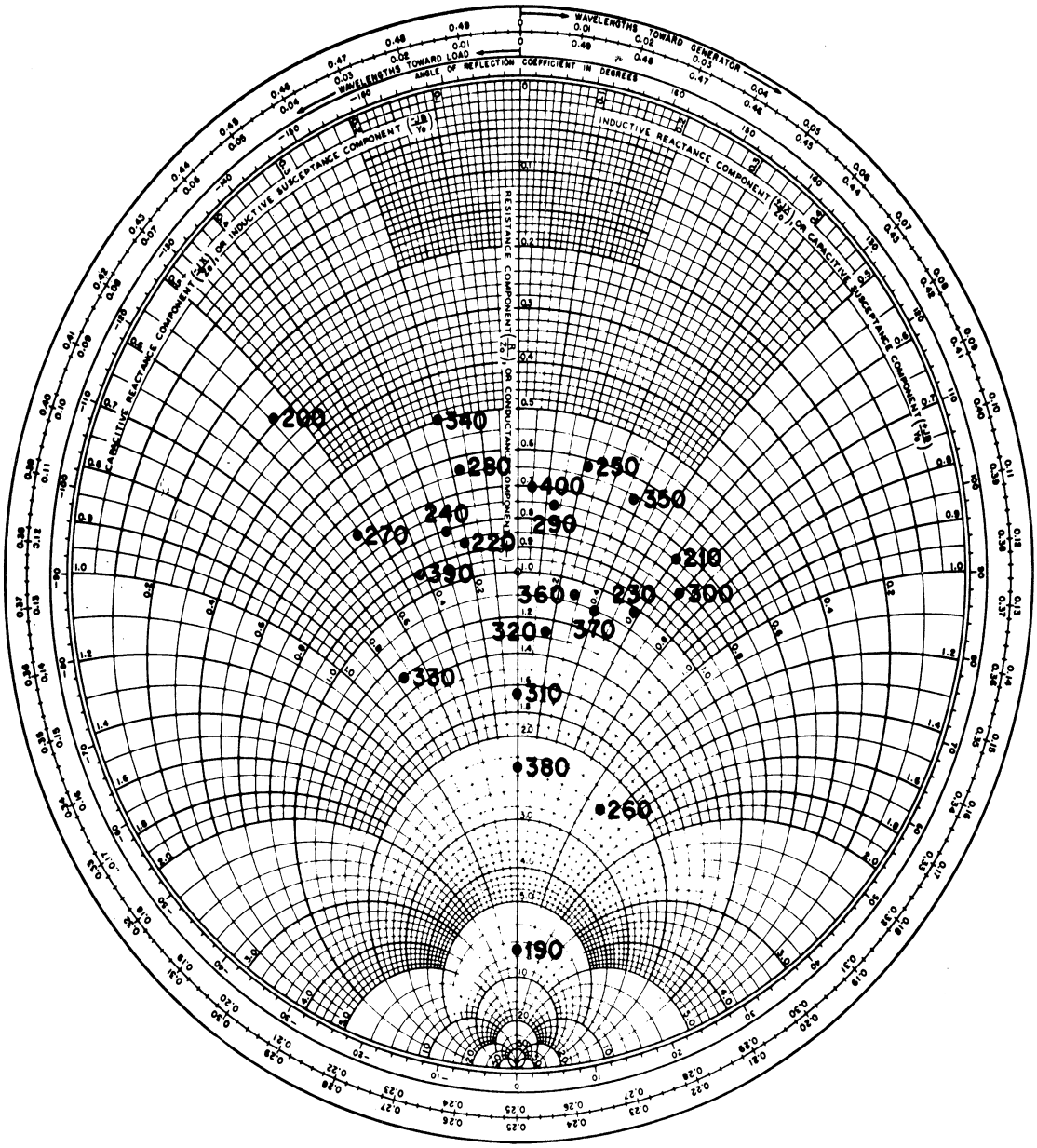

FIG. 2-24a: IMPEDANCE OF ANTENNA LPDA-2 MODIFIED TO INFINITE BALUN FEED (190 - 400 MHz).

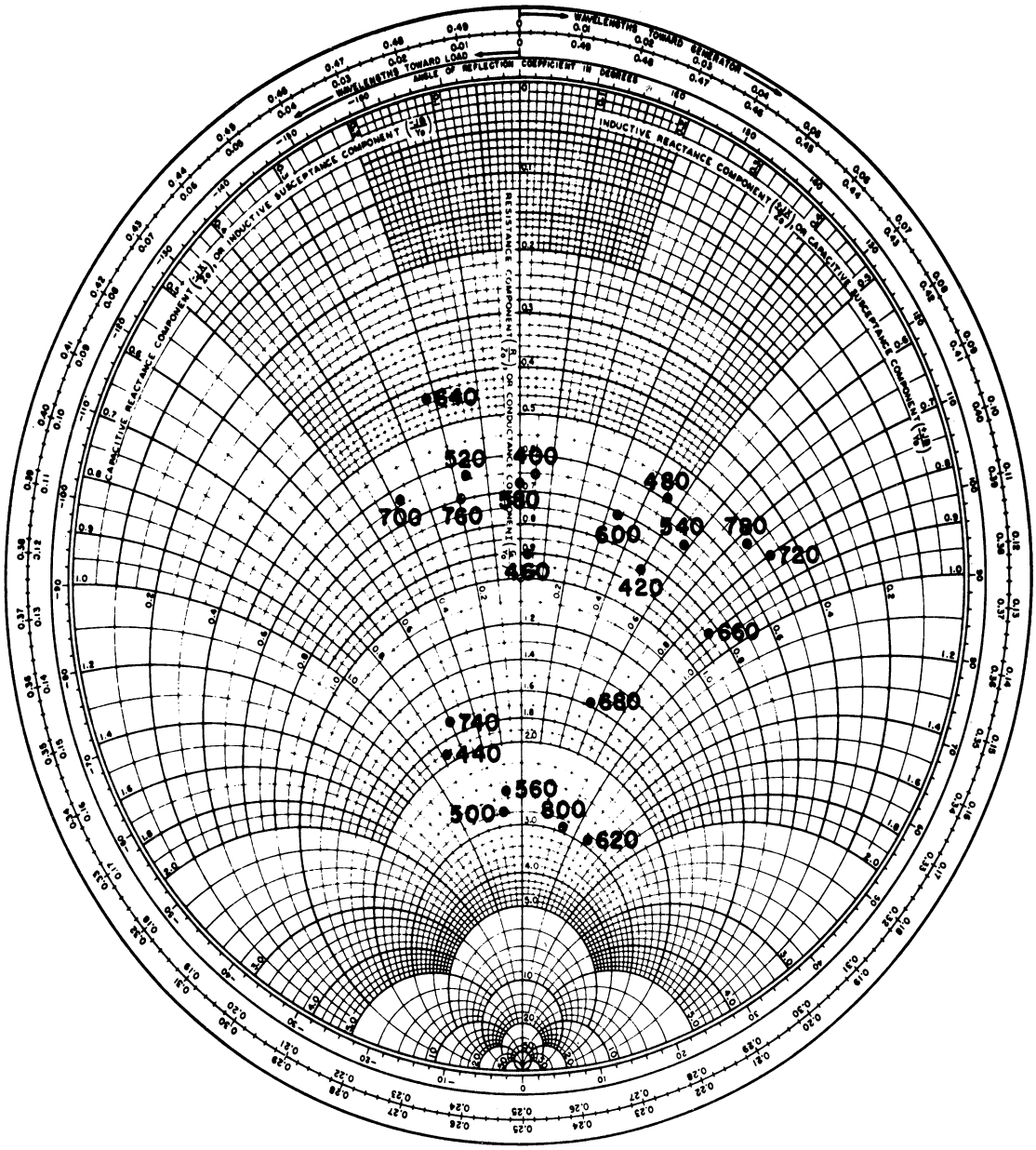

FIG. 2-24b: IMPEDANCE OF ANTENNA LPDA-2 MODIFIED TO INFINITE BALUN FEED (400 - 800 MHz).

nearfield probing techniques were applied to the antenna structure. It was found that the active region current distribution was substantially deformed within the region of bent elements. The apparent reason for this was the increased interference or coupling between the elements with bent ends. Despite the difficulty of increased VSWR and near-field deterioration on this particular model, the technique of bent or folded ends to foreshorten the elements has been successfully used by at least one antenna manufacturer. It is now felt that while this technique may be useful in shortening element lengths to nearly 0.5 of their unforeshortened lengths, the method seems less compatible with boom length foreshortening than other methods which incorporate impedance compensation. This reasoning is motivated by the need for decreased element coupling in order to successfully implement individual element broadbanding, which is deemed necessary for boom length foreshortening.

A modification was made on the design of LPDA-2 whereby the element at the lowest frequency end was bent in the opposite direction. This meant that right angle bends at the two ends of this dipole had the bent portion now pointing forward over several of the adjoining elements instead of pointing away from these elements. This type of modification produced a serious shortcoming in the radiation patterns. An undesirable backlobe developed below 180 MHz.

Still another possibility offering a slight improvement in the reduction of boom length is produced by using a slight bend on the longest dipole at it's center, and another bend back towards the apex near the end on the dipole. Figure 2-25 shows the arrangement used for this antenna, which is designated LPDA-6. The radiation patterns are shown in Fig. 2-26. These patterns are reasonably good and compare favorably with the patterns in Fig. 2-23 obtained for the antenna LPDA-2. This further reduction in boom length is 5 cm.

2.4.4 Study of Mixed Array with Zig-Zag Elements

An antenna was designed using a zig-zag configuration for the entire length of each electric dipole in the low frequency range up to a frequency of approximately 350 MHz. At higher frequencies straight electric dipoles were used. Below is a description of this antenna:

Antenna No. LPDA-7

Description: Zig-zag elements in low frequency sections;
Straight elements in high frequency section.

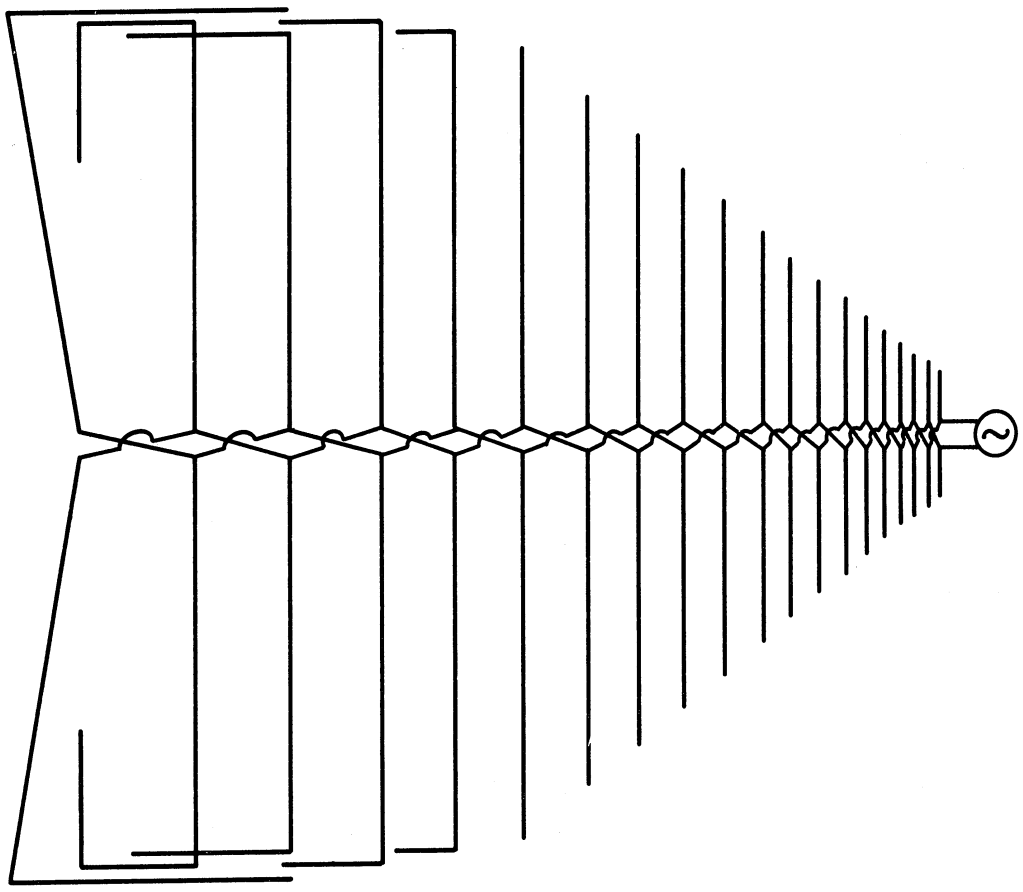

FIG. 2-25: ANTENNA LPDA-6: LONGEST DIPOLE 100 cm ($\lambda/2$ at 150 MHz)
SHORTEST DIPOLE 8.8 cm ($\lambda/2$ at 1700 MHz)
SIZE: 56 cm x 70 cm.

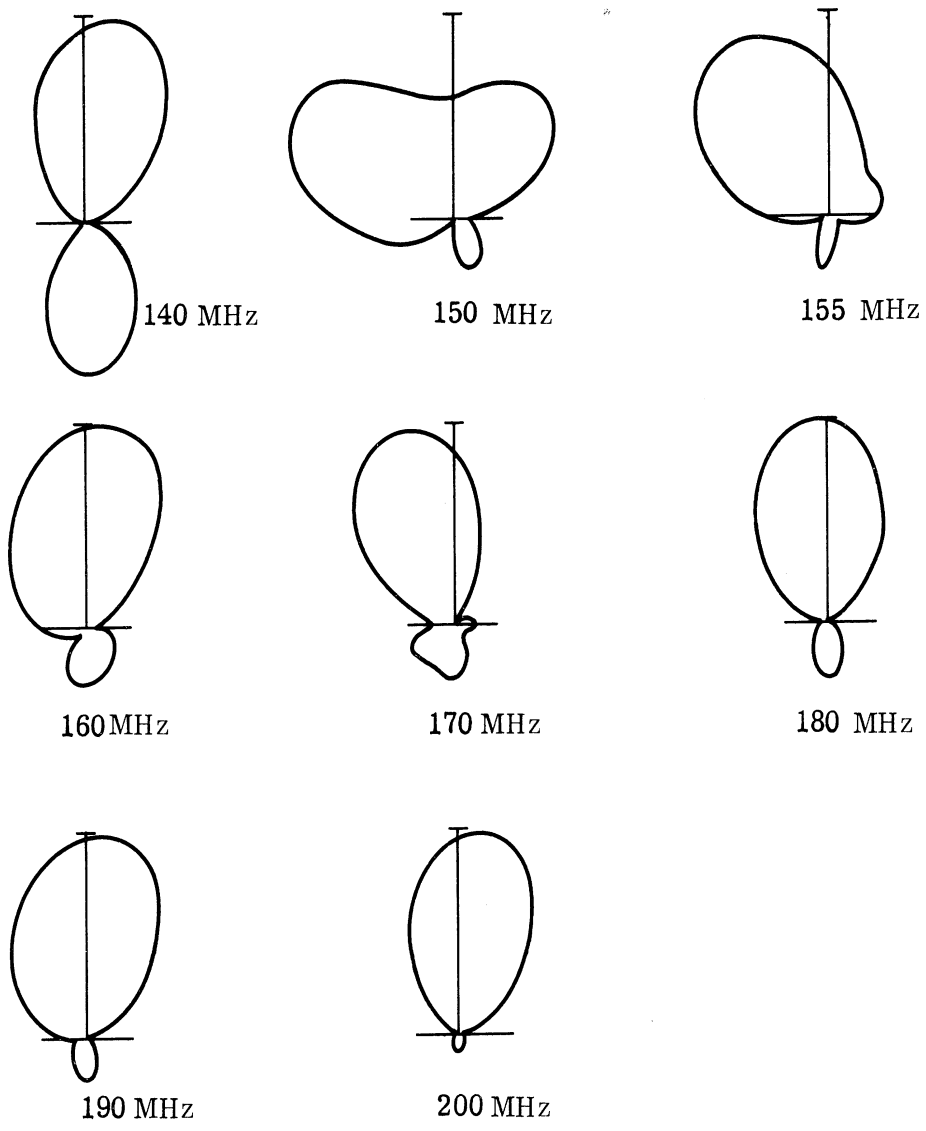

FIG. 2-26: LPDA-6 140 - 200 MHz E-PLANE LINEAR POWER PATTERNS.

$\tau = 0.86$

$\sigma = 0.096$

$\alpha = 20^{o}$ (half of the apex angle)

Size: Width of tip 7.0 cm,

Width across bottom 93 cm,

Length along boom 110 cm.

In Fig. 2-27 will be found the E-plane radiation patterns for this antenna. It is to be observed that there are some irregularities in the patterns at frequencies of 250 MHz, 255 MHz and 350 MHz. The patterns for the individual two sections of the antenna are not included in this report. However, they have been used in studying the behavior of the patterns for the entire frequency range.

Patterns were not taken below 150 MHz, but one would expect to find acceptable operation below 150 MHz due to the information obtained on zig-zag elements reported in Section 2.3.3. Some satisfactory radiation patterns were observed at frequencies below 150 MHz for the low frequency section of the array consisting only of zig-zag elements. When the last two bent dipoles of LPDA-2 were replaced by two bent zig-zag elements, the unwanted backlobe increased as is shown in Fig. 2-28. At the lower frequency limit, the backlobes of the radiation patterns are much larger than the ones with the bent dipoles.

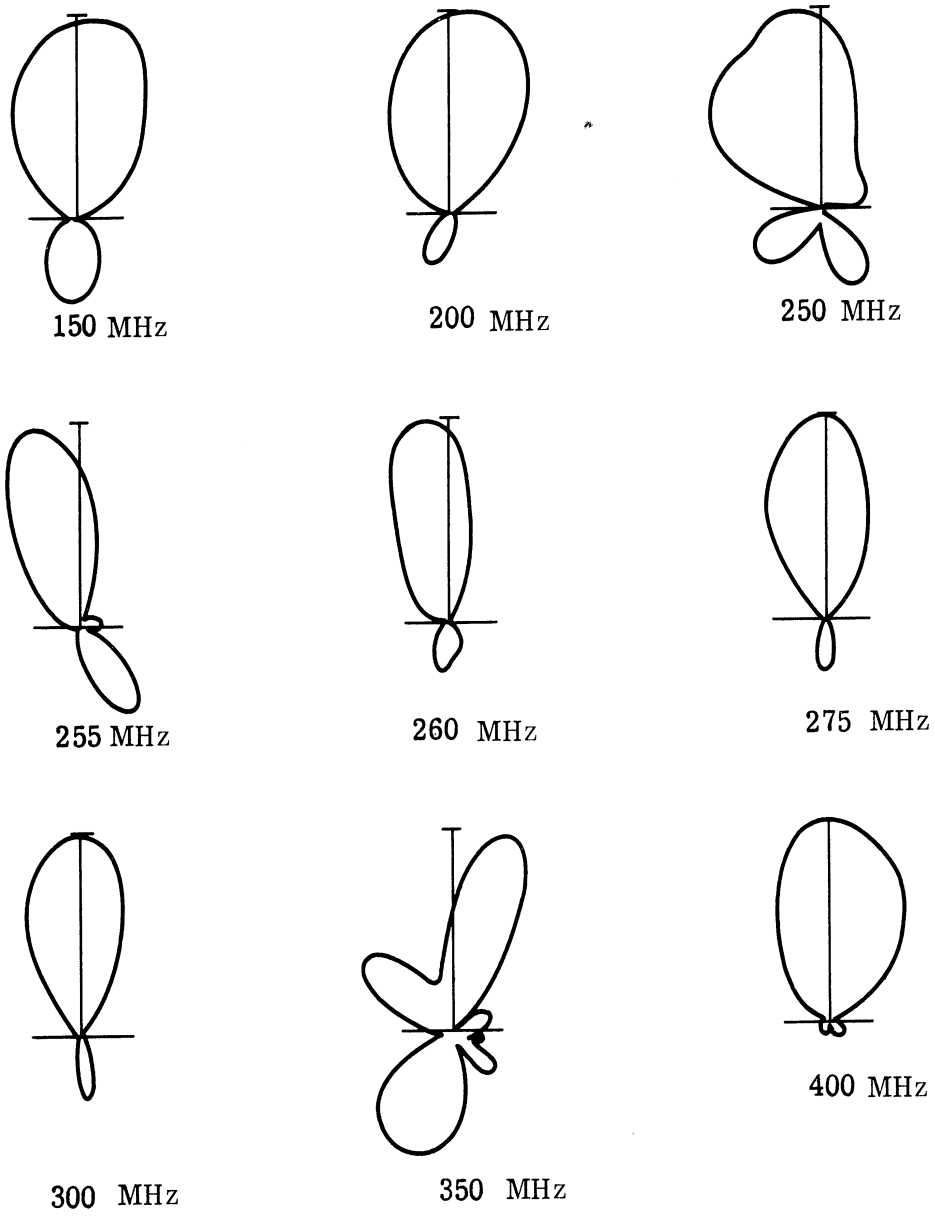

FIG. 2-27: LPDA-7 150 - 400 MHz E-PLANE LINEAR POWER PATTERNS.

Note: Patterns above 400 MHz are well behaved and similar to those of LPDA-1 (Fig. 2-18b).

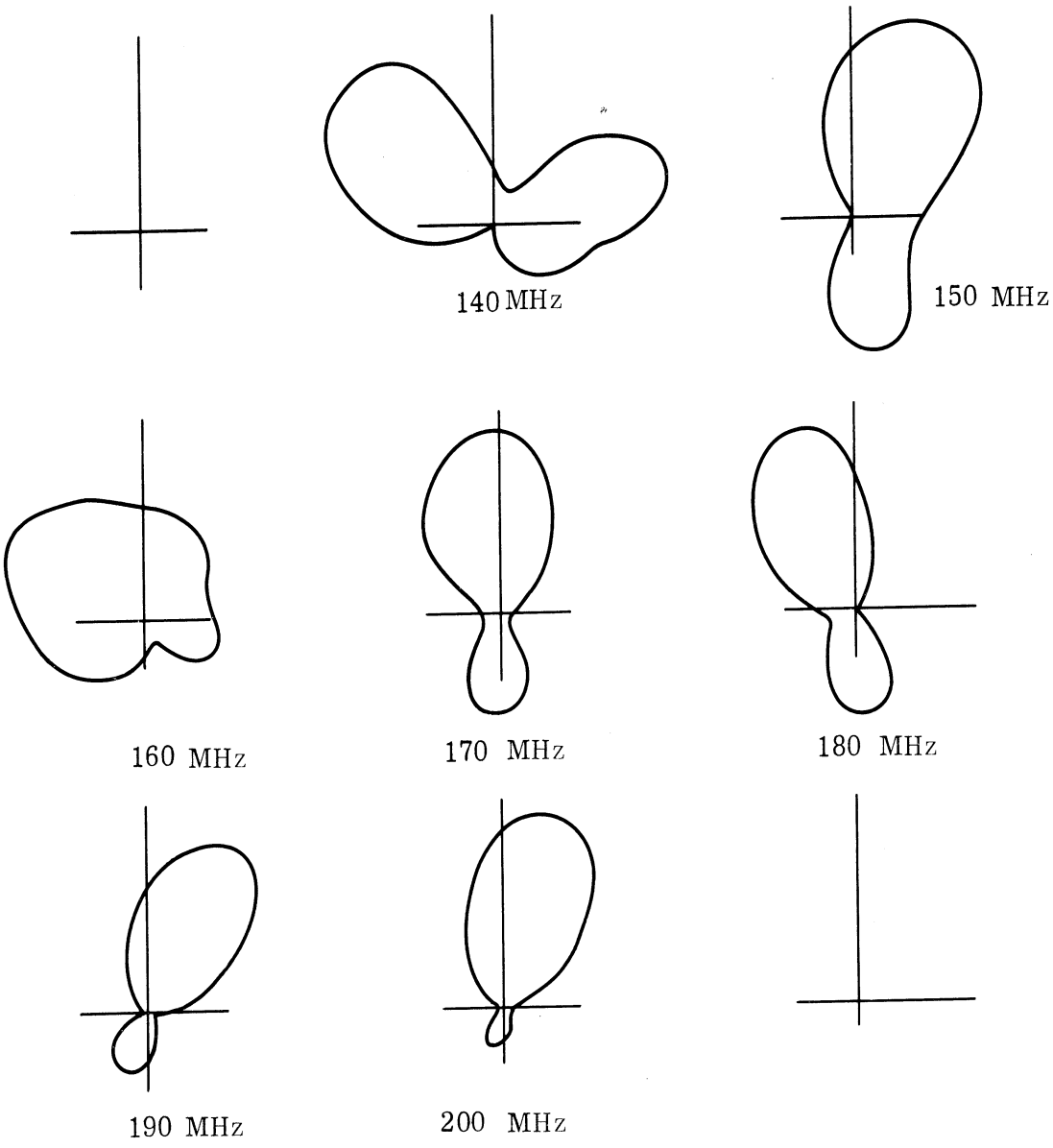

FIG. 2-28: E-PLANE LINEAR POWER PATTERNS OF LPDA-2 WITH THE LAST TWO BENT DIPOLES REPLACED BY TWO BENT ZIG-ZAG DIPOLES.

III

LOADED CONICAL HELIX ANTENNA

The purpose of this task is to develop a conical helix antenna covering a 50 - 1100 MHz frequency range that weighs less than 40 lbs and yet is one fourth the lineal dimensions of an unloaded antenna covering the same range of frequencies. The antenna is to have a hemispherical pattern shape, 0db gain with respect to a circularly polarized isotropic source, a VSWR of less than 2.5 to 1 with respect to a 50 Ω source, and a capability of handling at least 150 watts of continuous power. In addition, the backlobe should be at least 8db down from the main lobe and polarization is to be circular within 1.5 db.

In addition, the study was to include information on the feasibility of extending these techniques to the High Frequency Range (HF). For the exploratory development model for which the partial specifications were listed in the first paragraph, the contract monitor expressed a desire that the antenna would be no longer than 4 feet and be capable of handling at least 50 watts of CW power when fed with an Anzac H-9 hybrid.

The design and testing of the exploratory development model is discussed in Section 3.1, while the remaining sections discuss various techniques for reducing the size of a conical helix that were studied under this contract.

3.1 Design and Testing of the Exploratory Development Model

3.1.1 Design

The design of the exploratory development model was based on the coiled conductor slow wave structure winding discussed in Section 3.2. A 2 to 1 reduction in size was assumed, and then the design curves of Dyson (1965) were used to obtain an antenna with a height of 4 feet. A wrap angle of 85° was used, since this results in a relatively small variation with frequency of the pattern shape. The result was that the cone angle was 74° and the radius of the base was 4 feet. The side of the inscribed square was calculated to be 4.25 feet, since a square pyramidal antenna was built. A square pyramid is more readily adaptable to collapsible construction than is a cone. The conversion from the conical to the pyramidal geometry was made using the formulas of Tang and McClelland (1962).

The helical slow wave structure winding used on part of the antenna was based on antenna 228, which is discussed in Section 3.2. The pitch angle of the winding on the prototype is the same as that of antenna 228, namely 8°. The winding on the

model was scaled from antenna 228 by the ratio of the wavelength of the lowest operating frequency of both antennas. Thus the diameter of the winding of the model is 3/4" times the ratio of 400 to 50, or 6". The reason frequency scaling was used is that the diameter of a helix slow wave structure measured in wavelengths is the parameter which determines the slowing factor.

The winding diameter at the base was then scaled as it was wound around the cone by the scaling factor of the cone, τ, through the first 3-3/4 turns from the base. This location corresponds to the top of the active region for 50 MHz, assuming the 2 to 1 reduction is achieved. From the 3-3/4 through the 5-3/4 turn, the slowing factor was scaled linearly to unity from that on the lower turns of the antenna.

The scaling of the slowing factor was accomplished by maintaining the diameter of the winding calculated by the scaling factor of the cone. However, the pitch angle of each quarter turn was scaled so that the sine of the pitch angle, and hence the slowing factor, would vary linearly to one with the last turn of the transition region. The end of the transition region corresponds to the top of the active region at 200 MHz. Thus, the transition region will have some effect on all patterns taken from 60 to 600 MHz, since at least part of the active region will be in the transition region for this range of frequencies.

The helices used for the windings were wound on NEMA grade XXX paper phenolic tubing (MIL-P-3115-PBE). The stock size tubing closest to the desired size was used in construction. The winding data are given in Table III-1. The term winding number used in the table refers to quarter turns, which are numbered consecutively from the base, starting with turn number one. Above winding number 22, a regular winding of number 20 enameled wire is used.

The frame of the antenna is constructed out of NEMA grade G-10 epoxy fiberglass tubing (MIL-P-18177-GEE). Tubing of 1 in. O.D. by 1/16 inch thick was used exclusively. The tubing is joined at the tip and the corners with 1/4 inch thick G-10 sheet stock. All joints were bonded together with epoxy.

The antenna is fed at the tip by a pair of RG-8/U coaxial cables. The cables are connected at the base to an Anzac H-9 hybrid. The input impedance of the hybrid is 50 Ω.

The principles used in designing the exploratory development model were: 1) The design of the winding was based on antenna 228 which is discussed in Section 3.2; 2) The first turn of the exploratory development model was obtained by scaling the diameter of the winding of antenna 228 by the ratio of the wavelength of the lowest

TABLE III-1

Winding Data or the Exploratory Development Model

Winding No.	Diameter (inches)	Pitch (turns/in.)	Closest Tubing O. D. Available (in.)
1	6.00	0.277	6-1/8
2	5.524	0.41	6-1/8
3	5.086	0.445	5-1/8
4	4.683	0.484	4-5/8
5	4.311	0.524	4-5/8
6	3.969	0.57	4-1/8
7	3.655	0.62	3-5/8
8	3.365	0.67	3-5/8
9	3.099	0.75	3-1/8
10	2.853	0.794	2-5/8
11	2.628	0.86	2-5/8
12	2.419	0.935	2-5/8
13	2.226	1.015	2-1/8
14	2.050	1.1	2-1/8
15	1.888	0.7	1-5/8
16	1.738	0.523	1-5/8
17	1.600	0.42	1-5/8
18	1.473	0.352	1-1/2
19	1.356	0.298	1-1/2
20	1.249	0.25	1-1/8
21	1.150	0.198	1-1/8
22	1.059	0.140	1-1/8

frequency of operation of antenna 228, to the wavelength of the desired lowest frequency of operation of the exploratory development model; 3) The bottom 3-3/4 turns of the model depend upon the first turn of the model by the scaling factor of the cone, which results in the ratio of the diameter of the winding at any two points being the same as the ratio of the distances of those points from the apex of the cone; 4) Finally, for the transition region, turns 3-3/4 through 5-3/5, were obtained by using the diameter obtained in step three while varying the sine of the pitch angle so that the slowing factor of the slow wave structure would vary linearly from zero to one.

3.1.2 Testing of the Exploratory Development Model

The far field radiation patterns of the exploratory development model did not meet all of the pattern specifications for the antenna. However, even though the pattern specifications were not met, the antenna appears to be radiating over the 50 to 1100 MHz frequency band. Figure 3-1 shows how the antenna was mounted during testing, and Fig. 3-2 shows the far field radiation patterns for the antenna.

The backlobe of the patterns at the measured frequencies is higher than the 8db. level specified, except at 170, 200, 700, 800, 1000, and 1100 MHz. However, above 700 MHz, the main lobe starts to split up for at least one cut.

The polarization ratio was measured at five frequencies and is summarized in Table III-2.

TABLE III-2

Polarization Ratio of Exploratory Development Model

Frequency (MHz)	Polarization Ratio (db)
120	12
250	1
500	4
900	3
1100	1.5

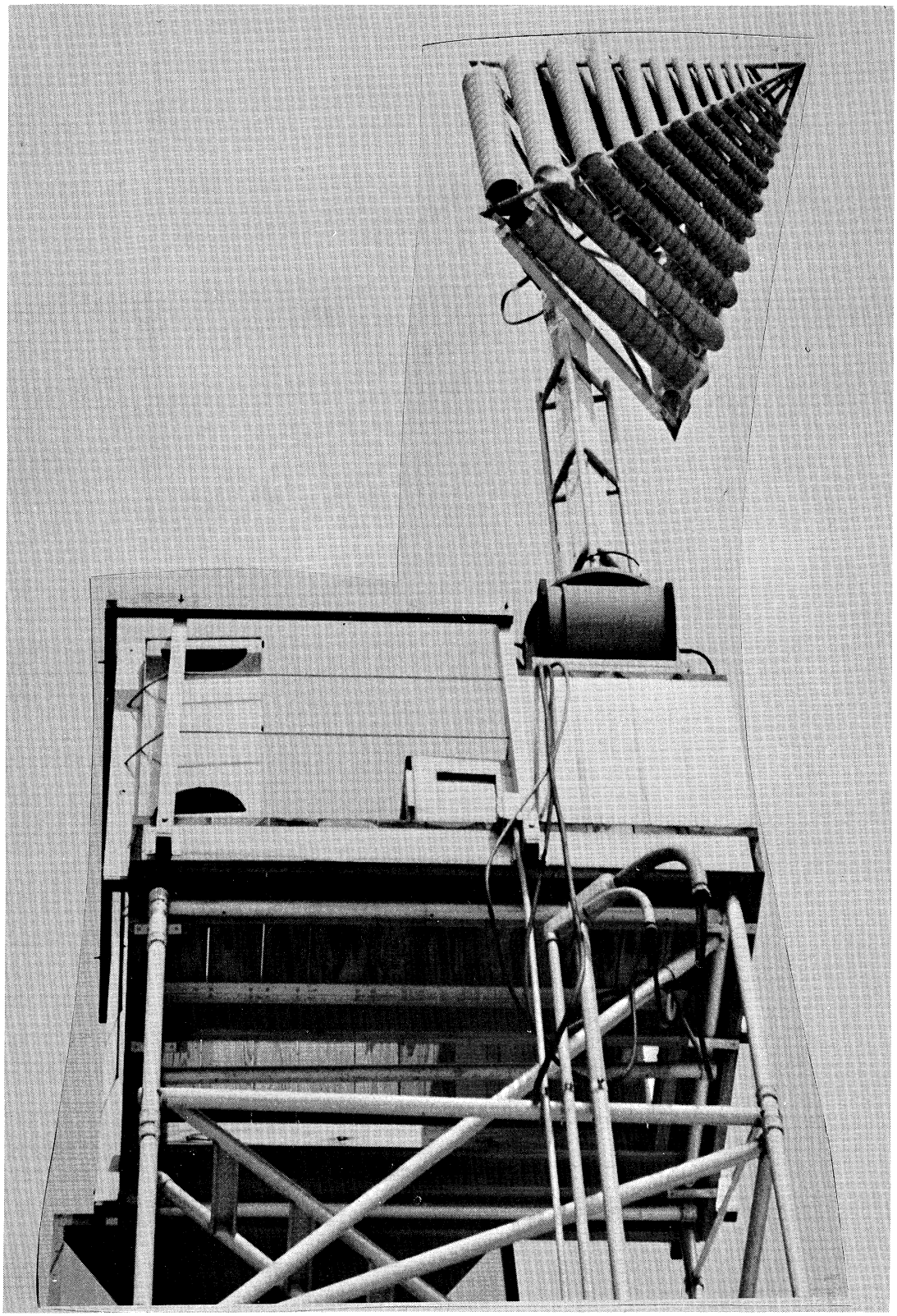

FIG. 3-1: EXPLORATORY DEVELOPMENT MODEL FOR TASK 2, A BIFILAR PYRAMIDAL HELIX WITH A HELICAL SLOW WAVE STRUCTURE WINDING.

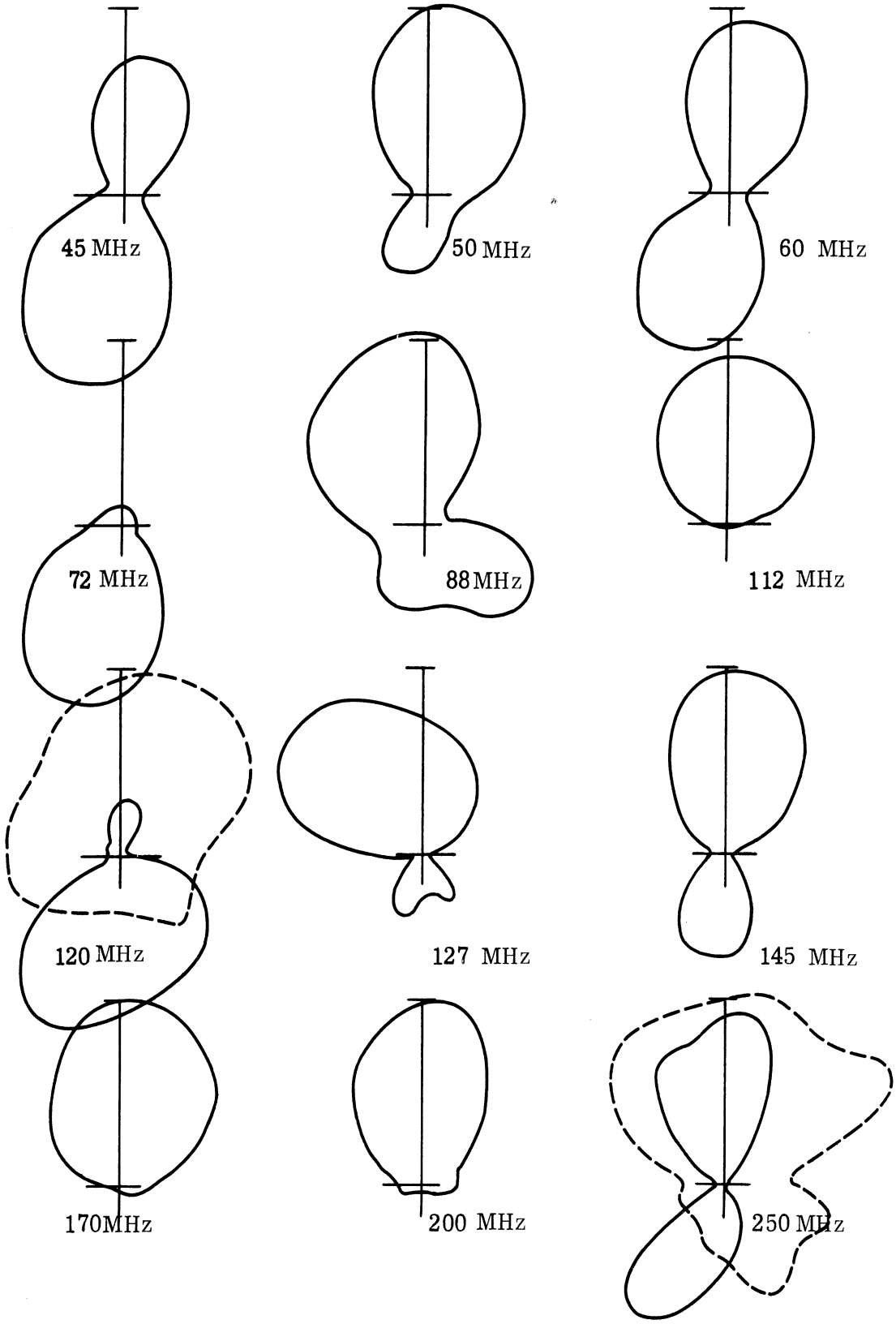

FIG. 3-2a: LINEAR POWER RADIATION PATTERNS OF THE EXPLORATORY DEVELOPMENT MODEL, TASK 2. (Horizontal polarization is shown in solid lines, vertical polarization is shown in dashed lines).

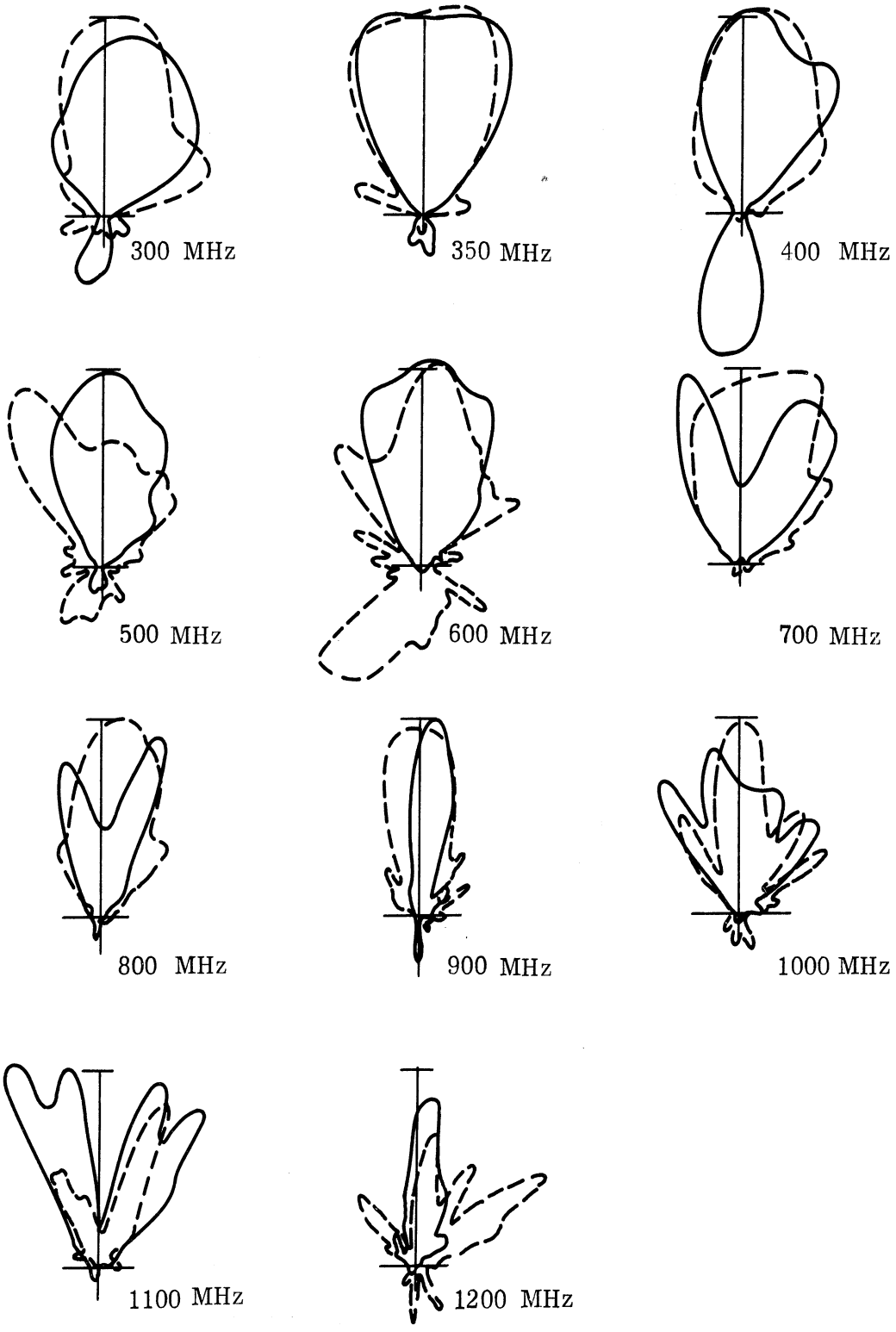

FIG. 3-2b: LINEAR POWER RADIATION PATTERNS OF THE EXPLORATORY DEVELOPMENT MODEL, TASK 2. (Horizontal polarization is shown in solid lines, vertical polarization in dashed lines).

Thus, over any given part of the frequency range of the antenna, at least one of the specifications on the pattern is not met. The gain and the low value of VSWR indicate that the antenna is radiating over most of the band. A plot of the VSWR is shwon in Fig. 3-3, and the gain in Table III-3.

TABLE III-3

Gain of the Exploratory Development Model

Frequency (MHz)	*Gain over a linear isotropic source (db)
120	0.36
400	4.33

The gain was measured by the substitution method using a halfwave dipole as a standard gain source. The dipole was assumed lossless and corrections were made for the mismatch of the antennas to the transmission line.

The phase angle of the reflection coefficient was not measured because at several frequencies there was interference of sufficient magnitude to unbalance the phase bridge. However, the interference was not strong enough to interfere with amplitude measurements. Table III-4 lists the measured values of VSWR.

TABLE III-4

The VSWR of the Exploratory Development Model

Frequency (MHz)	VSWR	Frequency (MHz)	VSWR
50	5.7	300	1.5
60	1.4	350	1.8
74	10.8	400	1.9
88	2.2	500	1.9
120	1.7	600	1.8
125	1.5	700	1.9
150	2.3	800	2.0
175	1.5	900	1.6
200	1.3	1000	2.8
250	1.1	1100	2.5

* Only desired forward lobe considered.

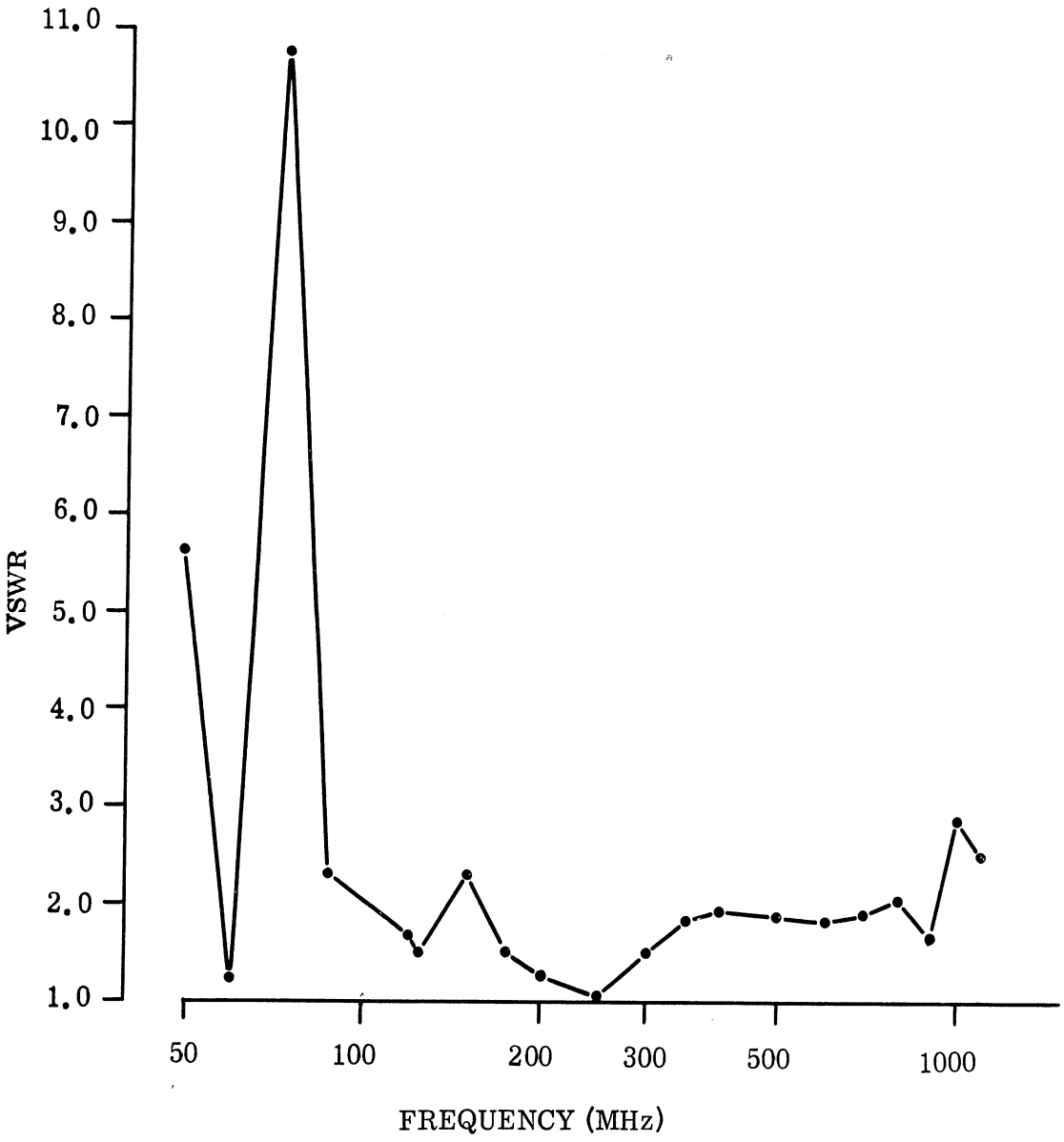

FIG. 3-3: VSWR OF THE EXPLORATORY DEVELOPMENT MODEL MEASURED AT THE END OF 8 FT OF RG-8 COAXIAL CABLE.

Based on the results obtained with helix antennas with helical slow wave structure windings (see Section 3.2) the poor performance of this antenna was not entirely unpredictable. As was pointed out earlier, if the slow wave structure winding is filled with ferrite, then radiation patterns meeting the specifications would almost certainly have been observed down to 25 MHz but with an antenna far heavier than specified.

The weight of the antenna is 46 lbs. Of this weight, about 15 lbs is due to the frame of the antenna and the remainder, about 30 lbs, is due to the windings.

3.2 Slow Wave Structure Windings

A study was performed on a helical antenna wound with a helix slow wave structure (coiled wire). Figure 3-4 shows a picture of the test antenna. The antenna is bifilar wound and fed at the tip with a hybrid. The antenna is wound on a 3" I.D. 1/16" thick piece of NEMA grade XXX (Mil-P-3115-PBE) paper phenolic laminate tubing 29" long. The pitch is 4" and there are seven turns per winding. Each winding is single coiled conductor on a 3/4" O.D., 3/32" thick piece of Tygon vinyl tubing. The coiled conductor consists of No. 20 enameled wire and has a pitch of 1/3".

This design was a compromise. Most helix antenna theory is based on windings that are thin in the radial direction. However to get a helix to operate as a slow wave structure, the pitch angle must be small and the circumference must be a fairly large fraction of a wavelength. Thus a trade off must be made between a diameter large enough to operate as a slow wave structure, yet small enough to approximate a wire winding.

If the antenna were wound with wire (not coiled) on a tube equal to the mean diameter of Antenna 228, it would have a center frequency of about 800 MHz. Figure 3-5 shows the far field patterns taken on Antenna 228. Notice that there is alsmot a 2:1 reduction in frequency of operation, but not a 4:1 reduction as would be predicted by the phase velocity of the slow wave structure (Okubo, 1965).

At 400 and 500 MHz, the patterns have a well defined main lobe, although there are sizable back and sidelobes. If the slow wave windings were wound on a conical helix instead of a helix, the backlobes would be much smaller due to the reflector effect of the windings in back of the active region. The pattern at 300 MHz is completely unexplainable. The large backlobe appears only over about a 50 MHz bandwidth around 300 MHz. At 200 MHz the antenna appears to be moving into the region where broadside radiation occurs.

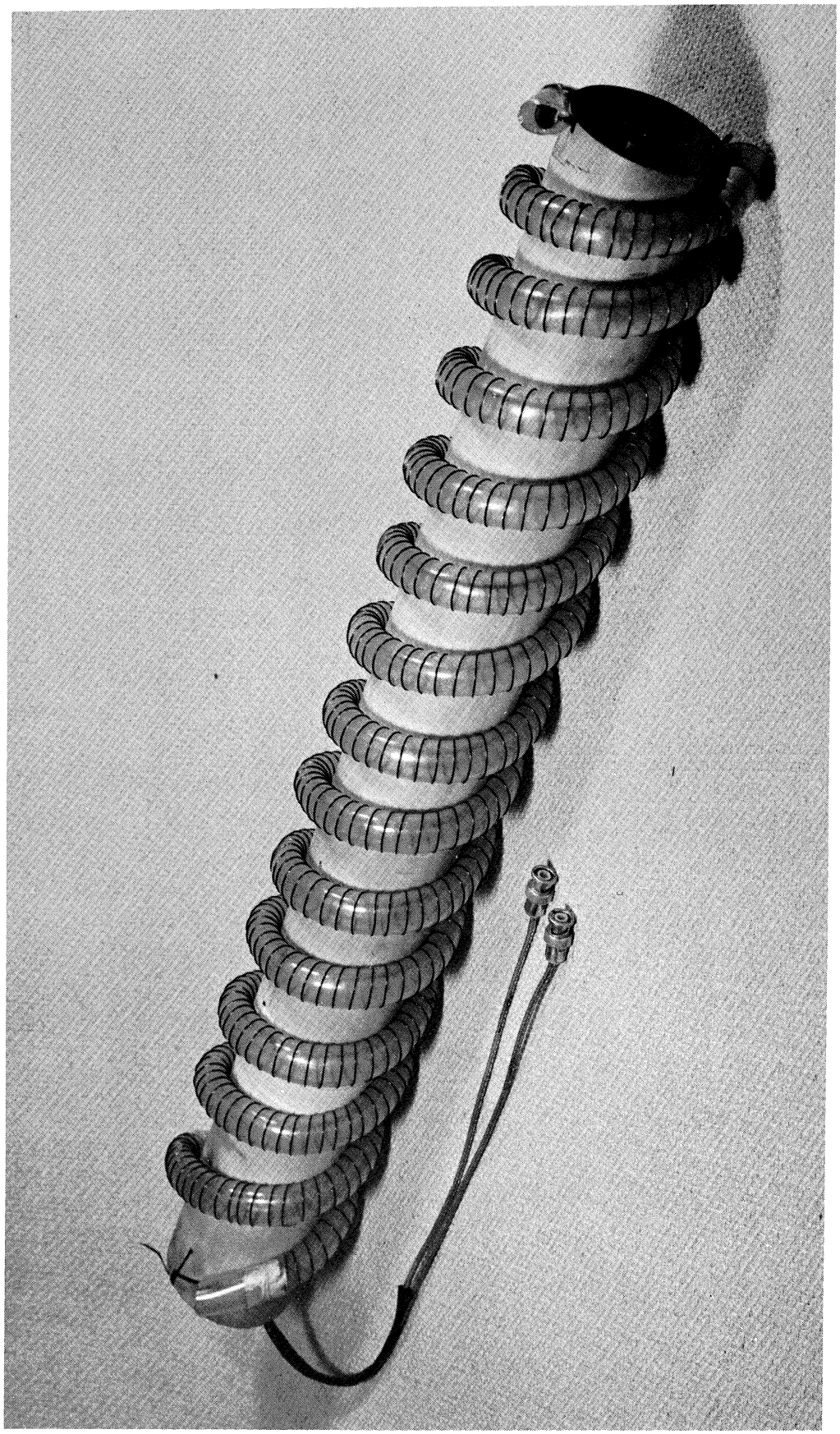

FIG. 3-4: ANTENNA 228, BIFILAR HELIX WITH A HELICAL WINDING.

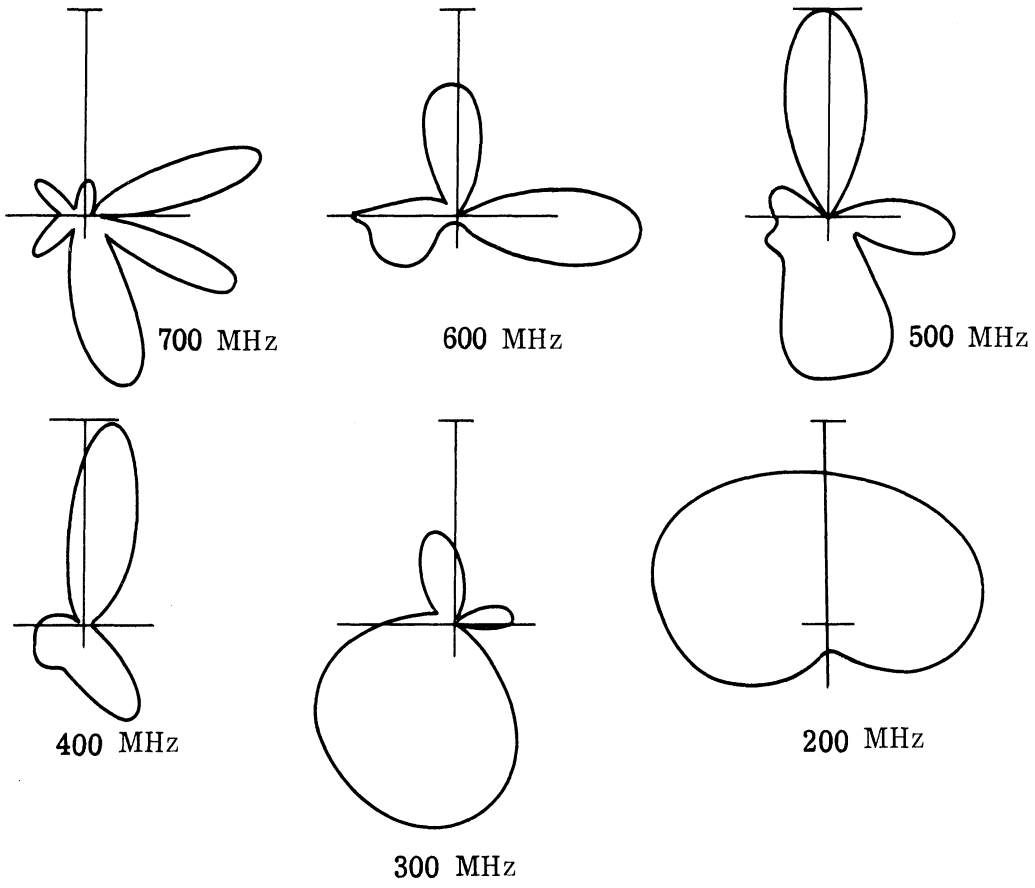

FIG. 3-5: ANTENNA 228, BIFILAR HELIX WITH A HELIX WINDING.

In an effort to better understand how the antenna operates, near field probing of the antenna was done at 0.1λ between antenna and probe (Fig. 3-6). The patterns are very unusual and not at all like those of a regular helix antenna, which usually show a strong amplitude at the tip and very rapid decay towards the base. Indeed, near field probing patterns at 800 MHz are very similar to the near field patterns of regular helix antennas, except for the humps in the middle of the patterns.

The input impedance of the antenna, shown in Fig. 3-7, seems to indicate a size reduction to around 400 MHz.

As a further aid in understanding the operation of Antenna 228, a plot was made of phase velocity along the slow wave structure normalized to the speed of light and versus frequency (Fig. 3-8). The data were obtained from Sensiper (1951, p. 66). Observe, that Fig. 3-8 is for a pitch angle of 10^{o}, whereas the pitch angle of the slow wave structure of Antenna 228 is closer to 8^{o}. However, the difference is not very critical. Curves for both the sheath model of a helix and the tape model with a tape width-to-pitch ratio (x) of 0.1 were replotted.

Note that even though the phase velocity is increasing somewhat as the frequency is decreasing, this does not explain the large backlobe at 300 MHz. It does not appear to be from the normal forward fire mode which occurs higher in frequency than the backfire mode. Possibly, the extraneous effects are from the large winding, or additional mutual coupling.

Later on in the contract period, another source of phase velocity curves was discovered that is much more detailed in the range of interest than were those of Okubo and Sensiper. Li and Beam (1957) use the small argument approximations for the Bessel functions used in the mathematical solution of the sheath helix problem and plotted up the resulting solutions. Their paper is an excellent source of information for designing helix slow wave structures that have a diameter much smaller than a wavelength. This special case covers the design of coiled conductors for winding helix antennas. Li and Beam's design data confirm that the slow wave structure winding was designed for a four-to-one reduction in phase velocity.

As a further check on the best position of the coiled slow wave structure winding, the winding of antenna 228 was reversed and far field patterns were taken. This reversing of the winding tended to create a greater angle between the windings of the slow wave structure winding and the axis of the antenna. A picture of the antenna with the reversed winding is given in Fig. 3-9. The far field patterns are shown in Fig. 3-10. As can be seen from Fig. 3-10 there appears to be little effect on the far

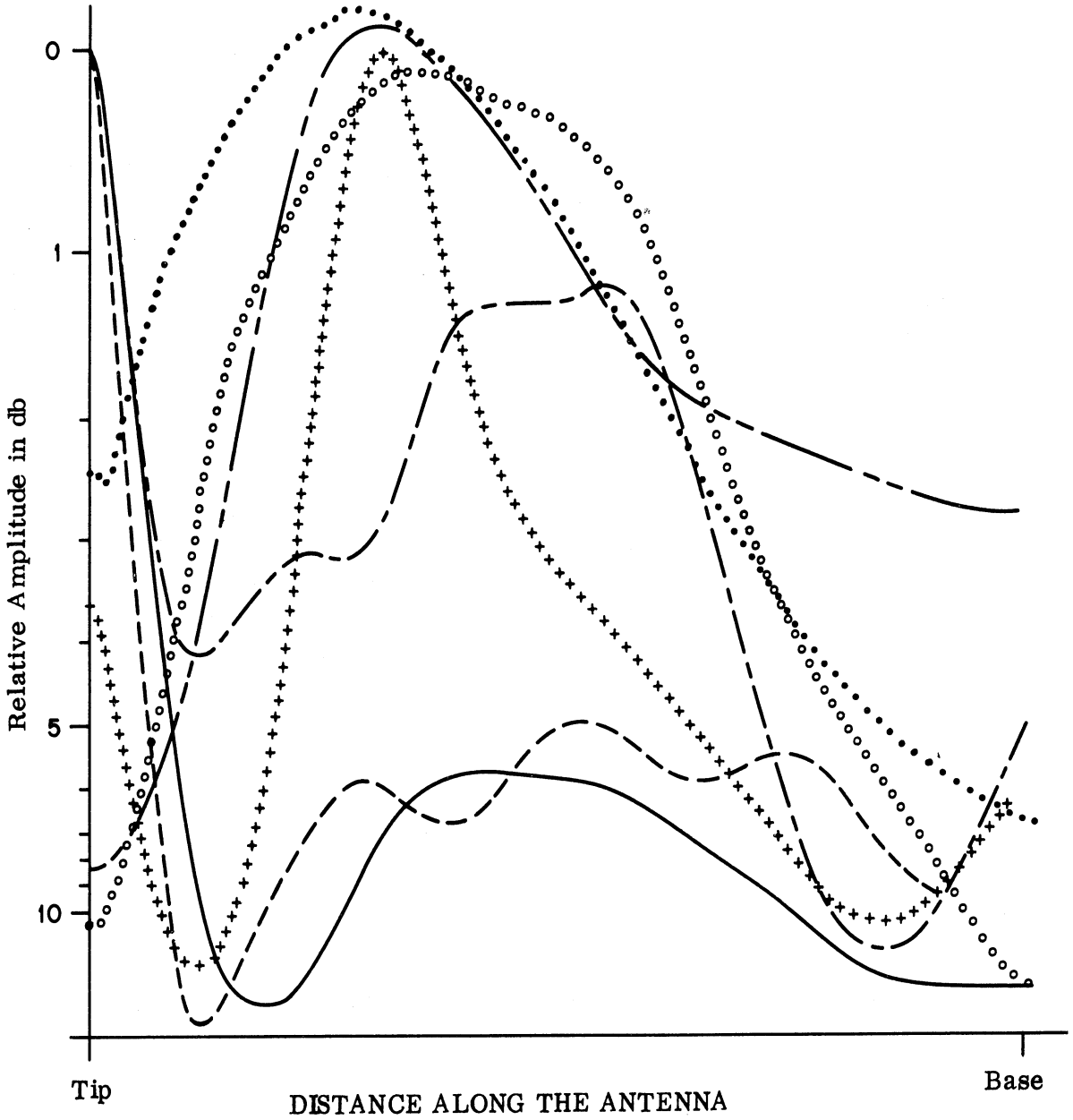

FIG. 3-6: NEAR FIELD PATTERNS OF ANTENNA 228, BIFILAR HELICAL WINDING HELIX AT 0.1 λ.

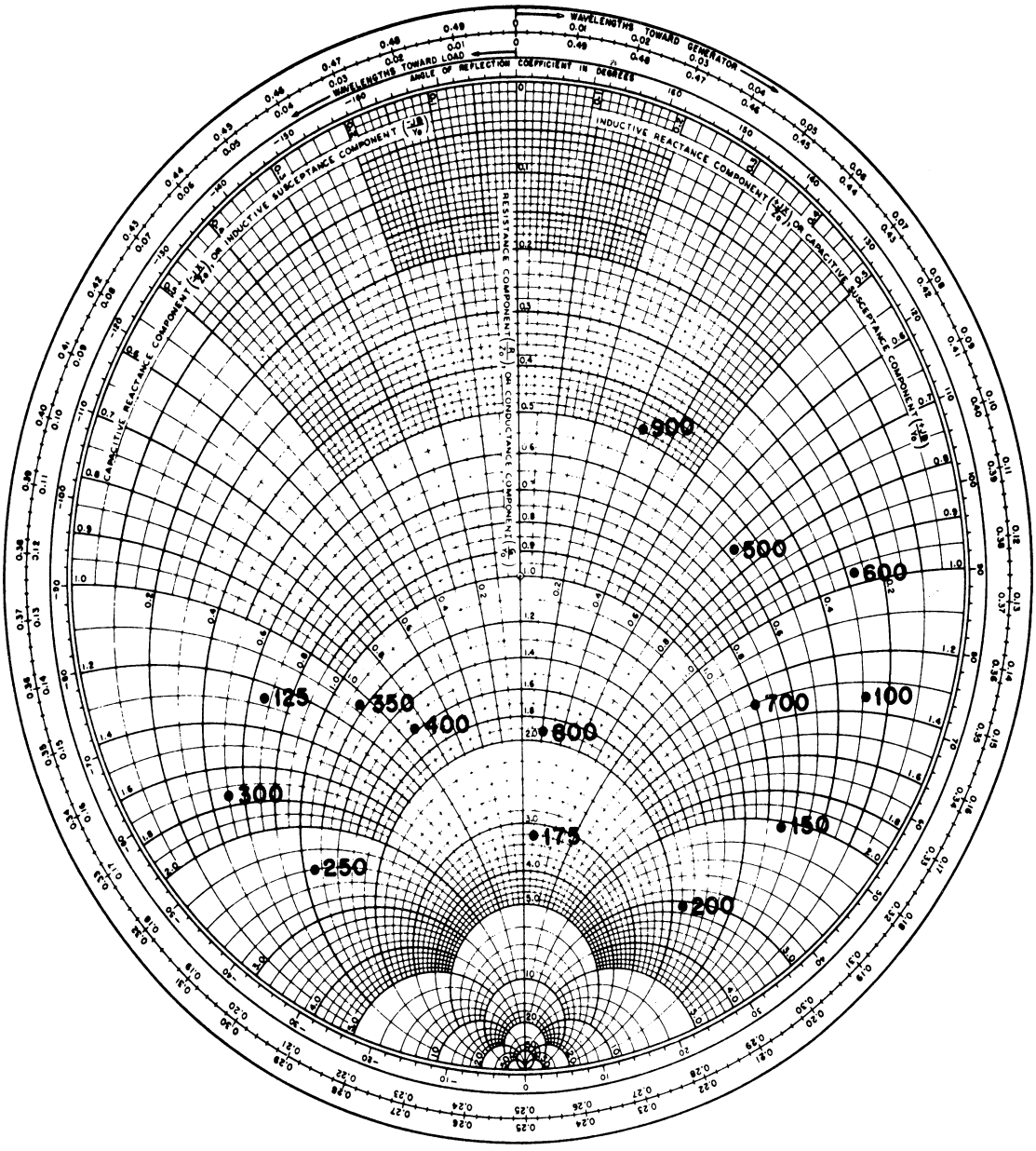

FIG. 3-7: IMPEDANCE OF ANTENNA 228 UNLOADED.
(Frequency in MHz)

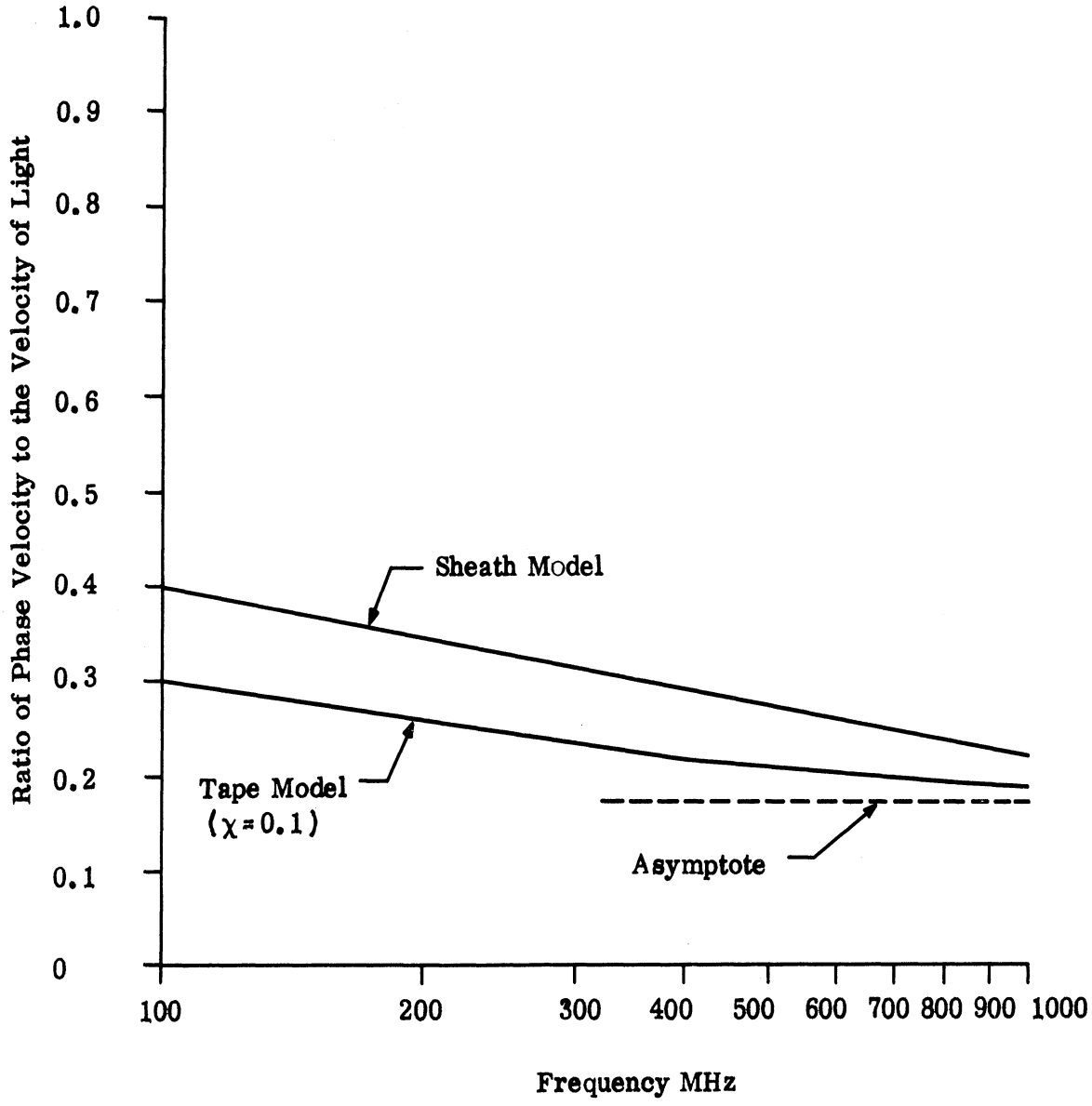

FIG. 3-8: PHASE VELOCITY FOR A 3/4" DIAMETER 10^{o} HELIX.

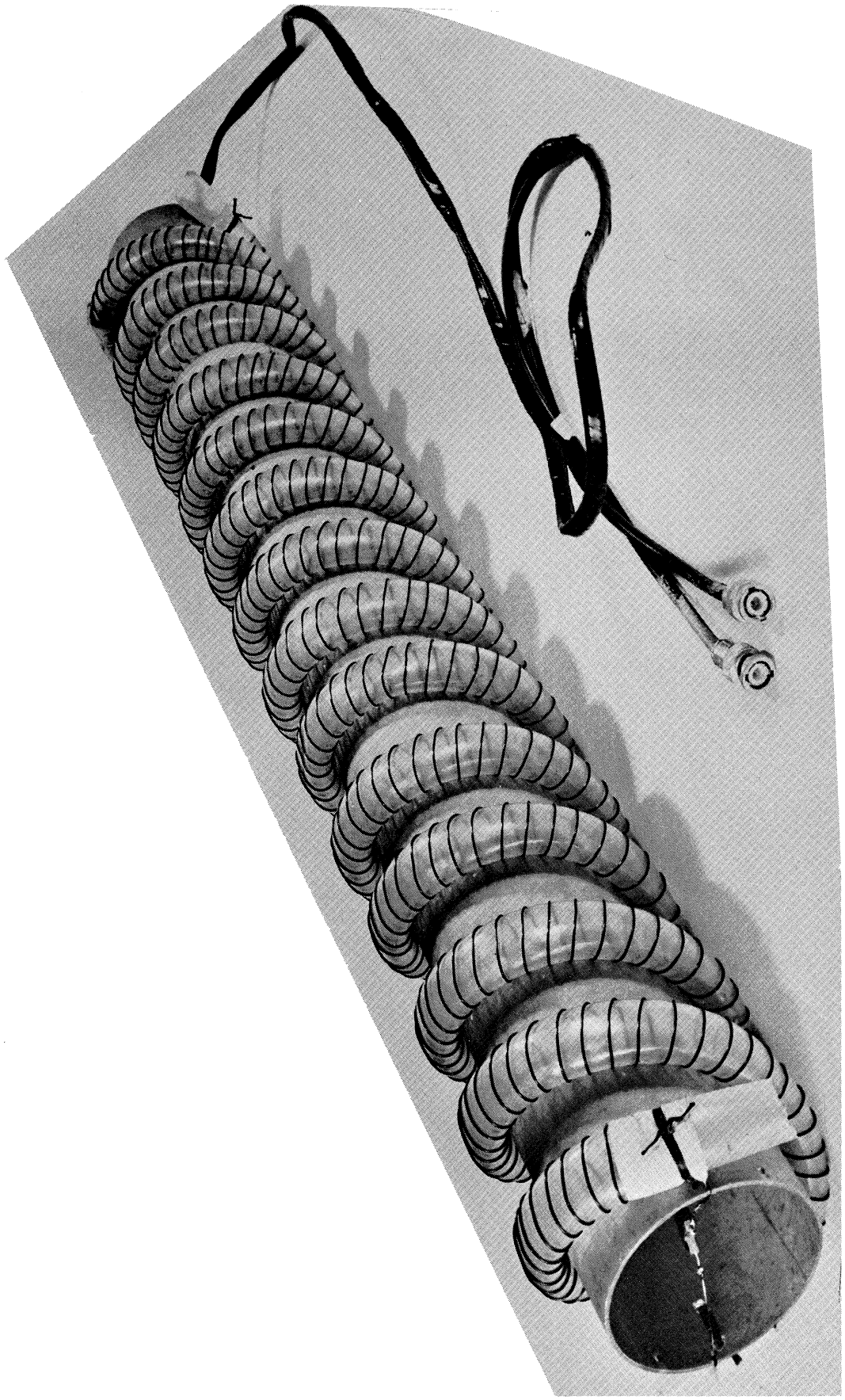

FIG. 3-9: ANTENNA 228 WITH THE WINDING REVERSED.

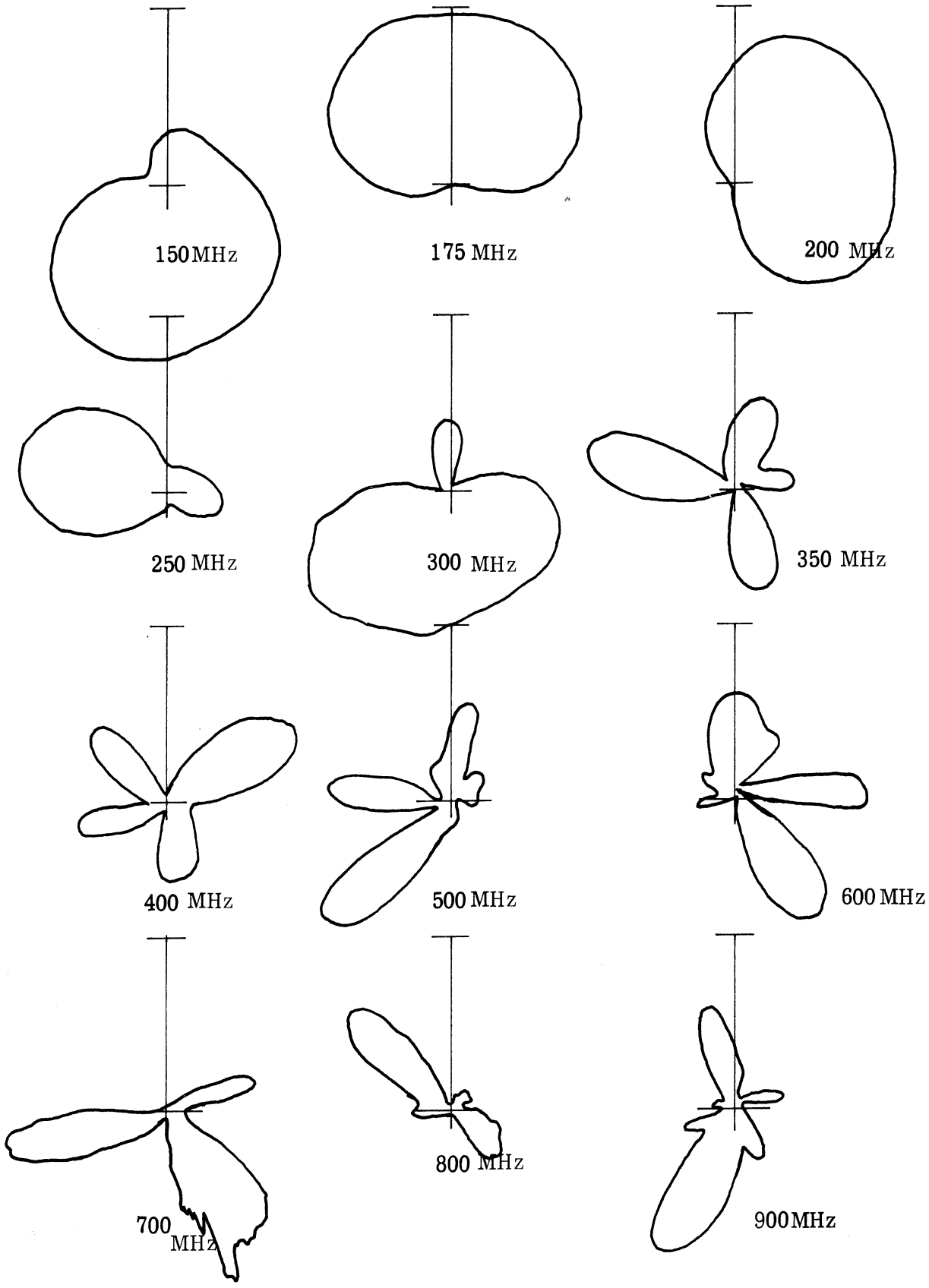

FIG. 3-10: ANTENNA 228, A BIFILAR 14^{o} HELIX, WITH WINDING REVERSED.

field patterns of the antenna. Even the unexplained large backlobe appears at 300 MHz. The bandwidth over which this backlobe occurs is the same also (from about 270 to 330 MHz). Thus it appears that the orientation of the individual windings of the slow wave structure with respect to the axis of the antenna has little effect on the operation of the antenna.

3.3 Discrete Component Loading

Discrete component loading appears to be a promising way of achieving significant reductions in the lower part of the HF (3 to 30 MHz) band. During the period of this contract, the concept was checked out and found to agree fairly closely with theory. Although all tests were at UHF and were performed using inductors instead of capacitors, it is reasonably certain that loading of antennas with capacitors in the HF band could definitely reduce the size of the antenna by a factor of greater than two-to-one.

The parallel wire transmission line model for a bifilar helix appears to be a good approximation to the actual boundary value problem of such a helix. The transmission line model assumes the bifilar helix to be a parallel wire transmission line wrapped around a circular cylinder. The diameter of the helix corresponds to the spacing between the wires of the transmission line. Assuming this to be the case, it seems logical that if additional capacitance were shunted across the transmission line, then the phase and group velocity of the transmission line would be reduced. Thus, a smaller helix antenna could be made "resonant", and hence a size reduction could be achieved. Even though the concept appeared to be intuitively plausible, the condition that the diameter of the helix corresponded to the spacing of the transmission line seemed disturbing. To verify the concept, three experiments were conducted. The three experiments consisted of three different configurations of capacitor loading. The rationale was that one of the configurations should show some effect on the patterns of the antenna. Figures 3-11 through 3-19 show pictures of each of the three types of capacitor loading and the corresponding far field patterns and input impedance for each type.

As can be noted by observing the patterns of the three types, only type II loading produced any significant effect on the patterns. Type II loading is the type that would be expected to have an effect according to the transmission line model. However, the patterns definitely do not indicate a significant size reduction has occurred.

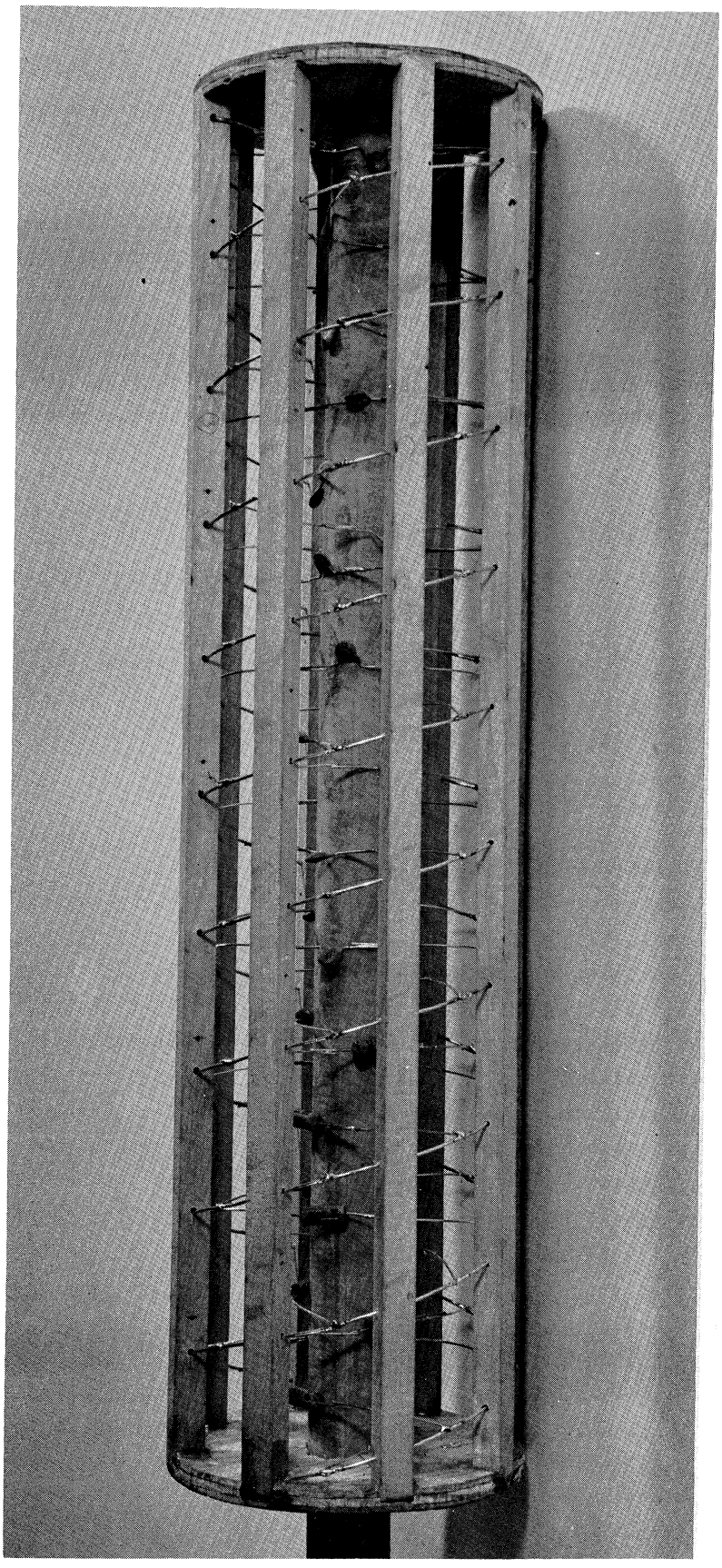

FIG. 3-11: PHOTOGRAPH OF ANTENNA 224 WITH 12 pf CAPACITORS IN TYPE II LOADING.

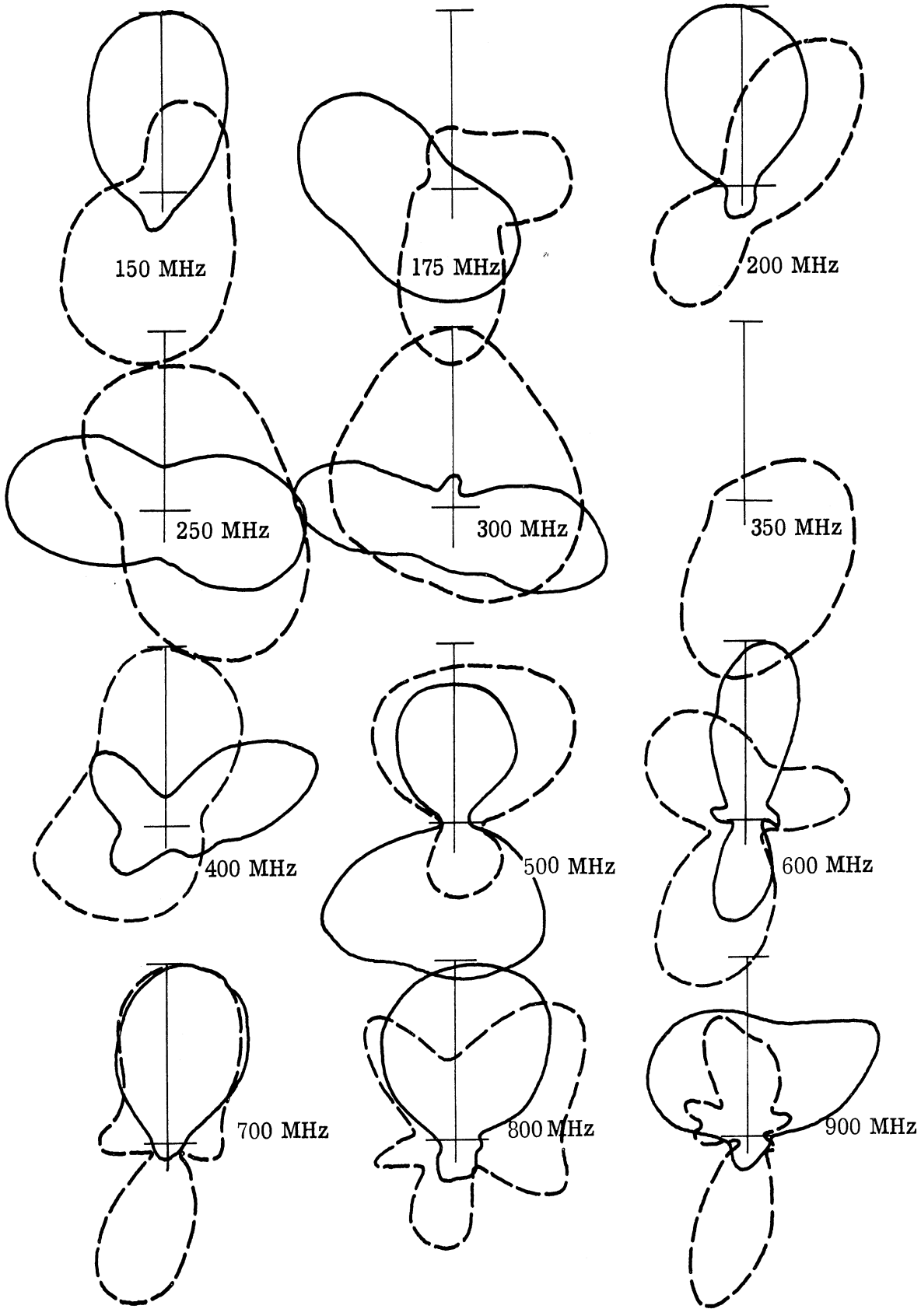

FIG. 3-12: RADIATION PATTERNS OF ANTENNA 224 WITH 12 pf CAPACITORS IN TYPE II LOADING.

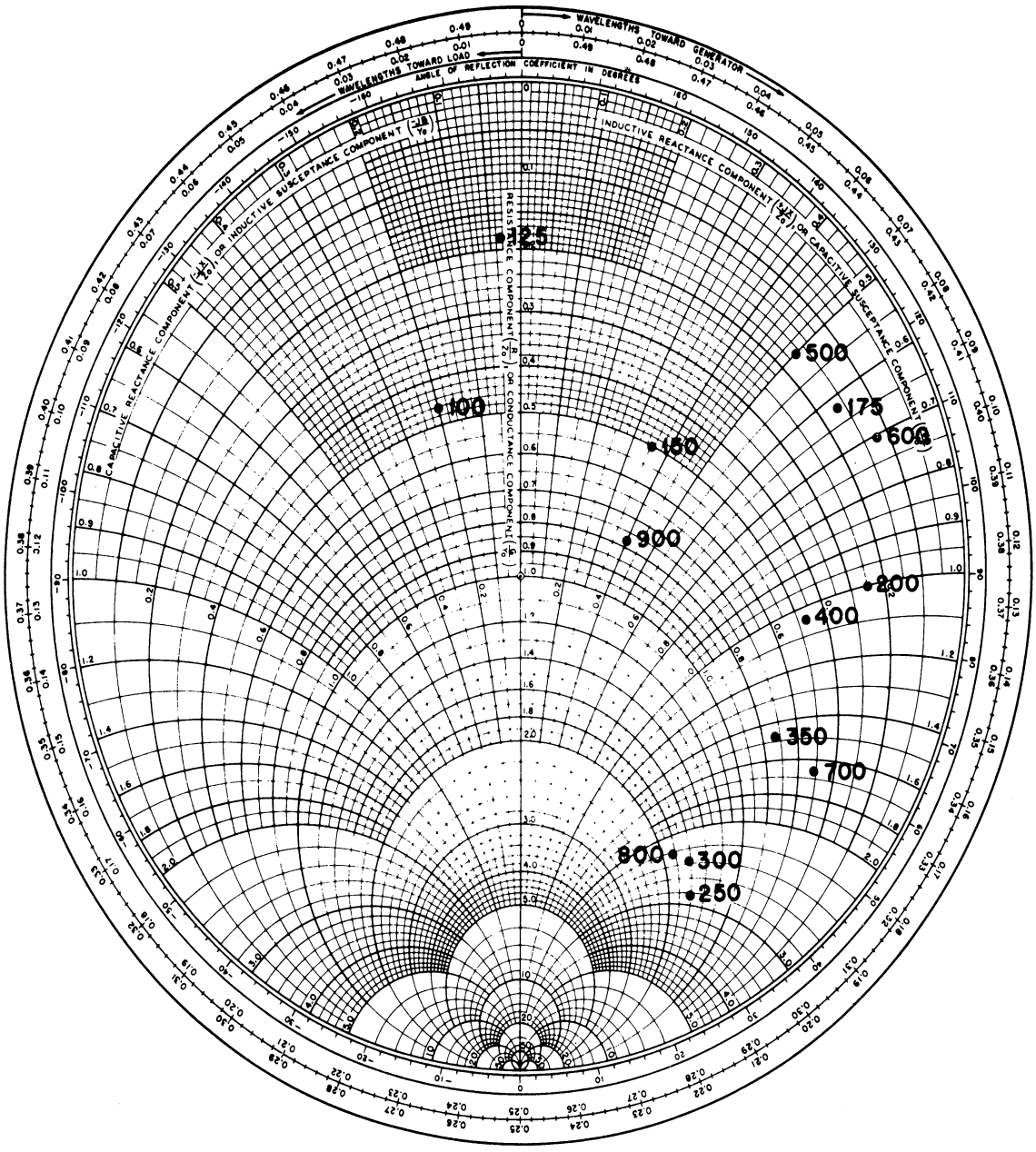

FIG. 3-13: IMPEDANCE OF ANTENNA 224 WITH 12 pf CAPACITORS IN TYPE II LOADING.
(Frequency in MHz)

FIG. 3-14: PHOTOGRAPH OF ANTENNA 224 WITH 12 pf CAPACITORS IN TYPE I LOADING.

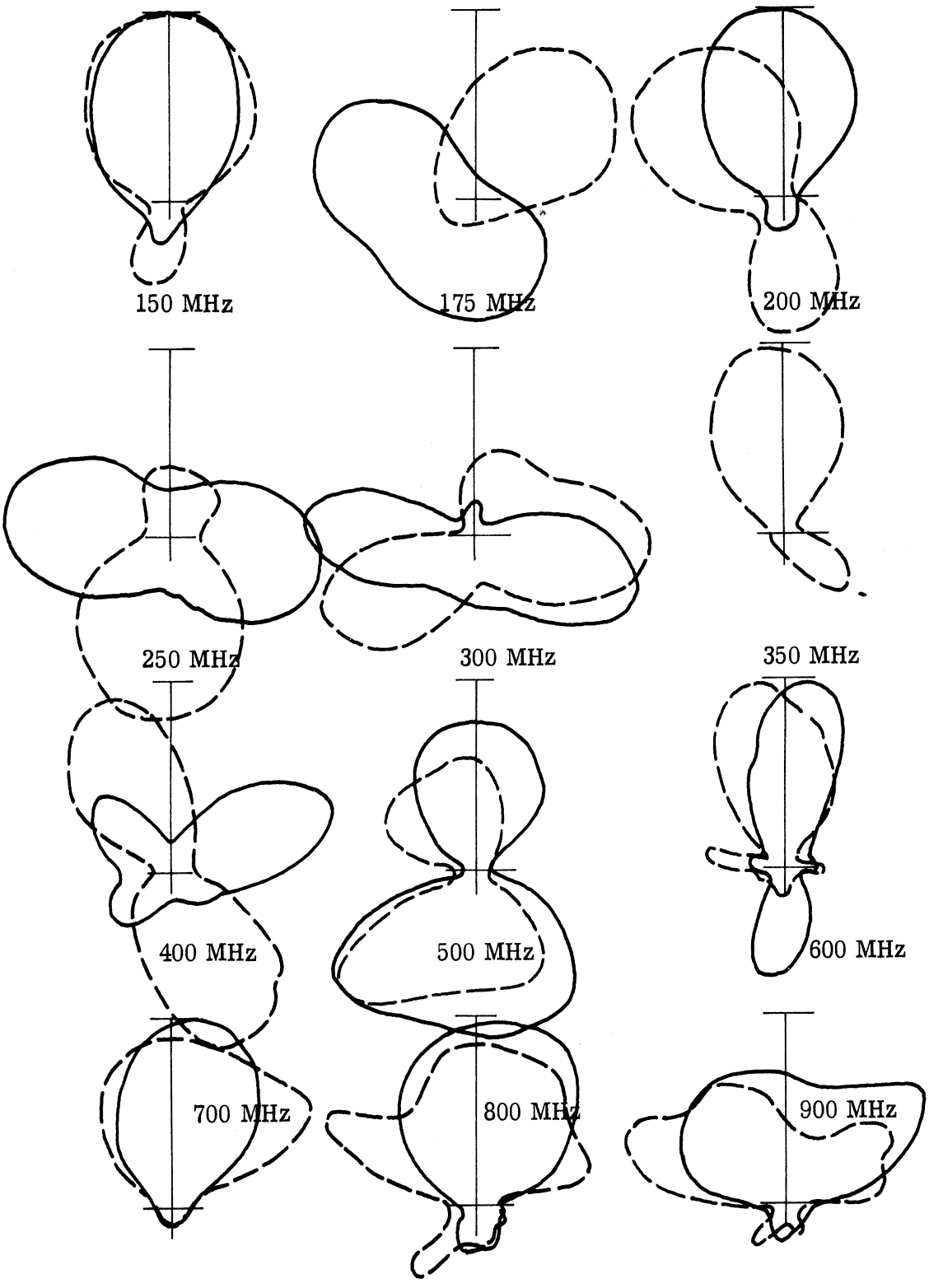

FIG. 3-15: RADIATION PATTERNS OF ANTENNA 224 WITH 12 pf CAPACITORS IN TYPE I LOADING.

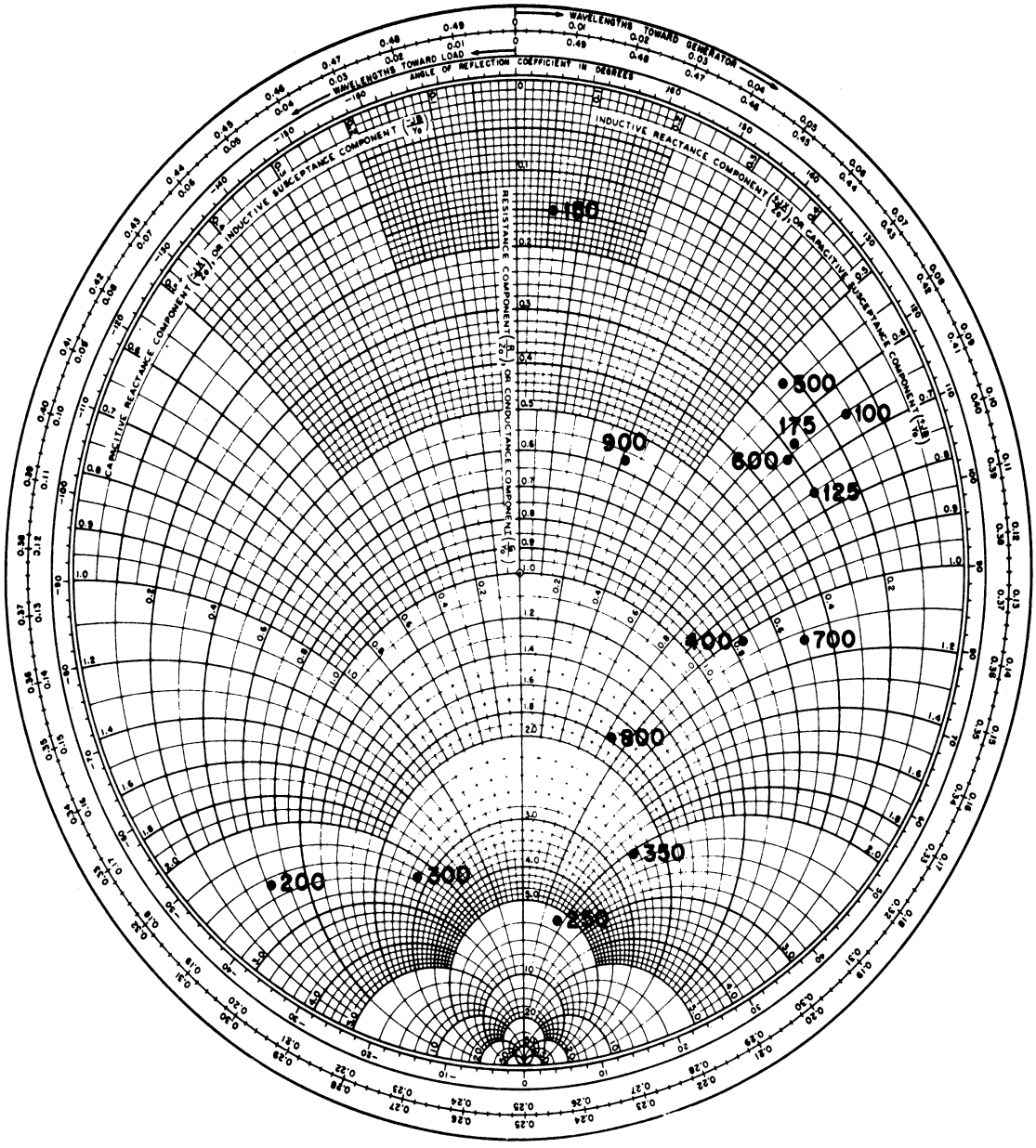

FIG. 3-16: IMPEDANCE OF ANTENNA 224 WITH 12 pf CAPACITORS IN TYPE I LOADING.
(Frequency in MHz)

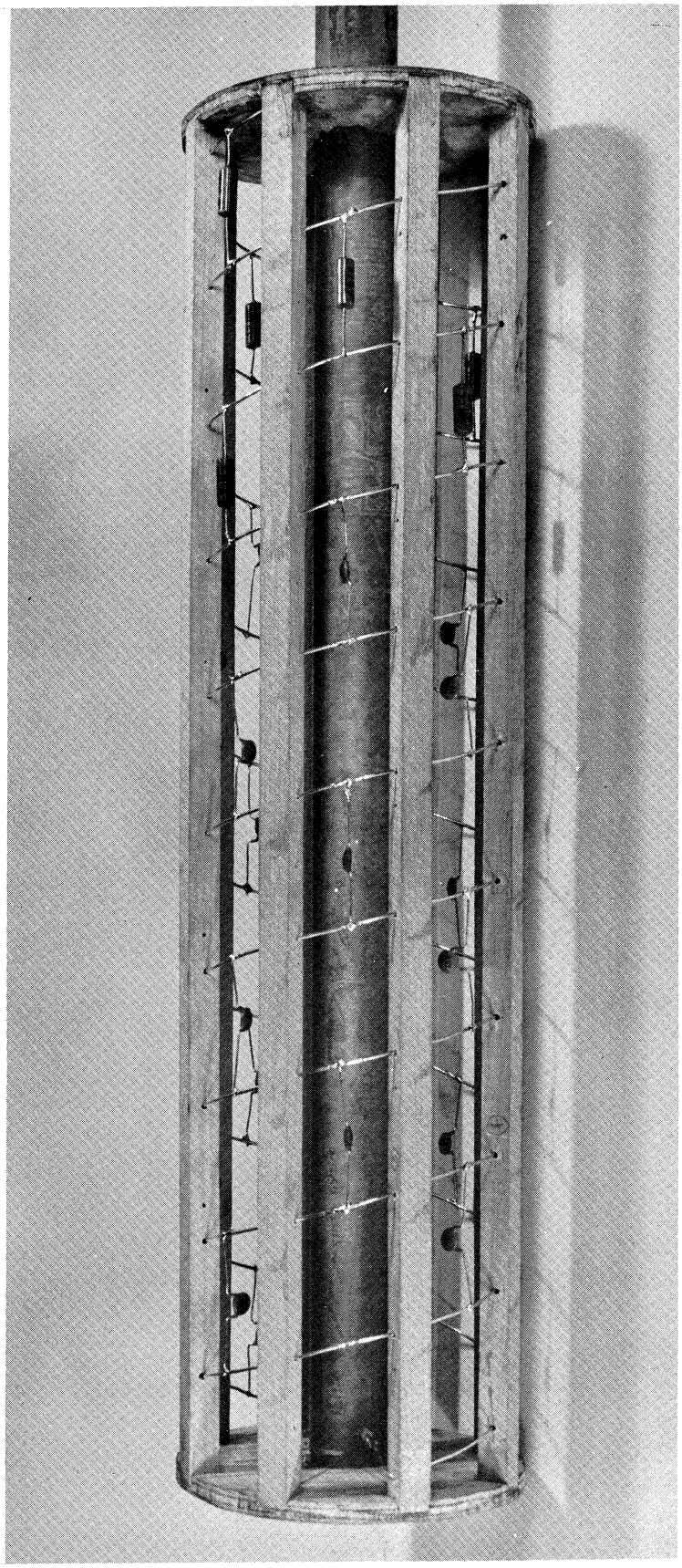

FIG. 3-17: PHOTOGRAPH OF ANTENNA 224 WITH 12 pf CAPACITORS IN TYPE III LOADING.

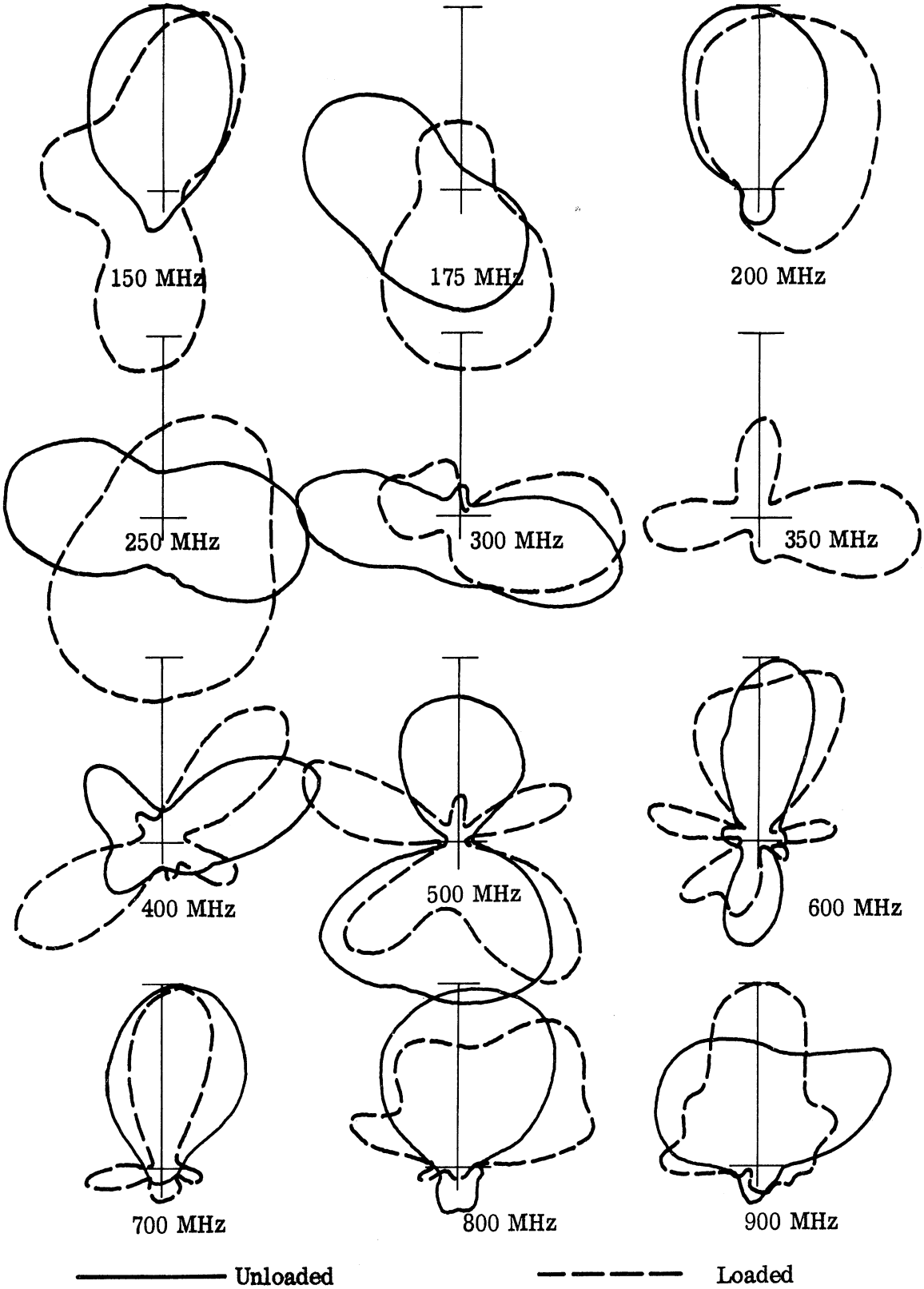

FIG. 3-18: RADIATION PATTERNS OF ANTENNA 224 WITH 12 pf CAPACITORS IN TYPE III LOADING.

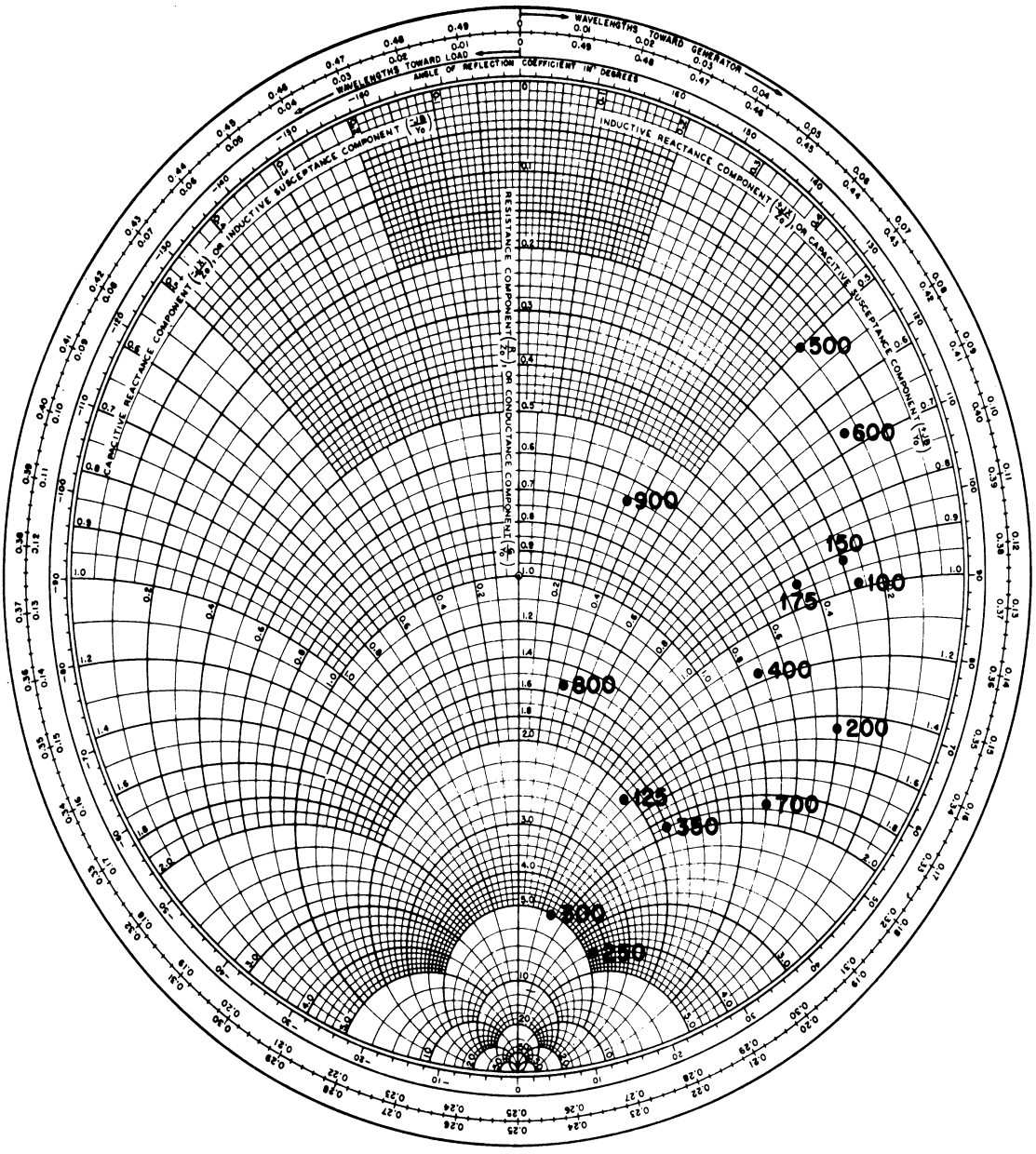

FIG. 3-19: IMPEDANCE OF ANTENNA 224 WITH 12 pf CAPACITORS IN TYPE III LOADING.
(Frequency in MHz)

Since the characteristic impedance assumed in the selection of the capacitors was 50 Ω, and not 790 Ω as would be predicted by the transmission line theory, larger capacitors were used in the type II configuration and additional patterns were taken. The results are indicated in Fig. 3-20.

The results were quite unexpected at the time they were observed, but agree closely with the theory derived later. Notice that between 860 and 870 MHz, the antenna switches from forward fire to backward fire radiation. The other interesting feature is that below 400 MHz, the amount of power radiated by the antenna is very small.

As it turned out, for the frequencies involved in the experiments, the capacitors connected across the diameter of the antenna were acting as inductors due to the inductance of the lead length. An article by Robert Pierce (1966) discusses this topic and gives formulas for calculating the inductance of the lead length. These formulas apparently assume that the current distribution along the lead is uniform. This is equivalent to assuming that the length of the lead is much less than a wavelength. Under the conditions of the experiment, this results in a value of inductance that is too large.

However, by calculating the value of the inductance according to Pierce's formulas and solving the transmission line model produced as a result, it can be shown that below a certain frequency (1155 MHz using Pierce's formula for inductance) the transmission line does not transmit energy, but attenuates it. Details are given in Appendix A.

Similarly, by using the inductance calculated using Pierce's formulas and making an analysis of the periodically inductive loaded transmission line that results, a characteristic equation can be obtained that can be solved for the $k - \beta$ diagram shown in Fig. A-2. This more exact analysis predicts both the attenuation, forward fire, and the backward fire modes that were observed on the antenna; this analysis predicted the shifts from different types of operation to occur at higher frequencies than were observed. Full details are given in Appendix A.

However, this analysis and the experiments do indicate that if a helix or conical helix antenna is loaded with capacitors at frequencies low enough so that the inductance of the lead length is not important, then worthwhile reductions in size can be achieved. Calculations indicate that this limit imposed by the inductance of leads is about 30 MHz, although reduced size antennas of this type could probably be successful up to 50 or 100 MHz. Appendix A gives the details.

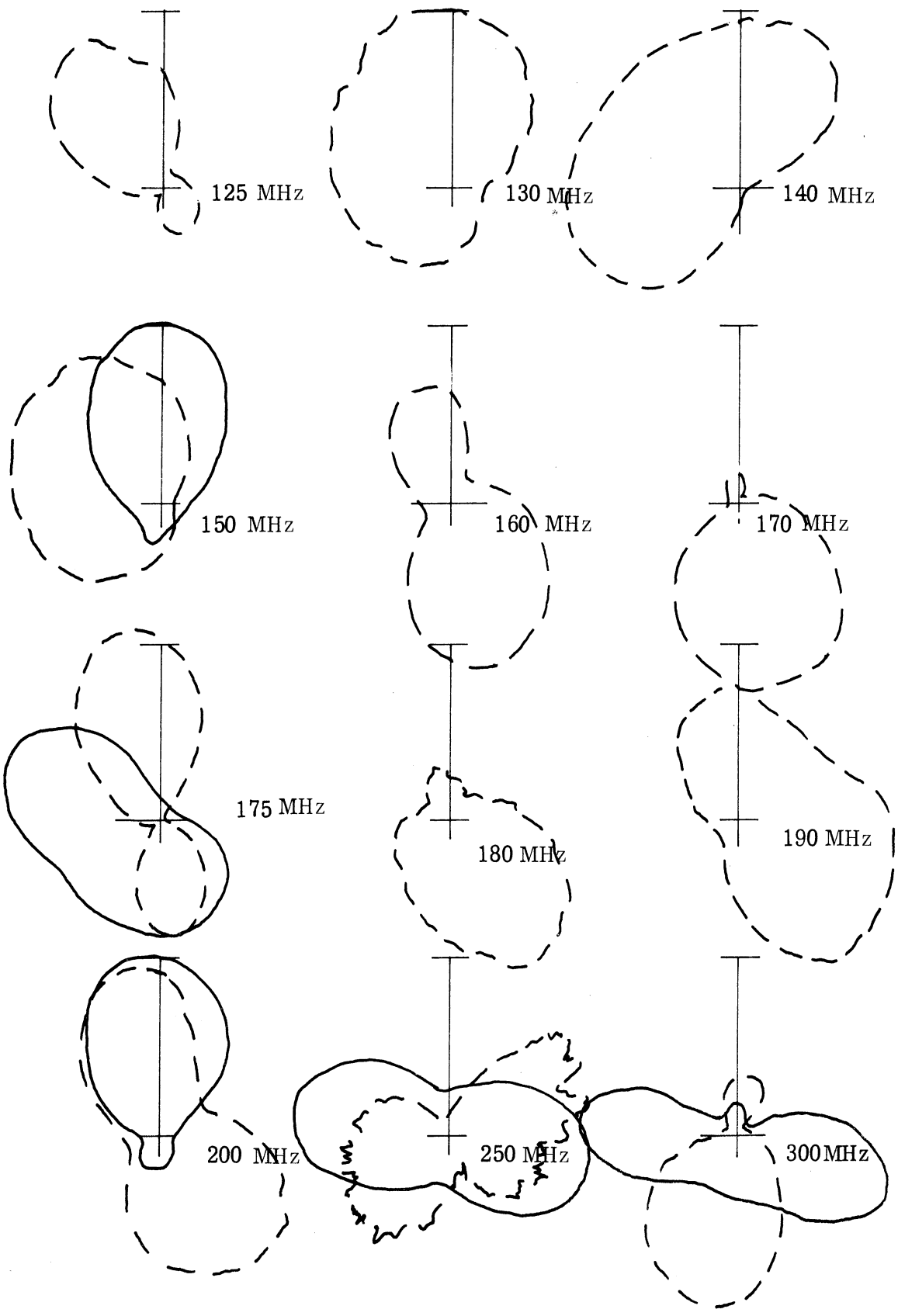

FIG. 3-20a: ANTENNA 224, A BIFILAR HELIX, LOADED WITH 120 pf. CAPACITORS IN A TYPE II LOADING.

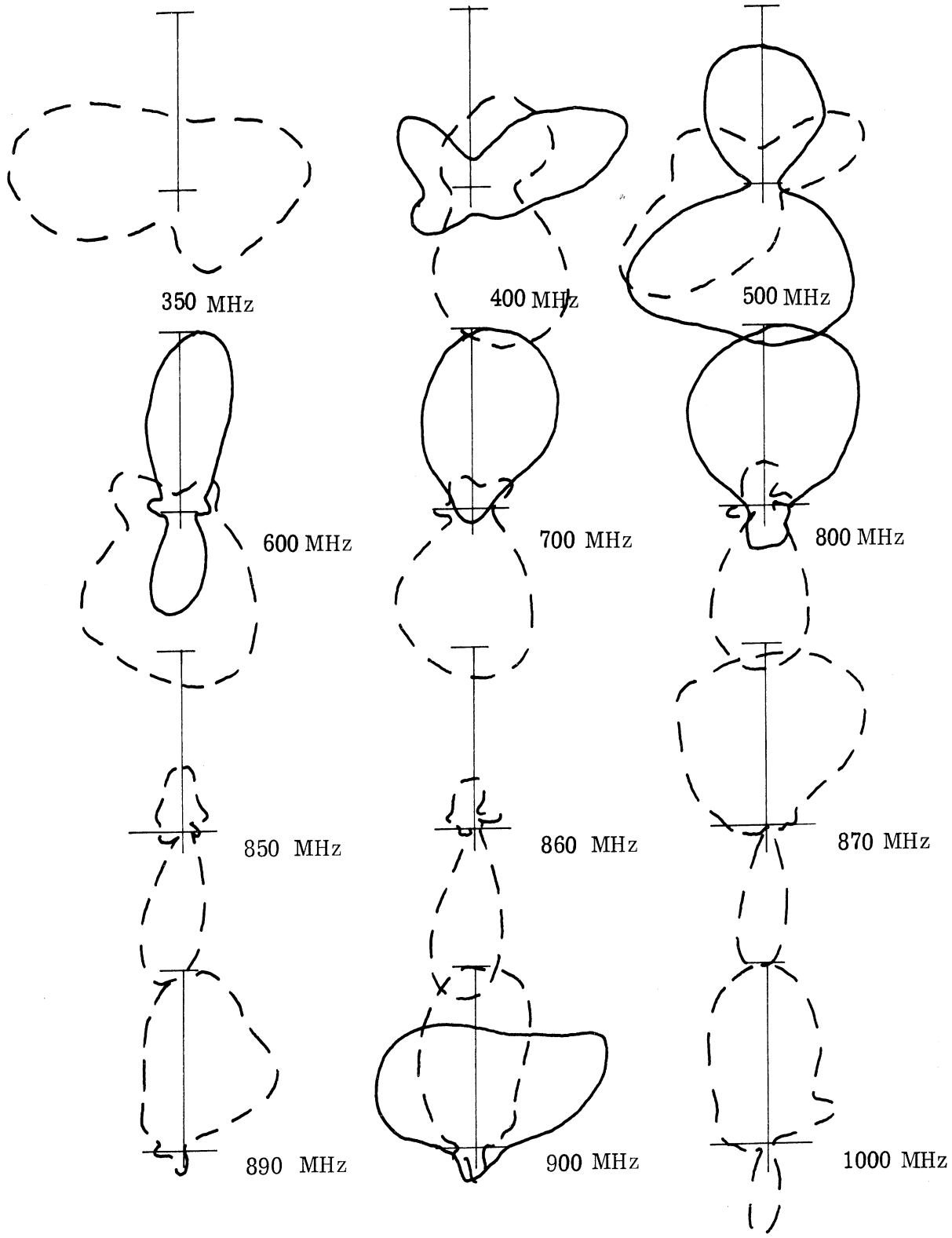

FIG. 3-20b: ANTENNA 224, A BIFILAR HELIX, LOADED WITH 120 pf. CAPACITORS IN A TYPE II LOADING.

Thus, discrete capacitor loading appears to permit significant size reductions for antennas operating in the HF band

3.4 Metal Loading

There are several reasons why metal loading could be desirable for size reduction of conical helical antennas. First, it is possible to make lighter metal loading than is commercially available in isotropic bulk material. Second, anisotropies may be introduced that offer the possibility of suppressing undesirable modes that occur with isotropic material. A helical antenna in free space can radiate all of the energy fed to it in either the zeroth or -1 modes. However, when the currents of the antenna are on the interface between free space and a magneto-dielectric medium, several modes may be necessary to satisfy the boundary conditions. These higher modes will radiate if the antenna is large enough. If a bifilar antenna is not large enough, the energy will be reflected from the end of the antenna and will either radiate in positive modes, or travel to the feed of the antenna and be absorbed (or reflected). The excitation of these higher modes produces a high backlobe when the $\pm$ 1 mode is radiated and high sidelobes when the other $\pm$ modes are excited.

Several metal loading techniques have been contemplated and some experimental work was performed on one of the promising techniques, a metal core inside the antenna. Figure 3-21 illustrates a typical core and the antenna into which it was inserted.

The rationale for doing this is based on considering the antenna as a transmission line. Figure 3-22 shows a diagram of a few sections of a distributed parameter transmission line, together with a summary of the pertinent relationships of a transmission line. Considering a helical or conical helical antenna in terms of a transmission line, radiation from the line occurs when the circumference of the helix times the propagation constant of the line is equal to approximately an integral multiple of 2π. As with a travelling wave antenna, if the phase velocity of the transmission line can be reduced, the physical dimensions of the antenna will be reduced.

Filling the interior of the helical antenna with a material where $\mu > 1$, $\epsilon > 1$, reduces the phase velocity (and increases the phase constant) much as would filling the interior of any transmission line. However, when radiation occurs for the odd modes of propagation, the opposite sides of the helical structure are π radians out of phase. Thus, there should be a net equivalent polarization across the helix. Hence, there is a capacitance between opposite sides of the helix (Fig. 3-23). Note that with an isotropic dielectric loading, this capacitance is increased, but so is the

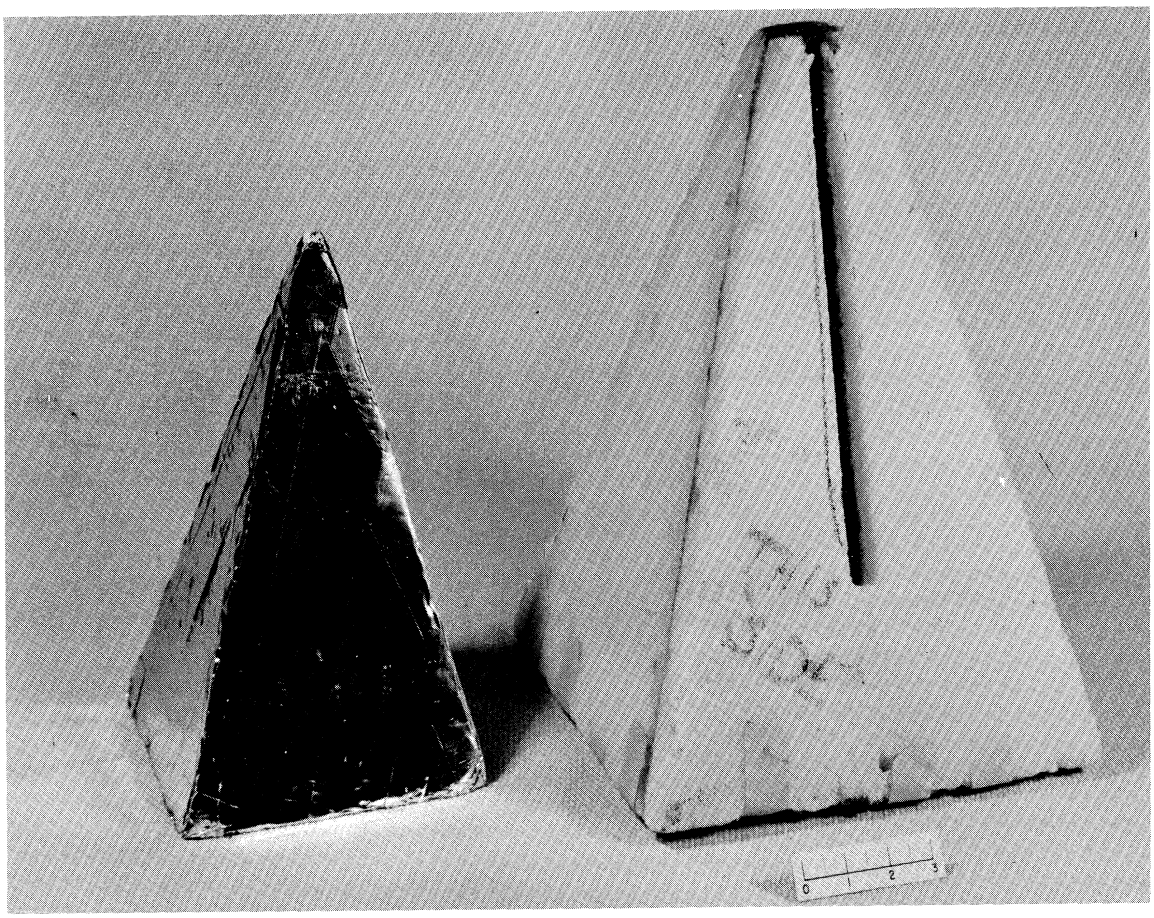

FIG. 3-21: ANTENNA 223: 500 - 900 MHz PYRAMIDAL HELIX AND METAL TAPE-COVERED STYROFOAM CORE.

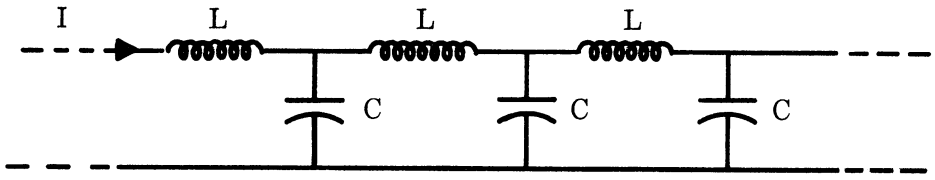

$$\frac{dV}{dx} = L\frac{dI}{dt} \qquad V = V_o \; e^{j(\omega t \pm \beta z)}$$

$$\frac{dI}{dx} = C\frac{dV}{dt} \qquad I = I_o \; e^{j(\omega t \pm \beta z)}$$

$$= \frac{V_o}{Z_o} \; e^{j(\omega t \pm \beta z)}$$

$$\beta = \frac{2\pi}{\lambda} = \frac{\omega}{v_p} = 2\pi f\sqrt{LC}$$

FIG. 3-22: TRANSMISSION LINE RELATIONSHIPS

capacitance between adjacent turns of the helix. This latter condition results in adding capacitance in series with the inductance of Fig. 3-23. This reduces the effective inductance and tends to increase the phase velocity. If this capacitance is not increased by a dielectric while the capacitance across the helix is increased, it is possible that much smaller antennas can be built.

As a result of such arguments, it was decided to insert metal cores inside the conical helix antennas. The charge distribution on the antenna induces equal, but opposite, charges on the metal core (Fig. 3-23). The result is a shorter distance between charges or a larger capacitance. This artificial dielectric should not increase the capacitance between adjacent turns.

No mathematical analysis has been made of this approach, however, a series of experiments was conducted to test the principle. The results are promising, but not as expected. Near field measurements seem to indicate that a size reduction is accomplished by a solid metal core, but several higher modes are excited and they complicate the interpretation. The far field patterns have very high backlobes and wide beamwidths. Reflected waves may be causing some pattern degradation.

Two attempts were made to suppress any higher modes that might exist. The first involved replacing the core with metal rings. It was hoped that the rings would act as a mode filter and permit only the backfire mode to exist. Unfortunately, they did not.

The second attempt consisted of placing absorber across the base of the antenna to absorb the higher minus modes that did not have room to radiate before they were reflected. This attempt was more successful and the modes reflected off the base were suppressed quite well.

Figure 3-24 shows the near field patterns of antenna 223 with a metal core tapered so that the distance between the windings and core is always 1/3 of a radius. The core consists of a block of styrofoam wound with aluminum tape. The tape is sealed in such a manner that the effect is of a continuous piece of aluminum covering the foam core. The core is positioned in the center of the antenna. No absorber was used in this experiment. Notice that the major peaks of the curves have widened and that a large part of the radiation occurs nearer the tip as compared with the unloaded case (Fig. 3-25). The latter, of course, is the desired result. Above 500 MHz there are minor zones of radiation closer to the base. At 900 MHz there are three such minor peaks. These are caused by higher modes of radiation.

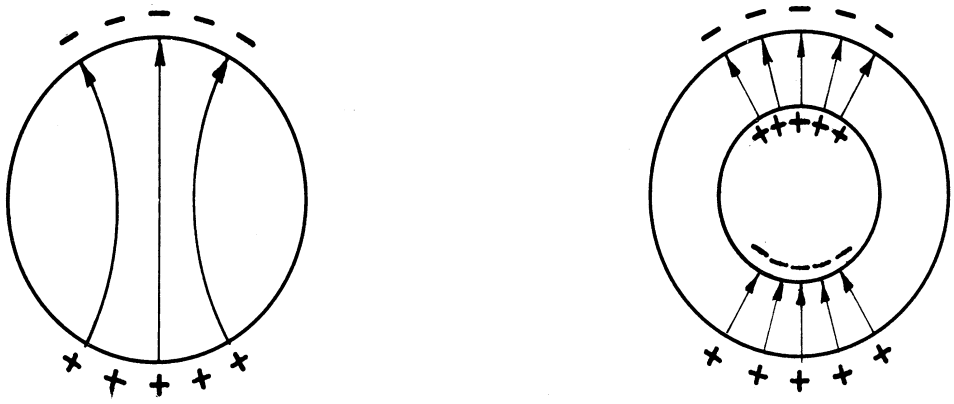

FIG. 3-23: INSTANTANEOUS CHARGE DISTRIBUTION ON A HELIX ANTENNA WITH AND WITHOUT METAL CORE (The Arrows Indicate the Electric Field).

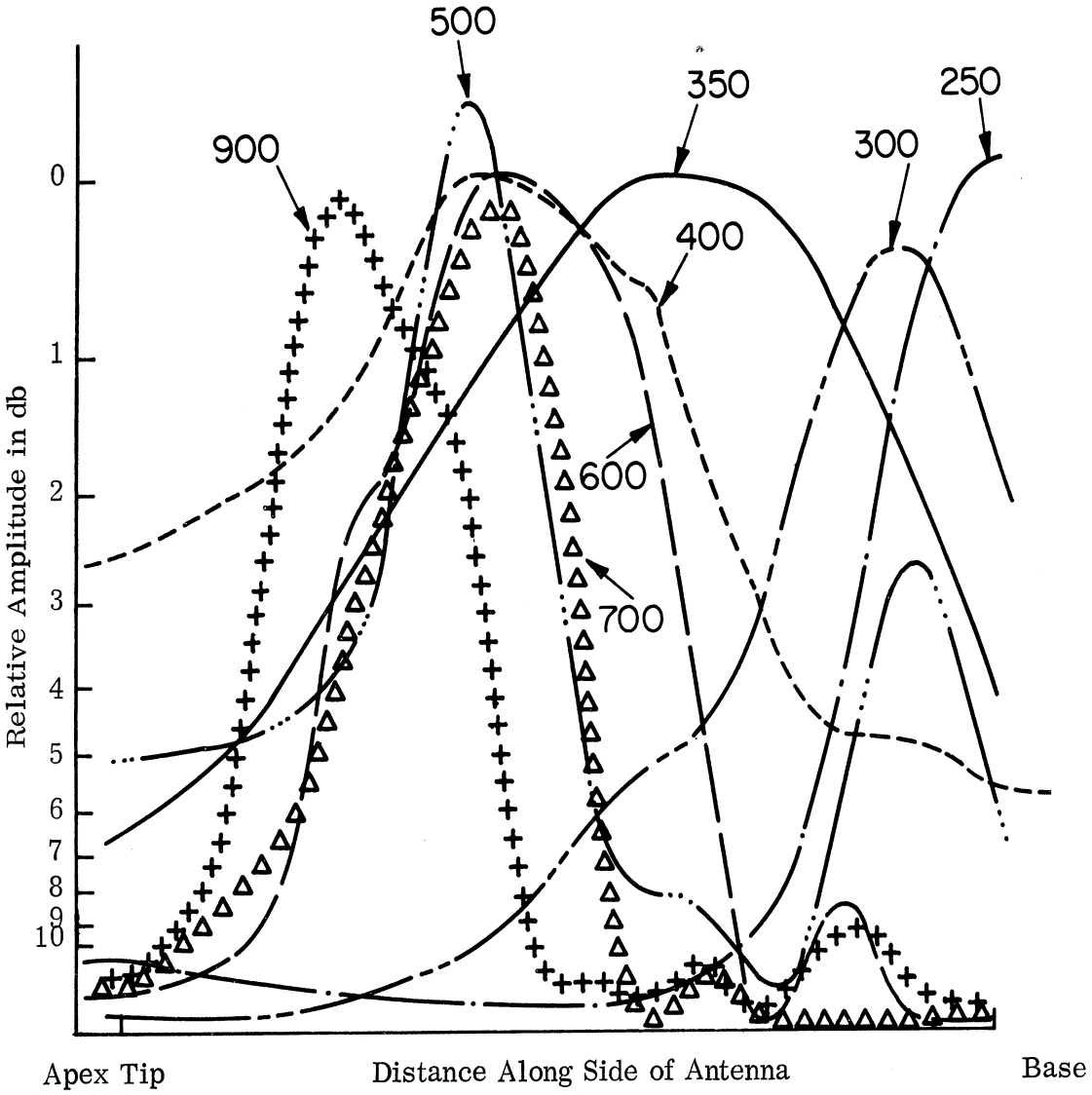

FIG. 3-24: ANTENNA 223 WITH A METAL CORE 1/3 RADIUS INSIDE OF THE WINDINGS. (Frequency in MHz)

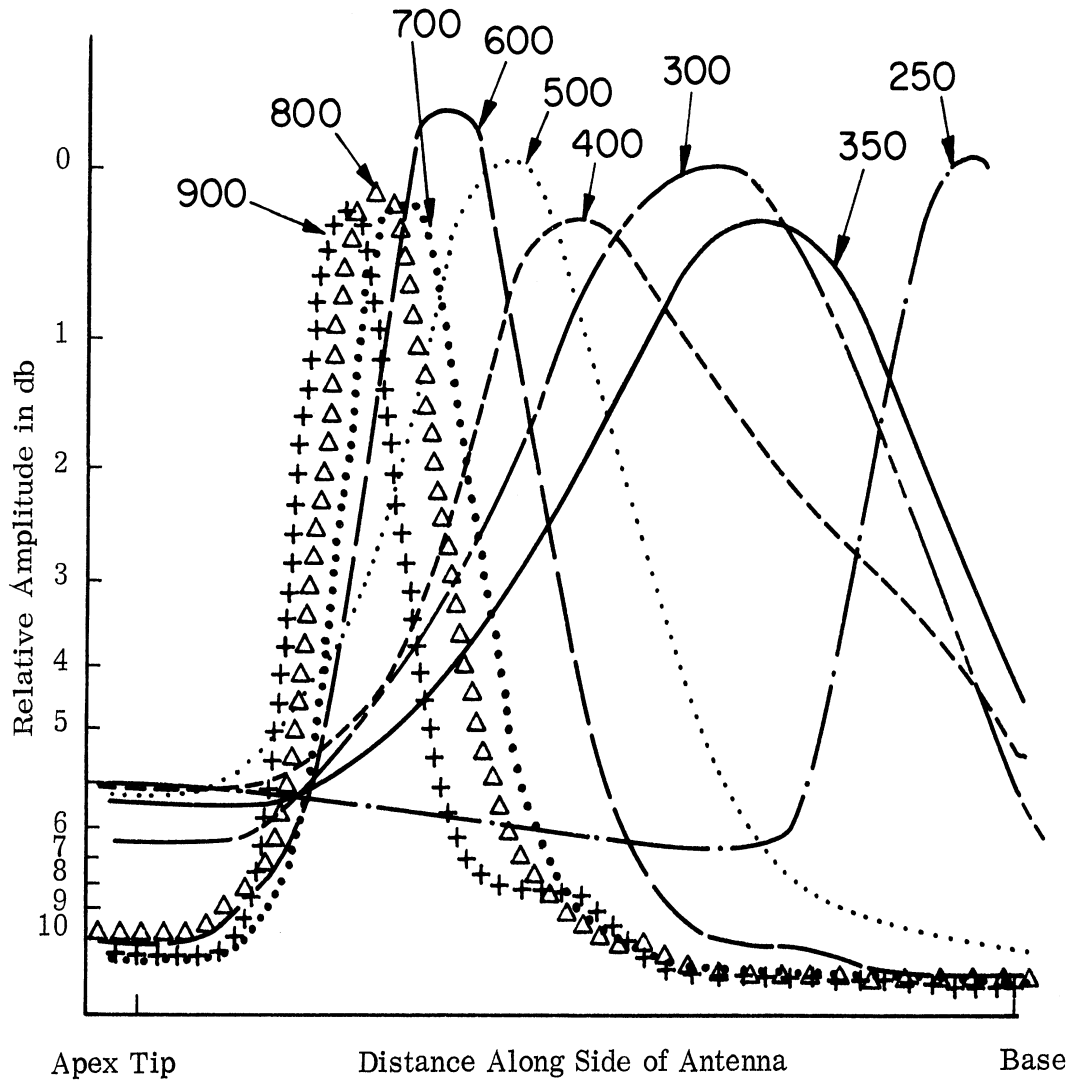

FIG. 3-25: ANTENNA 223 WITH NO LOADING.

(Frequency in MHz)

Figure 3-26 shows the far field patterns of antenna 223 with the same metal core. Note that the high backlobe shows up at most frequencies. This is apparently due to the + 1 mode. Notice the distortion of the main lobe and the sidelobes at 600, 700, 800, and 900 MHz by the higher + and - modes. Except for the other modes, the antenna appears to radiate quite well down to 300 MHz.

Figure 3-27 is the near field pattern of antenna 223 with a metal core similar to the previous one, but with 1/8 of a radius spacing. Again the probe was .1λ from the antenna. Note that the higher modes of radiation are stronger than the -1 mode for some frequencies. It appears, however, that the antenna is a good radiator even at 300 MHz. At 250 MHz the level of the signal received from the probe was very low. The objectionable feature would be the high side and back lobe levels.

The shape of the metal core was altered to try to reduce the intensity of the higher order modes. Figure 3-28 shows the near field patterns of antenna 223 with a metal core that is similar to the antenna in shape, but 3/4 scale. The core is positioned in the center of the antenna with the core and antenna bases coinciding. Note that the patterns bear a close resemblance to the shape of the patterns of the antenna in air. However, there definitely are reflections and radiation of higher order modes. It is encouraging to see that the near field peaks at the lower frequencies are closer to the tip than for the same antenna with no loading.

The Eccosorb WG (Emerson and Cuming) material was used to absorb possible reflections in this metal core experiment. Figure 3-29 shows the patterns obtained from antenna 223 with a metal core inside the windings and 1/8 radius away from the windings. A 3 x 10 x 10 inch piece of absorbing material covered the base of the antenna. A comparison with the patterns of the same experiment without the absorber reveals a rapid decay of the field amplitude occurring towards the base of the antenna. This is the result predicted. The patterns are similar to those of the same antenna with no loading. This is the shape necessary for a fairly good axial pattern.

For a better understanding of the effects of metal cores, an experiment was conducted with a dielectric loading and a metal core behind the dielectric. Figures 3-30 and 3-31 show the near field pattern. The 1/8 radius core was inserted in the antenna and Emerson and Cuming K-10 Hi-K dielectric was inserted between the core and the windings. The plots are unusual to say the least. Even at 250 MHz, which was the lowest frequency consistent with reliable operation of the signal source, the antenna was definitely radiating. Yet, the reflections appear to have increased.

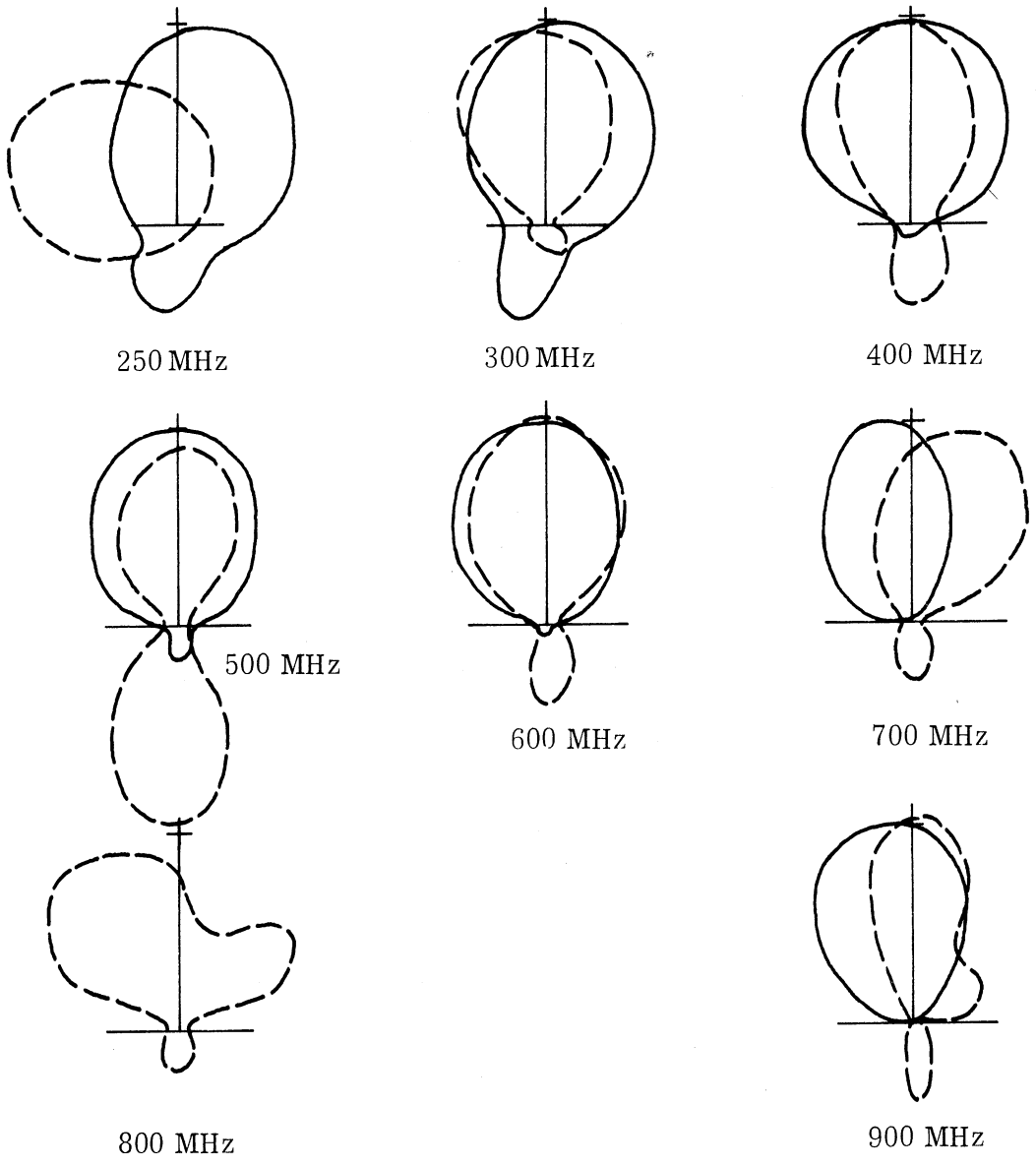

FIG. 3-26: PYRAMIDAL HELIX NO. 223 WITH A METAL CORE LOADING 1/3 RADIUS INSIDE OF THE WINDINGS.

_____ Unloaded _ _ _ _ _ _ _ Metal Core

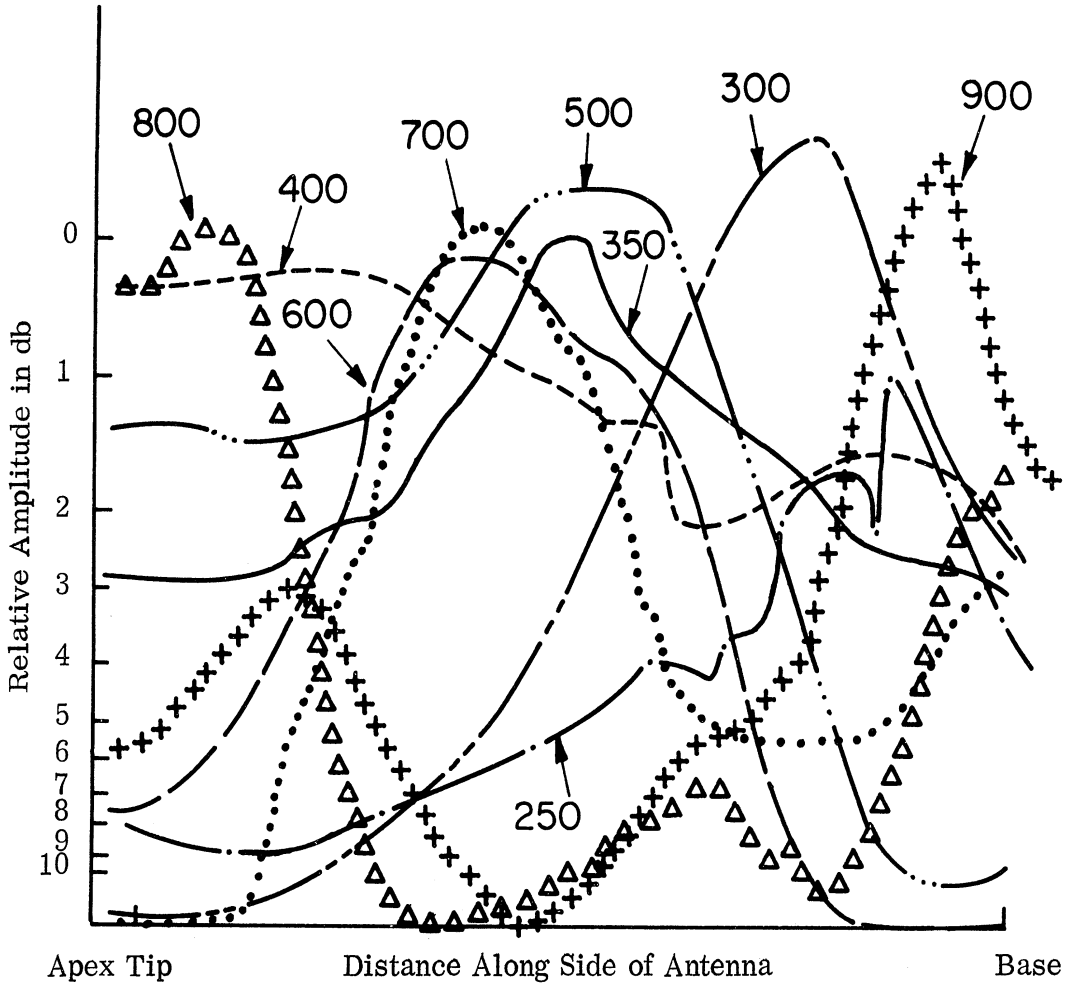

FIG. 3-27: ANTENNA 223 WITH A METAL CORE 1/8 RADIUS FROM WINDINGS.
(Frequency in MHz)

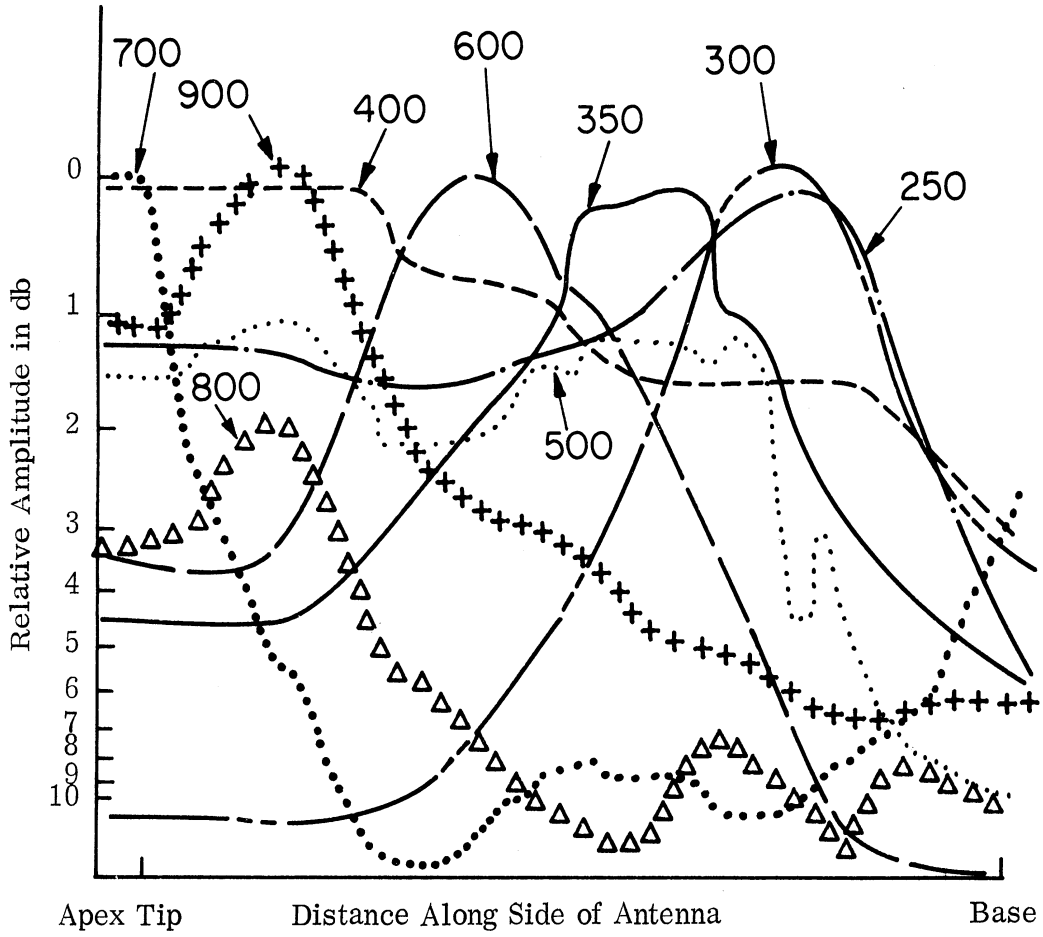

FIG. 3-28: ANTENNA 223 WITH A PYRAMIDAL METAL CORE THAT IS 3/4 THE ANTENNA SIZE. (Frequency in MHz)

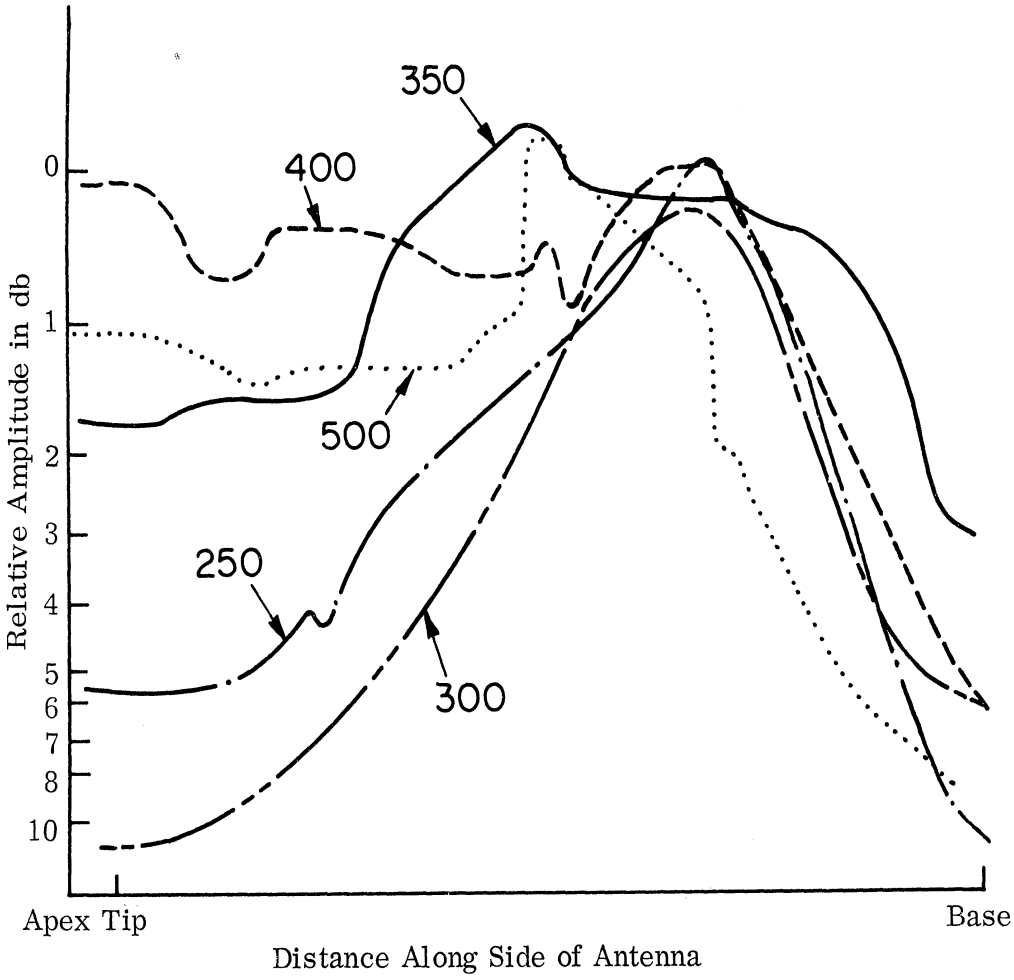

FIG. 3-29: ANTENNA 223 WITH A METAL CORE 1/8 RADIUS FROM THE WINDINGS AND WITH THE BASE COVERED WITH A 10" x 10" x 3" PIECE OF ECCOSORB WG. (Frequency in MHz)

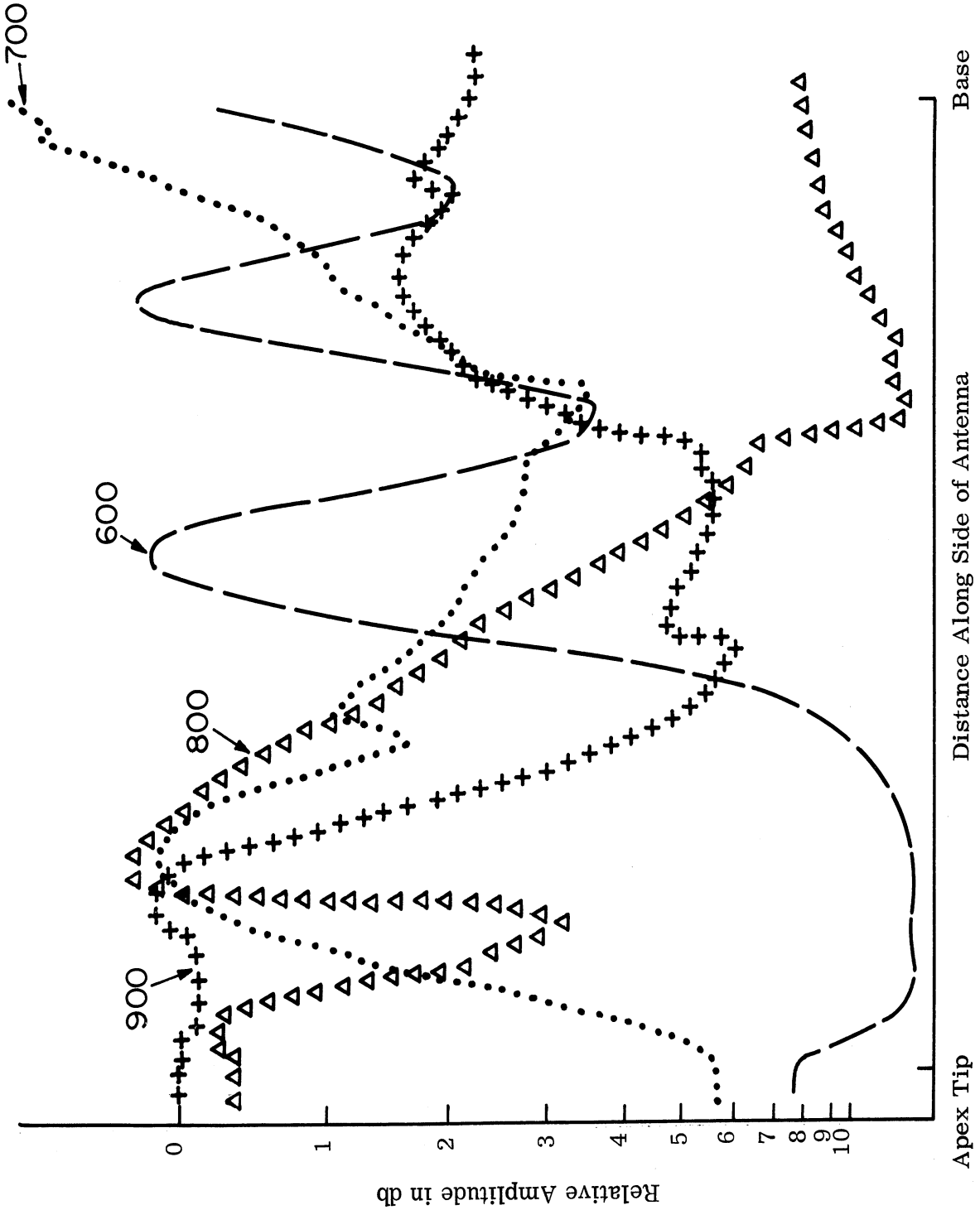

FIG. 3-30: ANTENNA 223 WITH K-10 IN BETWEEN A METAL CORE AND THE WINDINGS (METAL CORE 1/8 RADIUS INSIDE THE WINDINGS) (PART I).
(Frequency in MHz)

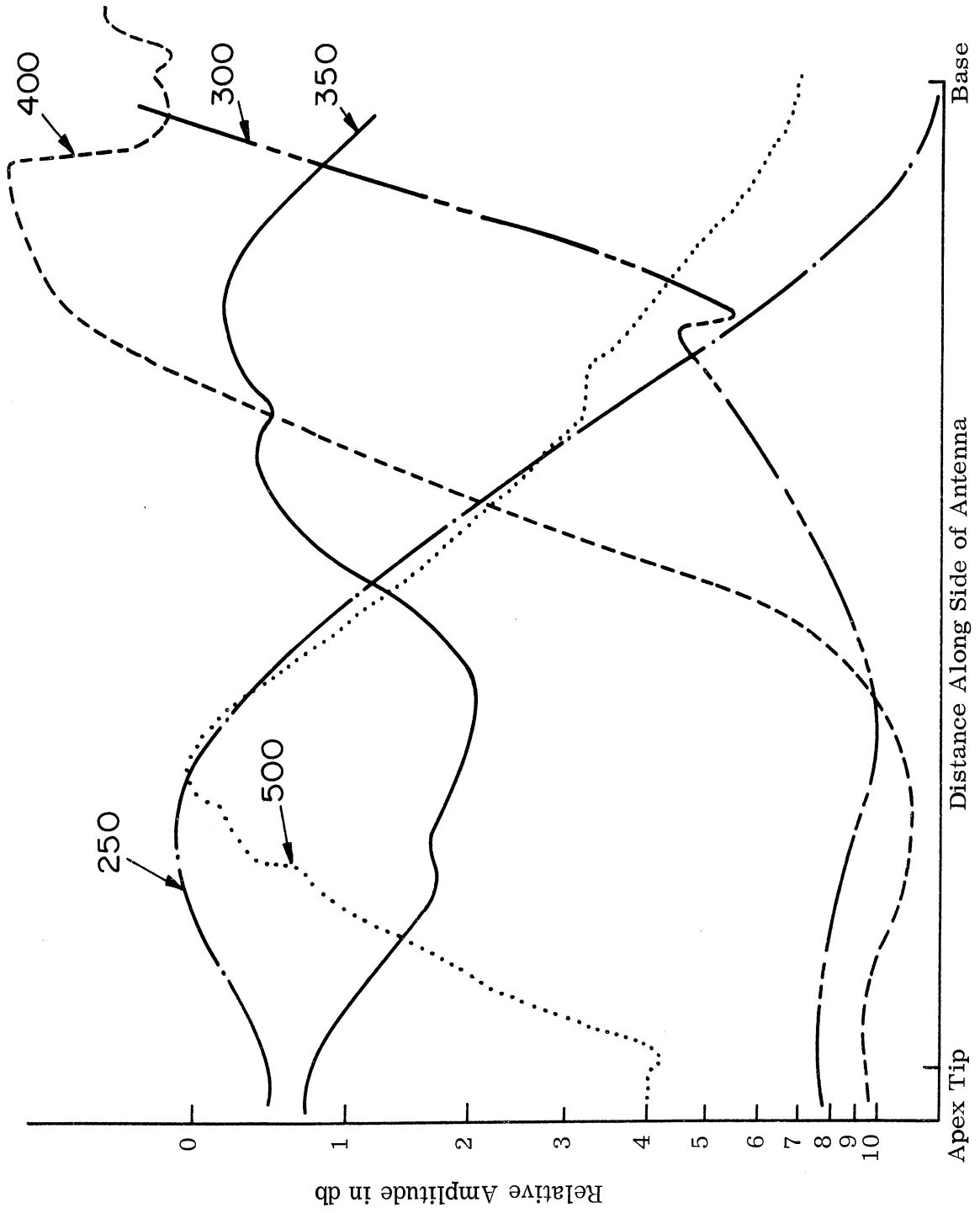

FIG. 3-31: ANTENNA 223 WITH K-10 IN BETWEEN A METAL CORE AND THE WINDINGS (METAL CORE 1/8 RADIUS INSIDE THE WINDINGS) (PART II).
(Frequency in MHz)

Since helix studies have been shown to be basically related to conical helix studies, several metal-core-loaded helices were studied in the near field chamber. Figure 3-32 shows measurements of the helix antenna 217 without loading. The measurements were taken along the side of the antenna, not along the length of the conductor. It can be seen that the frequencies 700 - 800 MHz have the best near field patterns for this backward-fire helix, since the near fields decay rapidly from the feed point to near zero, indicating that the currents have decayed due to radiation near the feed point. In addition, the frequencies 600 and 900 MHz have large standing waves indicating that these frequencies have relatively poor operation. The helix itself was designed for a center band around 800 MHz. In Fig. 3-33 the near fields of antenna 217 are shown with a 3" diameter metal core inside the helix. This core was intended to be a loading for the helix. If true loading occurs, other frequencies would show better operation than the 700 - 800 region seen in the unloaded case. As can be seen in Fig. 3-34, 700 MHz continues to be the best frequency and 600 and 900 MHz continue to be poor frequencies on either side of the best frequency, thus bracketing the bandwidth of this antenna. Hence, the metal core loading has not basically changed the characteristics of this antenna by shifting the resonant frequency region. If any effect occurs, it is in addition to the resonance near 700 - 800 MHz. Figure 3-34 shows near field patterns of the metal loaded helix taken at the lower frequencies to check a fairly promising far field radiation pattern. It was hoped that this much lower frequency of operation would indicate that the metal core was loading the antenna to a lower frequency of operation. It is seen, at both 160 and 210 MHz, that little change in the near field pattern occurs with the introduction of the metal core. The near field pattern at 250 MHz shows that some degradation occurs with metal loading. The unloaded near field pattern is interesting because it appears that even when unloaded it has an excellent near field pattern at this frequency. This occurs even though it is far from the nominal region of operation, 700 - 800 MHz, normally accepted for far field axial radiation. Figure 3-35 shows the far field patterns of the bifilar helix with and without loading of the metal core. They indicate that the far fields are definitely broken up by the introduction of 3" metal cylinder loading at the frequencies 400 MHz and above, even though the near field measurements at these frequencies showed relatively small change. At 250 MHz, only the loaded pattern is shown, which has some forward directivity but severe sidelobe problems. It can be concluded that no promising loading effects were seen in loading the bifilar helix 217, such as the 1/8 radius spacing of antenna 223, are required to have much effect on the antenna.

In conclusion, loading of conical helices with metal cores appears to produce some size reduction. Both near and far field patterns tend to show this. A definite statement as to how much effective size reduction could be achieved would be difficult to make at this time. The excitation of higher modes by metal cores

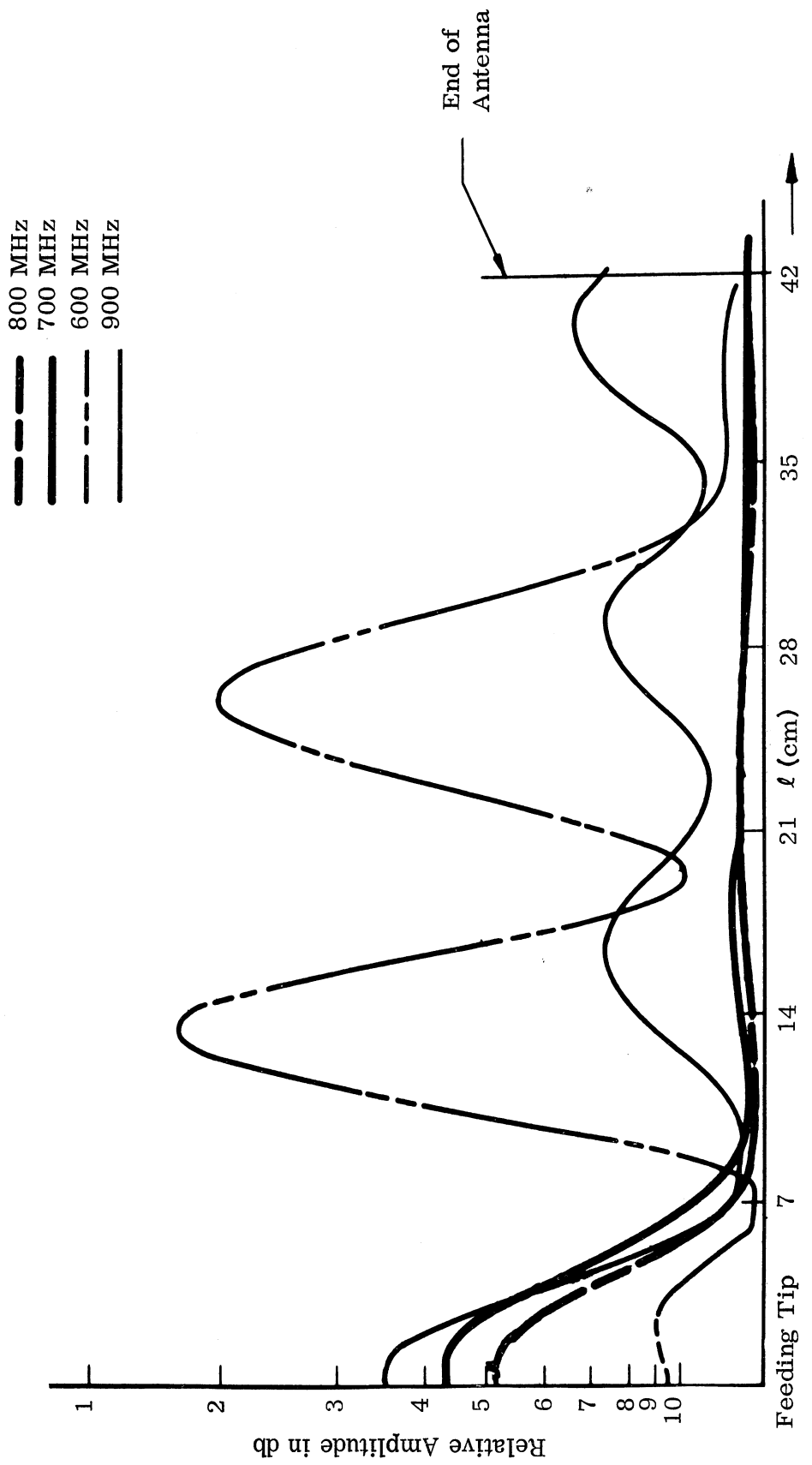

FIG. 3-32: NEAR FIELD AMPLITUDE OF ANTENNA NO. 217. PROBE POSITION $\lambda/6$ ABOVE ANTENNA SURFACE, NO LOADING.

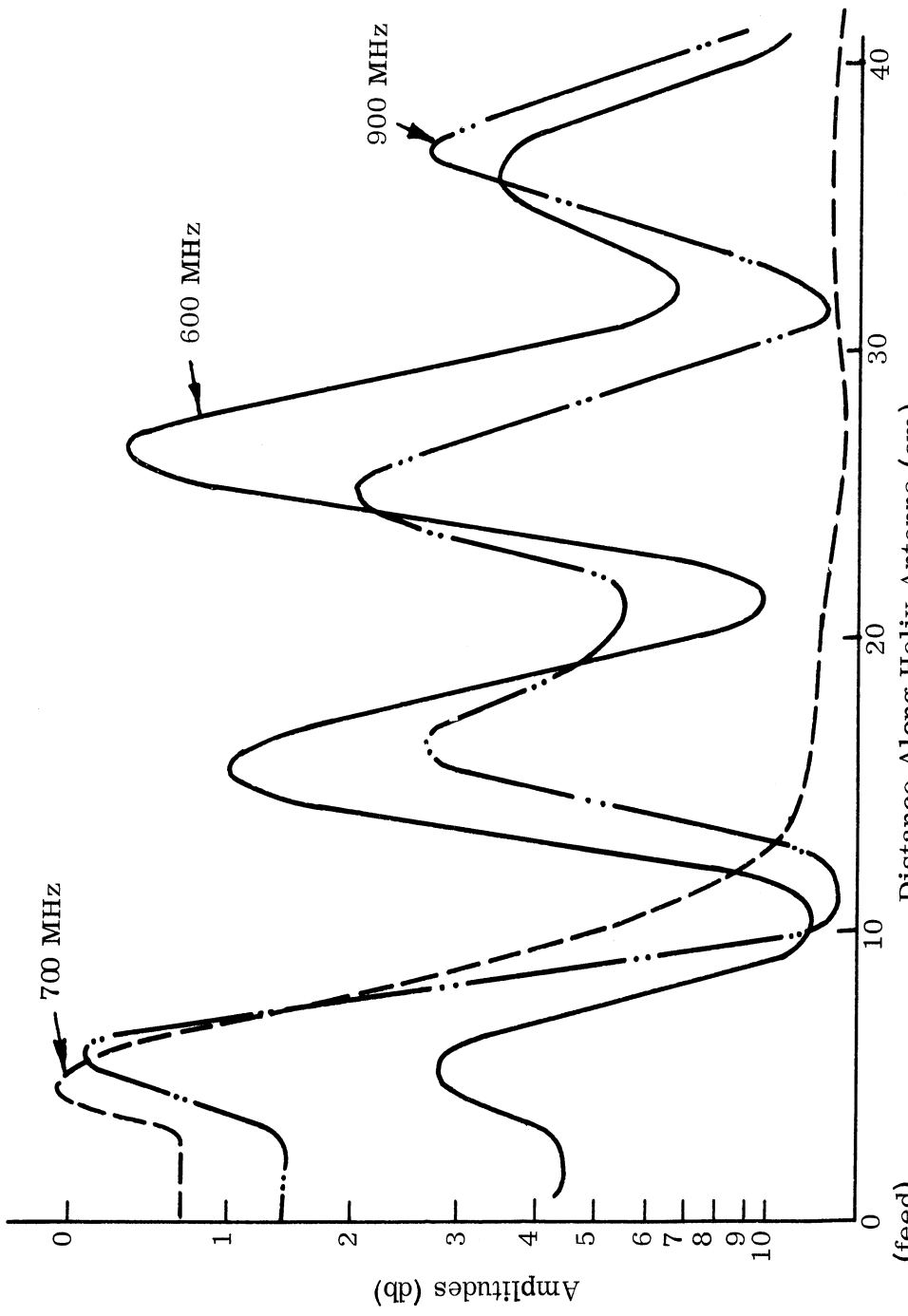

FIG. 3-33: NEAR FIELDS OF HELIX NO. 217 WITH 3" DIAMETER METAL CORE

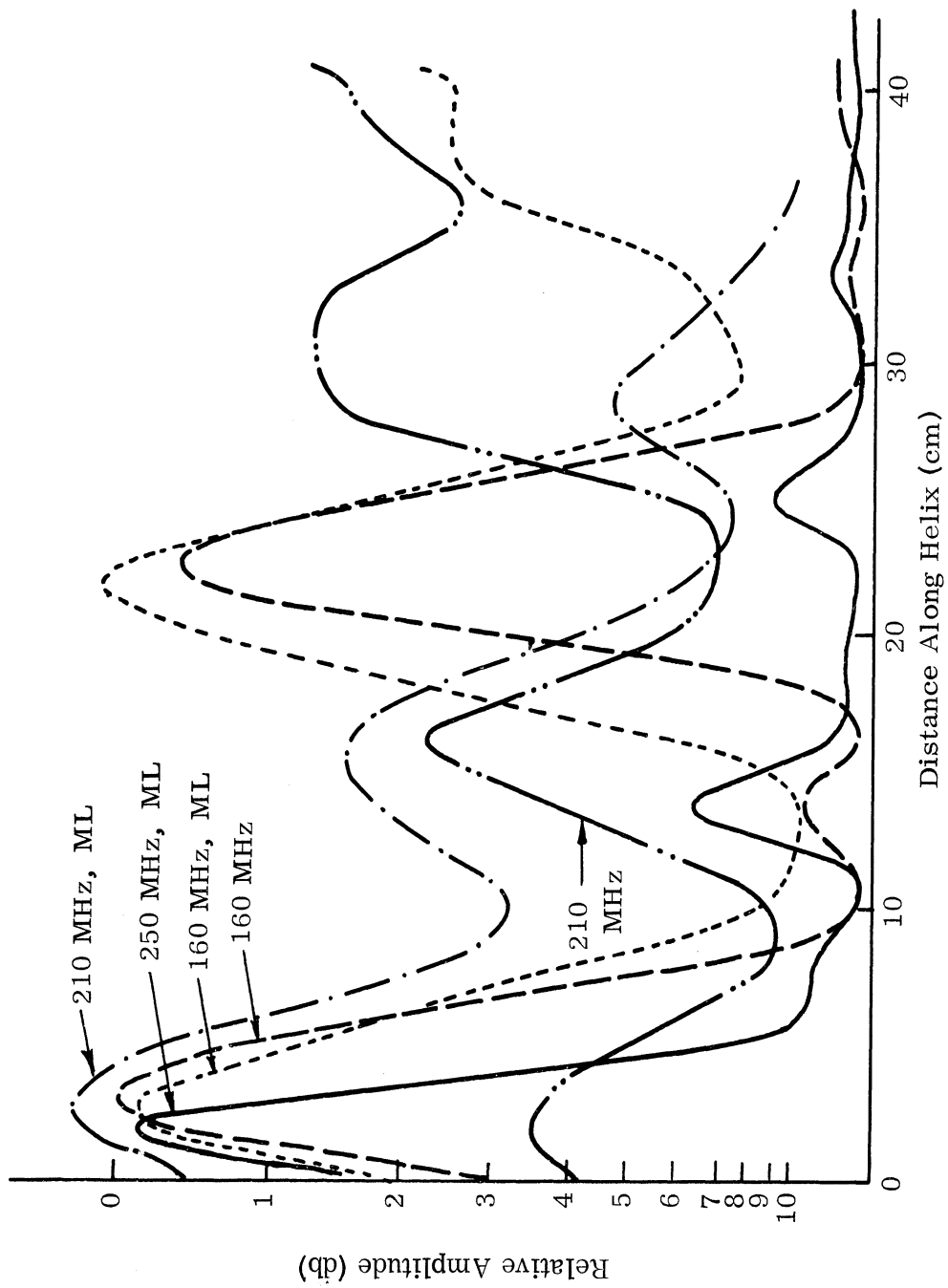

FIG. 3-34: NEAR FIELDS ALONG HELIX NO. 217, WITH AND WITHOUT 3" DIAMETER METAL CYLINDER LOADING (ML INDICATES METAL LOADINGS) DIAMETER OF HELIX NO. 217 = 4.65"

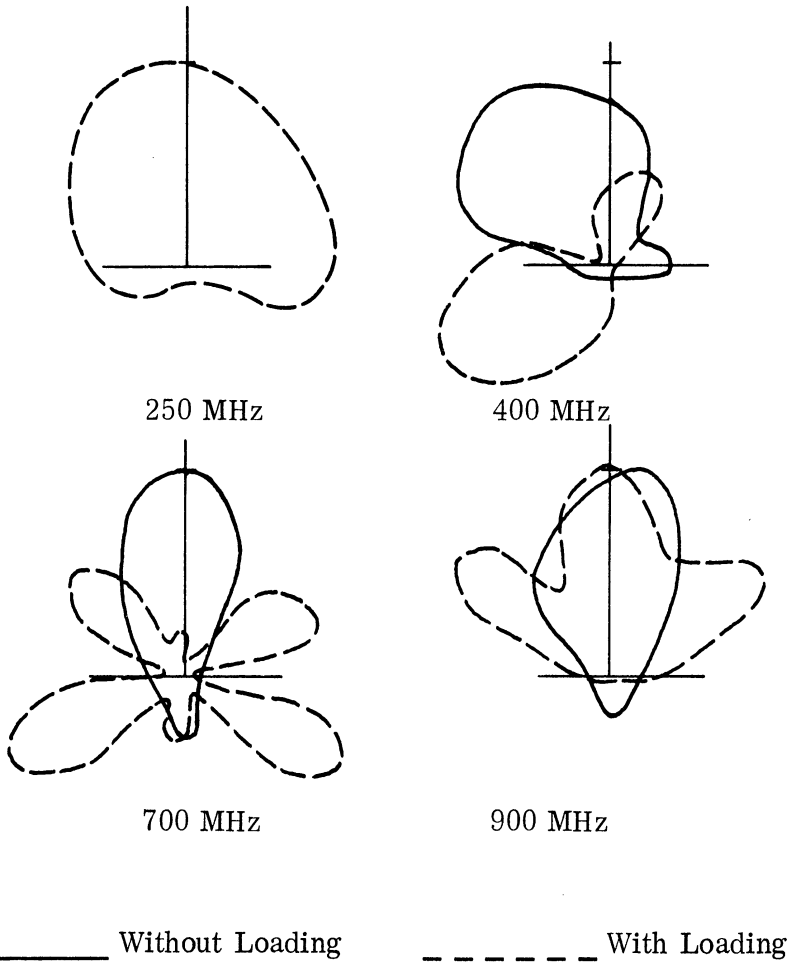

FIG. 3-35: BIFILAR HELIX 217 (4.5" Dia.) WITH AND WITHOUT 3" DIAMETER METAL CYLINDER LOADING.

obscures the facts. Since this experimental work was performed, a theoretical study of the problem has appeared (Neureuther, 1967). This tends to confirm the experimental results that metal cores will not produce significant size reductions.

3.5 Dielectric Loading

3.5.1 Dielectric Loading of Conical Helices

It is well known that a conical helix antenna can be considered a series of infinitesimally small helix antennas centered on the axis of the cone with progressively larger diameters toward the base. Although not strictly true, this is a good approximation which can be justified by experiment.

The following generalizations can be made about conical helix antennas. 1) Increasing the cone angle increases both the half-power beamwidth and the backlobe level. 2) Increasing the wrap angle slightly decreases both the beamwidth and sidelobe level. These conclusions have been verified experimentally and theoretically (Dyson, 1965).

Similarly, the following conclusions can be surmised concerning a helix antenna. 1) Increasing the length of a helix reduces the beamwidth and the backlobe level of the field pattern. 2) On the basis of pattern shape, the broadest bandwidth occurs at a pitch angle of 18° (corresponding to a wrap angle of 72° for a conical helix with a cone angle of 0°, (Kraus, 1950).

Prompted by the results of many experiments on loaded and unloaded helices and conical helices, a theory has been devised to explain and summarize the results of loading (Hong, et al, 1966; Shestopalov, et al 1961). Hong and Rassweiler, using a sheath helix model, point out that the diameter of a helix antenna can be reduced by the multiplicative factor $\sqrt{(1 + 1/\mu) / (1 + \epsilon)}$. Shestopalov, et al (1961) derive results that lead to the same formula based on a variational solution of tape helix model. Nothing is said, however, about length. Hong and Rassweiler (1966) apply this formula to the conical helix on the assumptions mentioned previously.

If only the diameter can be reduced, a loaded helix or conical helix will give the same field patterns only if the pitch angle is decreased to its former value (i.e. increase the wrap angle). Since the pitch distance along the axis and π times the diameter are legs of the right trinagle which has the winding length per turn as the hypotenuse, this is a necessary condition. Reducing the diameter without reducing the pitch would increase the pitch angle, which is one of the specified parameters for helix and conical helix antennas.

The second conclusion drawn is that in a conical helix antenna, a loaded antenna will produce approximately the same antenna patterns as an unloaded one only if the cone angle is reduced to the point that the length of the loaded and unloaded cones are the same. This is clear if the conical helix is considered a series of helices of infinitesimal length whose diameters are progressively increasing toward the base of the cone. The length of each infinitesimal helix comprising the loaded cone can maintain the same length as its unloaded counterpart only if the cone angle decreases. That is to say, the radius and the distance from the tip to the plane of the base of a conical helix form legs of a right triangle which has an element of the cone as its hypotenuse. Thus, to maintain the same length of the cone when the diameter is reduced, the cone angle must be reduced.

The experimental data taken on this project and published in the previous reports on this contract (Ferris, et al 1965, 1966a, 1966b) all verify this theory. Note that in the loaded sections of the conical helices, the near field patterns appear to "run out of antenna" from which to radiate even though the energy appears to move up the cone. It is also noted that when the antenna radiates from the loaded region, the beamwidth and backlobe levels are up and the efficiency is down.

Lengthening the conical helix in the loaded region (by reducing the cone angle) would definitely reduce the backlobe level and decrease the beamwidth. This would be analogous to lengthening an unloaded helix or conical helix. A further improvement would be achieved by increasing the wrap angle. This could be thought of as increasing the number of turns per inch in the loaded region. However, the effect would not be too great since the critical antenna pattern parameters are not a sensitive function of the wrap angle.

Applying this to the prototype delivered May 1966, the electrical performance could probably have been improved by 1) increasing the wrap angle in the loaded region, and 2) decreasing the cone angle.

In conclusion, it appears that magneto-dielectric loading of conical helices will not reduce the length appreciably, but will reduce the diameter of the bases.

3.5.2 Experiments Involving Very High Dielectrics

It is possible that a thin layer of a very high dielectric material could give a reduction in size and still be relatively lightweight due to the small amount of material used. Powdering such a dielectric and dispersing it in a light foam could produce a very lightweight dielectric but with a very much reduced dielectric constant. An additional experiment involving dielectric loading of a helical antenna was conducted to check these possibilities.

Barium titanate (Ba TiO_3) and titanium dioxide (TiO_2) were used as a loading material because the dielectric constant in solid form range from about 80 to almost 1000, depending on the form of the crystal structure. The materials were tested in powdered form.

Although these powders have not been tested for basic properties, the effects when loaded into helix antennas were ascertained. A reduction of more than 2:1 was hoped for if the dielectrics were of sufficiently high ϵ. The theory indicates that large reductions should be possible with very high dielectric constants, even though the theory has drastic limitations on its validity for a high dielectric constant.

Figure 3-36 shows the near fields of a small 2" diameter helix antenna (No. 218) when unloaded. The helix has a resonance frequency of approximately 1700 MHz and a band of operation from 1600 - 1800 MHz, consistent with the small size of the helix. A series of measurements was made in the near and far fields of Antenna 218 when fully loaded inside with these powders. Figure 3-37 shows the near field of Antenna 218 when loaded with a full core of powdered barium titanate. A frequency of about 1200 MHz is seen to be the resonant frequency where the field drops quickly, indicating a small, highly active region near the feed point. When compared with the region 1600 - 1800 MHz for the unloaded antenna, it is seen that a reduction down to approximately 2/3 of the unloaded diametrical size has been achieved. In antenna patterns, titanium dioxide powder was used for both antenna 217 and 218 to observe any change in resonant frequency.

Figure 3-38 shows antenna patterns of the bifilar helix Antenna 218 filled with titanium dioxide powder. It is apparent that except for 400 MHz, no substantial change for the better is indicated with the titanium dioxide powder, and that very little change of any sort occurs. At 400 MHz, however, the powder substantially imporves the forward lobe of the antenna. This indicated some effectiveness of the powder exists at low frequencies, but certainly not as great as a 2:1 reduction in diameter. An even lesser effect is noted in Fig. 3-39 which shows helix Antenna 217 loaded with titanium dioxide powder. Although the high end of the helix pattern is improved with the titanium dioxide, for reasons that have not as yet been discovered, the low frequency end is slightly worse with loading than without. Frequencies lower than 400 MHz would have been desirable and therefore, Fig. 3-38 is of more value in seeing the low frqueency behavior of dielectric powder.

A tentative conclusion is that the powders have rather low dielectric constant in spite of the high dielectric constant of the solid forms of the chemicals. The Lichtnecker Rule (Condon, 1958) for the dielectric constant of a solid-air mixture is $\log (\epsilon_{total}) = \alpha \log (\epsilon_1)$, where α is the percentage of solid material and ϵ_1 is the

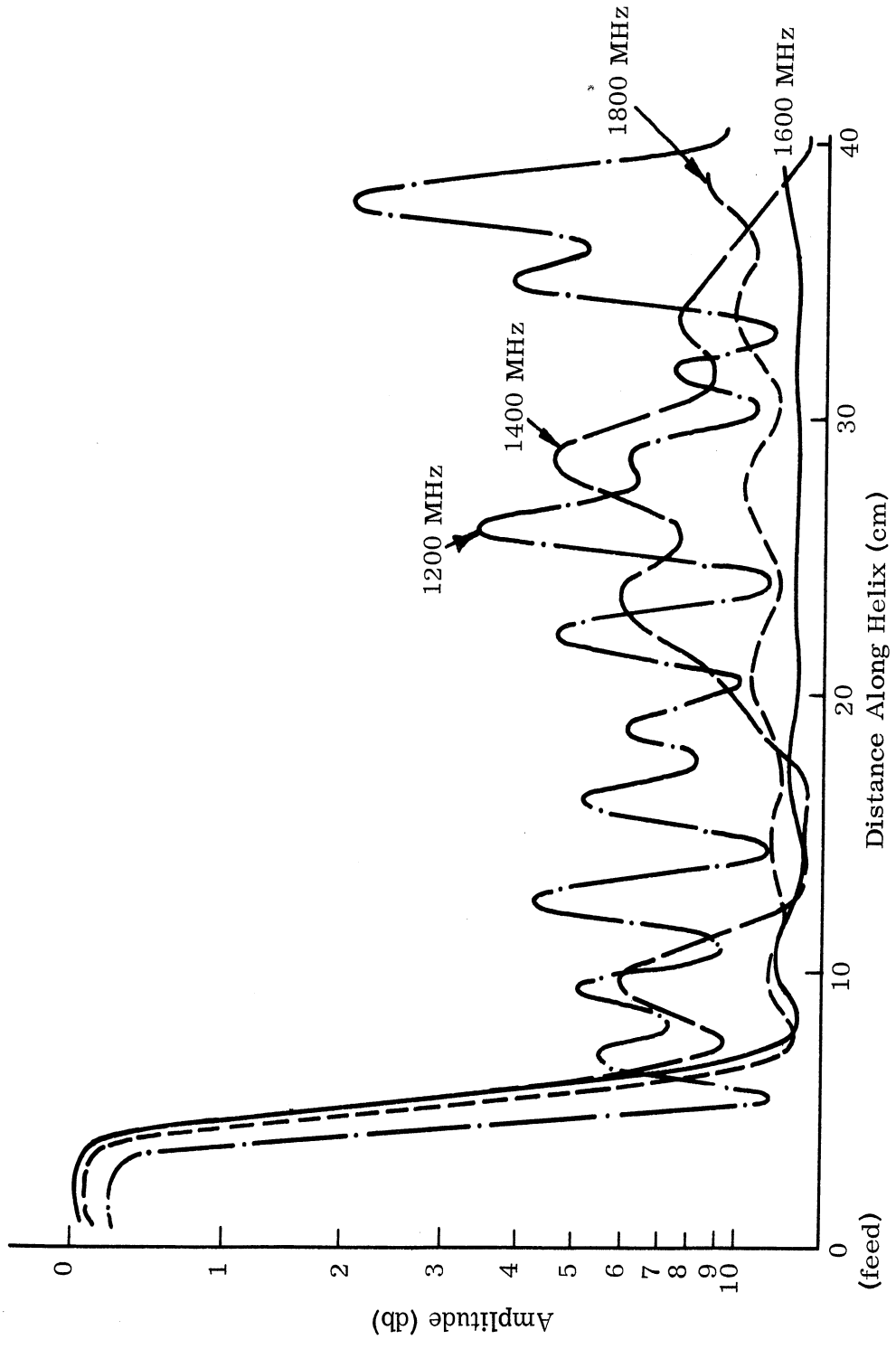

FIG. 3-36: NEAR FIELDS ALONG HELIX NO. 218 UNLOADED

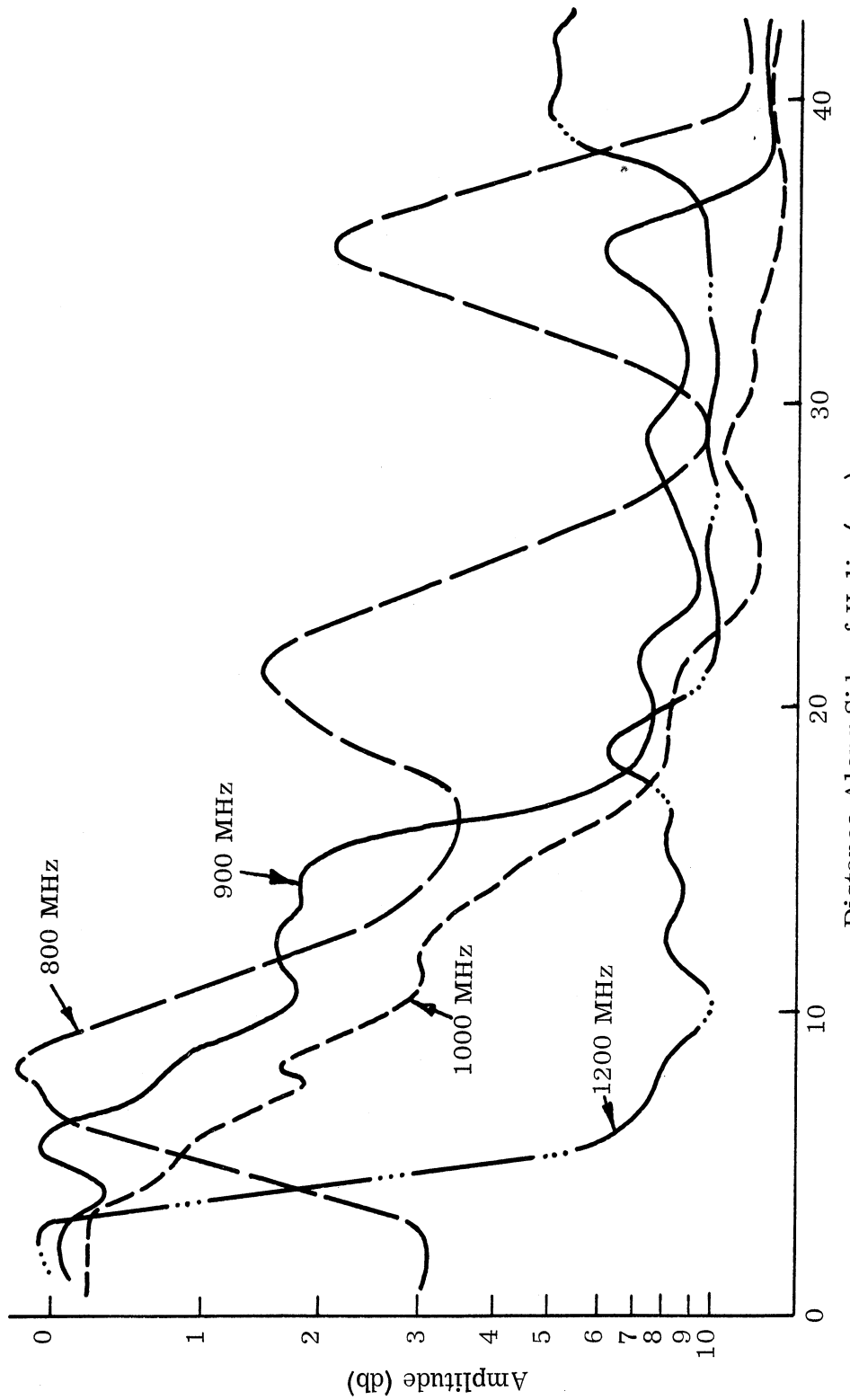

FIG. 3-37: NEAR FIELD OF ANTENNA 218 WITH POWDERED $BaTiO_3$ FULL CORE LOADING (PROBE DIST. $=\lambda/10$)

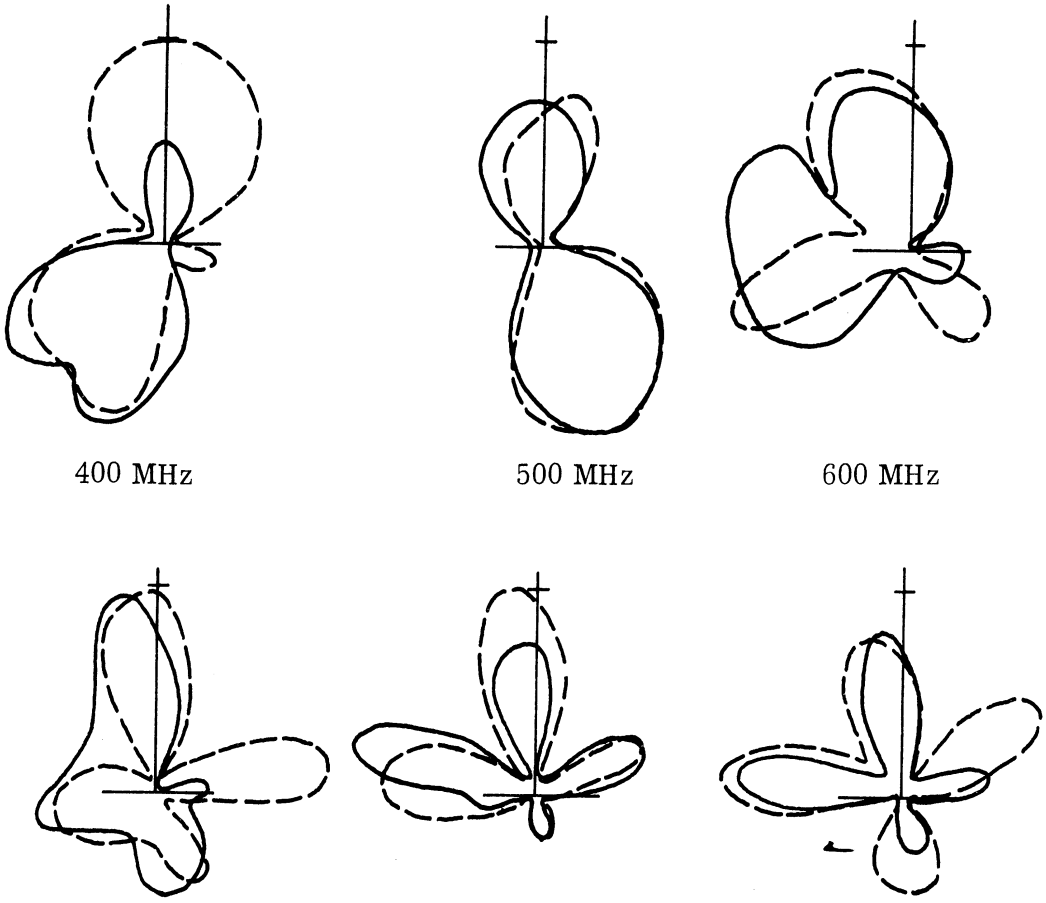

FIG. 3-38: BIFILAR HELIX NO. 18 FILLED WITH TiO_2 POWDER

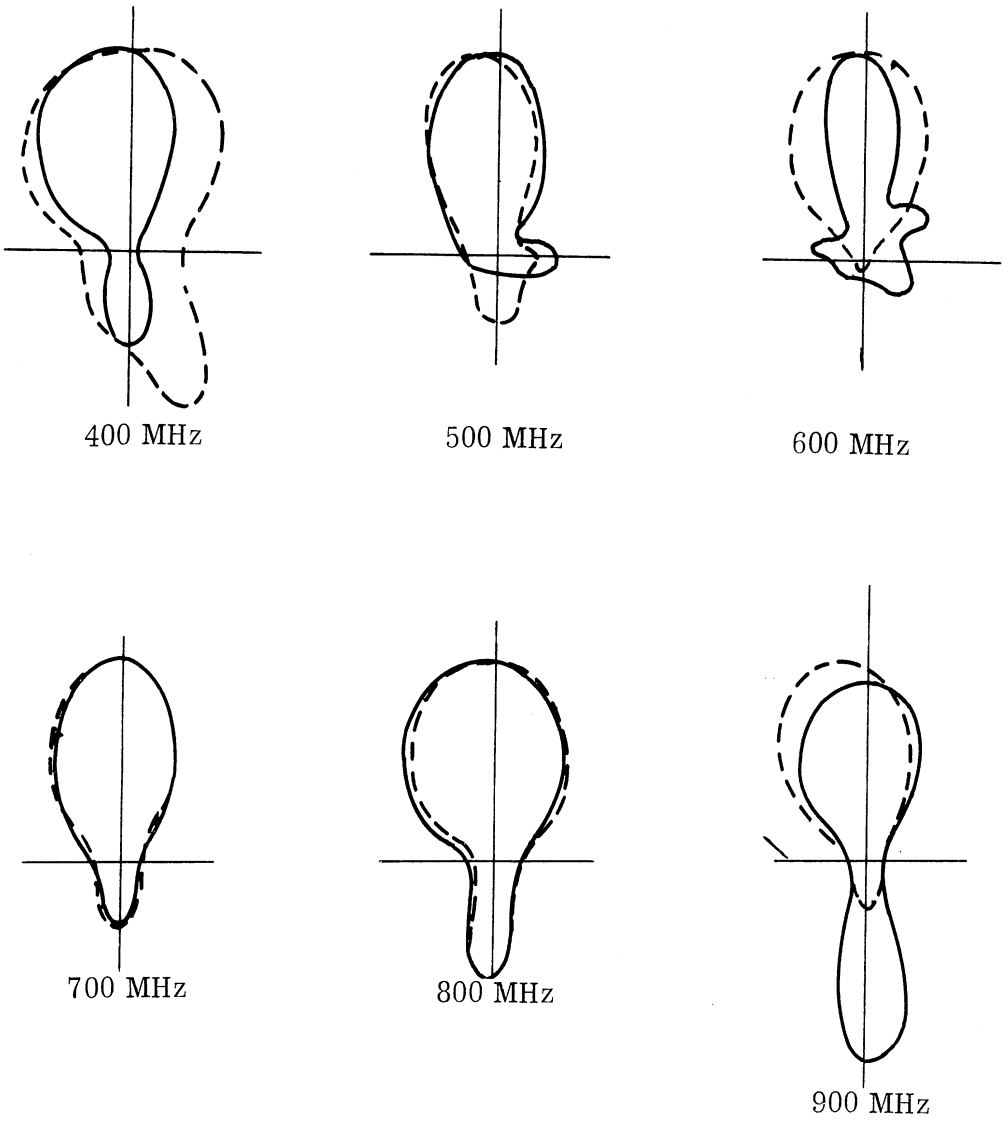

FIG. 3-39: TiO_2 LOADING OF BIFILAR HELIX NO. 217
3/8" LAYER INSIDE. 400 - 900 MHz.

dielectric constant of the solid material. For the case of $BaTiO_3$, the resulting ϵ of the powder was less than 10, thus verifying the experimental results.

3.6 Higher Mode Suppression

One of the problems encountered in reducing the size of conical helices has been the excitation of higher modes. With some loadings, these modes propagate along the structure and radiate, causing high backlobes or sidelobes. The interim report covers several techniques (Ferris, et al, 1966). Two additional techniques have been given consideration in this report period.

The first is the use of multifilar windings to suppress higher modes. Multifilar helices have been used successfully as antenna (Gerst and Worden, 1966). The reason is that a helix with n windings cannot support either the first n modes or their harmonics. Thus, power is not lost in exciting these modes since they cannot exist. Hence, the efficiency is high.

One drawback to this construction is that each winding must be fed so that the phase difference between successive windings is $2\pi/n$ radians, where n is the number of windings. Since high power versions of equipment for producing the required phase shifts over a 22 to 1 bandwidth are both expensive and difficult to make, this technique has its drawbacks. However, the mechanical construction of such an antenna is relatively easy.

An interesting feature of the Gerst and Worden paper is the size reduction and high bandwidth obtained with a multifilar helix. Unfortunately, the techniques described apply only to the forward-fire mode of operation. This is the type of helix operation originally discovered by Kraus (1950). The backward fire of Patton (Walter, 1965), which is almost always used to excite a conical helix, is not amenable to size reduction by this technique. This technique is discussed more thoroughly in Section 3.7.

The other higher mode suppression technique considered was the use of a resonant turn placed in back of a conical helix to act as a director. For many years radio amateurs have been using such a technique in an antenna they call the Cubical Quad (Orr, 1959). The cubical quad antenna consists of equal sized loop antennas cut to resonate at a particular frequency. One is fed at the midpoint of a side, while the other has an open circuited transmission line connected at the corresponding midpoint. The second loop is tuned by adjusting the length of the shorted transmission line until the loop acts as a director. Design parameters are given by Orr for both two element and three element antennas.

Antenna 223 L-2, which is a scale model of the prototype delivered last spring under Task 3, was modified to test the application of the tuned loop reflector to a conical helix. It may be recalled that in the dielectric loaded region of this antenna, higher modes were excited that produced a high backlobe. The modification consisted of adding a polyfoam core which protruded out the back, making an extension of the winding planes of the antenna. A turn was wound on this extension at one-tenth wavelength (at 250 MHz) from the plane of the base of the antenna. The one-tenth wavelength spacing is about the minimum feasible distance indicated by Orr's data. The 300 Ω twin lead transmission line tuning stub was adjusted to different lengths while taking patterns at 250 MHz. Some effect on the backlobe was noted, but the maximum effect was no more than about 1 or 2 db. Apparently this technique is not efficacious and, besides, it increases the required axial length.

3.7 Multifilar Windings

3.7.1 Introduction to the Mulfifiler Helix

A reduction in conical helix antenna diameter may be accomplished by changing the phase velocity of the current on the antenna wires, but the radiation leakage rate still may require the antenna length to remain essentially constant in order that a sufficiently long active zone may occur. One possible way to avoid the radiation leakage-rate problem is to use a forward-fire helix mode.

Recently, quadrafilar and octafilar helix antennas have been built that show a great reduction (4:1 or more) in diameter over a standard conical helix can be achieved (Gerst and Worden, 1966). The reduction in diameter actually occurs because the pitch angle of the helix is made rather large (22^{o} or more). A study of the $k - \beta$ diagram is helpful in understanding the relation between pitch angle and size. Higher order modes that would occur on the conventional monofilar antenna are suppressed by the use of several windings and an appropriate feed to excite the desired forward-fire (Kraus' T_1) mode. The actual sizes are determined in Gerst and Worden (1966) as a function of the number of windings on the helix; Table III-5 shows, for four different windings on a helix, the maximum and minimum normalized helix sixes, C_λ (circumference in wavelengths), for a single mode operation with maximum bandwidth. The pitch angle necessary to achieve this maximum bandwidth is also shown. Of course, these sizes, C_λ, are usually used to calculate the frequencies of operation for a given size helix. For the quadrafilar antenna, Table III-5 shows that a helix diameter of $.33\lambda$ still allows forward radiation. In contrast, the log conical antenna requires a base circumference greater than 1.0λ for complete radiation at the lowest frequency. A circumference of 1.2 to 1.5λ has been found necessary for small pitch angles and wide cone angles if no base

loading is used. Thus an approximately 4:1 reduction in diameter of the quadrafilar helix over the log-conical helix is accomplished.

In another report (Syracuse, 1966), an unclassified portion shows more details of the measurements of this antenna, and shows that the length of a quadrafilar helix must be greater than $.3\lambda$ for VSWR < 3.0. Thus a 50 MHz quadrafilar helix antenna is still limited to 2 meters (approximately 6 feet) minimum length for effective forward radiation and reasonable VSWR, even though a more than 4:1 reduction in diameter can be achieved. With this knowledge of a limitation in the possible length reduction of the forward-fire helix, it would appear desirable to investigate the backward-fire multifilar conical helix.

TABLE III-5

Helix Parameters for Greatest Bandwidth for Four Different Windings, $C_\lambda = 2\pi R/\lambda$ condition-forward radiation*

Type of Helix Winding	Largest C_λ		Smallest C_λ		Pitch
	Theoretical	Experimental	Theoretical	Experimental	
Monofilar	1.5		.67		22^o
Bifilar	1.8		.54		32^o
Quadrafilar	2.2	1.5	.43	.33	42^o
Octafilar	3.0		.32		54^o

3.7.2 Ground Plane Size

Most characteristics of the quadrafilar helix have been investigated in the references cited. However, a topic that appears to have been omitted from studies to date is the size of the ground plane necessary to launch the forward radiation mode. Pictures in the report by Syracuse (1966) show a ground plane more than four times as large as the helix. If such a ground plane is necessary, its size partially invalidates the diameter reduction of the quadrafilar over the conical helix.

*Reference, Gerst and Worden, 1966; Syracuse, 1966.

A quadrafilar helix was constructed in this laboratory, antenna 236, with a rather small ground plane, 4" x 4" square. The far field patterns are shown in Fig. 3-40. Since the helix was 2" in diameter, the frequency corresponding to a one wavelength circumference is 1900 MHz; the frequency corresponding to .33λ which would be according to Table III-5 the lowest frequency of operation with a large ground plane, is 630 MHz. Figure 3-40 shows that indeed, even with a small ground plane, the lowest frequency of operation is 650 MHz. Thus the antenna appears to be a good candidate for an antenna of reduced size. Additional patterns were taken using only the shield of the four BNC panel connectors as a ground plane. The shields were all connected together and patterns were taken. The patterns were essentially the same as those shown in Fig. 3-40.

3.7.3 Nested-Helix Antenna

Although forward-fire multifilar helices can be made with bandwidths of 8:1 or more, the forward-fire helix does not have a constant beamwidth characteristic such as the log-conical device. A backward-fire multifilar log-conical helix is a definite possibility; however, another possible solution for a 22:1 bandwidth coverage is to use the usual bifilar conical helix for most of the frequency range and a quadrafilar helix for the low frequency end. The physical arrangement could be as in Fig. 3-41, with the small high frequency log-conical antenna inside the large, low frequency quadrafilar helix. Figure 3-42 shows a possible feed network for such an antenna, using a low-pass filter to eliminate excitation of the quadrafilar at the high frequency end of operation.

In order to check whether the outer quadrafilar helix windings would interfere with radiation from the inner, conical helix at high frequencies, an experiment, the conical helix, antenna 234, was approximated by the pyramidal helix which had a base 2.5" square, corresponding to a cutoff frequency of approximately 1400 - 1700 MHz. The pyramidal helix was placed inside a quadrafilar helix, antenna 237, of 4" diameter (nominal frequency range, 350 MHz-1600 MHz) in two different positions, as shown in Fig. 3-43. Far field antenna patterns were taken, as shown in Fig. 3-44, to ascertain the amount of shielding effect the outside quadrafilar antenna would have upon the radiation patterns of the pyramidal helix. As can be seen in Fig. 3-44, the outside antenna had considerable effect, even when the pyramid was placed at the open mouth of the helix and especially at the low frequencies where the active zone of the pyramid is near its base, nearer to the surrounding helix, and further back from the mouth of the helix. Position 2 gave better patterns than position 1, even though in position 2 the pyramidal helix is further recessed into the surrounding quadrafilar than in position 1. The reason is probably that the quadrafilar is contributing to the radiation in position 2.

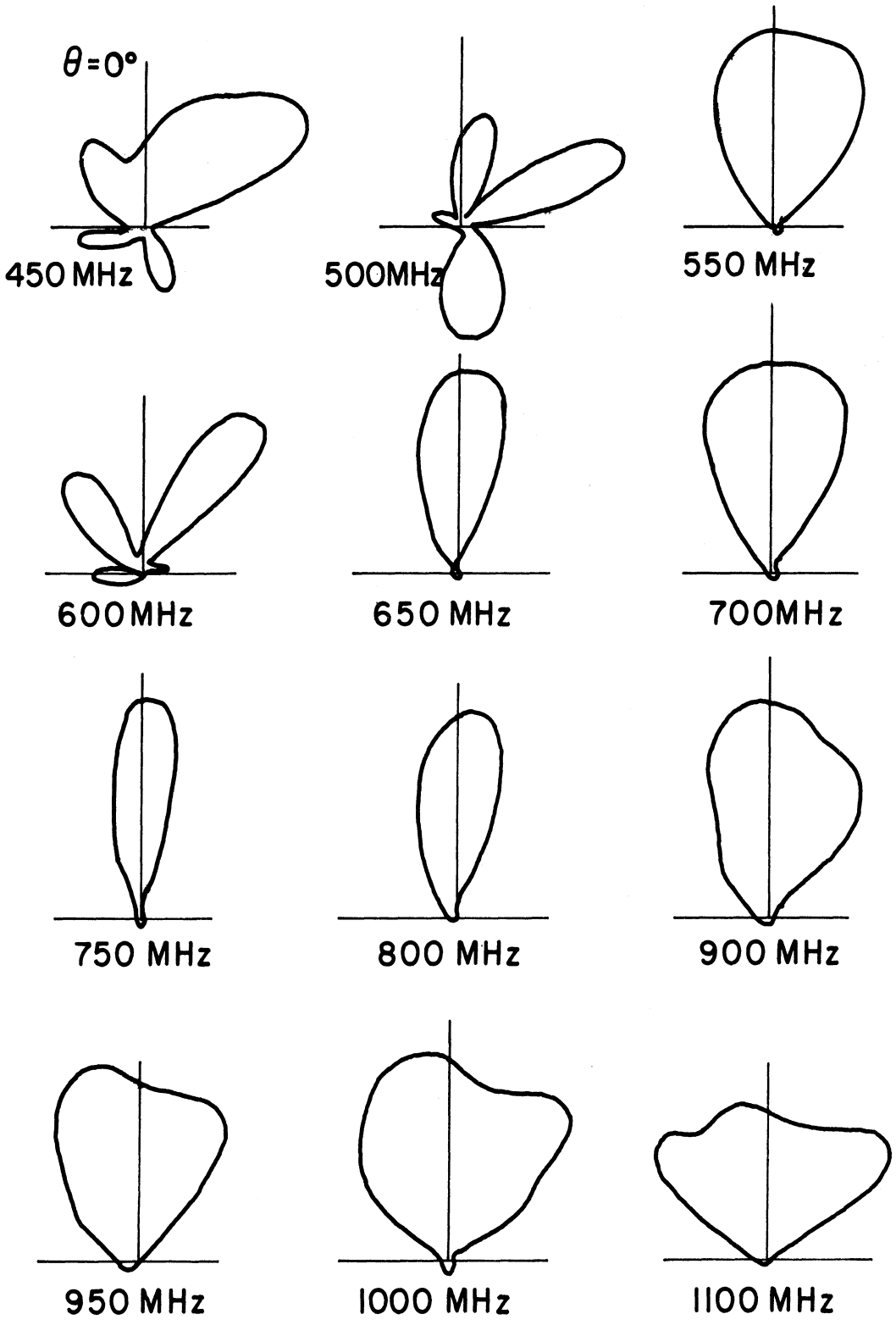

FIG. 3-40: THE QUADRAFILAR HELIX, Antenna 236, 2" Diameter, Plots of $|E_\theta|^2$.

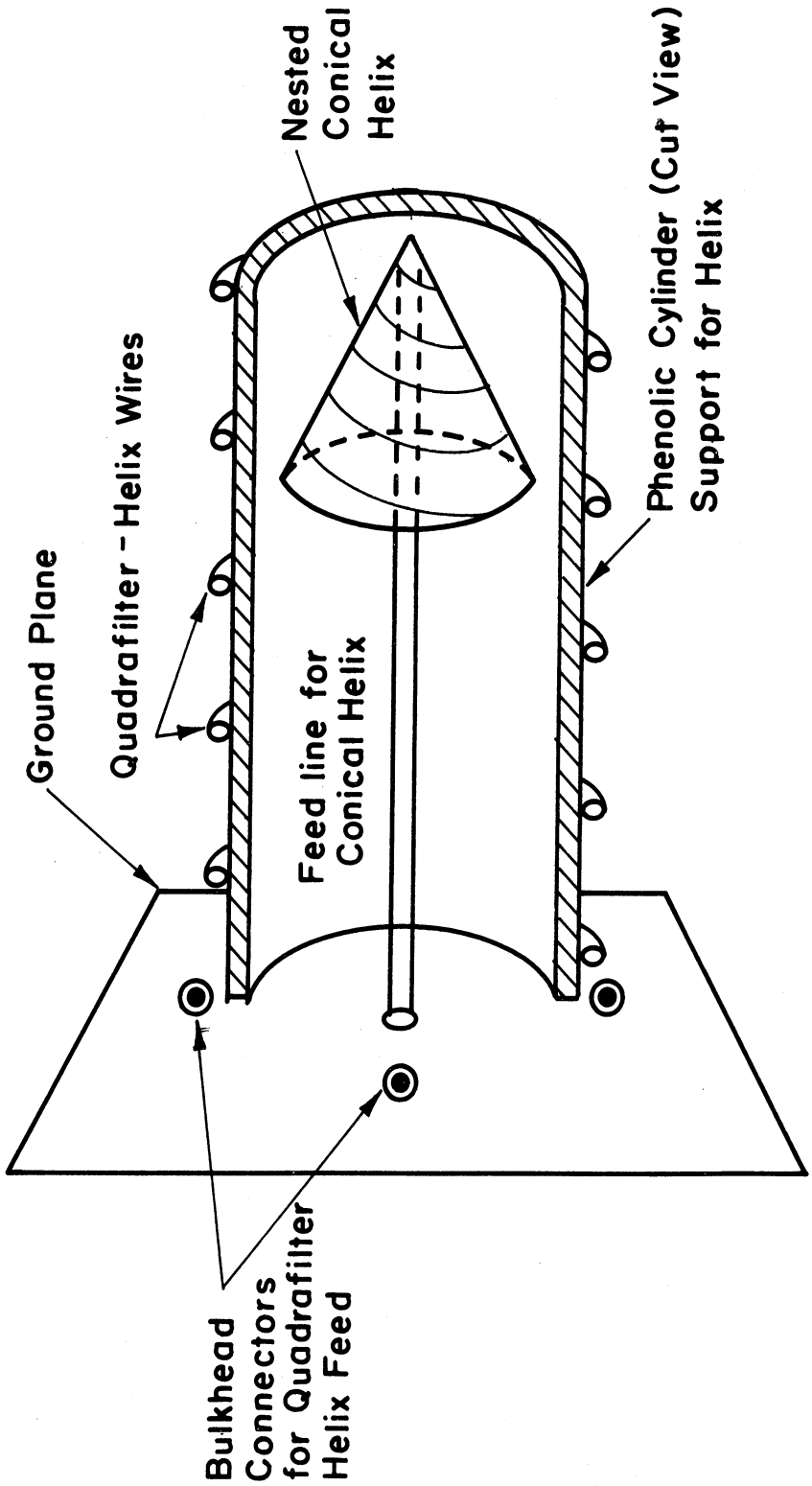

FIG. 3-41: A NESTED HELIX ANTENNA.

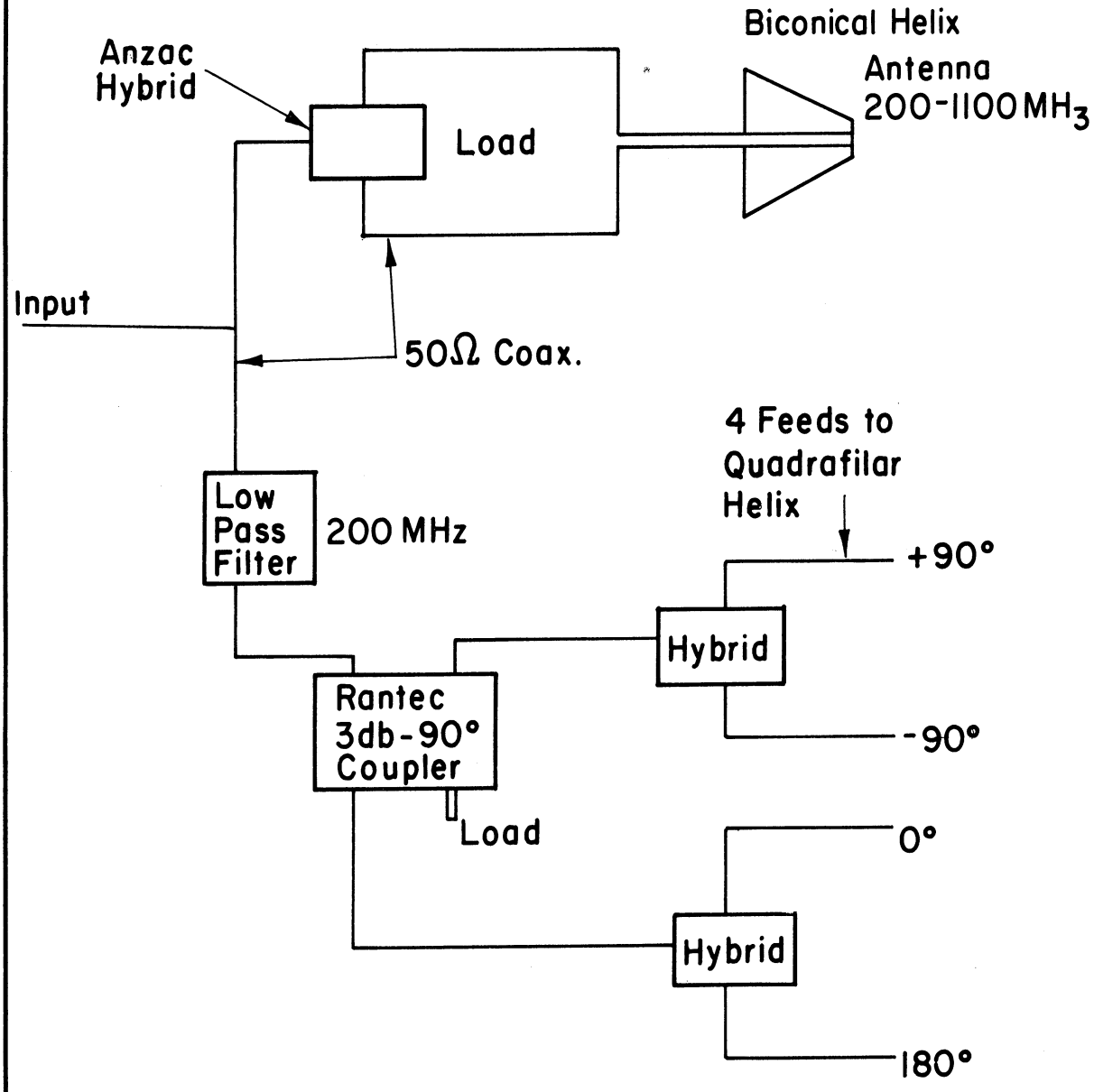

FIG. 3-42: FEED NETWORK FOR NESTED HELIX ANTENNA.

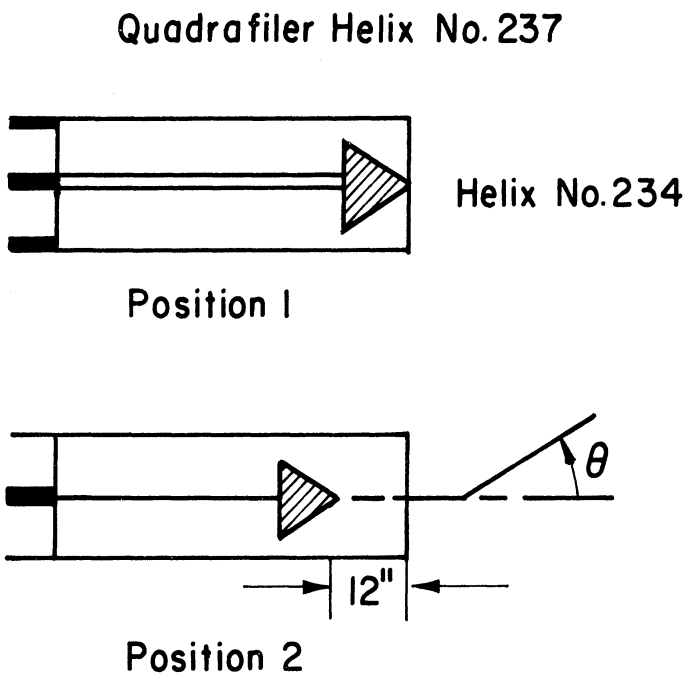

FIG. 3-43: POSITIONS OF NEXTED HELICES FOR ANTENNA PATTERNS.

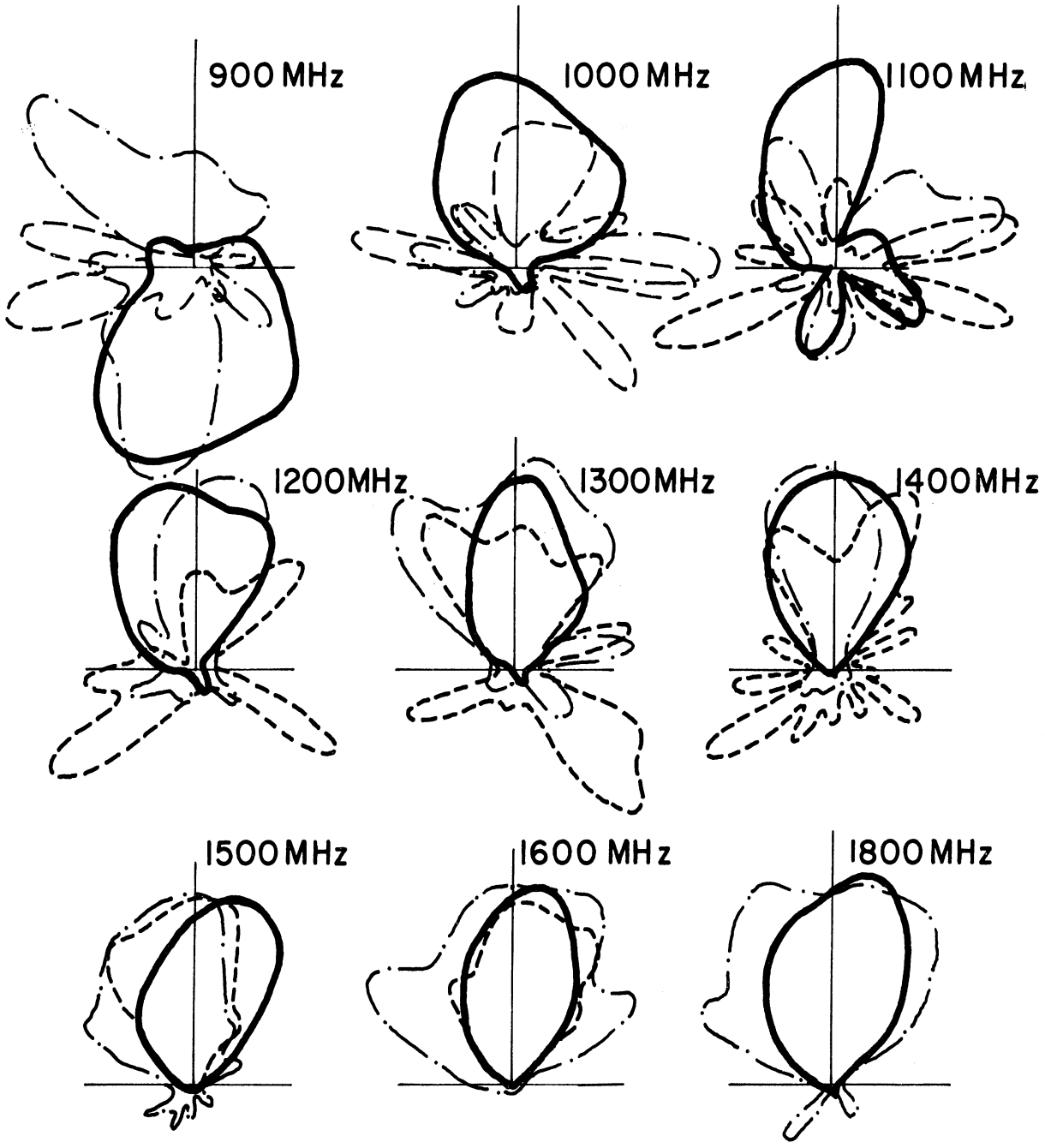

FIG. 3-44: INTERFERENCE OF UNFED QUADRAFILAR HELIX WITH FED NESTED PYRAMIDAL HELIX ; (---) Pos. 1, (—·—·—) Pos. 2 in previous figure; plots of $|E_\phi|^2$, (——) Pyramidal Helix Only.

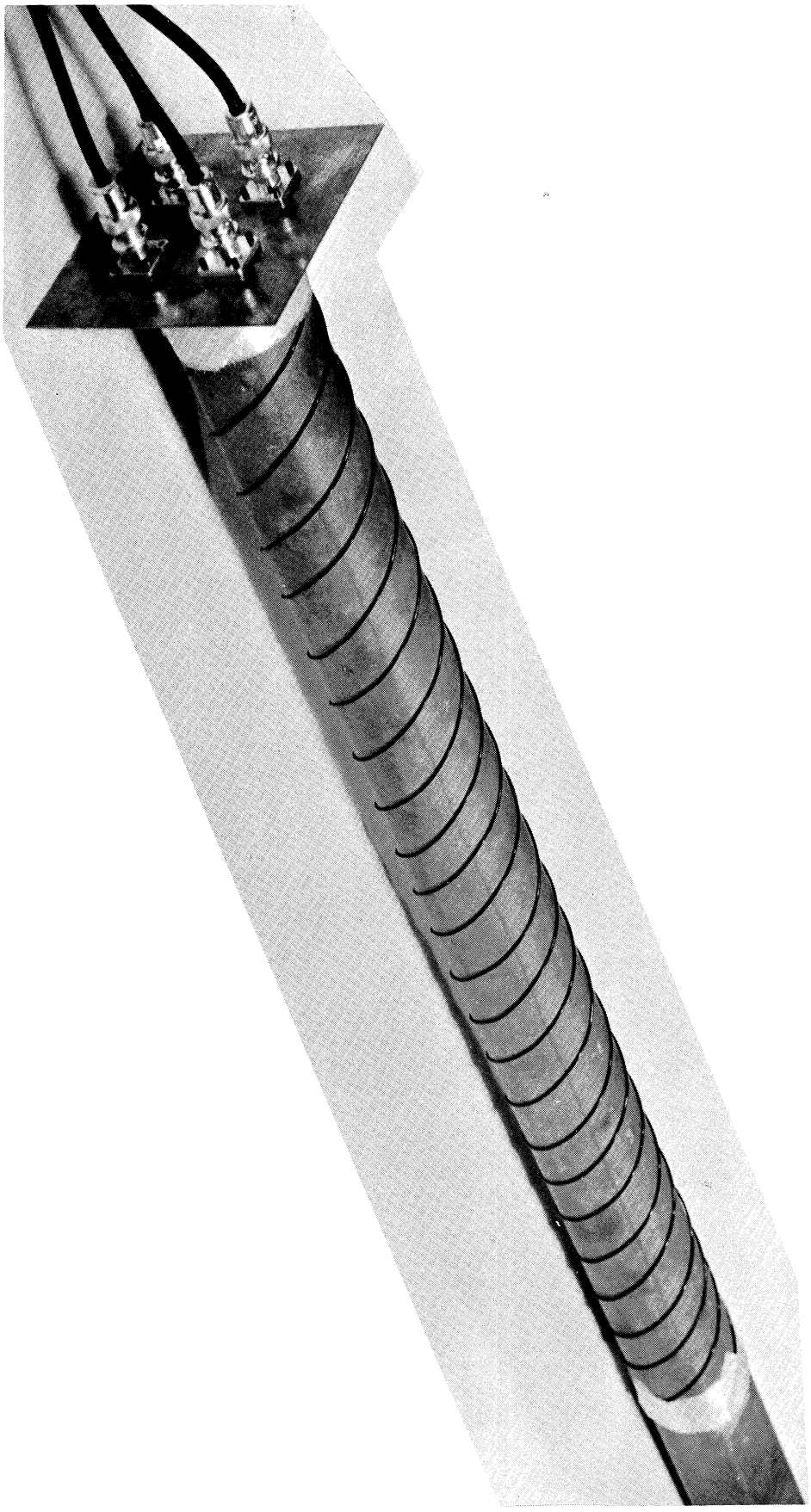

FIG. 3-45: ANTENNA 236, QUADRIFILAR HELIX ANTENNA.

As a result of this interference measurement and the lack of knowledge about the ground plane, as well as the difficulty in obtaining an adequate 3 db 90^{o} coupler for the feed network, the quadrafilar helix was not used in the delivered prototype, but remains a promising prospect. Table III-6 is the characteristics of all the multifilar helices discussed.

TABLE III-6

Characteristics of Multifilar Helices.
(all constructed of No. 18 wire)

Antenna No.	Type	Diameter (inches)	Pitch Angle ψ
236 (see Fig. 3-45)	Quadrafilar Cylindrical	2.1	40^{o}
237	Quadrafilar Cylindrical	4.2	40^{o}
234	Bifilar Pyramidal (35^{o} Cone Angle)	2.5" base	5^{o}

IV

BROADBAND OMNIDIRECTIONAL ANTENNA

4.1 Introduction

The design goals for the omnidirectional antenna are: 1) 10:1 frequency band coverage (0.1 to 1.0 GHz), 2) gain is to be 1.5 db above an isotropic source, and 3) the maximum diameter of the antenna is not to exceed two inches.

Antennas considered during this study may be categorized into two groups: 1) frequency sensitive trap elements, and 2) reactively loaded elements. The objective of the frequency sensitive trap elements was to utilize the traps to limit the current distribution to specific sections of the antenna, to effect the required radiation pattern and impedance characteristics. Experimental results employing the current trapping techniques (300-3000 MHz) have not proven to be satisfactory since at the design frequencies of this study high VSWR characteristics (> 3:1 with respect to the 50 Ω line) were observed for several trap antenna configurations. The currents flowing along the surface of several of these antennas were measured and the data revealed that significant current was flowing at the tip of the antenna, indicating the trap elements were not functioning as hypothesized. Antenna patterns for the trap configuration displayed a minimum of lobing, which was desirable. However, the main beam tended toward end fire at the higher frequencies typical of what may be expected for the current distributions measured. Because the traps did not properly control the flow of current along the surface of the antenna, the study of the trap concept was discontinued.

The second concept considered was the reactively loaded antenna described by Hallén (1962). Hallén's theory for the reactively loaded antenna suggests the use of uniformly spaced discrete reactive elements. The reactance (of each discrete element) is to vary such that it is a minimum at the feed and progressively increases to a maximum at the antenna tip to effect a "reflectionless" antenna. Intuitively the "reflectionless" antenna may be achieved employing either capactive or inductive elements. The initial model built by the University of Michigan (designed for convenience to operate from 300 - 3000 MHz) was capactively loaded employing uniform capacitance (employing 1 mil dielectric material). Results from this antenna were encouraging and are described further in section 4.3. It was found that by increasing the dielectric thickness, i.e., increasing the capacitive reactance improved the high frequency performance of the antenna, i.e., reducing variations in the VSWR, but raised the lower usable frequency. The final version utilized a capacitive distribution that increased in accordance with the theory discussed in section 4.2. This antenna displayed the familiar reduced low frequency performance but maintained the lowest overall VSWR (< 3:1) characteristics.

4.2 Theoretical Discussion of a Reactively Loaded Antenna

In section 4.1, Hallén's concept of realizing a linear broadband antenna has been discussed briefly. In this section, a qualitative discussion is given of the required current distribution along the antenna (hence the required distribution of reactive loading) which will be followed by the discussion on the feasibility of using either inductive or capacitive elements for the antenna loading. A specific design employing an exponentially increasing capacitive loading will be discussed. Finally, some details of the preliminary studies on the analysis of a reactively loaded antenna will be included.

4.2.1 Discussion on the Required Current Distribution

According to Hallén (1962), the amplitude of the current distribution (along the antenna) should decrease gradually toward the free end of a linear antenna to realize broadband impedance. During the present study it has been learned that the antenna surface currents are to be restricted to within a wavelength of the antenna input over the frequency range of interest to ensure that a pattern maximum occurs in the plane normal to the antenna axis over a broad range of frequencies. These considerations led us to choose an exponentially decreasing current along the antenna. Since the amplitude of the current along the antenna depends on the impedance per unit length along the antenna, it was hypothesized that if the reactive loading increased exponentially toward the free end of the antenna, that the required current distribution would be closely approximated. This form of reactive loading would also lend itself to theoretical analysis, as will be discussed later. The degree of exponential taper depends on the type of loading (capacitive or inductive), and the required frequency range, i.e., 10 - 100 MHz or 100 - 1000 MHz.

4.2.2 Feasibility Model

It is theoretically possible to obtain the required current distribution employing either capacitive or inductive loading (with the appropriate exponential taper) to achieve the required broadband frequency of operation. However, there are two essential differences (associated with the two types of reactive loading) which one should note. Assuming that the size of the reactive elements is negligible compared to the antenna length, an antenna loaded with inductive elements will be electrically longer (due to decrease in phase velocity) as compared to an antenna loaded with capacitive elements, i.e., to have the same electrical length the physical size of an inductively loaded antenna will be comparatively shorter than a capacitively loaded antenna. The second difference is the inductive reactance increases with frequency while the capacitive reactance decreases with frequency. Because the inductive reactance is directly proportional to frequency this causes the current distribution

of an inductively loaded antenna to be restricted primarily to the antenna input as the frequency is increased. This is the manner in which the current distribution should change to ensure that the radiation pattern will have a maximum in the plane normal to the linear antenna over the broad frequency (10:1) band. However, the capacitively loaded antenna has the opposite effect, i.e., the current is not restricted to the input, rather it is free to flow to the free end of the antenna.

From the above discussion, it is evident the inductive loading is preferred to capacitive loading. However, it does not appear feasible to achieve pure inductive loading in the frequency range (> 100 MHz) under consideration. This statement is substantiated from unsuccessful experimental results to be given in section 4.3 for inductive loaded antennas. It is believed that the inductive loading is more suitable to low frequency (< 100 MHz) applications (section 4.5).

Although the inductive loading is shown to be more desirable than capacitive loading, it has been found that capacitive elements are easier to fabricate in the frequency range above 100 MHz. If an antenna length of $\lambda_o / 2$ at the lowest frequency of interest can be tolerated, an antenna with capacitive loading and having the desired impedance characteristics and acceptable radiation patterns over a broad frequency range (10:1) can be fabricated.

4.2.3 Specific Design of a Capacitively Loaded Antenna

According to Hallén (1962) a linear broadband antenna may be realized by loading the antenna with reactive elements whose reactance increases toward the free end of the antenna. The loading is to be such that the resulting variation in surface impedance per square (impedance per unit length/circumference of the antenna) includes $Z_o = 377\ \Omega$ within its range of variation to effect a match between the antenna and free space. From the discussion of the previous sub-section, it is evident that because of the capacitive reactance is inversely proportional to the frequency, the antenna length over which appreciable current exists will increase with frequency. Therefore, to properly control the radiation pattern (to ensure a pattern maximum in the plane normal to the antenna axis) most of the current should be confined to a portion of the antenna (near the input terminal) which is a small fraction of a wavelength at the lowest frequency of interest. This will cause the current distributions at the highest frequency of interest to be confined to a portion of the antenna which is slightly less than a wavelength. To confine an appreciable portion of the current to a small fraction of a wavelength, of the antenna, it is necessary to have a large taper in reactive loading.

The antenna under consideration is shown in Fig. 4-1. The total length of the conducting portion of the antenna is 10 inches which is approximately $\lambda/4$ at 300 MHz. A conducting cylinder, having a diameter of 0.5 inches, with a small hole in the center, has been cut into 40 elements each 0.25 inches in length. The conducting cylinders are placed on a dielectric rod (6-32 threaded nylon rod) with dielectric discs (which form the capacitive elements) of different thickness placed in between the conducting discs, as shown in Fig. 4-1. The final goal of this study is to develop an antenna which is broadband and has a pattern maximum normal to the antenna axis over a 10:1 frequency band.

In our design, an exponential increase in capacitive loading is assumed. Assuming the loading at the input of the antenna is zero, the thickness of the nth dielectric disc (counted from the feed point) can be written as,

$$t_n = c\,(e^{\alpha z_n} - 1) \qquad (4.1)$$

where (c) and (α) are arbitrary constants to be determined. z_n is the length of the (nth) dielectric disc from the feed point and is given approximately by (nd), with (d) being the length of each conducting cylinder (= 0.25 inches).

To determine the arbitrary constants (c) and (α), we need to impose two conditions on equation (4.1). Since one should use a small reactance near the input and allow it to increase toward the free end of the antenna, the thickness t_1 is assumed to be 1 mil. Another condition to be imposed on equation (4.1) is for the thickness of the dielectric of the capacitive elements, to be such that the resulting variation in surface impedance per square (impedance per unit length/ circumference of the antenna) to include $Z_0 = 377\ \Omega$ within its range of variation. Since the exact value of the capacitance, of the capacitive elements, at the high frequencies (> 100 MHz) is much smaller than the static capacitance and somewhat larger than that obtained by considering only the skin depth, it was decided to use the mean of these two. These considerations led us to choose $c = 12.5$ and $\alpha d = 1/12.5$ so that equation (4.1) becomes

$$t_n = 12.5\,(e^{\frac{n}{12.5}} - 1) \text{ mils} \qquad (4.2)$$

(with this choice, $\alpha \approx 2K_0$ where K_0 is the free space wave number at 300 MHz). The values obtained from equation (4.2) are given below.

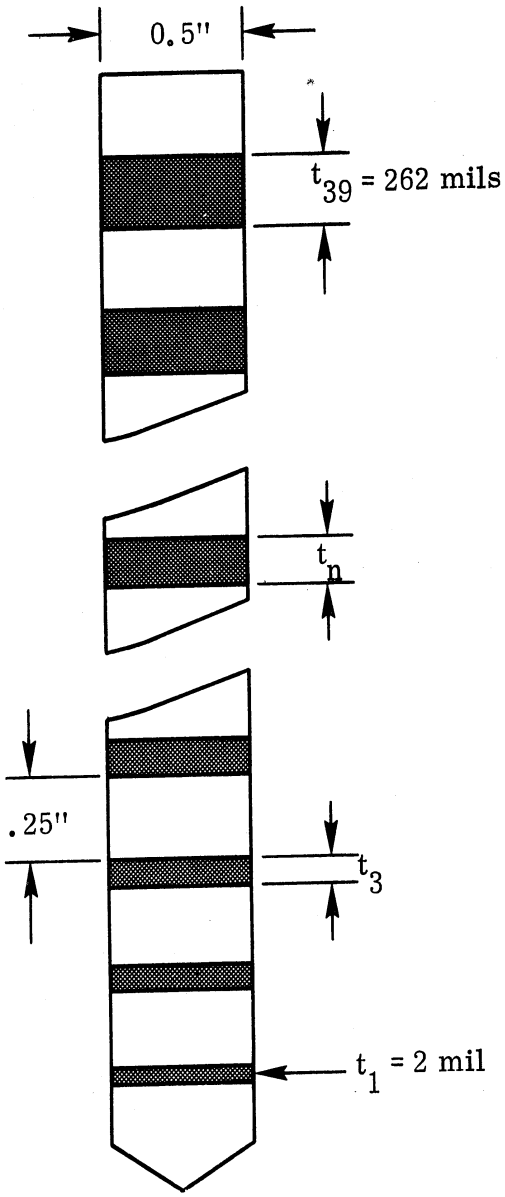

FIG. 4-1: LINEAR ANTENNA WITH EXPONENTIALLY INCREASING CAPACITIVE LOADING

n	1	2	3	4	5	6	7	8	9	10	11	12	13	
t_n	1	2	3	4	5	7	9	11	13	15	17	20	23	
n	14	15	16	17	18	19	20	21	22	23	24	25	26	
t_n	26	29	32	36	40	44	49	54	60	66	73	80	87	
n	27	28	29	30	31	32	33	34	35	36	37	38	39	
t_n	96	105	115	125	137	149	163	177	193	210	228	248	262	

The corresponding static capacitive reactance varied from .8Ω to 200 Ω, and from the skin depth approximation it varied approximately 200 Ω to 50 kΩ, at 300 MHz. It is assumed that the actual capacitance may vary from 100 Ω to 25 kΩ at 3 GHz, therefore Z_o = 377 Ω will be within the variation of capacitive reactance along the antenna. If (αd) is somewhat smaller than 1/12.5 this condition is still satisfied. A larger value than necessary was chosen for (αd), with the hope that the antenna current would be confined to the lower portion of the antenna at the highest frequency of interest. Consequently, the pattern will not vary significantly with frequency. Plexiglass is used for most of the dielectric discs except when the thickness is less than 10 mils where Visqueen and Baggie *(sandwich bags) spacers are used.

In the specific design given above, it is implicitly assumed that by increasing the exponential taper the impedance characteristics are not changed appreciably. However, if the exponential taper is appreciably large (to obtain pattern control) the antenna impedance may become capacitive at the lowest frequency of interest, resulting in a high VSWR. The same effect results if the capacitive loading is heavy (t_1 large). Therefore, one has to compromise on the values of (c) and (α).

Experimental results with the antenna employing the above values of (c) and (α) are included in section 4.3.3. The results show that the VSWR is < 3:1 from 900 MHz to 7.6 GHz. At the low frequency end (< 900 MHz) the VSWR increases rapidly as the frequency is decreased. The experimental radiation pattern shows that acceptable performance is achieved from 300 MHz to 3 GHz. As mentioned above, it is possible to improve the impedance characteristics at the low frequency

* registered trade mark.

end by decreasing the value of (c). To verify this possibility, an antenna was constructed whose capacitive elements were equal to one half (c is decreased to 6.25) that of the above design. The experimental results show that the VSWR is < 3:1 from 600 MHz to 7.6 GHz which was as expected. Further details on the experimental results and the current distribution are given in section 4.3.3.

4.2.4 Preliminary Study on the Analysis of Reactively Loaded Antenna

From the above it is evident that a broadband antenna may be designed using purely qualitative arguments. Since there is little available on the theoretical behavior of reactively loaded antennas, it was felt that some effort should be devoted to a theoretical study. A preliminary investigation has been conducted to solve for an approximate current distribution along the antenna. Theoretically it is possible to obtain the impedance and radiation characteristics of the antenna knowing the current distribution. There are three methods by which one might obtain an approximate current distribution. The difficulties and limitations of these methods will be discussed and the approach for completing the analysis will be indicated.

4.2.4.1 Method of Equivalent Voltage Sources

The antenna geometry is shown in Fig. 4-2. A perfectly conducting cylinder of length (2h) and radius (a) is excited at its center by a voltage source of potential V_o. 2N impedances are loaded symmetrically at an interval of distance d along the antenna. It is desirable to have $Z_N > Z_{N-1} > \ldots\ldots > Z_2 > Z_1$, (this condition is not used in the analysis). Assuming a perfectly conducting cylinder, the electric field at the surface must be zero except in the vanishing gaps at $z = 0, \pm d, \pm 2d \ldots \pm Nd$, thus

$$E_z(z) = -V_o\,\delta(z) + \sum_{n=1}^{N} Z_n I_n \left[\delta(z - nd) + \delta(z + nd)\right] \qquad (4.3)$$

where $\delta(z)$ is the Dirac delta function, I_n is the axial current along the antenna at a distance (nd) from the feed point, the symmetry condition $I(z) = I(-z)$ has been used in arriving at equation (4.3). The induced electric field can be written in terms of vector potential as

$$E_z^i(z) = -\frac{j\omega}{K_o^2}\frac{d^2 A_z}{dz^2} - j\omega A_z. \qquad (4.4)$$

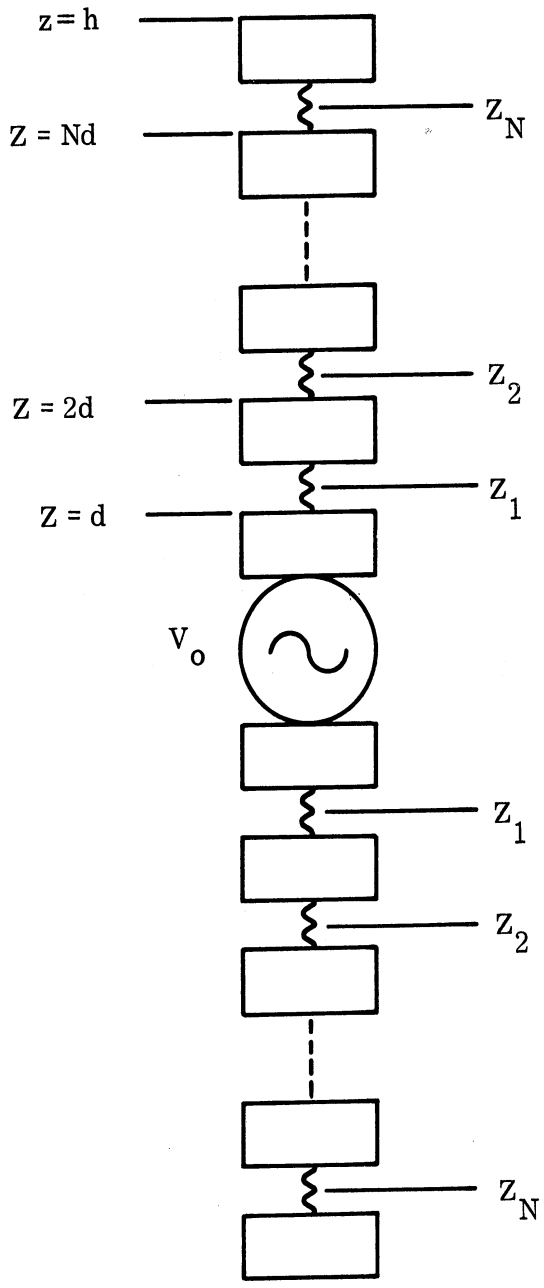

FIG. 4-2: ANTENNA LOADED WITH REACTIVE ELEMENTS

Equating (4.3) and (4.4) to satisfy the boundary condition gives a differential equation for the vector potential at the antenna surface as

$$\left(\frac{d^2}{dz^2}+K_o^2\right)A_z(z)=\frac{jK_o^2}{\omega}\left\{-V_o\,\delta(z)+\sum_{n=1}^{N}Z_n I_n\left[\delta(z-nd)+\delta(z+nd)\right]\right\} \tag{4.5}$$

Equation (4.5) has a complete solution (applying the physical symmetry of vector potential) given by

$$A_z(z)=Be^{jK_o z}+Be^{-jK_o z}+\frac{V_o}{2v}e^{-jK_o|z|}-\frac{1}{2v}\sum_{n=1}^{N}Z_n I_n\left[e^{-jK_o|z-nd|}+e^{-jK_o|z+nd|}\right] \tag{4.6}$$

where (v) is the velocity of propagation in free space.

In a rigorous theory, the above result could be used to obtain an integral equation for the current distribution. It is usually difficult to solve such integral equations, especially so in the present case. We will use an approximate method which is due to King (1965). It has been found by King that the ratio of vector potential $A_z(z)$, at a point on the antenna surface to the current $I_z(z)$, at the same point is essentially independent of (z) and determined primarily by the antenna dimensions. With this approximation, we have

$$I_z(z)=\frac{4\pi}{\mu o}\frac{A_z(z)}{\psi} \tag{4.7}$$

where (ψ) is called the "expansion parameter" which depends on the antenna dimensions and it is essentially constant over a major portion of the antenna (except at the end of the antenna where it becomes infinite). Using the approximation given by equation (4.7), in conjunction with equation (4.6), gives

$$I_z(z)=\frac{4\pi}{\mu o\psi}B\left(e^{jK_o z}+e^{-jK_o z}\right)+\frac{2\pi V_o}{\zeta_o\psi}e^{-jK_o|z|}-\frac{2\pi}{\zeta_o\psi}\sum_{n=1}^{N}Z_n I_n\left[e^{-jK_o|z-nd|}+e^{-jK_o|z+nd|}\right] \tag{4.8}$$

where ζ_o is the intrinsic impedance of free space. Equation (4.8) contains $N+1$ undetermined coefficients ($B, I_1, I_2, \ldots I_N$). Fortunately, there are $N+1$ boundary conditions,

$I_z(z) = I_n$ where $z = nd$ for $n = 1, 2 \ldots . N$, and $I_z(h) = 0$ which facilitates the determinations of the unknowns. Hence, equation (4.8) gives the approximate solution for the current distribution of the Hallen antenna, even though it may be too unwieldly to evaluate if N is too large.

4.2.4.2 Matrix Methods

The method to be used in this section is essentially due to Harrington (1967). He obtains a solution for the current along a wire antenna when it is excited by a voltage source. His solution is expressed as a matrix which is well suited for machine computation. Here we extend his method to include the effects of reactive elements loading the antenna. The resulting matrix for the current along the Hallén antenna is no more difficult to obtain than that of a simple wire antenna. In this respect the matrix method is well suited to Hallen's antenna and it is more accurate than the other two approaches.

A detailed explanation of the method will be found in Harrington's text. Here we review important results of that reference which will be useful for the purpose of our later discussions.

Basically the method involves 1) an approximation of the exact equation for conducting bodies by an approximate equation valid for thin wires, 2) replacement of the derivatives by finite difference approximations, yielding an approximate operator, 3) use of pulse functions for expansion functions, to give a step approximation to the current and charge, and 4) the use of point matching for testing.

To effect a solution, the wire is considered as (M) short segments connected together. The end points of each segment define a pair of terminals in space. These (M) pairs of terminals can be thought of as forming an (M) port network. One can determine the impedance matrix for the (M) port network by applying a current source to each port in turn, and calculating the open circuit voltages at all ports. The admittance matrix is the inverse of the impedance matrix. Once the admittance matrix is known, the port currents (current distribution on the wire) are found for any particular voltage excitation (applied field) by matrix multiplication. Let $[Z]$ be the impedance matrix of the (M) segments of the wire (see Harrington, 1967 for determining this matrix), and is given by,

$$[Z] = \begin{bmatrix} Z_{11} & Z_{12} \cdots\cdots\cdots Z_{1M} \\ Z_{21} \cdots\cdots\cdots\cdots\cdots Z_{2M} \\ \cdots\cdots\cdots\cdots\cdots\cdots \\ Z_{M1} \cdots\cdots\cdots\cdots Z_{MM} \end{bmatrix} \tag{4.9}$$

Then the current along the antenna is given by (Harrington, 1967),

$$[I] = [Y][V] \quad \text{where} \quad [Y] = [Z]^{-1} \tag{4.10}$$

and $[V]$ is the voltage matrix which is determined by the impressed fields. For an antenna excited in the nth interval, the applied voltage matrix is

$$[V] = \begin{bmatrix} 0 \\ \vdots \\ V_n \\ \vdots \\ 0 \end{bmatrix} \tag{4.11}$$

where V_n is the source voltage. From equation (4.10 and 4.11) the current distribution of the wire antenna, when it is excited by a single source at (nth) segment, can be obtained.

To apply equation (4.10) to the Hallén antenna, the effect of reactive loading will be included in the voltage matrix $[V]$. From the previous discussion, it is evident that the effect of the reactive elements can be taken into account, if one replaces those elements by equivalent voltage sources given by the product of the impedance of the reactive elements and the current on the corresponding segments of the antenna. For now, assume that the number of reactive elements are equal to the number of the antenna segments minus the number of sources applied to the antenna. For Hallén's antenna, when it is excited at one end of the antenna, this corresponds to a voltage matrix,

$$[V] = \begin{bmatrix} V_0 \\ I_2 \; Z_2 \\ I_3 \; Z_3 \\ \vdots \\ I_M \; Z_M \end{bmatrix} \tag{4.12}$$

where $I_2 \ldots . I_M$ corresponds to the currents in the corresponding antenna segments, $Z_2 \ldots . Z_M$ are the impedances of the loading elements, and V_o is the applied source voltage.

Writing (4.10) in a different form gives

$$[Z][I] = [V] \tag{4.13}$$

Notice that $[V]$ is given by (4.12) and

$$[I] = \begin{bmatrix} I_1 \\ I_2 \\ \vdots \\ I_M \end{bmatrix} \tag{4.14}$$

One can immediately write down

$$[Z_o][I] = \begin{bmatrix} V_0 \\ 0 \\ \vdots \\ 0 \end{bmatrix} \tag{4.15}$$

where $[Z_o]$ is the modified impedance matrix which includes the impedances of the loading elements and is given by,

$$\left[Z_o\right] = \begin{bmatrix} Z_{11} & Z_{12} \cdots\cdots\cdots\cdots\cdots Z_{1M} \\ Z_{21} & Z_{22} + Z_2 \cdots\cdots\cdots\cdots\cdots \\ \cdots\cdots\cdots\cdots\cdots\cdots\cdots\cdots\cdots \\ Z_{n1} \cdots\cdots\cdots\cdots Z_{nn} + Z_n \cdots\cdots \\ \cdots\cdots\cdots\cdots\cdots\cdots\cdots\cdots\cdots \\ Z_{M1} \cdots\cdots\cdots\cdots\cdots\cdots Z_{MM} + Z_M \end{bmatrix} \qquad (4.16)$$

From equation (4.15) and (4.16), it is clear that the effect of loading the antenna can be taken into account by simply adding the impedance of the loading element to the self impedance of the corresponding segment of the antenna. The same procedure could be used even if the number of segments are more than the number of loading elements (this may be desirable for better accuracy in determining the current distribution). From equation (4.15), $\left[I\right]$ can be found by inverting $\left[Z_o\right]$ and is given by

$$I = \left[Y\right]\begin{bmatrix} V_0 \\ 0 \\ \vdots \\ 0 \end{bmatrix} \text{ where } \left[Y\right] = \left[Z_o\right]^{-1}$$

$$= V_0\begin{bmatrix} Y_{11} \\ Y_{21} \\ \vdots \\ Y_{M1} \end{bmatrix} \qquad (4.17)$$

From this it is clear that $I_1 = V_0 Y_{11}$, $I_2 = V_0 Y_{21}$, etc. Hence Y_{11} gives the input admittance of the Hallen antenna.

4.2.4.3 Continuously Distributed Reactive Loading

Another approach which is considered employs a continuously distributed reactive loading along the length of the antenna. Above, we considered the effect of loading a wire antenna by discrete lumped reactive elements. When the spacing between those elements is a small fraction of the wavelength, it is not unreasonable to assume the loading to be continuous.

Let $Z_1(z)$ be the impedance loading per unit length of the antenna. Let $I_z(z)$ be the total axial current along the antenna which is driven at $z = 0$ by a delta function generator with emf V_o. Then it can be shown (King, 1965) that the axial component $A_z(z)$ of the vector potential on the surface of a cylindrical antenna will satisfy the one dimensional wave equation,

$$\left(\frac{d^2}{dz^2} + K_o^2\right) A_z(z) = \frac{jK_o^2}{\omega}\left[Z_1(z)\, I_z(z) - V_o\, \delta(z)\right] \tag{4.18}$$

where K_o is the free space wave number.

In a rigorous theory the above equation, for vector potential, should be solved after which one would then obtain an integral equation for the current distribution. Using the approximation which is due to King (1965) as mentioned in 4.2.4.1, it is seen that the ratio of vector potential, $A_z(z)$, at a point on the antenna surface to the current $I_z(z)$, at the same point is essentially independent of z and determined primarily by the antenna dimensions. Repeating equation (4.7), we have

$$I_z(z) = \frac{4\pi}{\mu_o}\frac{A_z(z)}{\psi} \tag{4.19}$$

where ψ is called the "expansion parameter". Using the approximation (4.19) in conjunction with equation (4.18), we obtain a second order differential equation for the current

$$\left[\frac{d^2}{dz^2} + K_o^2 - jK_o\, f(z)\right] I_z(z) = 0 \tag{4.20}$$

where $f(z) = \frac{4\pi}{\zeta_o \psi} Z_1(z)$

ζ_o is the intrinsic impedance of free space, and ψ is the expansion parameter at the current maximum.

Equation (4.20) can be applied to any (complex or real) impedance $Z_1(z)$ and on solving that differential equation with the boundary condition $I(h) = 0$, will give the current distribution on the loaded antenna (keeping in mind the approximations which led to equation 4.20).

Since our interest here is the reactive loading, it is assumed that $Z_1(z) = jX_L(z)$, hence equation (4.20) becomes

$$\left[\frac{d^2}{dz^2} + K_o^2 + K_o F(z)\right] I_z(z) = 0 \tag{4.21}$$

where $F(z)$ is a real function of z and is given by

$$F(z) = \frac{4\pi}{\zeta_o \psi} X_L(z).$$

Equation (4.21) can be solved exactly only for a few special forms of $X_L(z)$. Only approximate methods are available for the general case of arbitrary $X_L(z)$. In our study, a special form for $X_L(z)$ will be assumed in solving for $I_z(z)$.

Since for the Hallén antenna, $X_L(z)$ should increase with z, an exponential distribution will be assumed and is given by (assuming $X_L(o) = 0$)

$$X_L(z) = C\left(e^{\alpha z} - 1\right) \tag{4.22}$$

where C is an arbitrary constant which is positive for inductive loading and is negative for capacitive loading. The amount of reactance taper depends on the constant α.

Substituting (4.22) in (4.21) will result in a differential equation given by

$$\left[\frac{d^2}{dz^2} + K_o^2 - K_o K_1 + K_o K_1 e^{\alpha z}\right] I_z(z) = 0 \tag{4.23}$$

where $K_1 = \frac{4\pi C}{\varsigma_o \psi}$

To solve for the above equation, we let

$$v = \frac{2\sqrt{K_o K_1}}{\alpha} e^{\alpha z/2} \tag{4.24}$$

Substituting this in equation (4.23) results in a familar differential equation,

$$\left[\frac{d^2}{dv^2} + \frac{1}{v}\frac{d}{dv} + \frac{K_o^2 - K_o K_1}{v^2 \alpha^2} + 1\right] I(v) = 0 \tag{4.25}$$

Whose solutions are the Bessel functions $J_{\pm \nu}(v)$. Therefore,

$$I(v) = AJ_{-\nu}(v) + BJ_{+\nu}(v) \tag{4.26}$$

where $$\nu = j2\frac{\sqrt{K_o^2 - K_o K_1}}{\alpha}$$

and $$v = 2\frac{\sqrt{K_o K_1}}{\alpha} e^{\alpha z/2}$$

Note that ν is imaginary for both inductive and capacitive loading. However, v is real for inductive loading (K_1 is positive real) and it is imaginary for capacitive loading (K_1 is negative real). Applying the boundary condition $I(z) = 0$ at $z = h$, we obtain

$$\frac{B}{A} = R_1 = -\frac{J_{-\nu}(v_h)}{J_{\nu}(v_h)}$$

where

$$v_h = \frac{2\sqrt{K_o K_1}}{\alpha} e^{\alpha h/2}$$

Hence, the relative current along the antenna is given by

$$I_z(z) = J_{-\nu}(v) + R_1 J_{+\nu}(v) \qquad (4.27)$$

Due to the approximations involved, equation (4.27) gives only a first order current distribution. It is hoped that the matrix method will prove a better approximation. However, to obtain a better approximation for input impedance, a variational method could be used in conjunction with equation (4.27). It is suggested that this work be continued in order to better understand the reactively loaded antenna.

4.3 Experimental Results

Data in this section is presented in the order of the experimental development of the Hallén antenna, with the hope this presentation will give the reader a feeling for the changes in the overall performance achieved by non-uniform loading. The first reactively loaded antenna considered was a capacitive antenna designed to operate from 300 - 3000 MHz, as this frequency scaling reduced antenna construction cost and simplified the testing procedure. The first capacitive Hallén configuration consisted of 21 cylinders, 0.5 inches in diameter and 0.5 inches long. The cylinder at the input was tapered with a 90^o total included angle to reduce input capacitance. Uniform capacitance was provided (i.e., the capacitive reactance did not vary as a function of antenna length) using a double thickness of 0.6 mil Handywrap* spacers between each cylindrical section. To support the antenna it was placed in a hollow foam block.

4.3.1 Constant Reactance

The VSWR data (for a 10:1 frequency band) of the Hallén antenna (Fig. 4-3) was compared with similar data for a solid aluminum antenna (Fig. 4-4) of the same radius and overall length ($\simeq$11 inches) in Fig. 4-5 and 4-6. Two features are readily apparent, first, the VSWR near the free space quarter wave resonance is much greater for the Hallén antenna. However, the remaining VSWR data for the Hallen antenna is lower than that for the aluminum antenna. The higher VSWR near

* registered trade mark identification

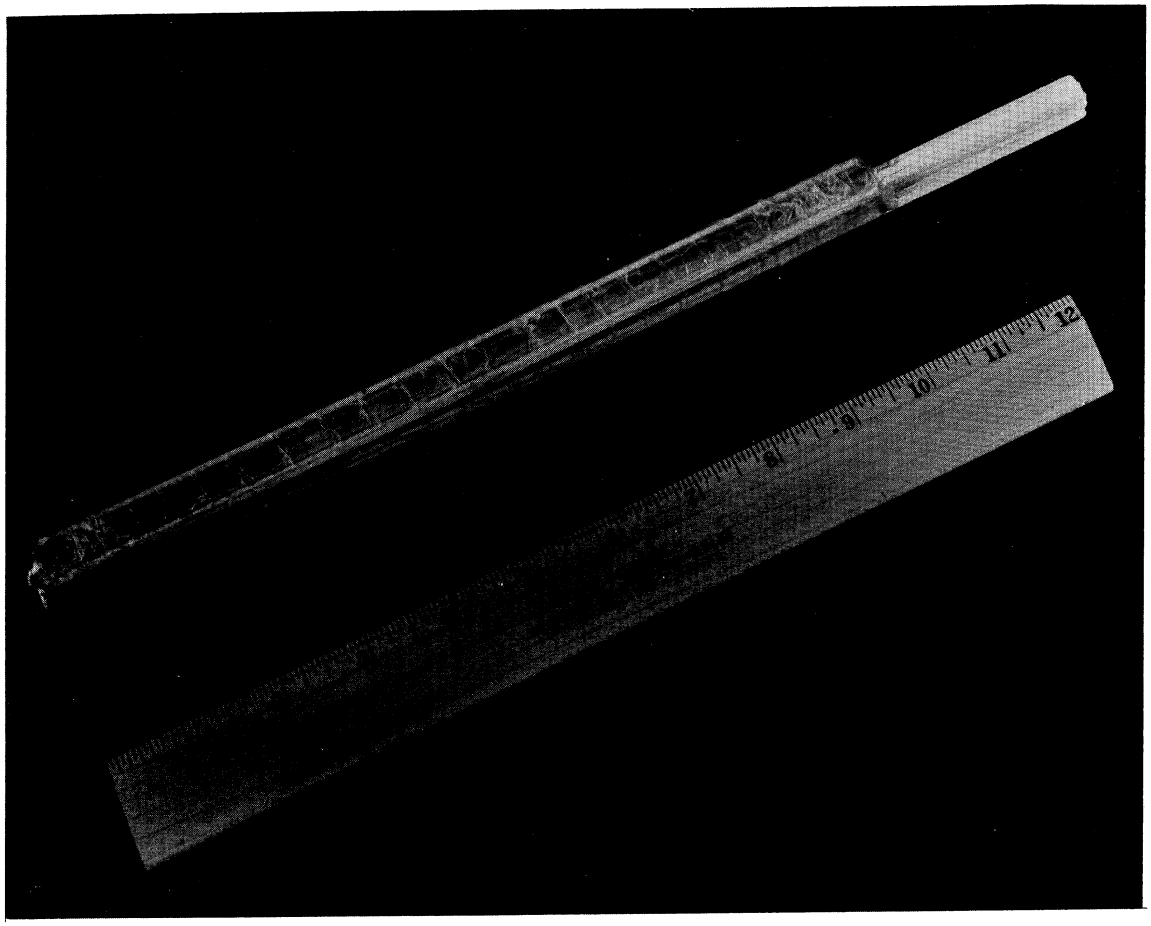

FIG. 4-3: HALLÉN ANTENNA WITH UNIFORM CAPACITANCE
(1/2" Diameter X 11" Long)

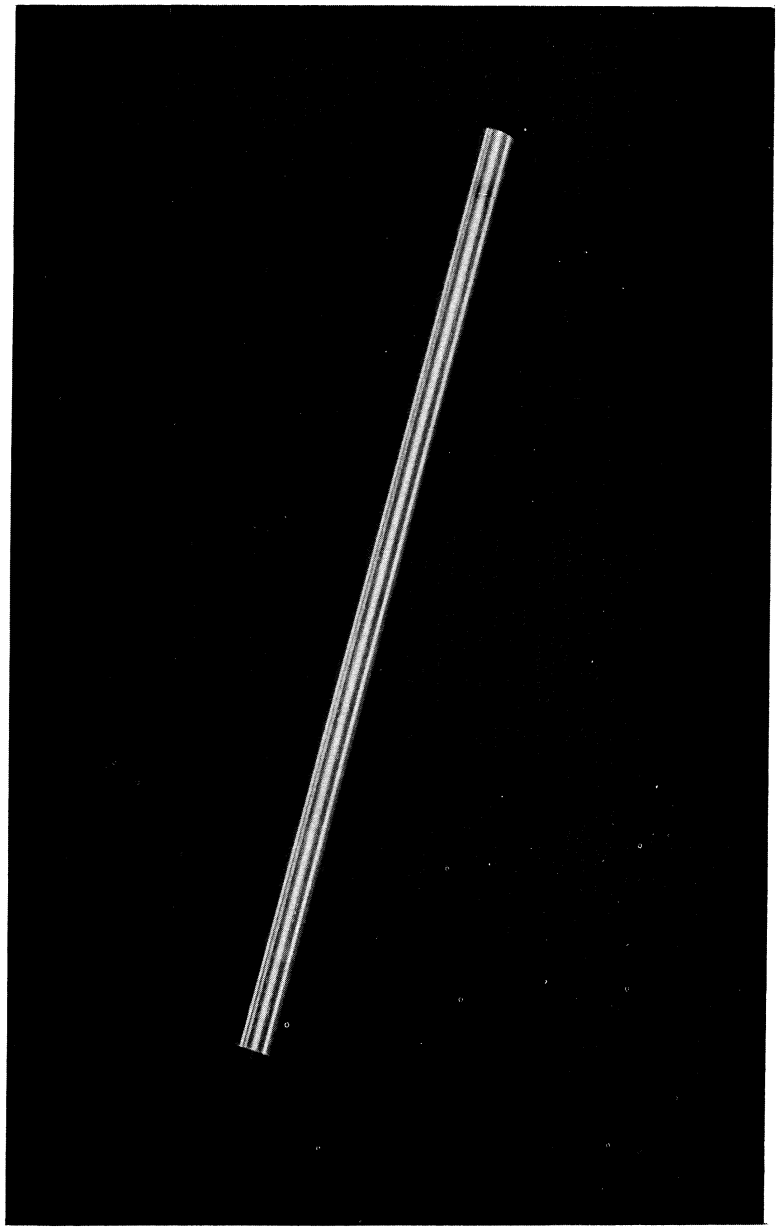

FIG. 4-4: SOLID ALUMINUM ANTENNA
(1/2" Diameter X 11" Long)

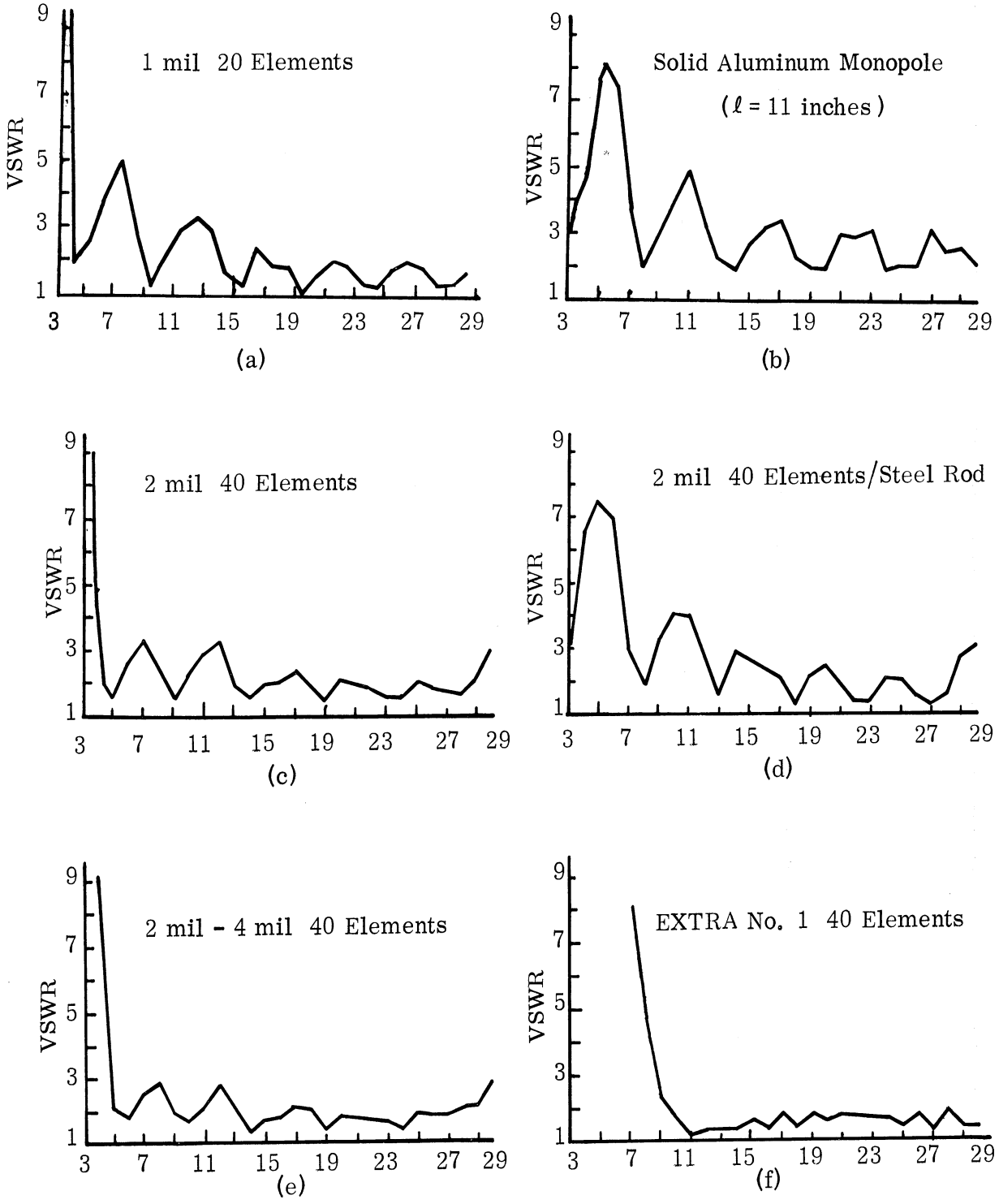

FIG. 4-5: VSWR CHARACTERISTICS OF HALLEN AND ROD ANTENNA OVER A FLAT GROUND PLANE (f = GHz)

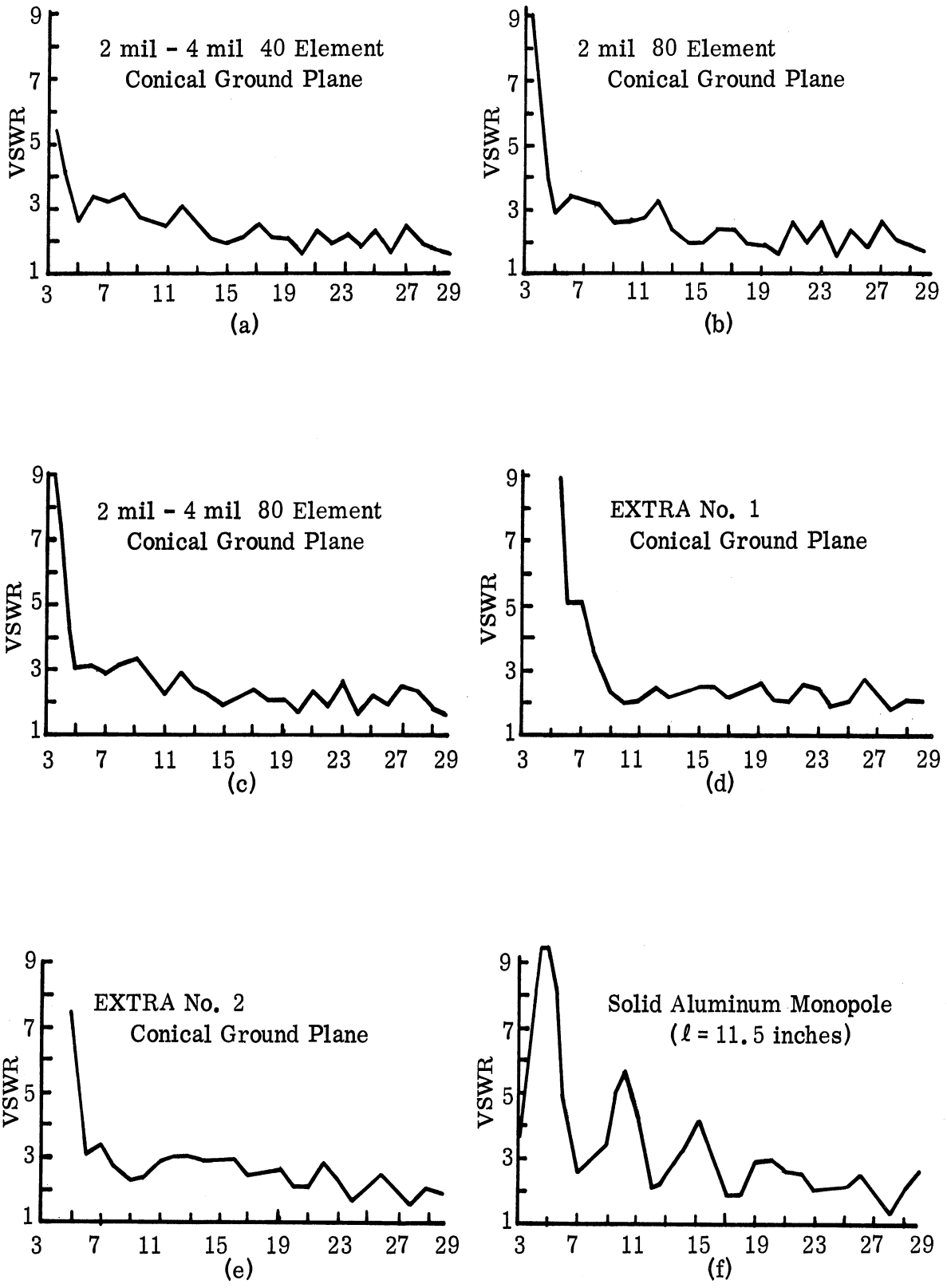

FIG. 4-6: VSWR CHARACTERISTICS OF HALLÉN AND ROD ANTENNAS OVER A CONICAL GROUND PLANE (f = GHz)

the quarter wavelength resonance may be explained in two ways. First, recall that an electrically short monopole inherently exhibits a capacitive input reactance. Therefore, capacitive loading (as for the Hallén antenna) increases the antenna capacitance such that the antenna input impedance is characteristic of an electrically short antenna. Alternatively in transmission line theory, it has been shown that transmission lines loaded with discrete capacitive elements may be considered as fast wave structures, $v > C$. Therefore, the increase in wavelength due to the capacitance would cause the apparent quarter wave structure to be electrically short, causing the antenna to have substantial capacitive reactance. The second feature (observed in the comparison of the Hallén and aluminum monopole) is that although VSWR characteristics appear to be similar for the two antennas, the VSWR maxima for the Hallén are always less than those for the solid antenna. Considering the two graphs of VSWR (Fig. 4-5a and b) it becomes apparent that the Hallén is most effective in reducing the reflections at the higher frequencies (1400 - 3000 MHz) as suggested in section 4.2. The first capacitive Hallén antenna was designed to have a distributed capacitance every 1/8 free space wavelength at the highest frequency of interest (3000 MHz). Periodic variations in VSWR with frequency indicated the antenna was frequency sensitive because of standing waves (due to reflections) on the antenna. As noted previously the desired current distribution should be an exponentially decaying current whose magnitude at the free end of the antenna is approximately 10db below the peak current at the input of the antenna. If this 10db current taper could be maintained over the first $\lambda/4$ to $\lambda/2$ (free space wavelength) from the antenna input at all frequencies of interest (in the 10:1 frequency band), the desired pattern and impedance characteristics would result. Figures 4-7 and 4-8 are typical radiation patterns showing the lobing structure of the first capacitive antenna. This lobing structure is typical of linear antennas which have a current standing wave of reduced magnitude on their surface.

The second version of the capacitive Hallén antenna (Fig. 4-9) consisted of 40 cylinders, each 0.5 inches in diameter and 0.25 inches long. Therefore, these cylinders are $\lambda/16$ free space wavelengths long at the highest frequency of interest. The foam support of the first antenna was replaced with a 6-32 nylon threaded rod. Each cylinder was drilled and taped for 6-32 thread and holes were cut in the dielectric spacers. Screwing the threaded elements together gave a more uniform separation between the cylinders. These spacers were cut from 2.0 mil thick polyethelene.

The shorter elements (0.25 inches) minimized the variations in the VSWR (Fig. 4-5c). Increasing the number of discrete capacitance elements further increased the total base capacitance, therefore, causing the antenna to appear electrically shorter than the first version discussed above. As was expected, the

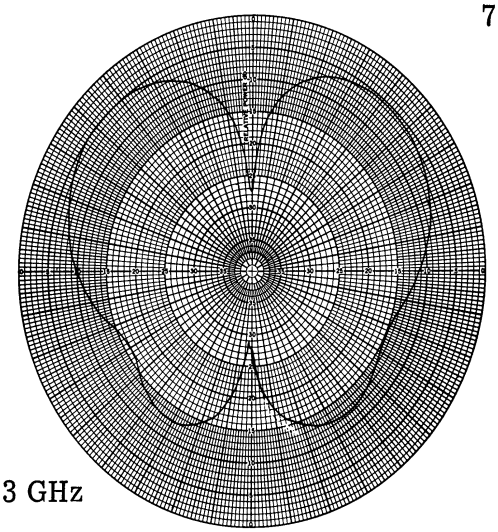

0.3 GHz

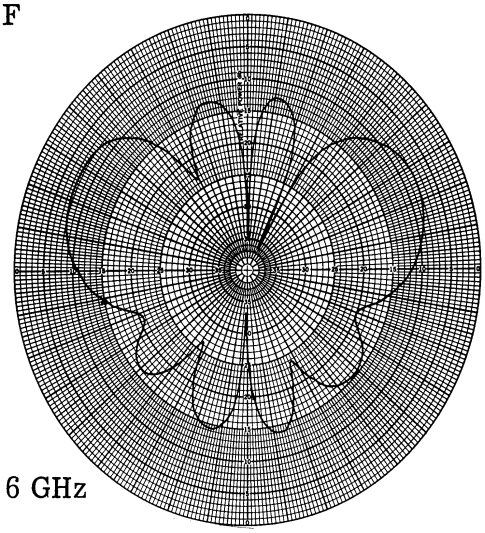

0.6 GHz

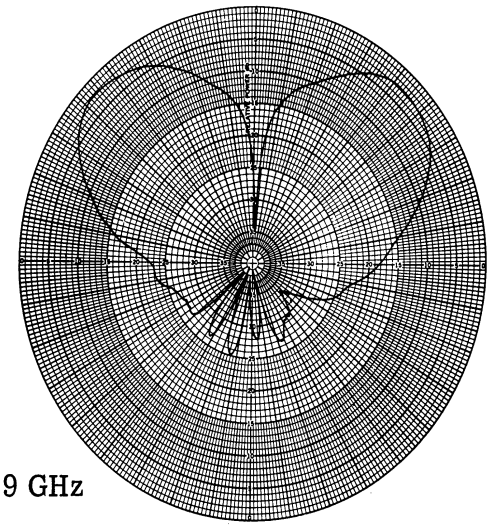

0.9 GHz

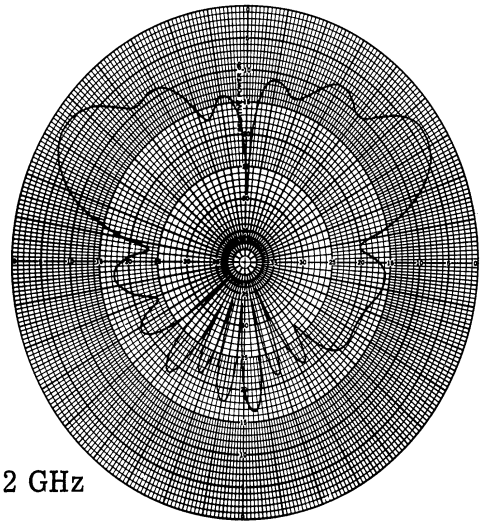

1.2 GHz

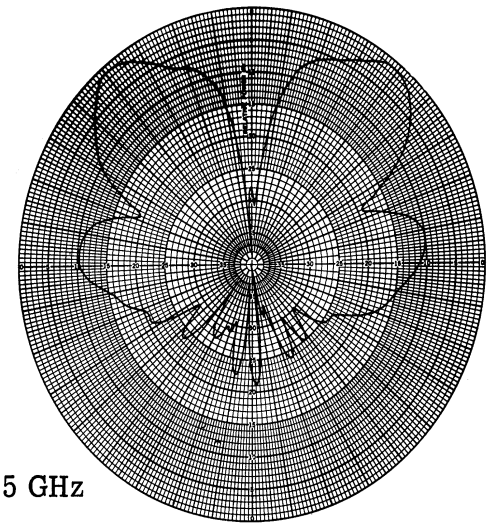

1.5 GHz

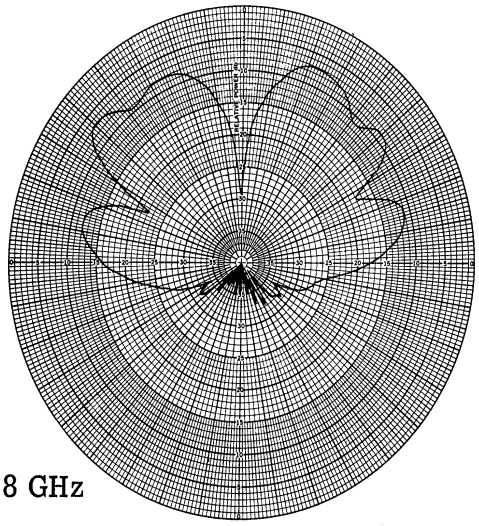

1.8 GHz

FIG. 4-7: ELEVATION PATTERNS OF 1 mil CAPACITIVE HALLEN ANTENNA OVER A CONICAL GROUND PLANE (0.3 - 1.8 GHz)

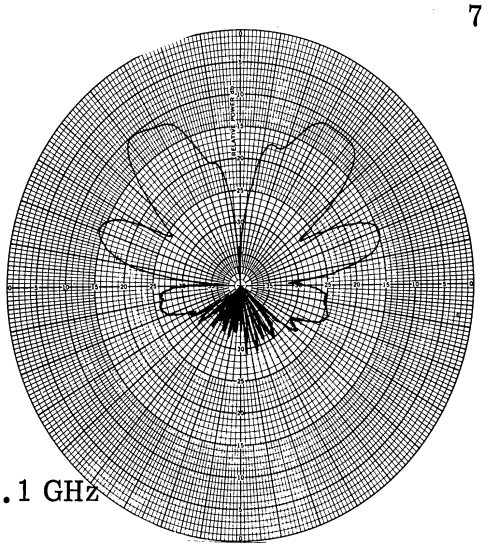

2.1 GHz

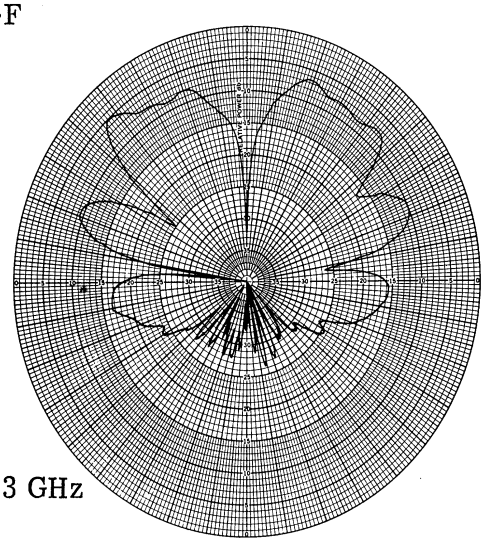

2.3 GHz

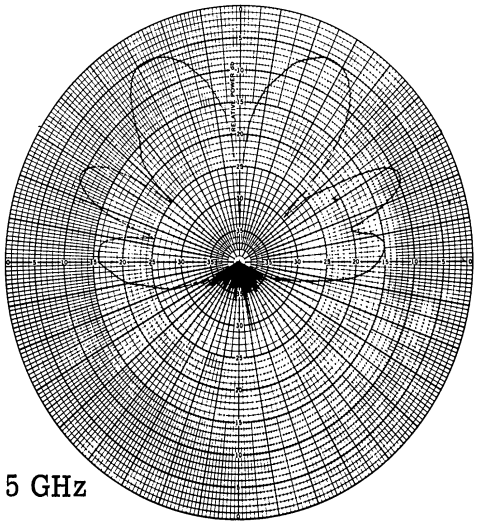

2.5 GHz

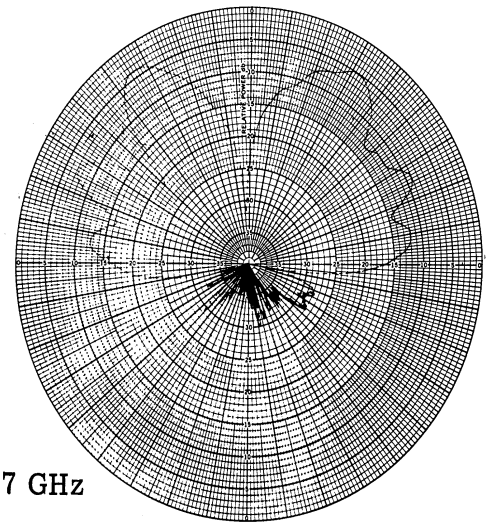

2.7 GHz

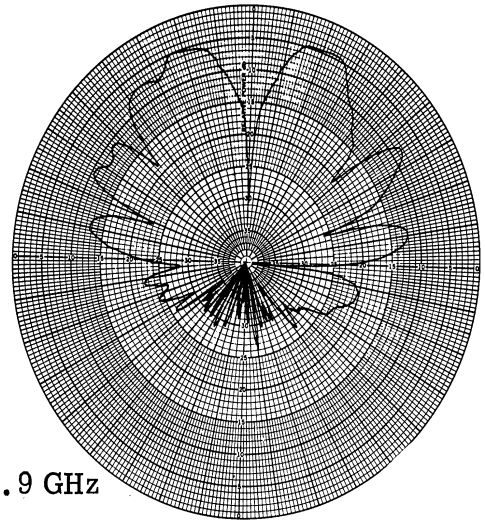

2.9 GHz

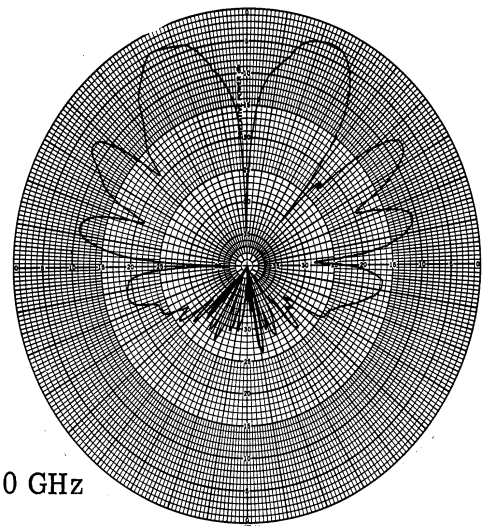

3.0 GHz

FIG. 4-8: ELEVATION PATTERNS OF 1 mil CAPACITIVE HALLÉN ANTENNA OVER A CONICAL GROUND PLANE (2.1 - 3.0GHz)

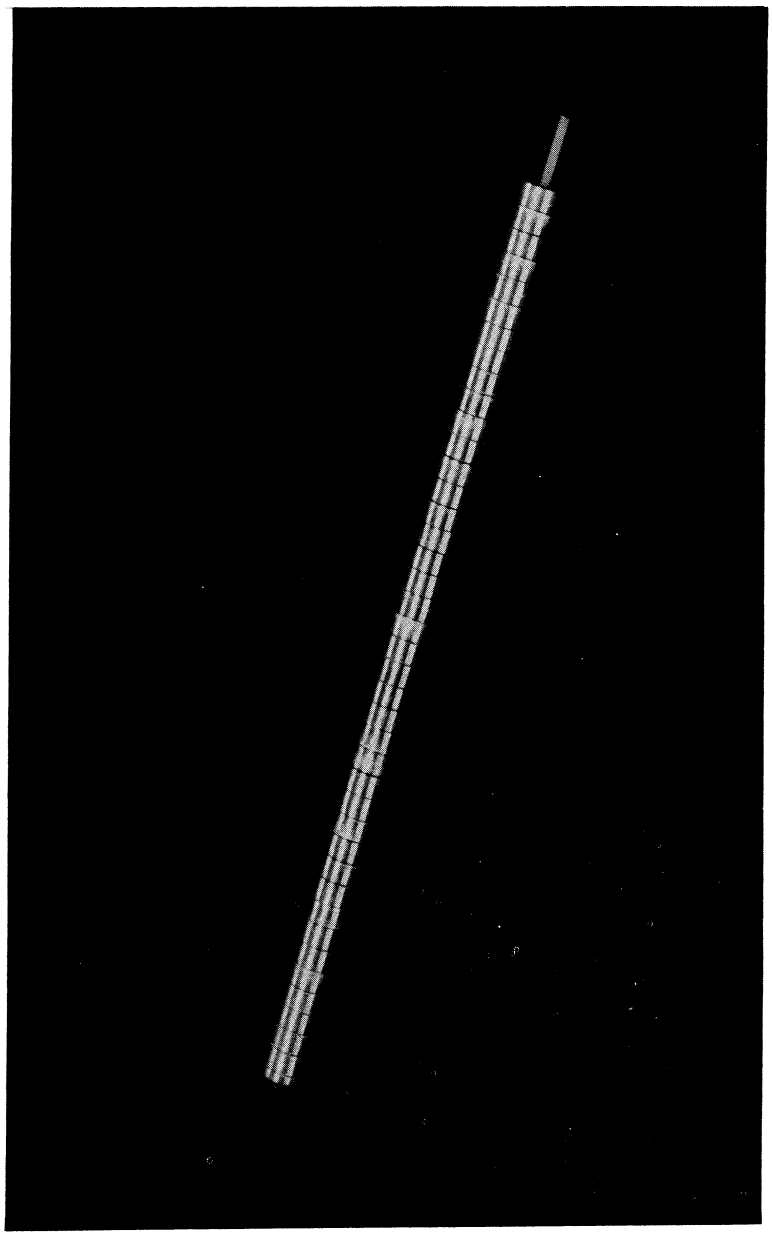

FIG. 4-9: 40 ELEMENT HALLÉN/2 MIL DIELECTRIC

first VSWR minimum occurred at a higher frequency (500 MHz) than was observed for the previous antenna (400 MHz). It is interesting to note that increasing the number of capacitive sections reduces the VSWR of the first maximum from 5.0:1 (for the previous antenna) to 3.3:1. Although the level of the VSWR peaks is not lowered by the shorter cylinders, the more constant level of VSWR suggests that the magnitude of the surface current standing waves have been reduced which is desired.

A third antenna (Fig. 4-10) consisted of 80 conductive cylinders 0.5 inches in diameter and 0.125 inches long. These cylinders were also threaded on a 6-32 nylon rod with 2 mil polyethelene spacers. This antenna was mounted on a conical ground plane having an included angle of 60^{o} and an axial length of approximately 15.5 inches. Typical VSWR data for this antenna is shown in Fig. 4-6b. Decreasing the cylinder length to less than $\lambda/16$ free space wavelength at the upper design frequency does not significantly decrease the surface current standing waves. However, increasing the number of capacitive sections per unit length increased the total input capacitance and again raised the lower usable frequency (i.e., increased the frequency at which the VSWR remained less than 3:1).

4.3.2 Capacitive Reactance

At this time the following question was raised. What is the reactance of each capacitive section in the frequency band of interest? Classical electromagnetic theory states that the capacitance is directly proportional to the area of the plates and the dielectric constant of the material between the plates. However, one must recall that the area involved is the true area of the plates only for the quasi-static case. At microwave frequencies, as the frequency increases, the charge accumulation is restricted to the edges with minimal charge density at the center. One would expect this because of the small separations between the plates, and further because the current density (antenna conductive current) is restricted to the surface of the antenna in accordance with skin depth expressions. Because of the reduction of the charge density at the center of the plates, the capacitance decreases (increases the capacitive reactance).

Several unsuccessful attempts were made to measure the capacitance associated with two 0.5 inch cylinders separated with a 1 mil dielectric spacer. These measurements were attempted at frequencies above 100 MHz. In general, it was found that the value of the capacitance measured was influenced by objects such as the necessary test equipment and test leads.

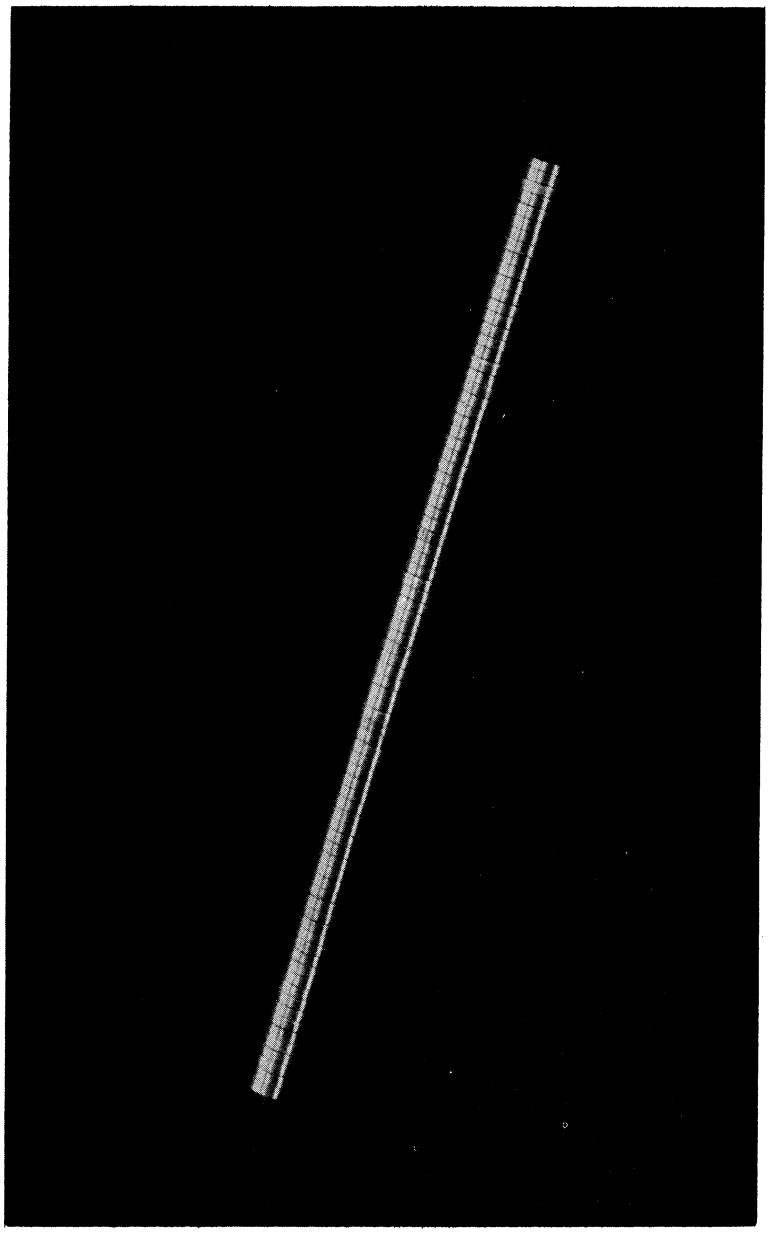

FIG. 4-10: 80 ELEMENT HALLÉN/2 MIL DIELECTRIC

Above it was hypothesized that charge density between the cylindrical discs would be restricted near the surface of the cylinder. Therefore, it was reasoned that the nylon threaded rod could be replaced with a metalic threaded rod. This change was made and VSWR characteristics were measured and are shown in Fig. 4-5d. This data clearly shows that currents are flowing in the interior region of the discs at the capacitive junction. It is interesting to note that the VSWR at 300 MHz is nearly the same as that for a solid monopole and departs from the high VSWR of the nylon rod antennas for this frequency. This is believed to be due to the currents that are flowing in this interior region (between the cylinder) and further, that this region has considerable charge storage capacity. Therefore, the capacitance is lower than that predicted from quasi-static formulation but higher than would be predicted if the charge were stored in an area proportional to the skin depth at these microwave frequencies. Conversely the capacitive reactance is greater than the predicted quasi-static reactance and lower than the skin depth reactance. From the data collected with the metal support rod, it does not appear feasible to build a capacitively loaded dipole such that the feed line is located inside of one of the dipole elements as is typical for vertical polarized mobile applications. Because of the poor VSWR characteristics associated with the metalic rod, the remainder of the experimentation utilized the dielectric rod support.

4.3.3 Variable Reactance Antenna

To further improve the electrical performance it became obvious that an increasing capacitive reactance was required in the region near the free end of the antenna. However, it was recognized that any increase in the capacitive reactance would detrimentally affect the lower frequency. In an effort to minimize this low frequency deterioration, 2 mil dielectric was placed between the first 20 cylinders and 4 mil dielectric between the remaining 20 cylinders of the 40 element antenna discussed previously. Figure 4-5e shows the improved performance with the antenna mounted over a 4 foot flat ground plane. The low frequency range of the antenna was not greatly affected by the presence of the increased reactance near the free end and increased capacitive reactance decreased the first two peaks of VSWR data in Fig. 4-5c to $< 3:1$. The former 4 foot diameter ground plane was replaced by a conical ground plane having an axial length of 15.5 inches and included angle of 60° to optimize the impedance and far field pattern characteristics. Although this particular capacitive antenna displayed a low reflection coefficient across the large bandwidth (8:1) the antenna patterns deteriorated by tending toward end fire at the higher frequencies.

Effects of the conical ground plane on the VSWR of the 2 mil, 80 element dielectric antenna and the 2 mil - 4 mil, 40 element antenna are shown in Fig. 4-6 a and b respectively. In general, the overall periodic pattern of the VSWR is reduced to an irregular variation of reduced magnitude, while the low frequency reflections are increased by the smaller ground plane.

Patterns for the 2 mil - 4 mil, 40 element antenna on a conical ground plane are shown in Figs. 4-11 and 4-12. Nulls in the patterns suggest that the phase of the conductive currents change along the length of the antenna. Since the angular position for nulls and half plane maximums are the same for antennas having either traveling or standing wave conductive currents, it is difficult to tell which is responsible for the nulls that are present in Fig. 4-11 and 4-12. When the antenna becomes electrically long, radiation along the long path causes the peak VSWR of solid metal monopoles to be reduced to acceptable levels of < 3:1. Existance of standing waves for electrically long antennas is revealed by a periodicity of the VSWR even though the peaks are of a reduced magnitude. Looking at the VSWR plot and the patterns for the 2 mil - 4 mil, 40 element antenna, it appears that the nulls in the far field pattern may be caused by a combination of the traveling wave and standing wave conduction currents with the major effect caused by the traveling wave. Here it becomes apparent that if current is allowed to flow along the entire length of the antenna with little or no restriction on current magnitude, the pattern for the electrically long antenna will exhibit a trend toward end fire with a large number of lobes to the broadside. These patterns graphically show the necessity to limit the current to the lower half wavelength (nearest the input) of the antenna for all frequencies of interest (10:1 frequency band).

A compromise between the physical length of the antenna and the high frequency performance resulted in the final version of the capacitive antenna (Fig. 4-13) described in the previous section (4.2). To simplify future discussions of the EXponentially Tapered Reactance Antenna, it will be referred to as "EXTRA". Increasing the capacitive reactance toward the antenna tip increases the thickness of the dielectric separators thereby increasing the overall antenna length. As indicated from previous data, this increase in total capacitive reactance also increased reflections at the lower frequencies and raised the lower usable frequency making the antenna physically long. The VSWR data of Fig. 4-5f substantiates this disadvantage but also shows the advantage of greatly reduced reflections with lack of periodicity gained by this particular loading. Data is presented on the flat ground plane to emphasize the very low level and lack of periodicity for the reflections. When placed on a conical ground plane (Fig. 4-6d) the overall level of reflections are increased with some increase in the periodicity. Far field patterns for this antenna as

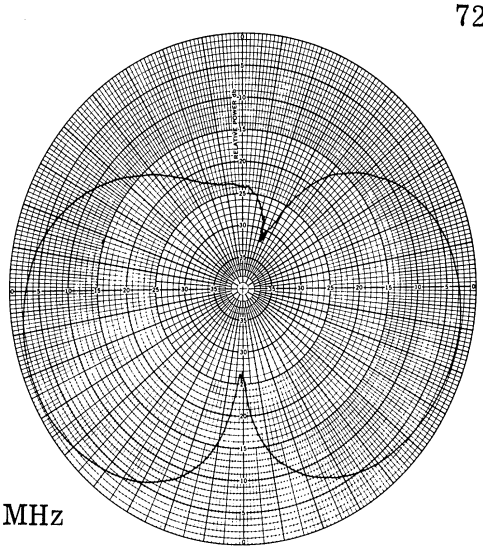

300 MHz

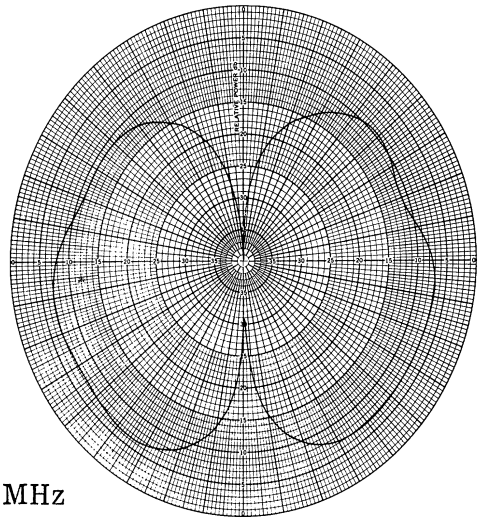

600 MHz

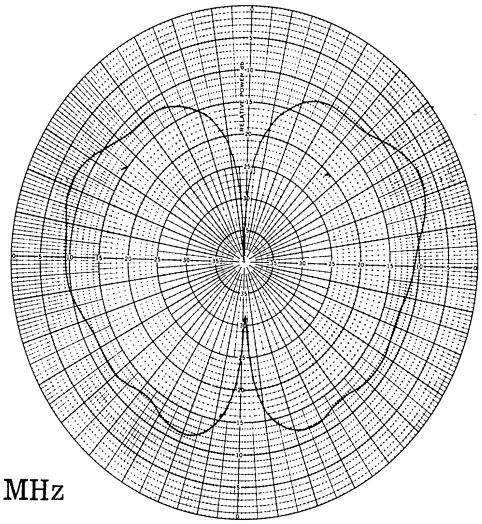

900 MHz

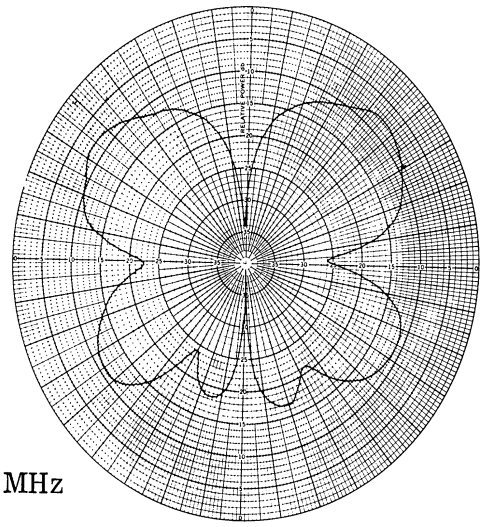

1200 MHz

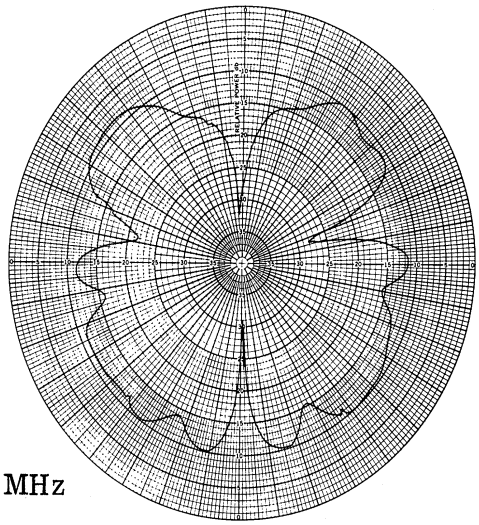

1500 MHz

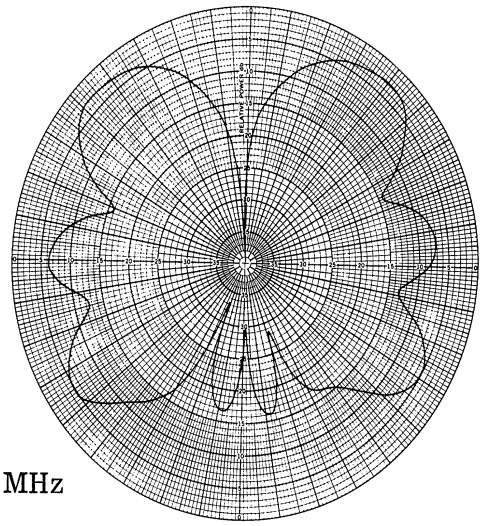

1800 MHz

FIG. 4-11: ELEVATION PATTERNS OF 2 mil - 4 mil 40 ELEMENT HALLÉN ANTENNA OVER A CONICAL GROUND PLANE (300 - 1800 MHz)

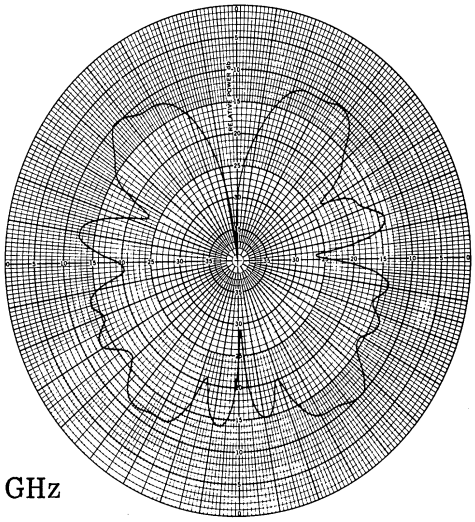

2.1 GHz

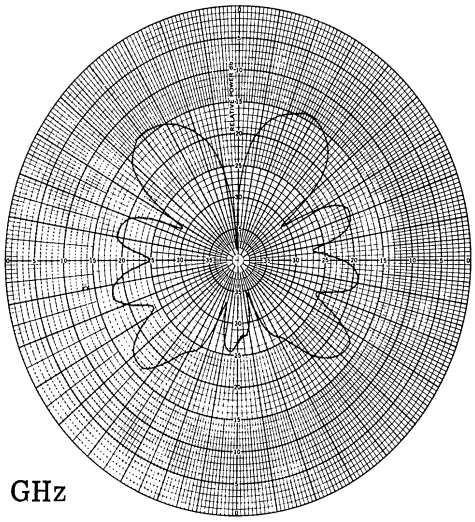

2.3 GHz

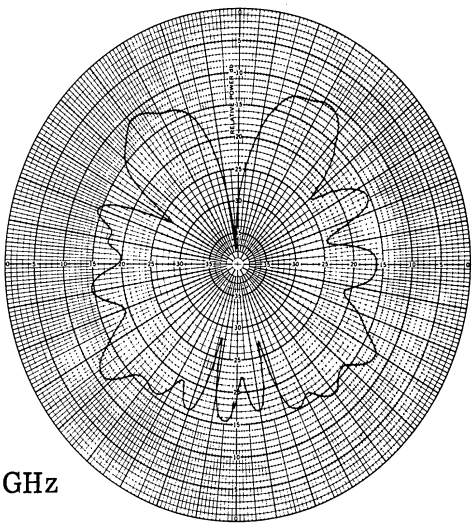

2.5 GHz

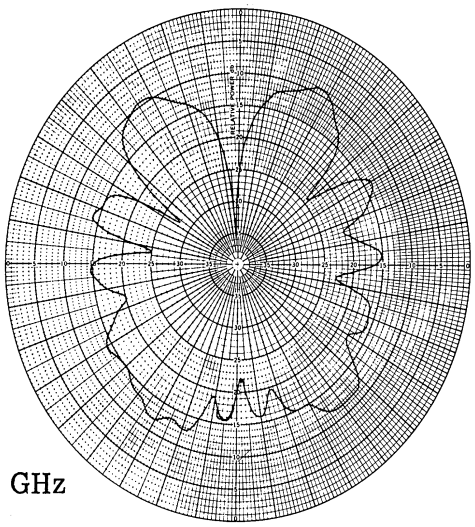

2.7 GHz

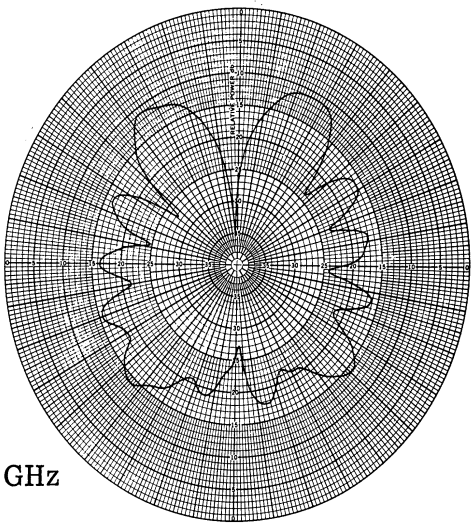

2.9 GHz

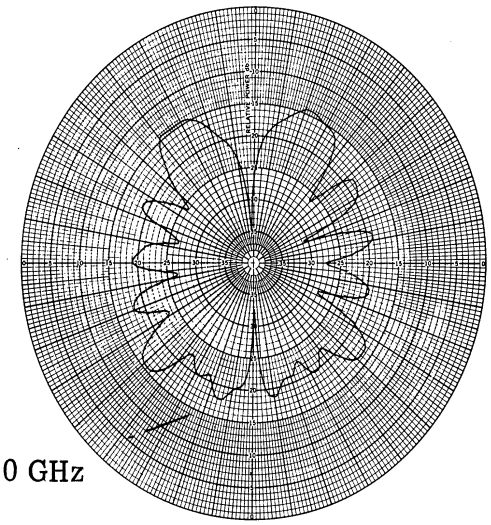

3.0 GHz

FIG. 4-12: ELEVATION PATTERNS OF 2 mil - 4 mil 40 ELEMENT HALLÉN ANTENNA OVER A CONICAL GROUND PLANE (2.1 - 3.0 GHz)

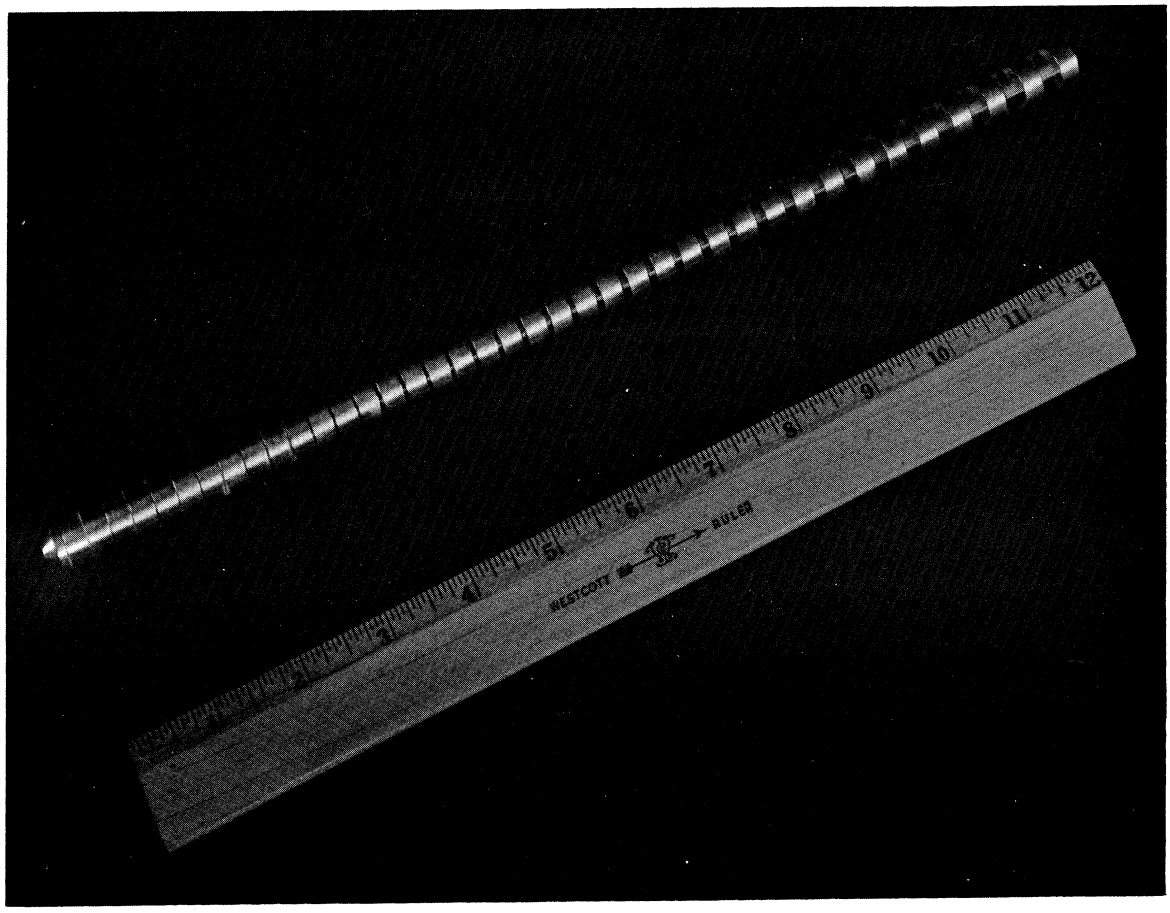

FIG. 4-13: EXTRA No. 1

compared to patterns for the 2 mil - 4 mil, 40 element antenna were greatly improved in the mid-frequency range (1500 - 3000 MHz). Although the antenna is physically $\lambda/4$ at 220 MHz, the antenna reflections are not within the contract requirements for VSWR until 900 MHz. Patterns are not shown for this particular configuration since data for an alternate design were very similar. The alternate design is discussed below.

To reduce the useful low frequency response of the antenna all of the capacitor separations were cut in half to reduce the overall capacitive reactance while maintaining the same taper. Decreasing the capacitor separations reduced the overall length of the antenna from 13-1/2 inches for the first model to 11-1/2 inches (Fig. 4-14). Figure 4-15 shows a solid aluminum antenna resonant near 300 MHz, EXTRA No. 1 and EXTRA No. 2. The VSWR was reduced at the lower frequencies (Fig. 4-6e), such that a VSWR of < 3:1 existed, above 800 MHz. For comparison the VSWR characteristics for a solid aluminum monopole (of the same length and diameter) is shown in Fig. 4-6f. It is important to note that the antenna has a VSWR only slightly above the design goal from 600 MHz. Patterns of Fig. 4-16 and 4-17 are similar to those that were recorded for the first version discussed above. The important difference between these last two antennas from the earlier versions is the improved coverage in the plane normal to the antenna axis because of reductions in the depth of the nulls. Reduction of null depth is believed to be due to the tapered current distribution with the variable capacitive loading. With the capacitive reactance exponentially increasing with length, the current should decay exponentially toward the antenna tip. If the current decreases exponentially to zero at the tip, the contributions from currents with changing phase will be minimal due to their decreased magnitude.

4.3.4 Surface Current Distributions

The current distribution of EXTRA No. 2 antenna with distributed capacitive loading and a solid aluminum monopole were measured and compared in Fig. 4-18, 4-19 and 4-20. Currents were measured by an external loop as it traversed the length of the antenna. At 3000 MHz, the current on the solid aluminum monopole displayed only a minor reduction in magnitude toward the tip. In contrast note the rapid current decay for the capacitive antenna. At the lower frequencies the decay is very rapid but as the frequency increases the decreased capacitive reactance reduces the effectiveness of the current control shown by the increased current magnitude toward the antenna tip. This increased current density toward the antenna tip is responsible for the trend toward end fire and minor current lobing that begins to appear at the higher frequencies. Of course the end fire trait is the most objectionable of the two. Just as for long antennas the greater the electrical length, the

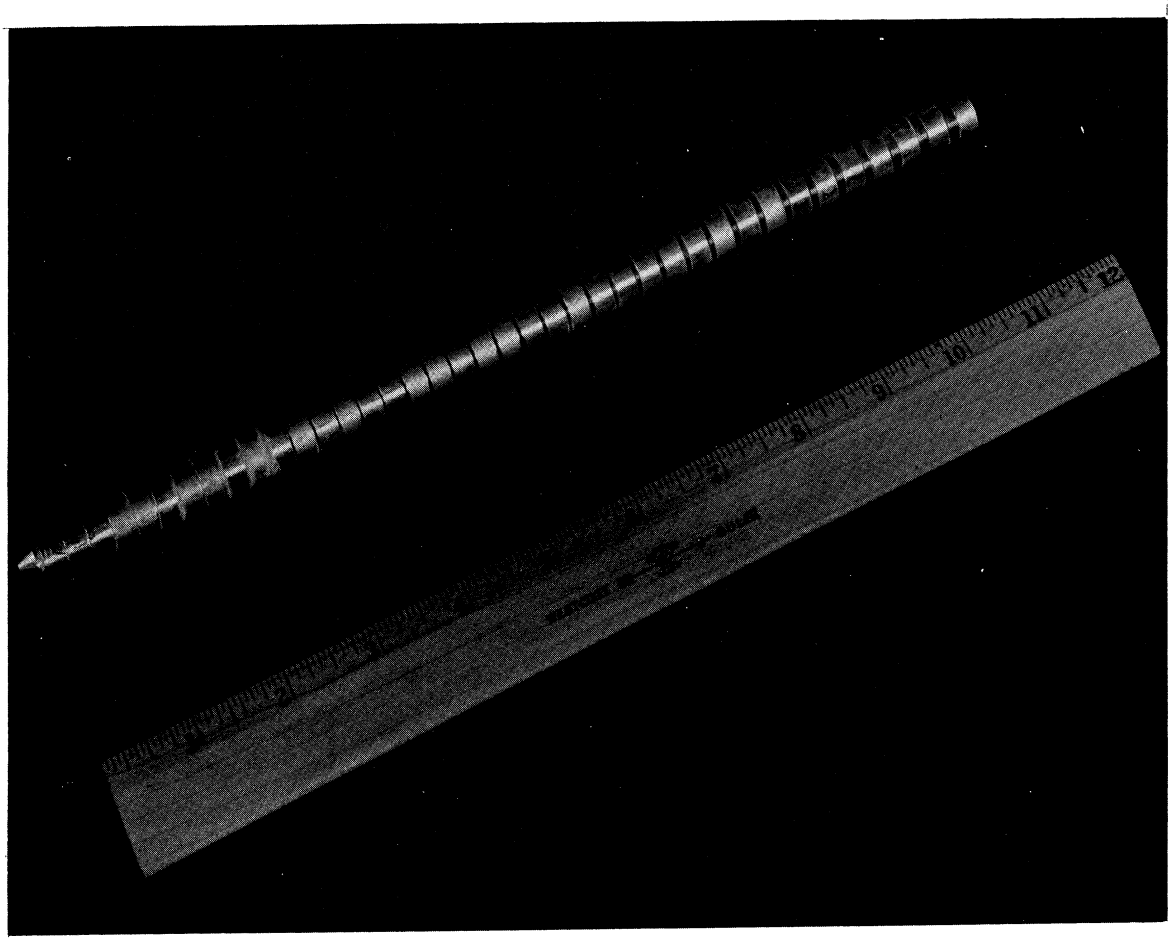

FIG. 4-14: EXTRA No. 2

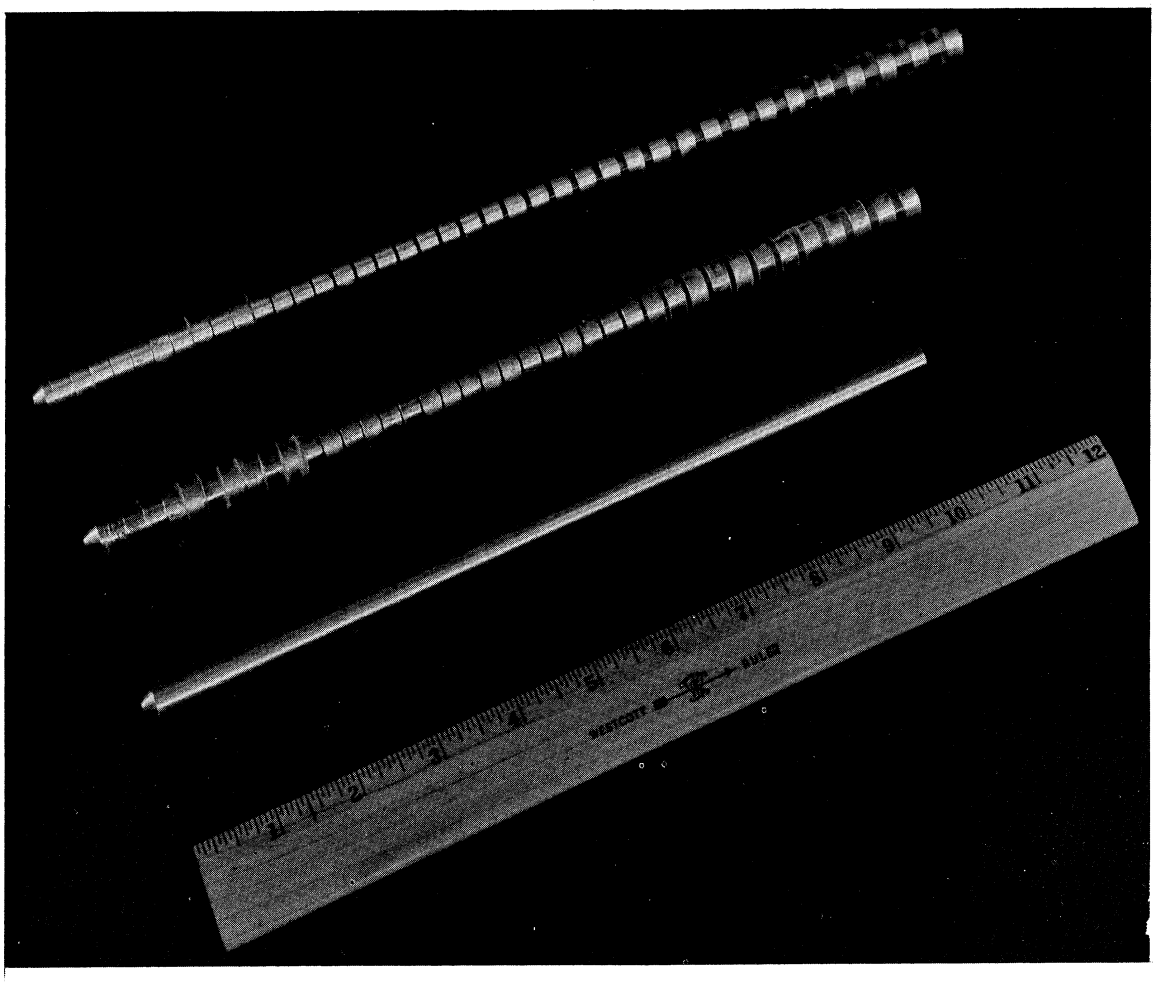

FIG. 4-15: COMPARISON OF ALUMINUM MONOPOLE AND EXTRA 1 AND 2 ANTENNA

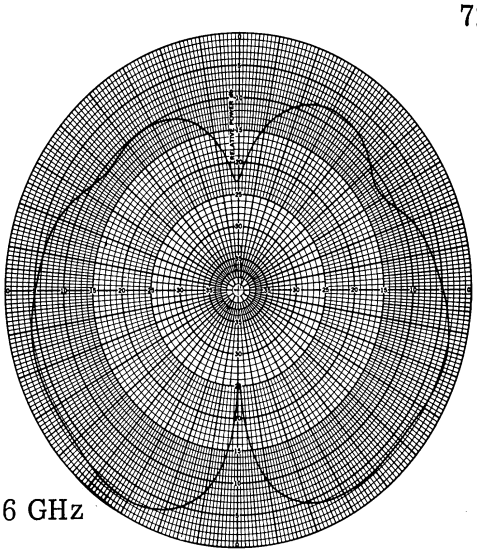

0.6 GHz

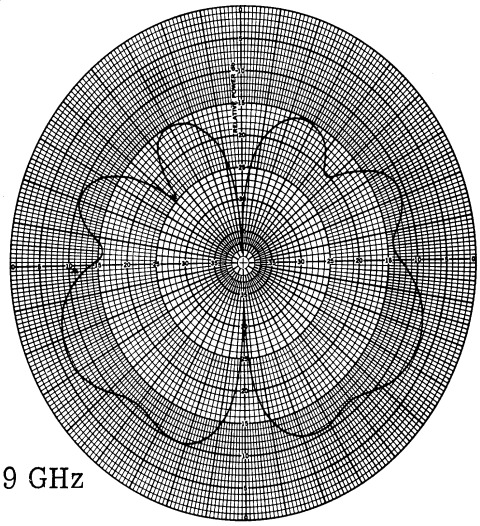

0.9 GHz

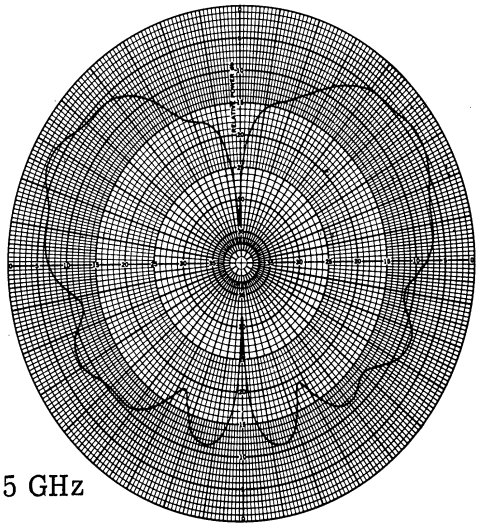

1.5 GHz

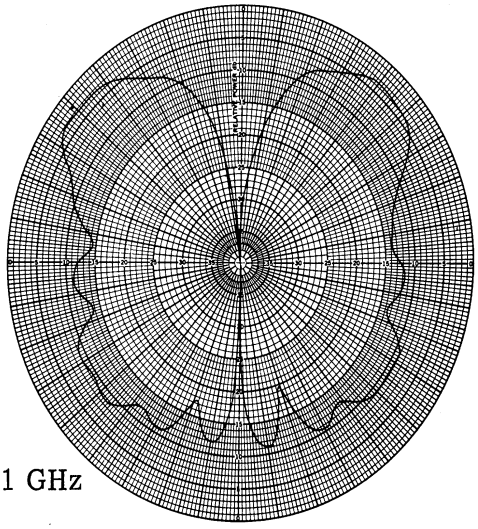

2.1 GHz

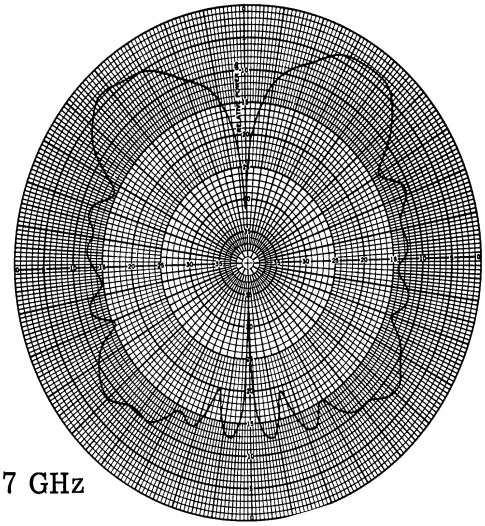

2.7 GHz

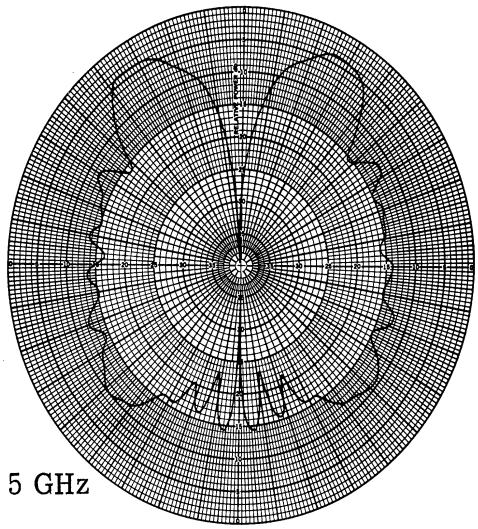

3.5 GHz

FIG. 4-16: ELEVATION PATTERNS OF EXTRA No. 2 ANTENNA OVER A CONICAL GROUND PLANE (0.6 - 3.5 GHz)

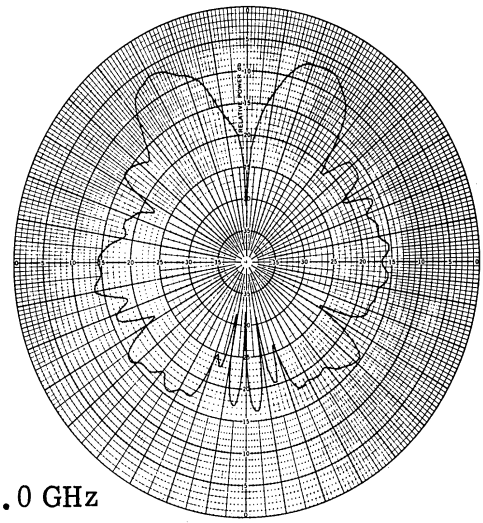

4.0 GHz

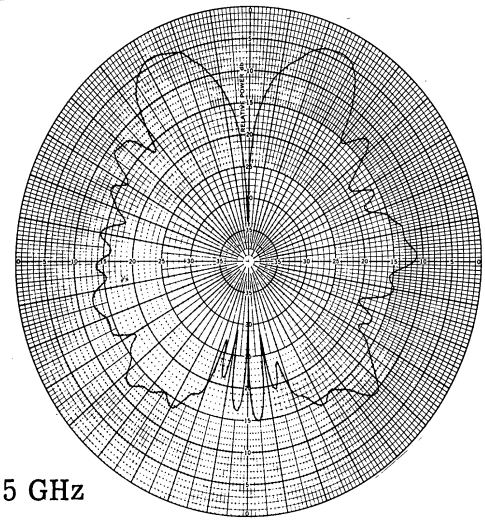

4.5 GHz

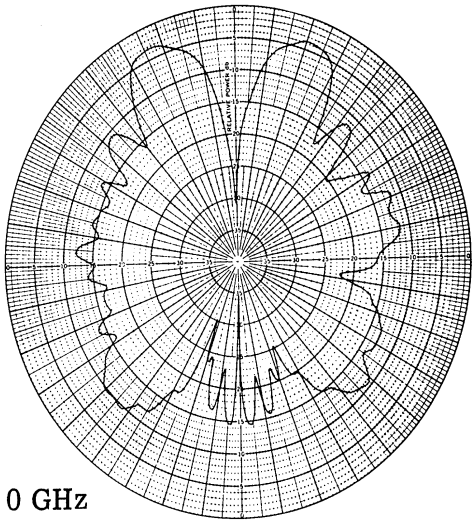

5.0 GHz

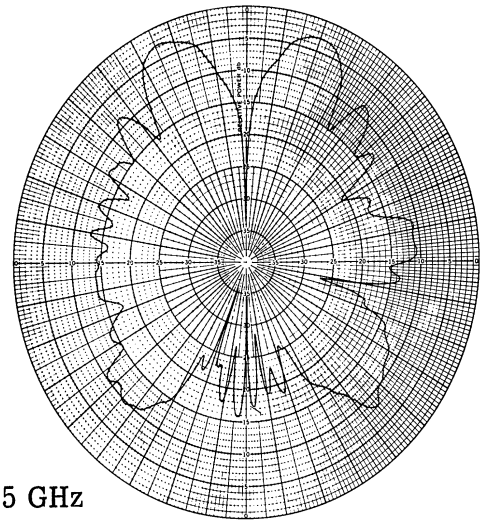

5.5 GHz

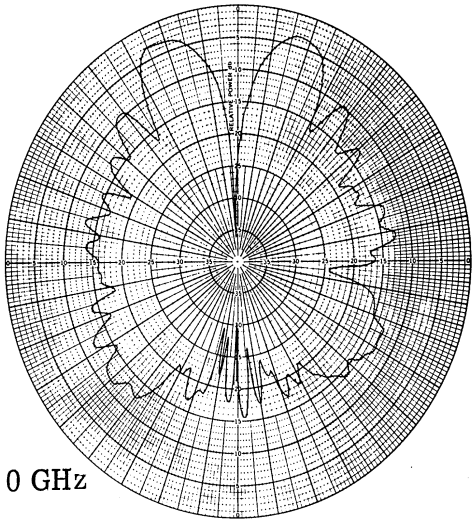

6.0 GHz

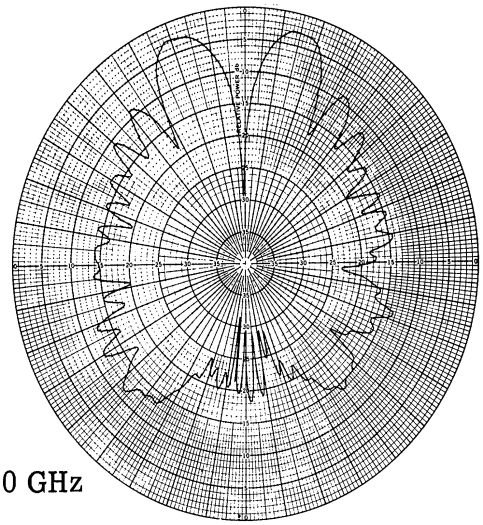

7.0 GHz

FIG. 4-17: ELEVATION PATTERNS OF EXTRA No. 2 ANTENNA OVER A CONICAL GROUND PLANE (4.0 - 7.0 GHz)

smaller the angle between the main lobe and principal axis of the antenna. At the higher frequencies the antenna appears to operate as a traveling wave antenna. Table 4-1 shows the similarity between angles of main beam and nulls for EXTRA No. 2 (from Fig. 4-16 and 4-17), and a traveling wave antenna. Values for the traveling wave antenna were taken from Jasik (1961). The effect of restricting the current near the input is more noticable at 2.1 GHz where the capacitive reactance is more effective. Here the first maximum was observed to occur near 44^{o} instead of the predicted 35^{o}. However, the succeeding nulls and maximums produced by the reduced currents toward the tip display closer agreement.

TABLE 4-1

	Traveling Wave $L = 2\lambda$	EXTRA No. 2 $F = 3.1$ GHz $L = 2\lambda$	Traveling Wave $L = 4.5\lambda$	EXTRA No. 2 $F = 4.5$ GHz $L = 4.5\lambda$
1st max.	35^{o}	44^{o}	23.5^{o}	27^{o}
1st min.	60^{o}	69^{o}	39^{o}	41.5^{o}
2nd max.	75^{o}	76^{o}	48^{o}	49.5^{o}
2nd min.	90^{o}	84^{o}	56.5^{o}	58.5^{o}
3rd max.	105^{o}	93.5^{o}	63.5^{o}	63.5^{o}
3rd min.	120^{o}	107.5^{o}	71^{o}	70.5^{o}

(as measured from principal axis)

It is interesting to observe the agreement between the two sets of data (of Table 4-1) when one recalls that the traveling wave data was obtained for an isolated straight wire, and the second set of data was for a finite antenna (EXTRA No. 2) over a finite conical ground plane. For example, as the frequency of the finite antenna is increased, the reduced capacitive reactance allows the current distribution to more closely approach that of the traveling wave antenna (i.e., higher current density toward the tip). The increased current density in the region near the tip causes the main beam to approach that predicted for the traveling wave antenna. However, the angle of maximum radiation for the finite antenna is somewhat greater than for the isolated straight wire. Based on Terman (1955) the following behavior may be expected for the attenuated current distribution associated with the exponentially tapered reactance of EXTRA No. 2: 1) the angle of maximum radiation will increase, and

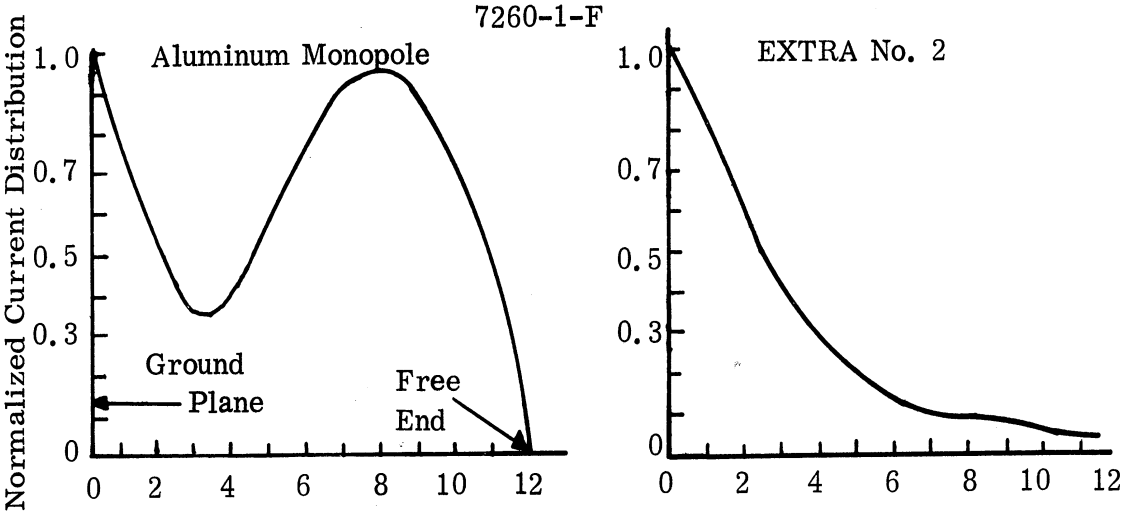

Surface Current Distribution at 600 MHz

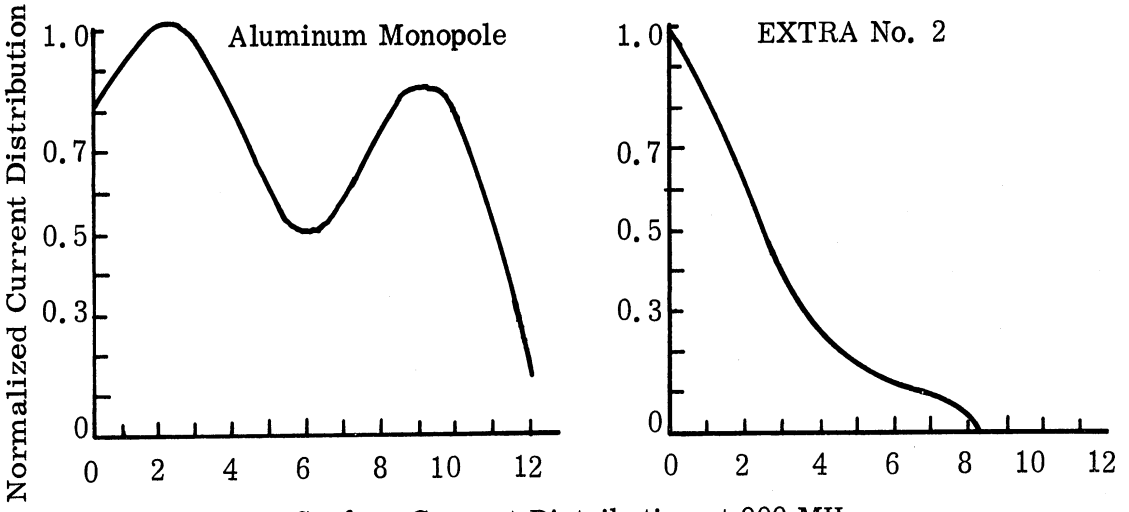

Surface Current Distribution at 900 MHz

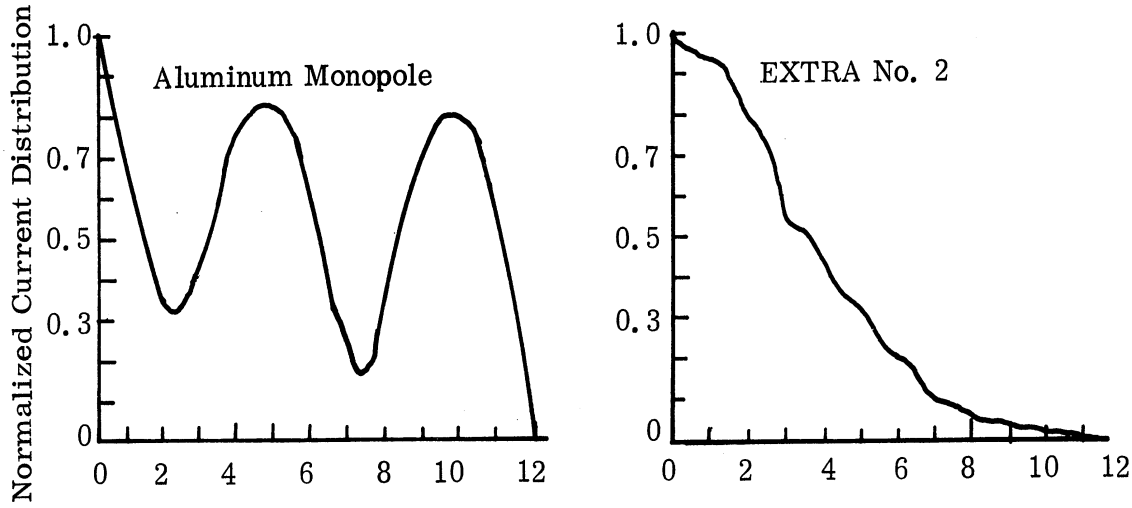

Surface Current Distribution at 1200 MHz

FIG. 4-18: SURFACE CURRENT DISTRIBUTION COMPARISON - ALUMINUM MONOPOLE AND EXTRA No. 2 (600-1200 MHz, ℓ = inches)

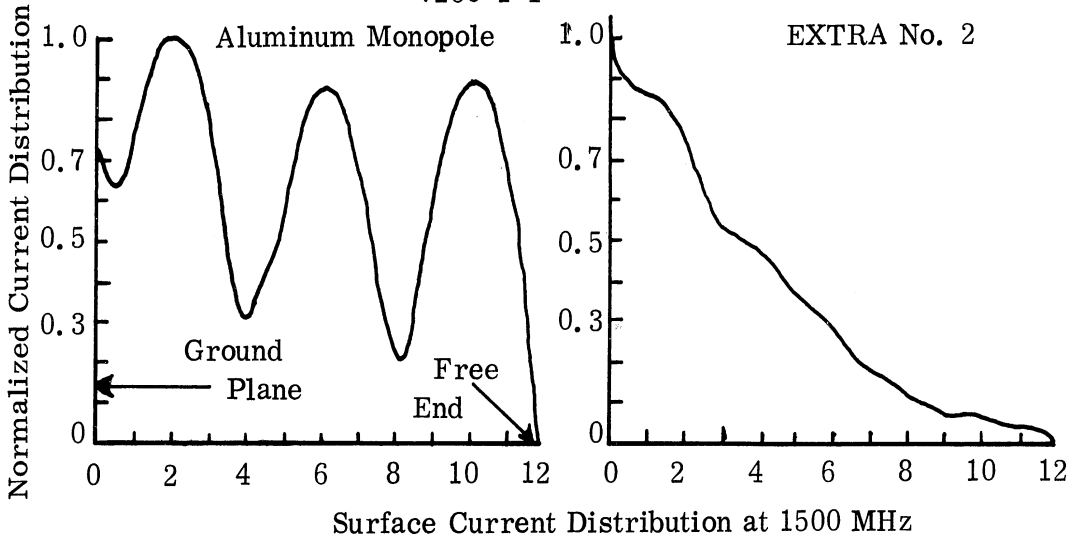

Surface Current Distribution at 1500 MHz

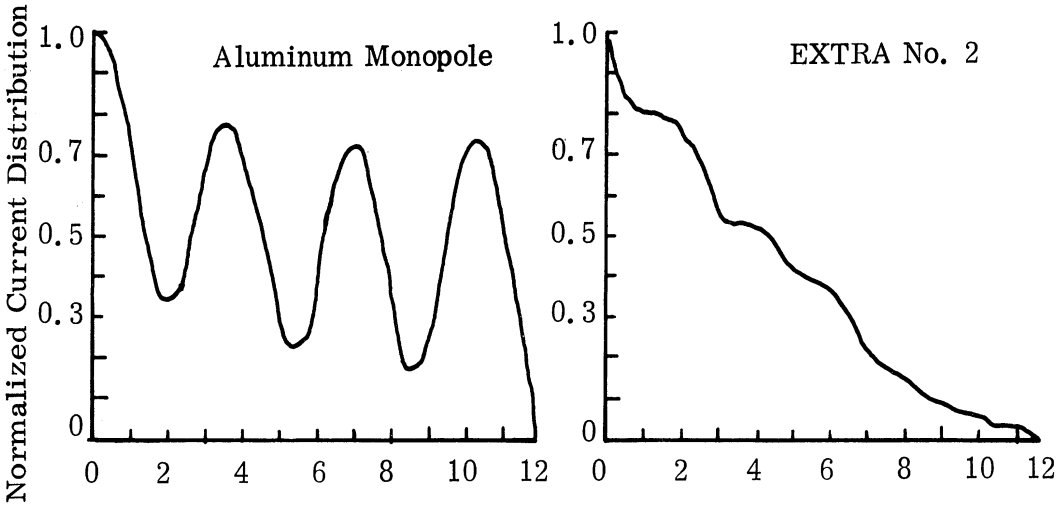

Surface Current Distribution at 1800 MHz

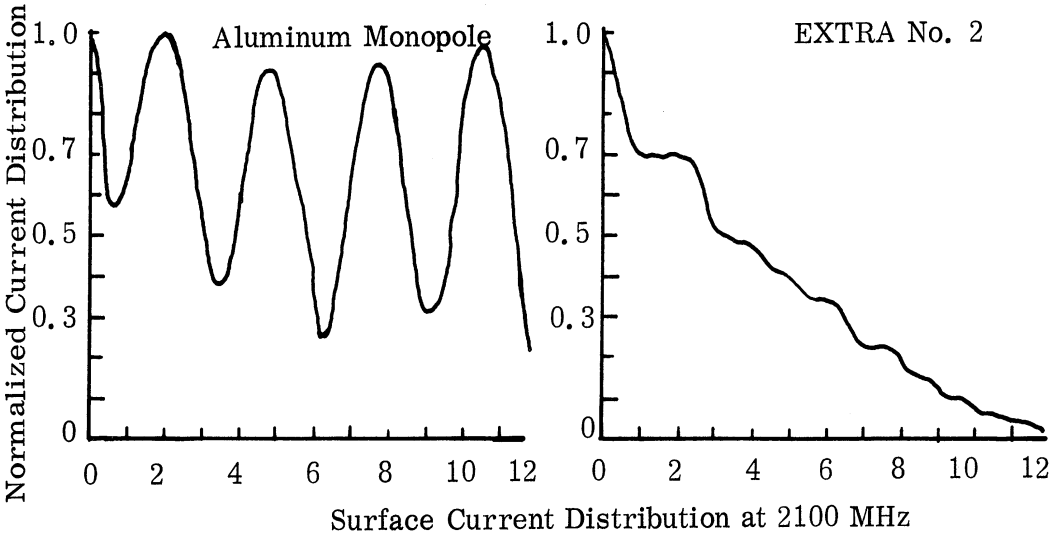

Surface Current Distribution at 2100 MHz

FIG. 4-19: SURFACE CURRENT DISTRIBUTION COMPARISON - ALUMINUM MONOPOLE AND EXTRA No. 2 (1500-2100 MHz, ℓ = inches)

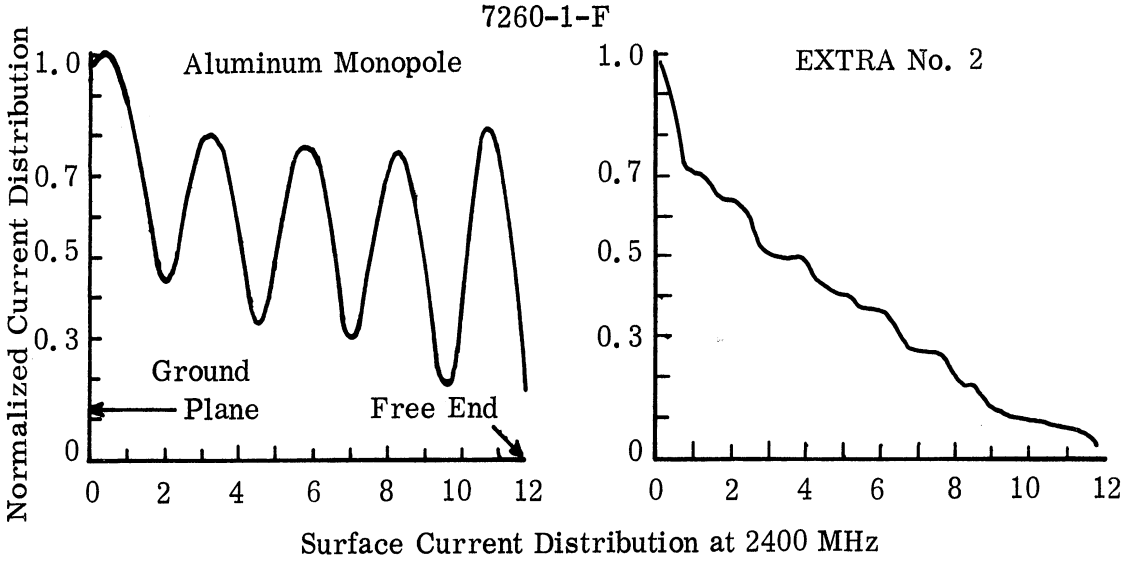

Surface Current Distribution at 2400 MHz

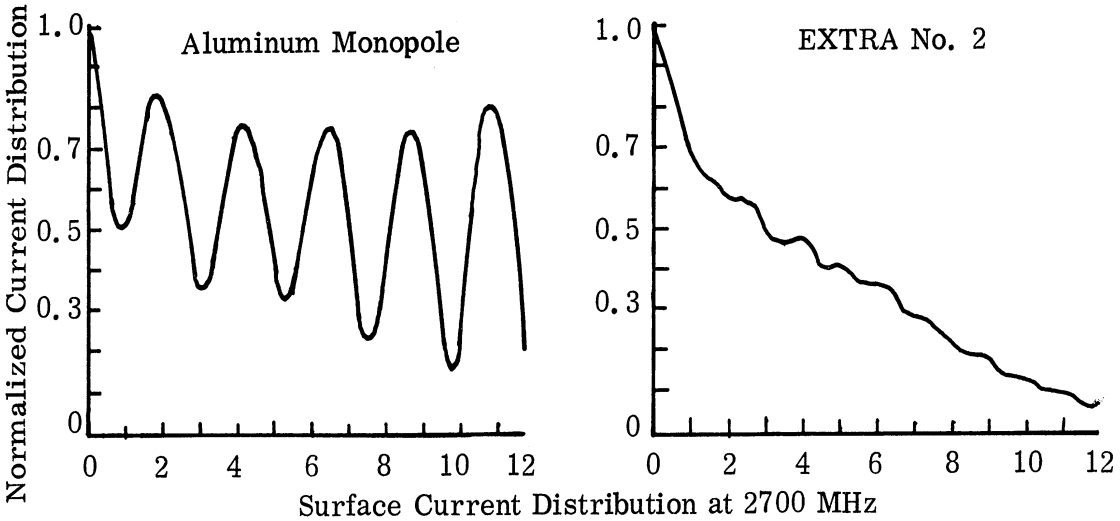

Surface Current Distribution at 2700 MHz

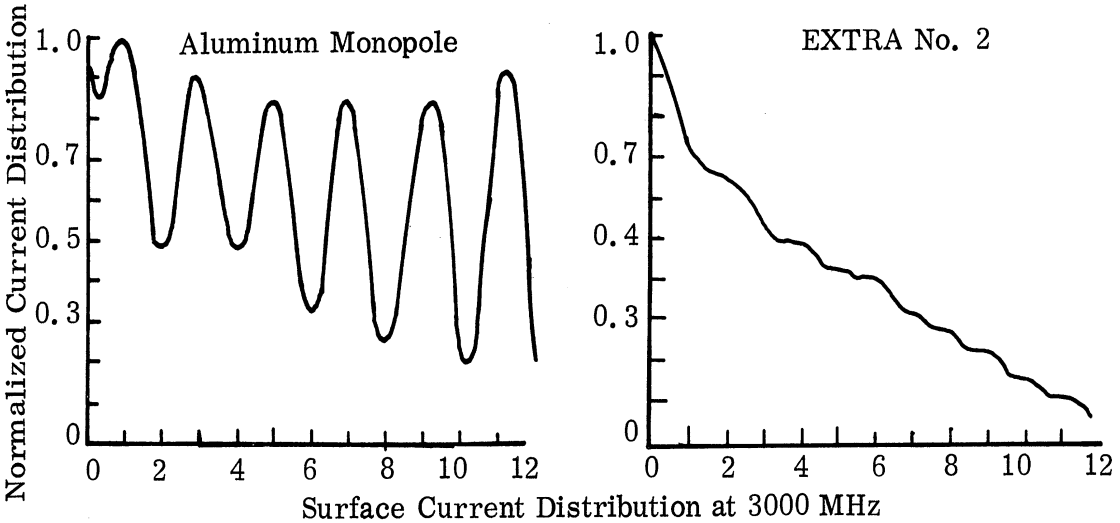

Surface Current Distribution at 3000 MHz

FIG. 4-20: SURFACE CURRENT DISTRIBUTION COMPARISON - ALUMINUM MONOPOLE AND EXTRA No. 2 (2400 - 3000 MHz, ℓ = inches)

2) there will be a reduction in null depth. Since the major lobe of EXTRA No. 2 (Fig. 4-16 and 4-17) tends toward end-fire as the frequency increases and from the current distribution (Fig. 4-18 - 4-20) it is probable that antennas typical of this configuration function in the same manner as long wire antennas ($1 > \lambda$) do at the higher frequencies. For this reason the bandwidth of the capacitively loaded antenna is pattern limited.

4.3.5 Prototype

Figure 4-21 shows the impedance of the prototype antenna mounted over a solid conical ground plane. It was requested that the delivered prototype employ a smaller ground plane employing radial rods. Initially the solid (conical ground plane) was replaced with a rod ground plane consisting of a 2 inch solid metal cone with a 60° total included angle and 8 rods, extending to form the same size as the solid conical ground plane. The impedance (Fig. 4-22) for this ground plane configuration varied primarily in phase which is believed to be due to the change in the ground plane configuration. Figures 4-23 and 4-24 are typical of the patterns for the rodded ground plane and are similar to the patterns for the solid ground plane data (Figs. 4-16 and 4-17). The rods were then cut in half and the impedance (Fig. 4-25) and patterns (Fig. 4-26 and 4-27) data retaken. It was observed that the VSWR increased at the lower frequencies and some pattern distortion occurred (deeper nulls) at the higher frequencies. Although the patterns from 1200 - 1800 MHz appear to be changed, careful examination reveals this is due to the short ground plane, therefore, reducing the rippling in the pattern such that the overall pattern shape remains similar to those of Fig. 4-23 and 4-24. For example, at 2500 MHz a large null occurs at 25° above the horizon because of the short ground plane. At 5500 MHz the pattern exhibits severe lobing for both rodded ground plane configurations. This lobing occurs at the higher frequencies (4000 MHz and above) because the spacing of the eight rods are greater than $\lambda/4$ apart. Patterns at 5500 MHz through 6500 MHz show the severest lobing. This is caused because a solid cone 2 inches long is employed to support the rods. This solid cone is approximately 1 wavelength and therefore enhances the current distribution at the higher frequencies.

It should be noted that the ground plane of the delivered prototype (Fig. 4-28) is considered to be electrically small at the lowest frequency of operation and remains small because of the use of rods (rod spacing varies as a function of cone length). King (1956) notes that a small ground plane may have an adverse affect on the far-field patterns even though the impedance of the antenna is nearly equal to its impedance over an infinite ground plane. One must remember that with an infinite ground plane the contributions to the far field patterns by the currents on the antenna and the

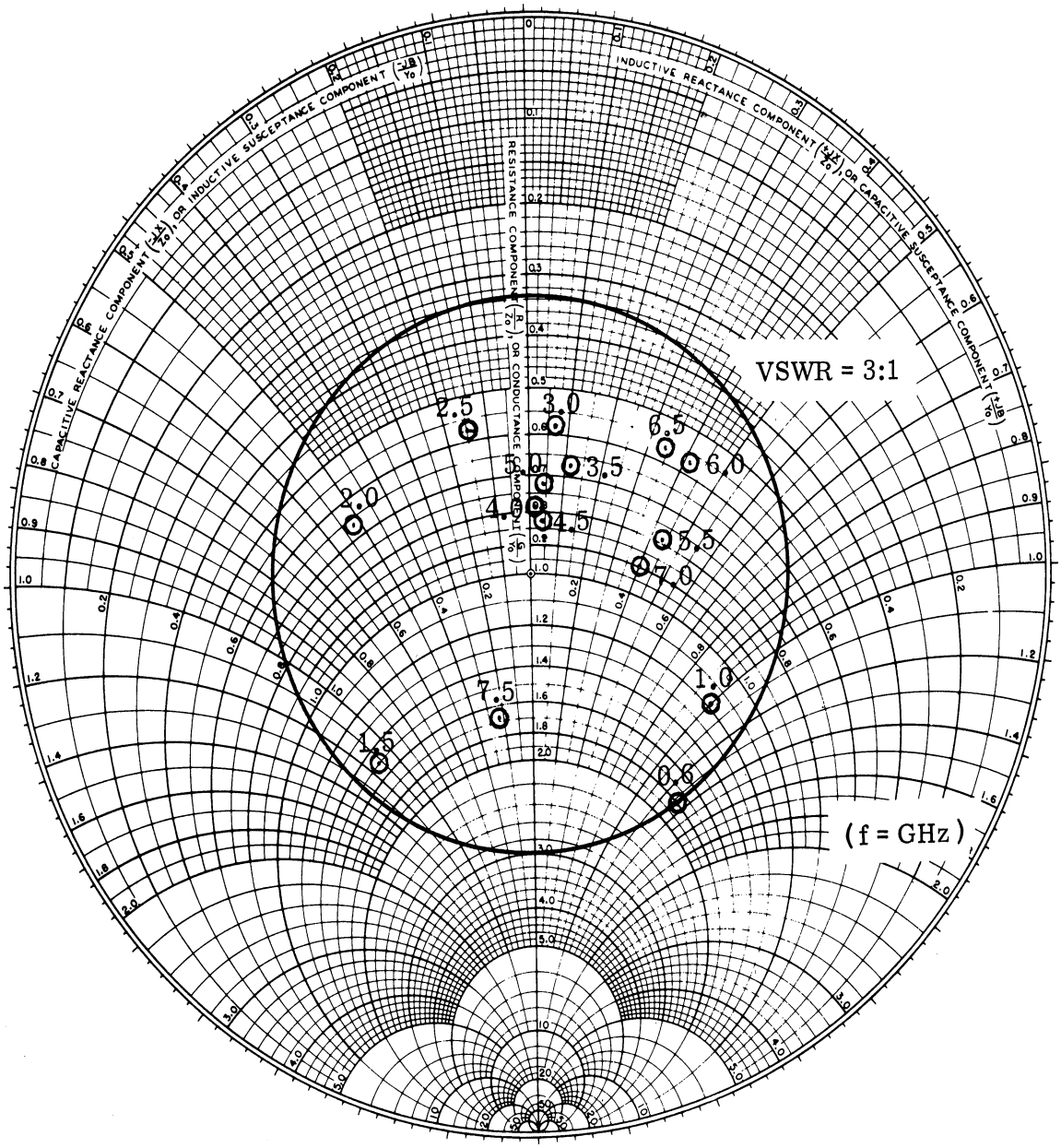

FIG. 4-21: IMPEDANCE PLOT OF EXTRA No. 2 OVER A SOLID ALUMINUM GROUND PLANE

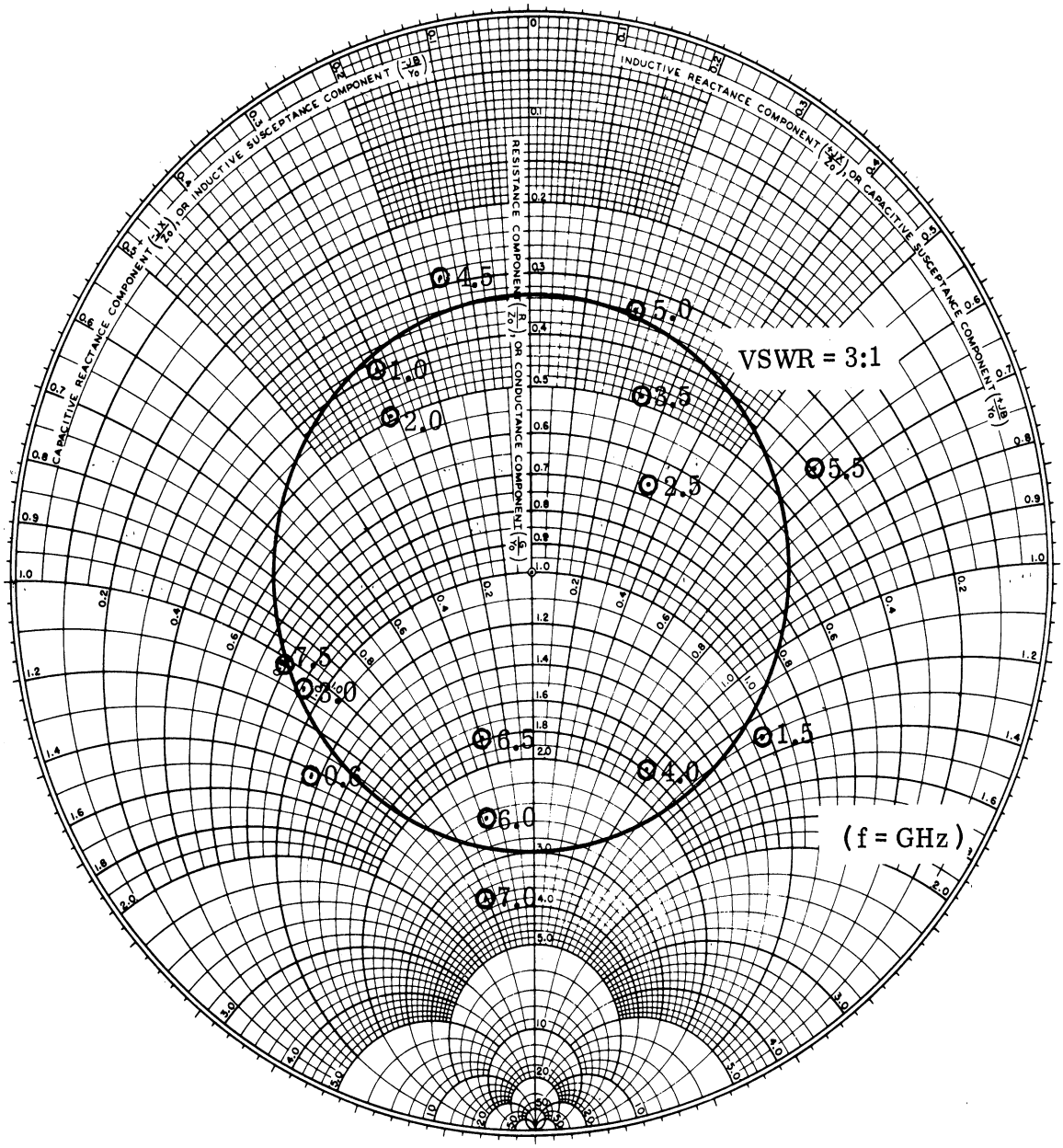

FIG. 4-22: IMPEDANCE PLOT OF EXTRA No. 2 OVER a 18 INCH, 8 ELEMENT ROD GROUND PLANE

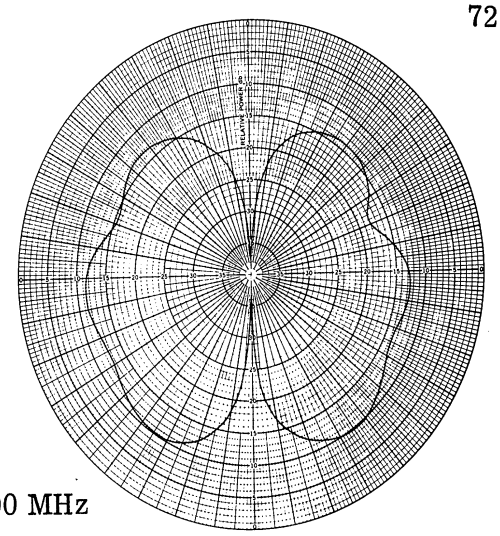

600 MHz

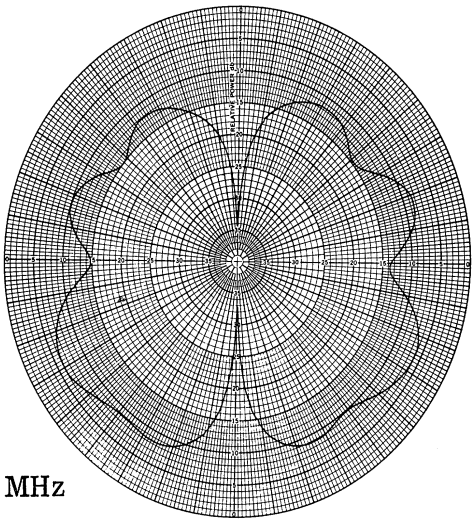

900 MHz

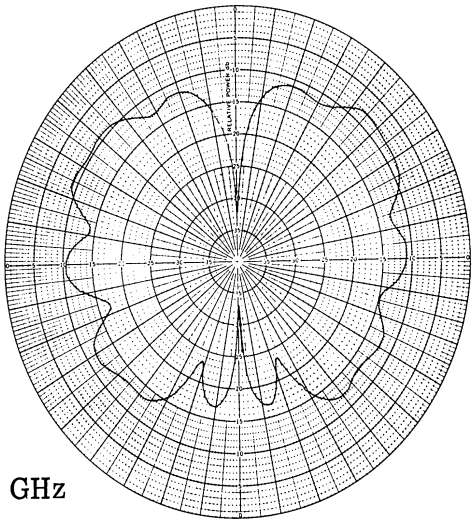

1.5 GHz

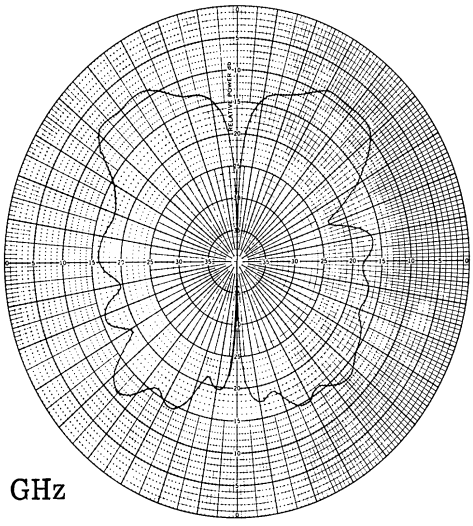

2.1 GHz

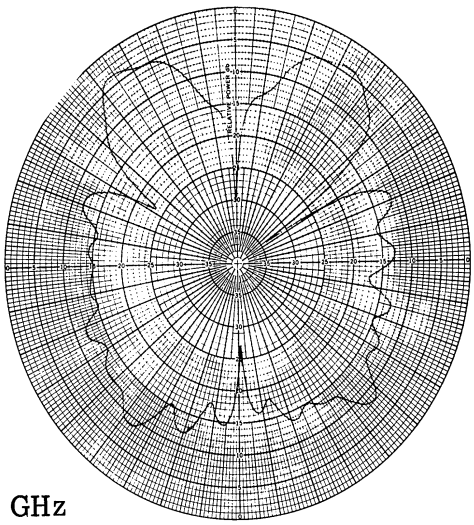

2.7 GHz

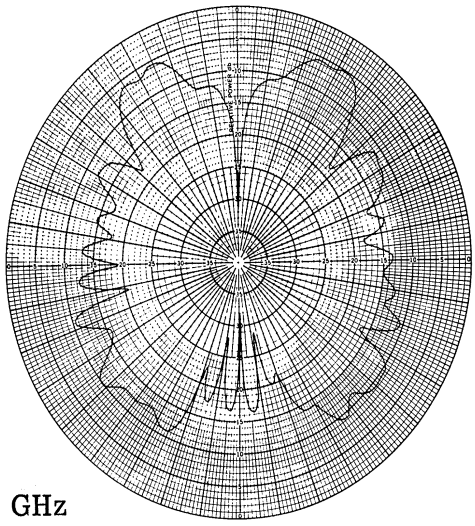

3.5 GHz

FIG. 4-23: ELEVATION PATTERNS OF EXTRA No. 2 EMPLOYING AN 18 INCH RODDED CONICAL GROUND PLANE (600 MHz - 3.5 GHz)

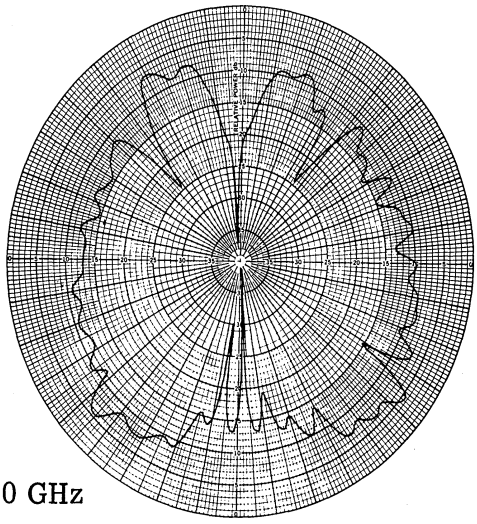

4.0 GHz

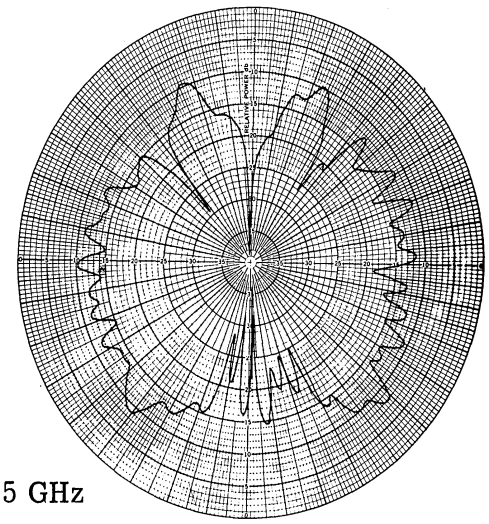

4.5 GHz

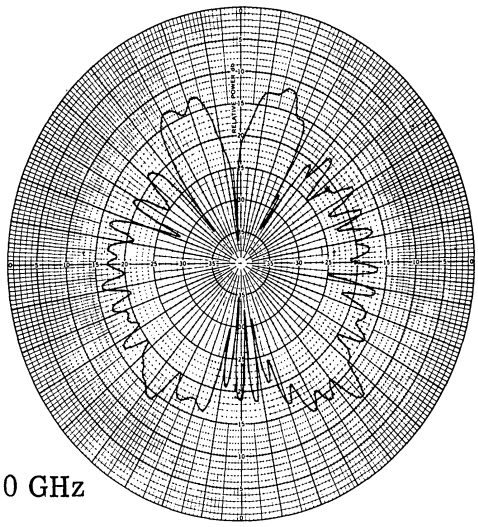

5.0 GHz

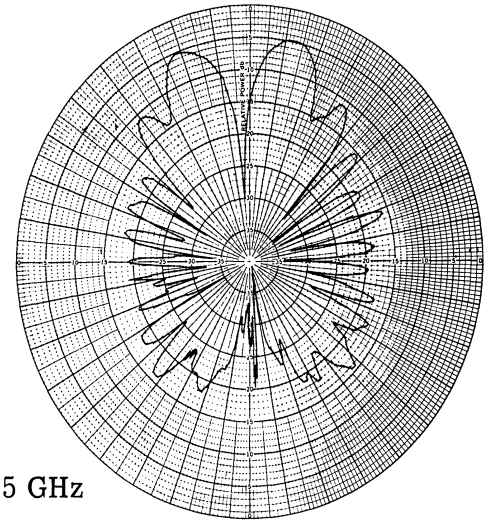

5.5 GHz

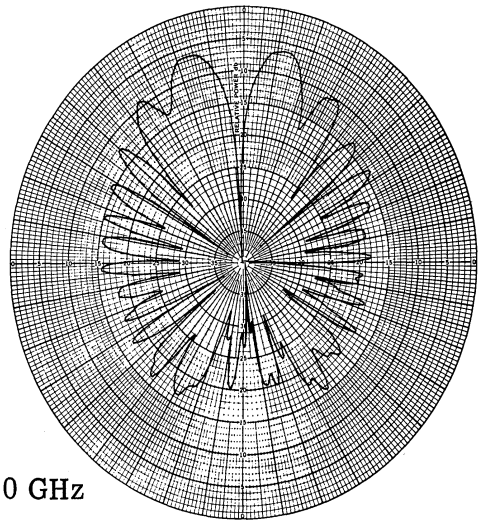

6.0 GHz

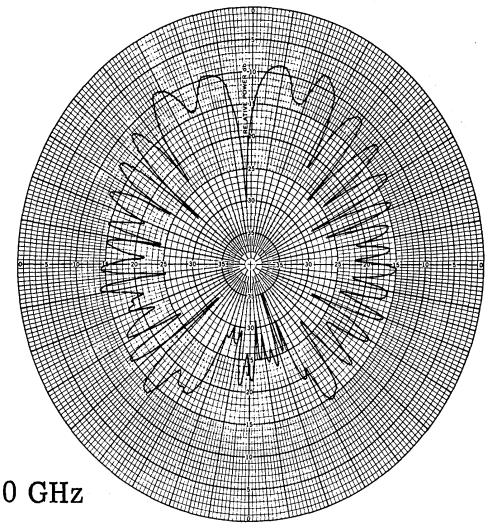

7.0 GHz

FIG. 4-24: ELEVATION PATTERNS OF EXTRA No. 2 EMPLOYING AN 18 INCH RODDED CONICAL GROUND PLANE (4.0 - 7.0 GHz)

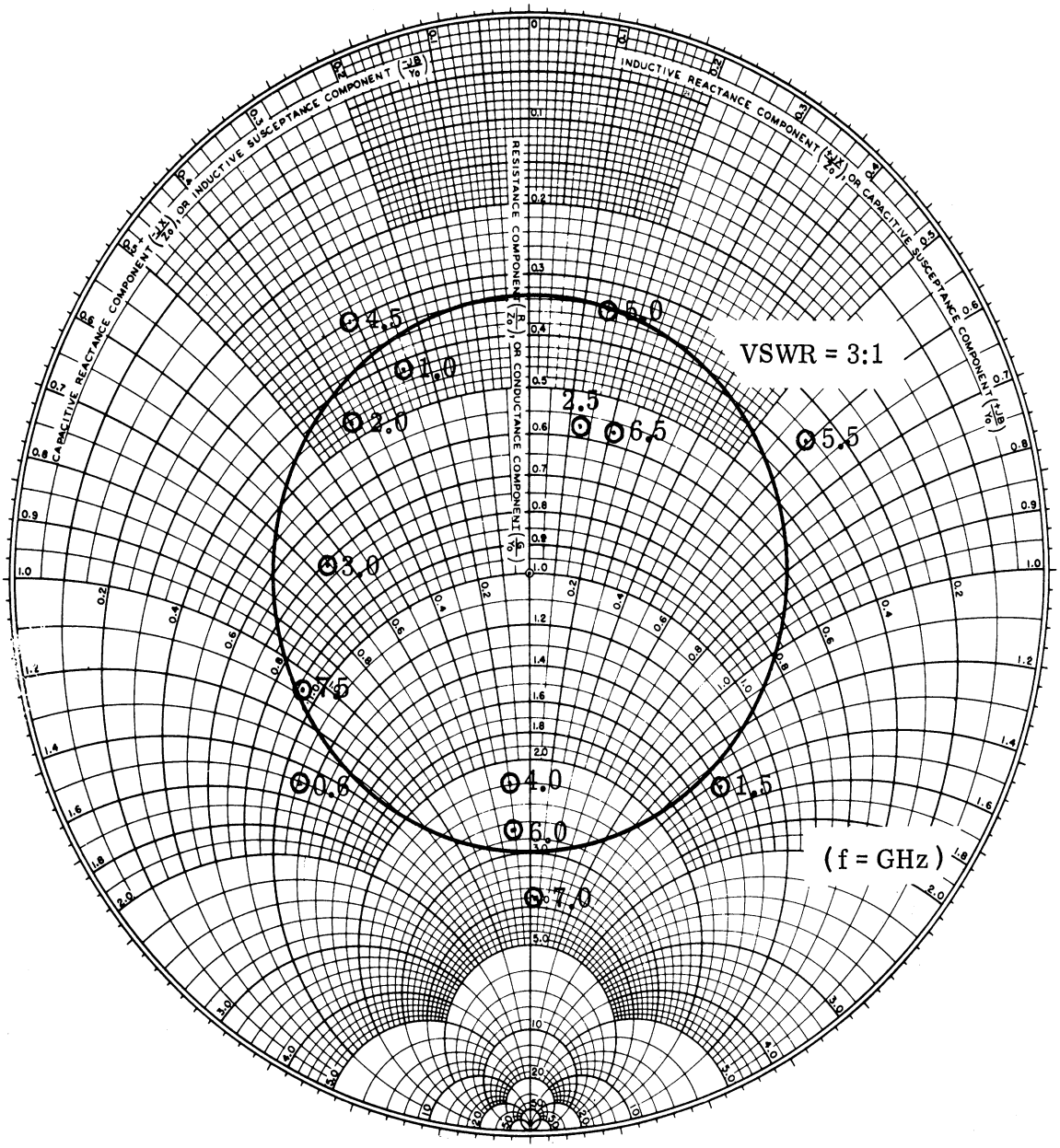

FIG. 4-25: IMPEDANCE PLOT OF EXTRA No. 2 OVER A 9 INCH, 8 ELEMENT ROD GROUND PLANE

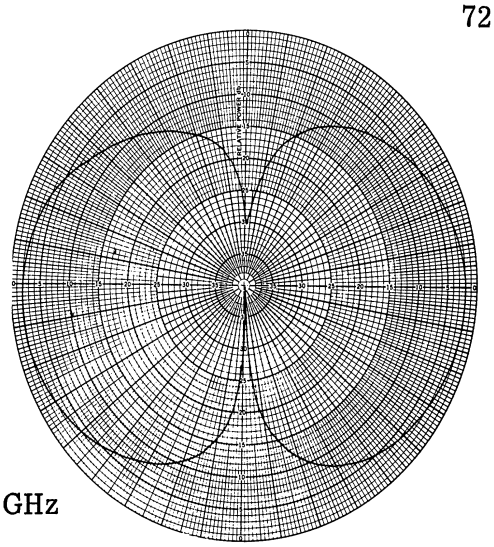

0.6 GHz

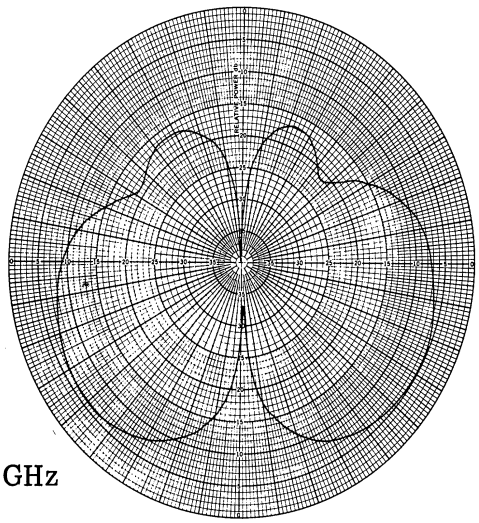

0.9 GHz

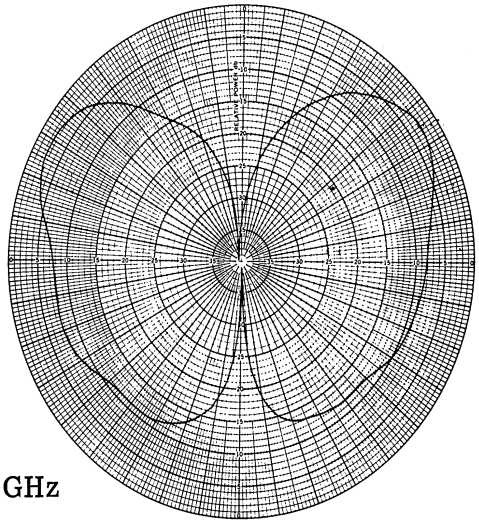

1.5 GHz

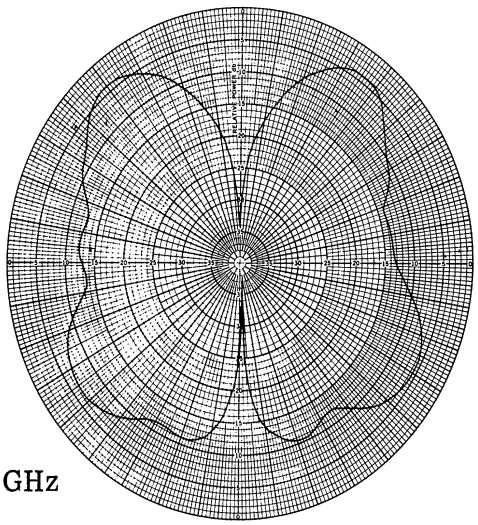

2.1 GHz

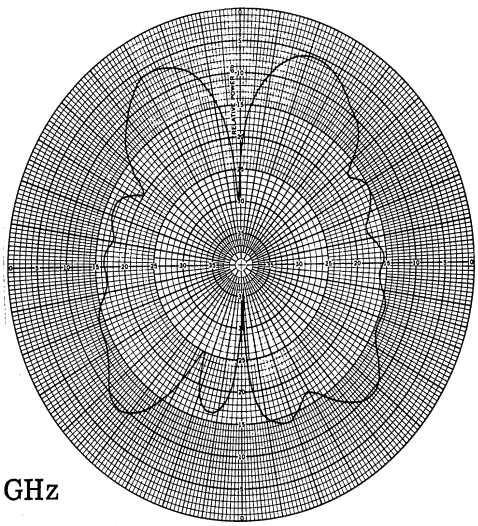

2.7 GHz

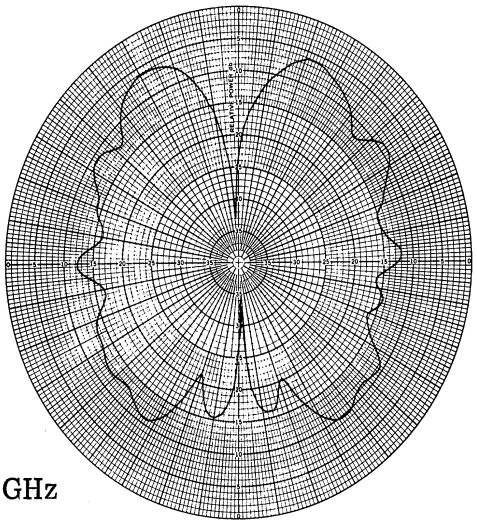

3.5 GHz

FIG. 4-26: ELEVATION PATTERNS OF EXTRA No. 2 EMPLOYING A 9 INCH RODDED CONICAL GROUND PLANE (0.6 - 3.5 GHz)

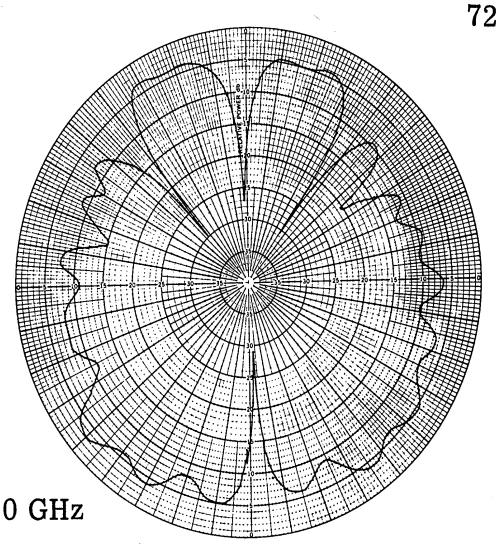

4.0 GHz

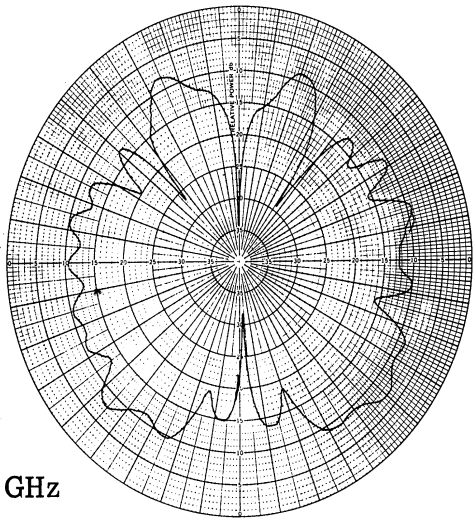

4.5 GHz

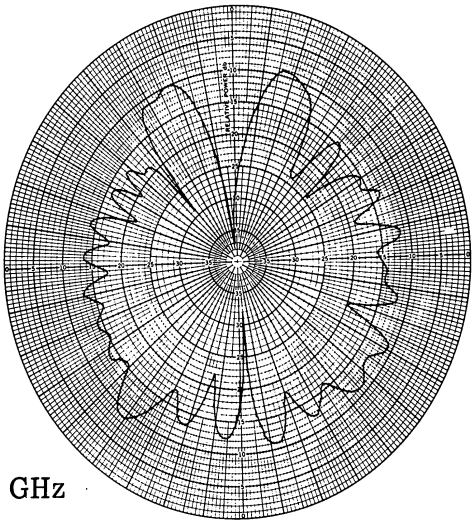

5.0 GHz

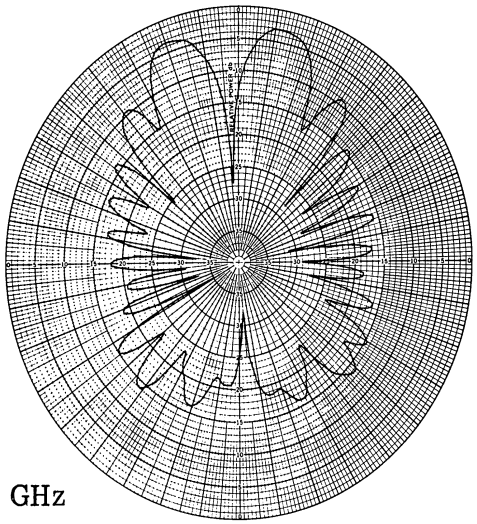

5.5 GHz

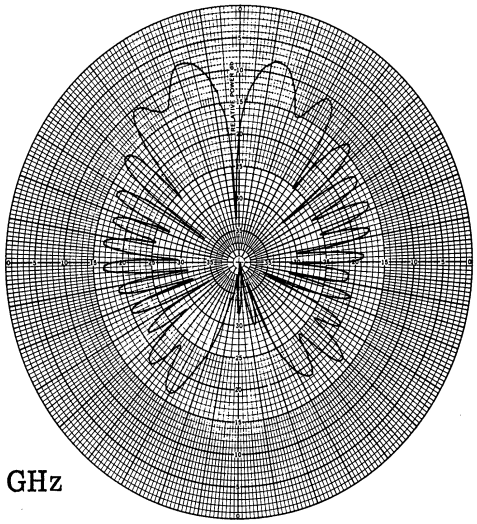

6.0 GHz

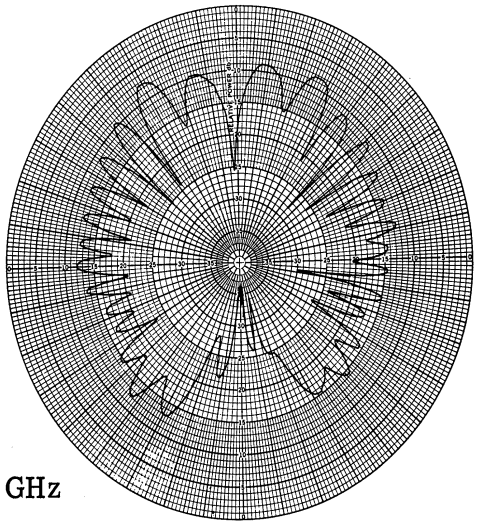

7.0 GHz

FIG. 4-27: ELEVATION PATTERNS OF EXTRA No. 2 EMPLOYING A 9 INCH RODDED CONICAL GROUND PLANE (4.0 - 7.0 GHz)

conducting ground plane are equal. Therefore, if the ground plane is symmetric with respect to ϕ (when the antenna is oriented along the (z) axis) and the ground plane is finite, the currents on the ground plane will be limited to the physical length of the ground plane causing them to exhibit a radial standing wave distribution instead of a traveling wave distribution. The absence of currents beyond the physical termination of the ground plane causes a null in the far-zone field, similar to that for the same antenna over an infinite imperfectly conducting ground plane. The radial attenuation of currents by an imperfect conductor reduces the amplitude of the traveling wave so that at distant points the current differs little from zero. When one employs either an imperfectly conducting ground plane or a finite perfectly conducting ground plane, the currents that contribute significantly to the far field pattern are those on the antenna and on the surface within a finite region of the ground plane around the base of the antenna. For the imperfectly conducting ground plane, the currents consist of attenuated traveling waves and for the finite conducting ground plane the currents are standing waves terminated abruptly at the edge of the ground plane. Although the traveling waves differ from the infinite conducting ground plane, the gradually attenuated traveling waves produce smooth far field patterns. The standing waves on the finite ground plane produce a pattern similar to the attenuated traveling wave, except that it has superimposed ripples, and a small but significant field below the ground plane. Further, when the ground plane is an integral number of half wave lengths long the standing wave is enhanced and the far field pattern exhibits large variations, i.e., deep nulls. This then explains the patterns in the 5500 - 6500 MHz region where the solid aluminum ground plane portion is approximately 1 wavelength and at 2500 - 3000 MHz where it is $1/2\lambda$ long. The rods tend to reduce the half wave resonance but at the wavelength resonance this effectiveness is limited due to the electrical separation (between the rods) in circumference.

Data presented above demonstrates the need for considering the broadband element and ground plane together as the antenna. For example, if the broadband element and a short ground plane are mounted over a vehicle, currents will be induced on the vehicle such that it must be considered part of the ground plane and will be instrumental in determining the shape of the far field pattern.

Two possible means of reducing nulls of the above antenna (EXTRA No. 2) are: 1) scalloping the edge of the solid aluminum cone to disturb the standing wave, and 2) employing additional rods of irregular lengths to reduce the electrical separation.

Gain data is shown in Figs. 4-29 and 4-30. The dotted line represents the isotropic level. Dipoles were used as a gain standard from 600 - 1400 MHz, and gain standard horns for the higher frequencies. The above data (Figs. 4-29 and 4-30)

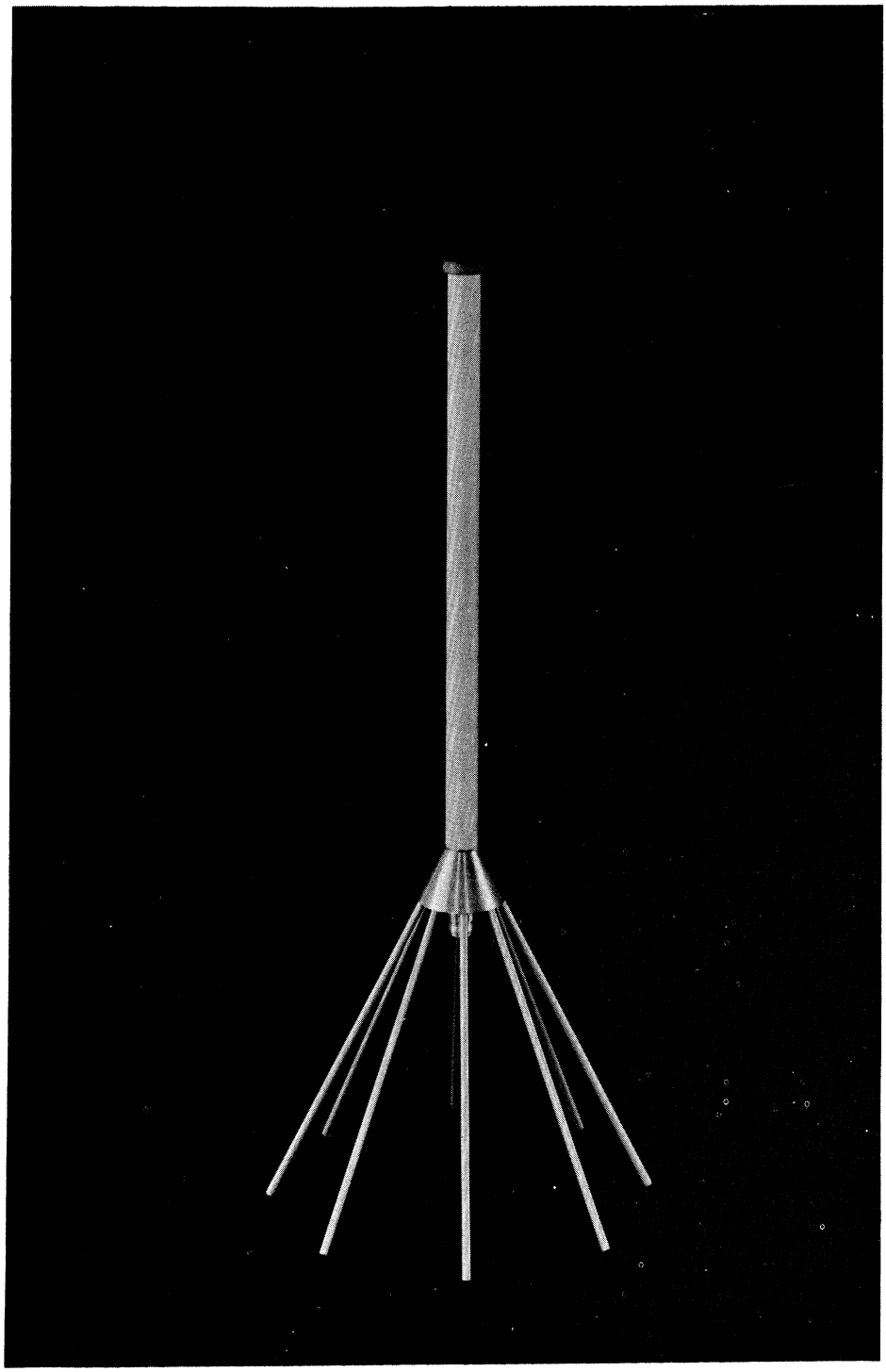

FIG. 4-28: DELIVERED PROTOTYPE (EXTRA No. 2)

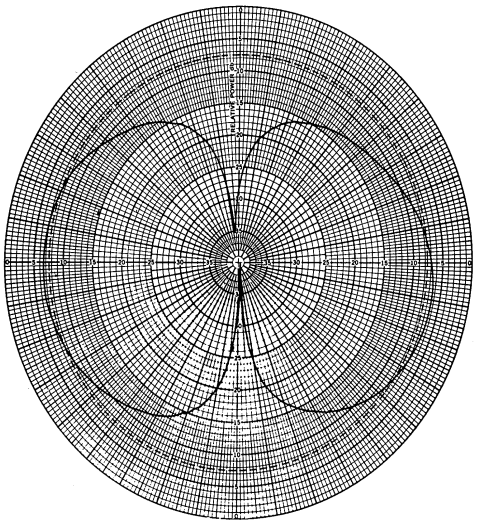

0.6 GHz

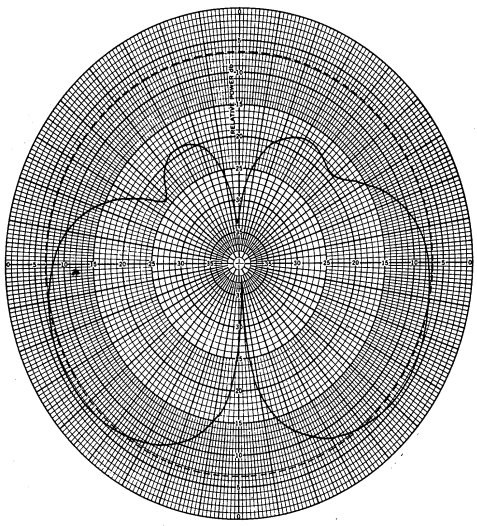

0.9 GHz

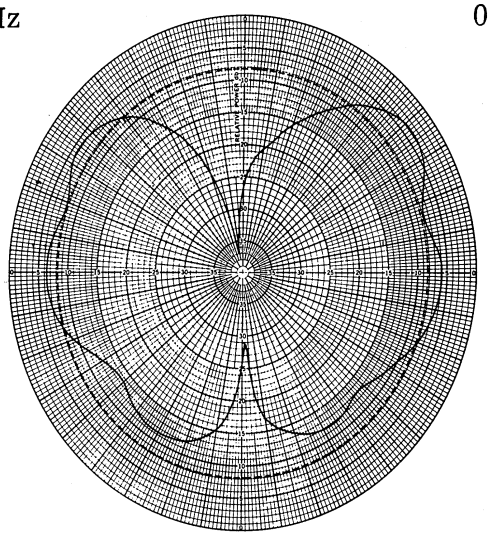

1.4 GHz

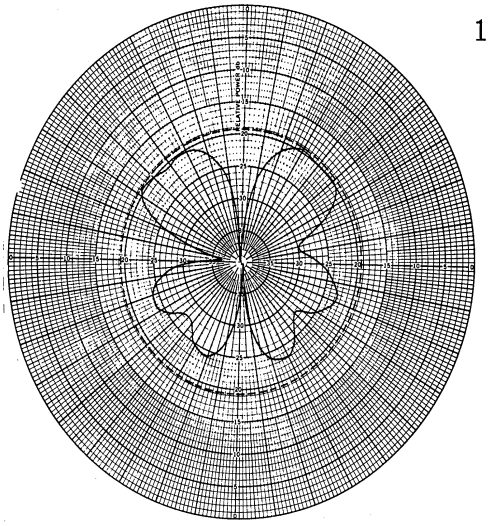

1.9 GHz

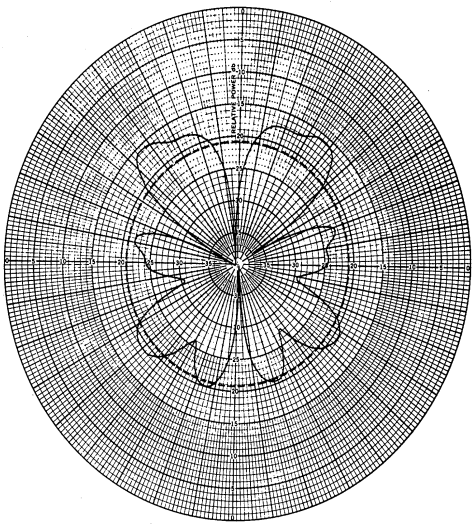

2.5 GHz

FIG. 4-29: GAIN PATTERNS OF EXTRA No. 2 RELATIVE TO AN ISOTROPIC SOURCE (0.6 - 2.5 GHz)

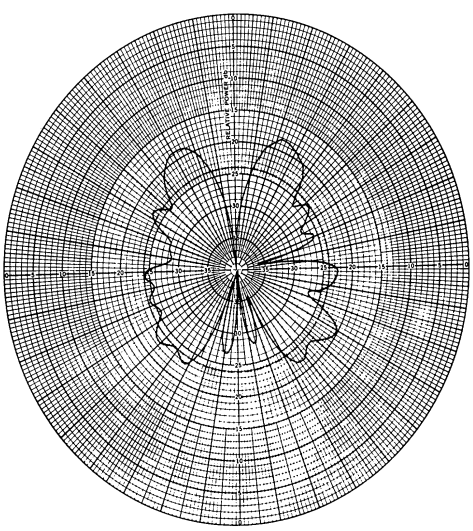

3.5 GHz

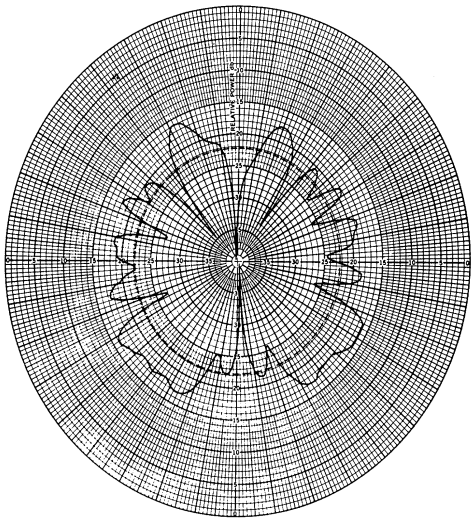

4.5 GHz

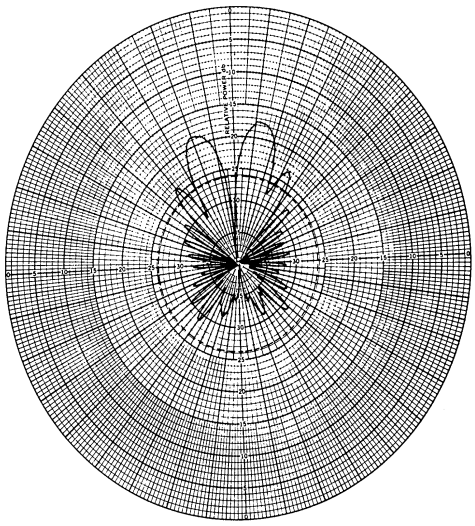

5.5 GHz

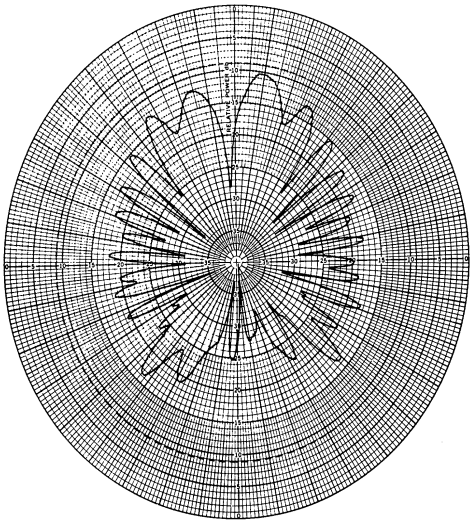

6.5 GHz

FIG. 4-30: GAIN PATTERNS OF EXTRA No. 2 RELATIVE TO AN ISOTROPIC SOURCE

shows that the capacitive loading slightly reduces the gain of the antenna. However, we should remember the gain is influenced by the ground plane, e.g., a vertical monopole over an infinite ground plane will have twice the gain of a vertical dipole. By changing from an infinite ground plane to a short conical ground plane, the gain of the monopole decreases.

4.4 Conclusive Remarks to the Capacitively Loaded Antenna

A thorough understanding of the broadband operating characteristics of the reactive antenna cannot be presented at this time. However, we may offer some interesting observations based on the surface current data presented previously and from reflectometer data. It should be noted that when one is measuring the surface current distribution of the antenna, both the forward and reverse currents are present but cannot be separated. Due to this ambiguity, it is sometimes difficult to properly interpret the surface current data. For example, questions still remain as to the cause for the type of current distributions that were observed in Figs. 4-18, 4-19 and 4-20. To assist in the understanding of the above data, a set of reflectometer data was collected in the frequency range of 1.0 - 2.0 GHz for a solid monopole (Fig. 4-31) and EXTRA No. 2 (Fig. 4-32) for two conditions each (with and without a dielectric sleeve).

From the reflectometer data, we find that the addition of the dielectric support tube (Fiberglass G-7) to the aluminum monopole reduces the phase velocity of the surface currents. This reduction in phase velocity is hypothesized because of the shift in the reflection coefficient of Fig. 4-31. From Fig. 4-31 the monopole appears to be longer when the dielectric sleeve is employed since the reflection coefficient curve for this configuration is shifted (toward the lower frequency) relative to the configuration without the sleeve. It is further hypothesized (and substantiated by the surface current data of Fig. 4-18, 4-19 and 4-20) that the surface currents of the aluminum monopole exist as standing waves as a result of the interaction between the incident and reflected surface current flowing on the monopole. The shift in the reflectometer data of Fig. 4-31 is explained since the dielectric sleeve retards the velocity of the incident and reflected conduction currents on the surface of the monopole. Because of this reduction in the phase velocity one may expect the impedance at the input to the monopole to be shifted in frequency as is apparent from Fig. 4-31.

From the surface current data on the EXTRA No. 2 antenna as shown in Fig. 4-18, 4-19, and 4-20, one may hypothesize that a traveling wave exists. This assumption appears to be valid since there is no apparent standing wave pattern in

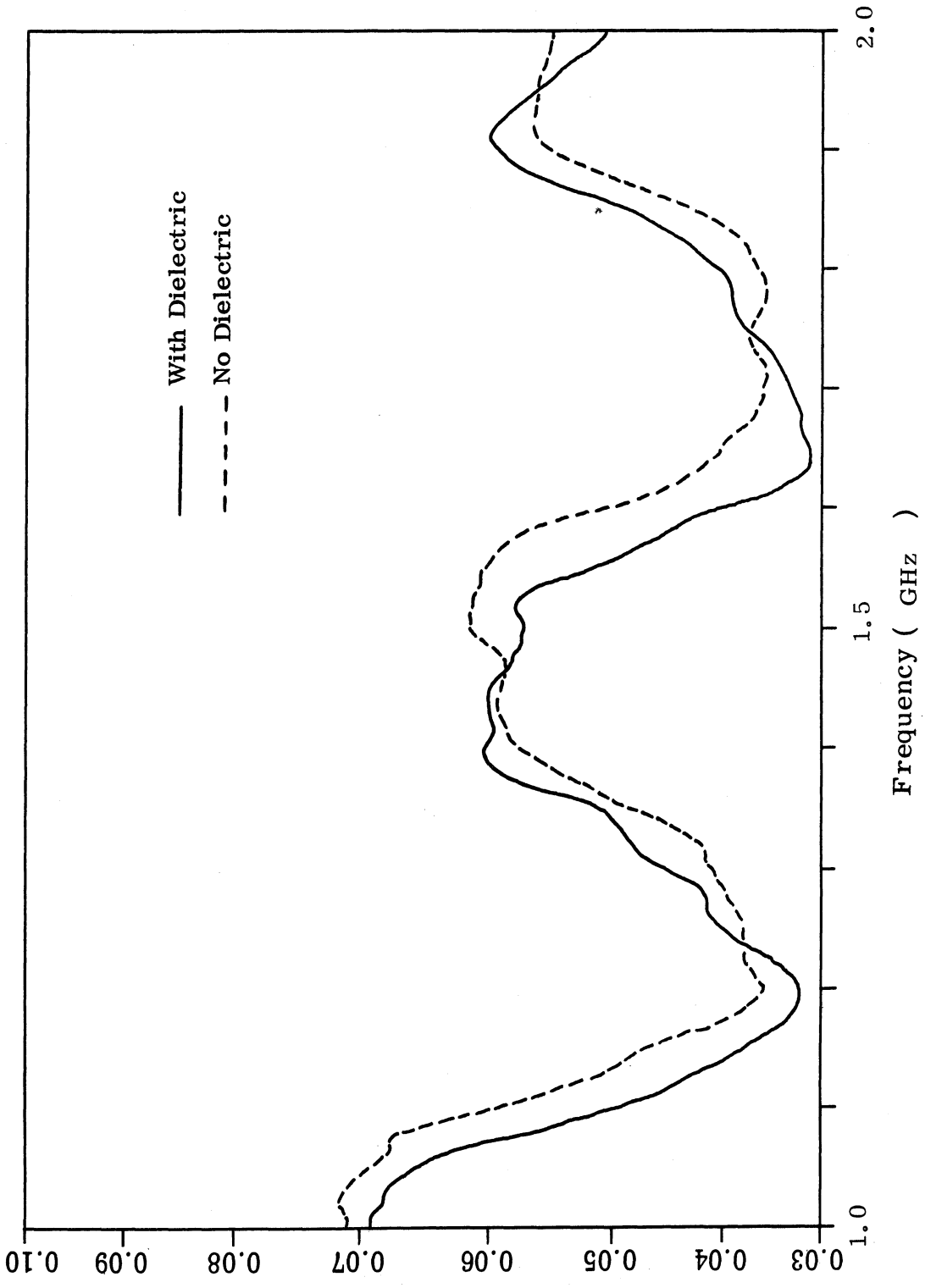

FIG. 4-31: ALUMINUM MONOPOLE REFLECTION COEFFICIENT
(ℓ = 11-1/2 inches) (ρ = 0.3 - 1.0)

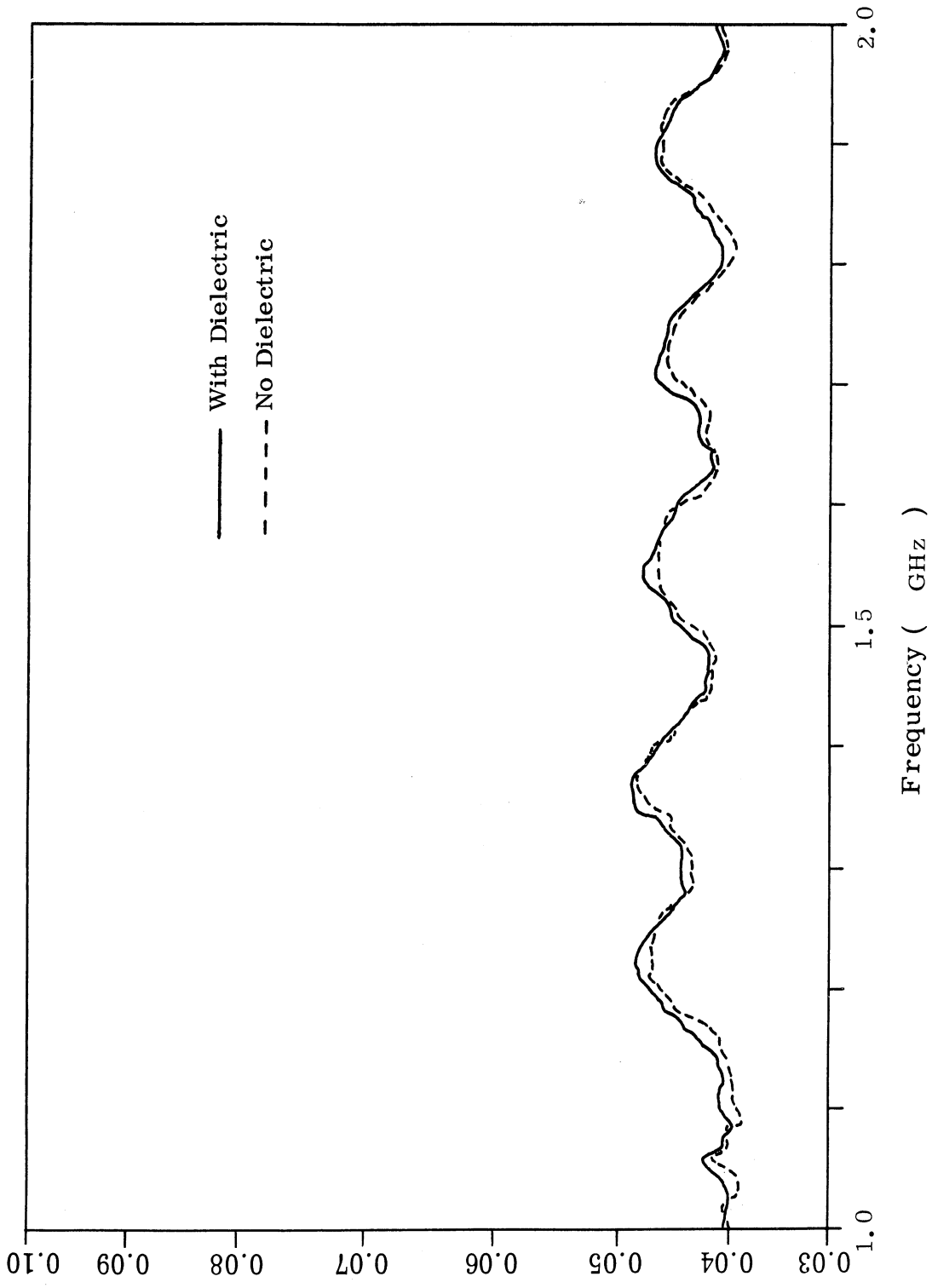

FIG. 4-32: EXTRA No. 2 REFLECTION COEFFICIENT
(ρ = 0.3 - 1.0)

the data. Further, it is obvious the incident current reduced to zero over a finite antenna length. Because of this current decay one may assume there is only an incident surface current and no reflected current from the tip of the antenna. The reflectometer data of Fig. 4-32 further substantiates this hypothesis since there is little change in the reflection coefficient with or without the dielectric sleeve.

A further observation that may be made in regards to the reactive loaded antenna is the manner in which the traveling wave (Fig. 4-18, 4-19 and 4-20) varies with frequency. Consider the classical equation for capacitive reactance ($X_C = 1/2\pi fC$) Assuming that C remains constant, we see that the capacitive reactance is inversely proportional to frequency. From the surface current data for EXTRA No. 2, we see that the current distribution becomes distributed over a longer length of the antenna as the frequency increases.

It is interesting to note that in Hallen's discussion of the reflectionless antenna (Hallén, 1962), he suggests the desirability of a current distribution that is limited to an incident traveling wave, i.e., the reactance should restrict the current such that there would be zero incident current at the antenna tip and there would be no reflected conductive current flowing. It is apparent from the above data that a reflectionless antenna can be fabricated employing capacitance. Further, the antenna will be broadband (frequency range 10:1) insofar as its impedance characteristics are concerned. With respect to pattern we will define a broadband pattern to be equivalent to the pattern of a $\lambda/2$ dipole over the frequency band of interest. This restriction was not stated by Hallén. To achieve this pattern it requires that the antenna incident conduction currents be restricted to the first $\lambda/2$ for the particular frequency involved. This requires that the distributed reactance along the length of the antenna be directly proportional to the frequency. Therefore, an inductive reactance is required since from the classical inductive reactance equation ($X_L = 2\pi fL$) we see that the inductive reactance is directly proportional to frequency. However, there are problems associated with employing inductancies at frequencies > 100 MHz as have been discussed previously (Ferris, et al, 1967). In the following section a few concluding remarks with regard to an inductively loaded reactive antenna are presented.

It was requested that consideration be given to the feasibility of employing inductive elements in series with capacitive elements, to reduce the physical length of the antenna (EXTRA No. 2). Previous experimental experience with inductive elements for the frequency range of interest suggests that they are not practical. Further, if one obtains a pure inductance at these frequencies, it is considered not advisable to employ series inductors in series with capacitive elements, simply

because the effective reactive loading is reduced thus defeating the very purpose of tapered capacitive reactive loading.

4.5 Inductive Antenna

Inductive loading appears attractive due to the fact noted previously that inductive reactance increases with frequency. The first impression is that this increased reactance would limit currents to the lower section of the antenna at the higher frequencies thus improving the far field radiation patterns. Pattern quality may not be increased as much as it first appears as will be shown later. A further discussion of the inductive concept was presented in the sixth quarterly report for this contract (Ferris, et al, 1967).

4.5.1 Experimental Results

Experimental models have been constructed to operate in both the 100 - 1000 MHz and 300 - 3000 MHz bands. Classical electromagnetic theory suggests the most logical method to obtain an inductance is to wind a conducting filament in the form of a coil. This was the first concept employed in the design of an inductive antenna. Reflectometer data (to be presented) graphically shows the results of different configurations considered. One of the first inductive antennas exhibited controlled patterns at discrete 100 MHz intervals over the frequency range of 100 - 1000 MHz. This antenna (Fig. 4-33) employed 48 coils each consisting of 10 turns of wire wound on a 1/2 inch diameter form with each coil spaced 1/2 inch between the adjacent ends. Figure 4-34 is a plot of the reflection coefficient as a function of frequency from 1 - 2 GHz. Although the antenna was designed to operate in the 100 - 1000 MHz range, this graph shows high oscillations in the VSWR characteristic. Generally the VSWR minimums were separated by 100 MHz in the 100 - 1000 MHz range. At these frequencies, the patterns (Fig. 4-35) were well behaved suggesting that the surface current distribution was also well behaved. Initial efforts to measure the surface currents associated with the antenna showed that the current was restricted near the antenna input. Further, as the frequency increased, the current distribution receeded toward the input terminal as expected for an inductively loaded antenna. It is not understood what produces the high VSWR's at periodic intervals. However, a possible explanation is presented below.

From the Smith Chart it would appear desirable for the total length of the conducting filament of the coil to be less than $\lambda/4$ long (at the highest operating frequency of interest to ensure that the coil will appear inductive). It is obvious however, that a ten turn coil wound on 1/2 inch diameter would consist of a filament far

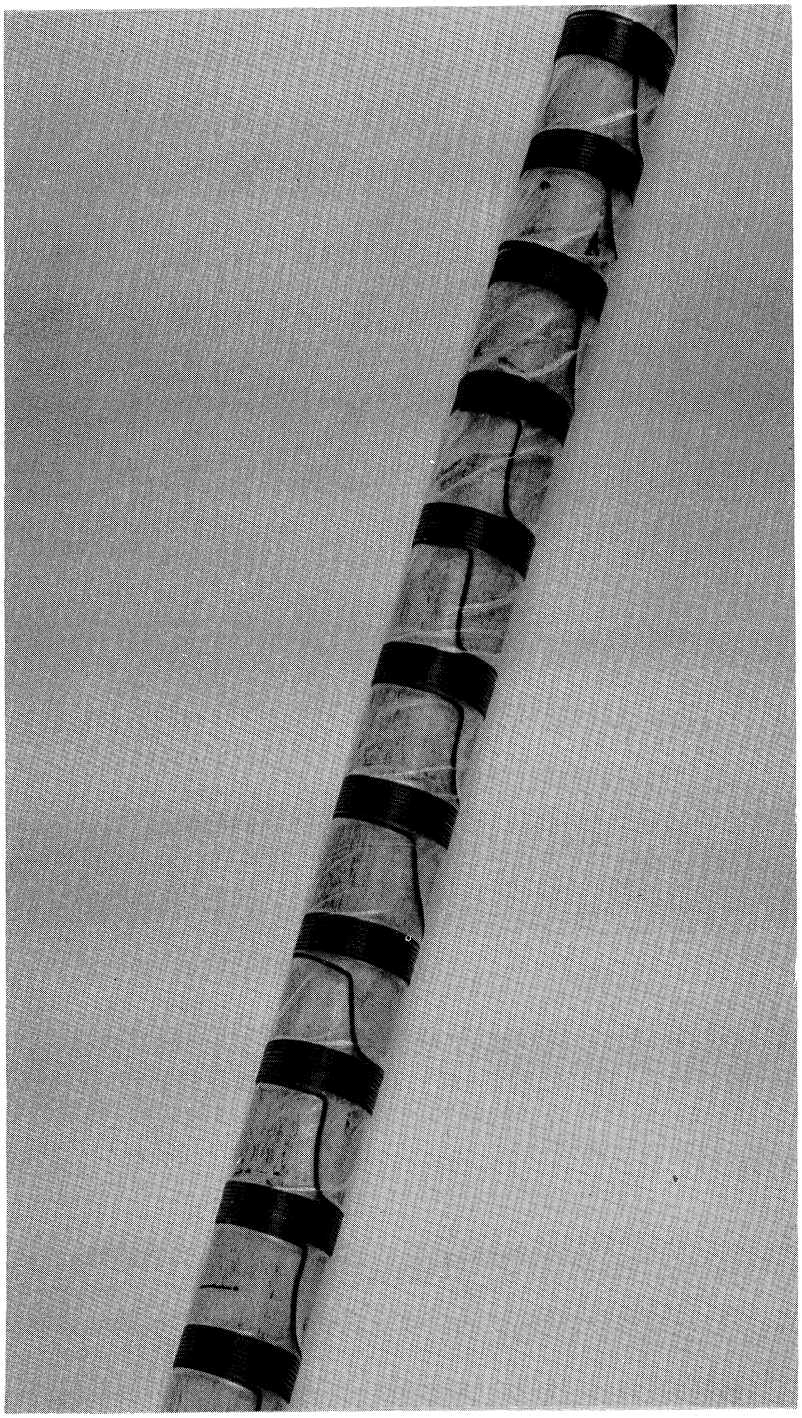

FIG. 4-33: INDUCTIVE LOADED ANTENNA (48 COILS - 1/2 INCH DIAMETER COIL)

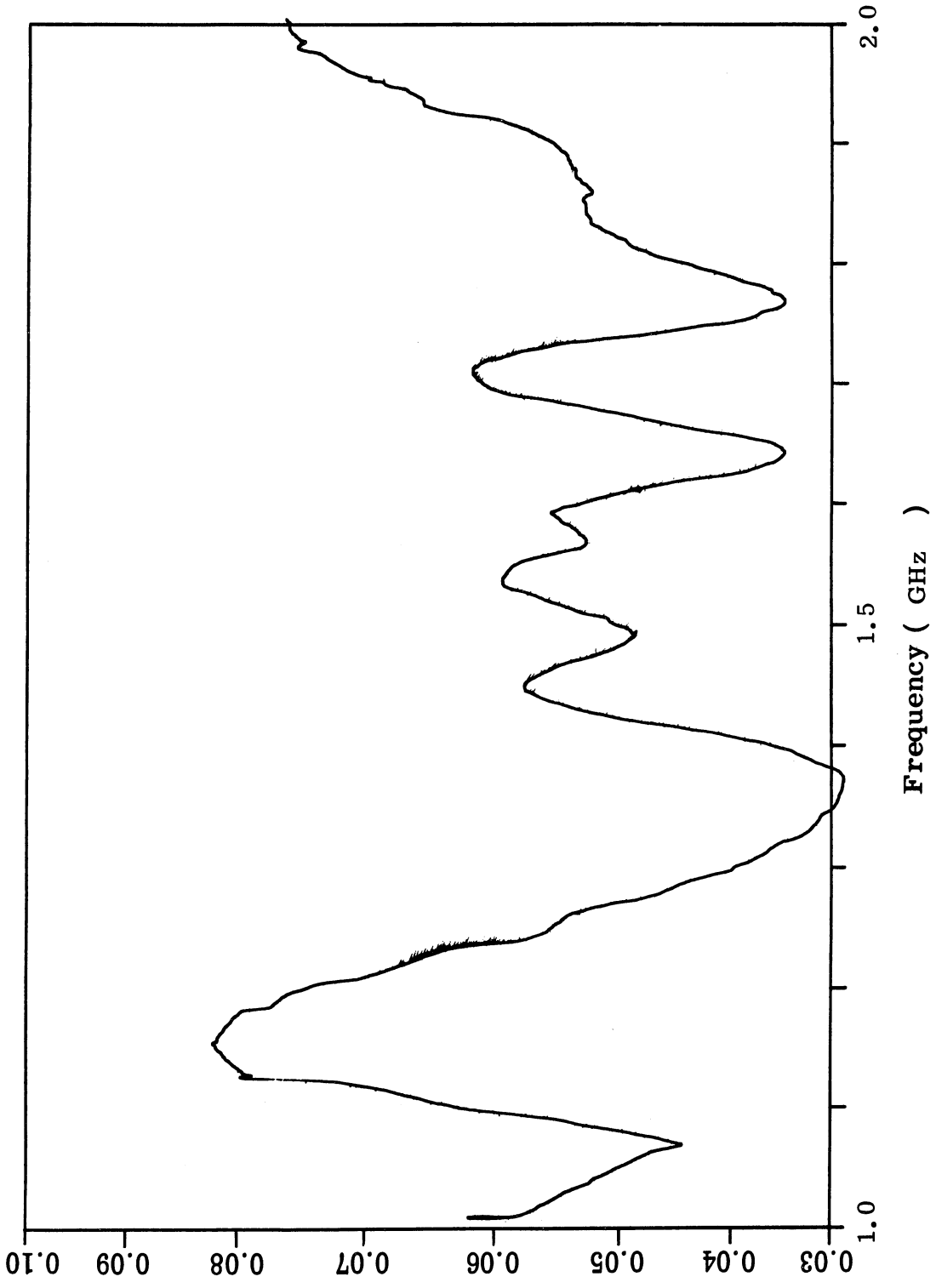

FIG. 4-34: REFLECTION COEFFICIENT OF (1/2 INCH COIL) INDUCTIVE LOADED ANTENNA

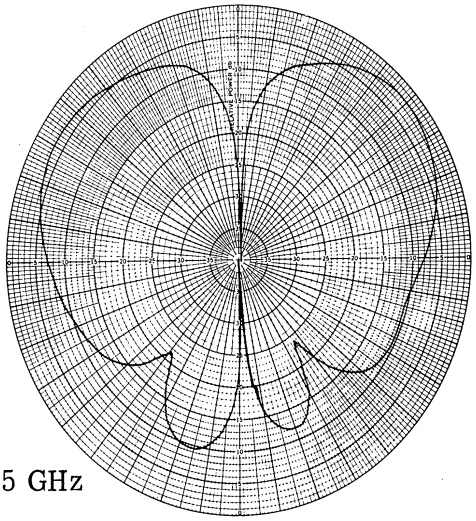

0.5 GHz

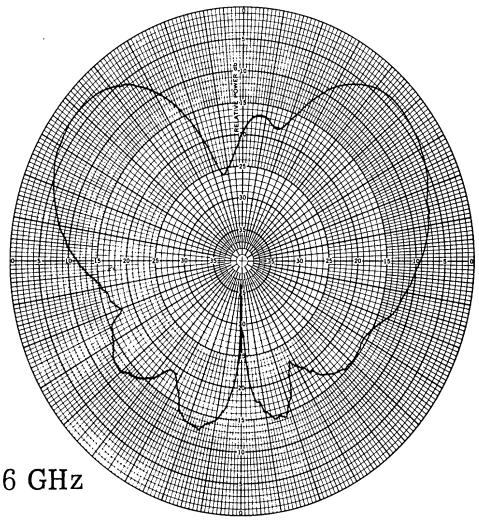

0.6 GHz

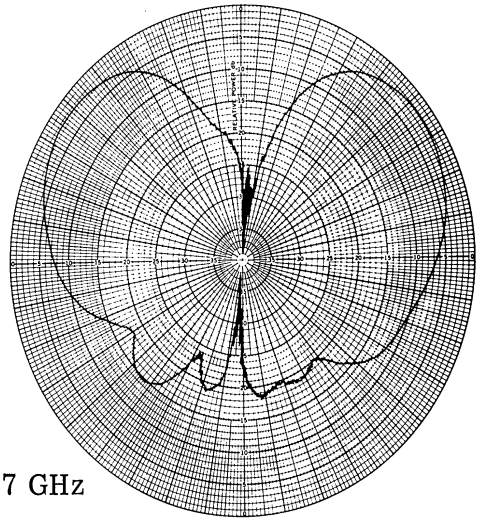

0.7 GHz

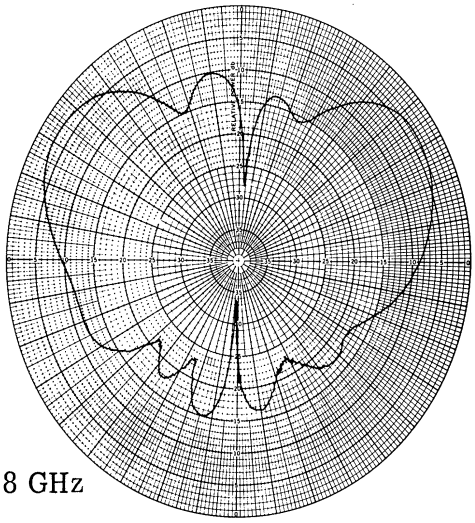

0.8 GHz

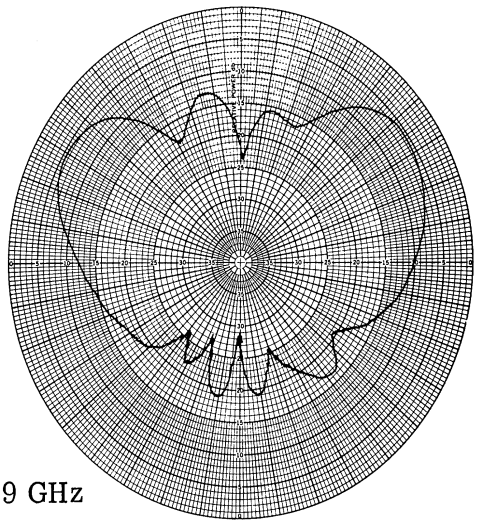

0.9 GHz

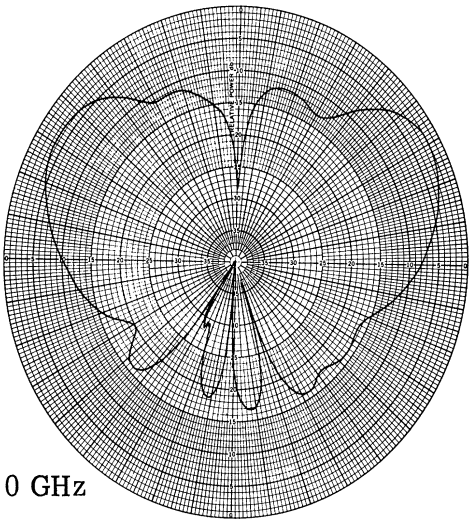

1.0 GHz

FIG. 4-35: ELEVATION PATTERNS OF THE 48 ELEMENT INDUCTIVE ANTENNA (0.5 - 1.0 GHz)

longer than $\lambda/4$ at 1000 MHz. To examine this hypothesis an antenna employing 55 coils each consisting of 10 turns of No. 28 wire wound on a 1/16 inch diameter Rexolite rod and spaced 1/2 inch between adjacent ends, was fabricated and tested. The total filament length was under $\lambda/4$ for frequencies below 2.0 GHz.

Figure 4-36 is a plot of the reflection coefficient as a function of frequency for this configuration. Periodicity between the nulls (i.e., low reflection coefficient) is greatly increased, and further the frequency separation between nulls remains approximately constant. The cause for this phenomena is not understood and, therefore, requires further consideration. It is to be noted that the majority of the coil antennas considered during this study displayed this uniform frequency separation between reflection coefficient minimums. Further, it was difficult to obtain radiation patterns from antenna configurations employing small diameter coils due to the extremely high reflection coefficient.

Consideration was also given to variations in the number of turns per coil and the spacing between coils, e.g., coil antennas have been designed to have uniform separation between turns and log periodic, and uniform spacing between coils. It is interesting to note that as the coil diameter was increased the reflectometer data exhibited smaller reflection coefficient variations (a reduction in the maximum reflection coefficient). It is reasoned that as the coil size is increased, the lowered reflections are due to radiation from the coils.

As an example of the above discussion a coil antenna consisting of several different coil diameters with uniform separation between the coils (Fig. 4-37) was constructed. A typical set of reflectometer data is shown in Fig. 4-38. It is interesting to observe that this data is similar to that of Fig. 4-36. Since inductance is directly proportional to the diameter of the coil, this antenna was fed from the small diameter end. The antenna was designed to have increasing inductance toward the tip and was to operate from 300 - 3000 MHz and was $\lambda/4$ (10 inch long) at 300 MHz. As can be seen from the reflectometer plots, the VSWR was periodic and did not display promising broadband capabilities. Patterns for this antenna were discouraging due to the severe lobing.

Because of the lack of success with the coil antennas, consideration was given to other techniques for achieving the required inductance. Formulas for the self inductance of a single wire (Ferris et al, 1967) show the inductance is inversely proportional to the wire diameter. With this in mind several antennas of the inductive geometry were designed. All were designed on the principal of current constriction to develop areas of increased inductance. Figure 4-39 and 4-40 show two

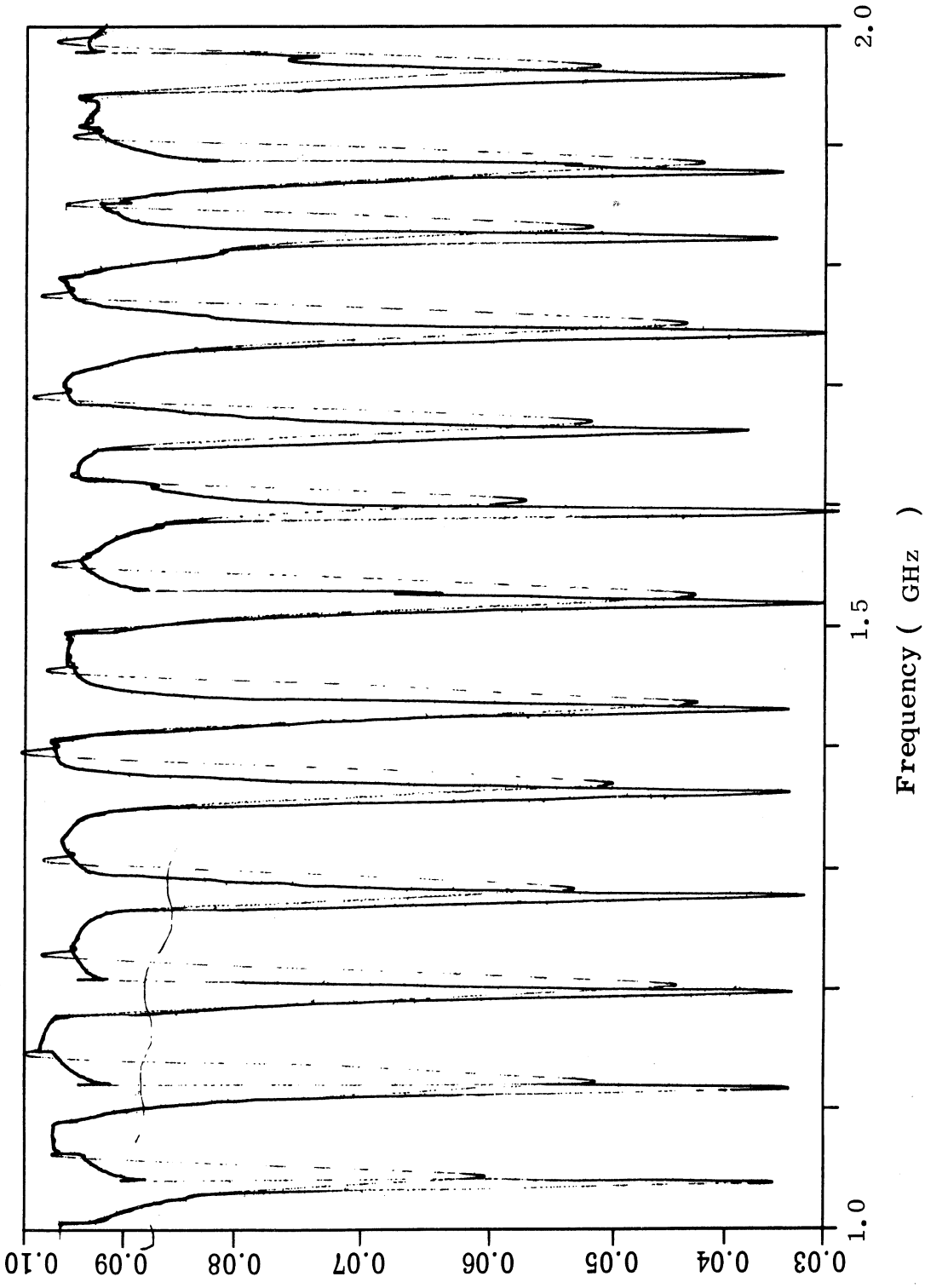

FIG. 4-36: REFLECTION COEFFICIENT OF (1/16 INCH COIL) INDUCTIVE LOADED ANTENNA

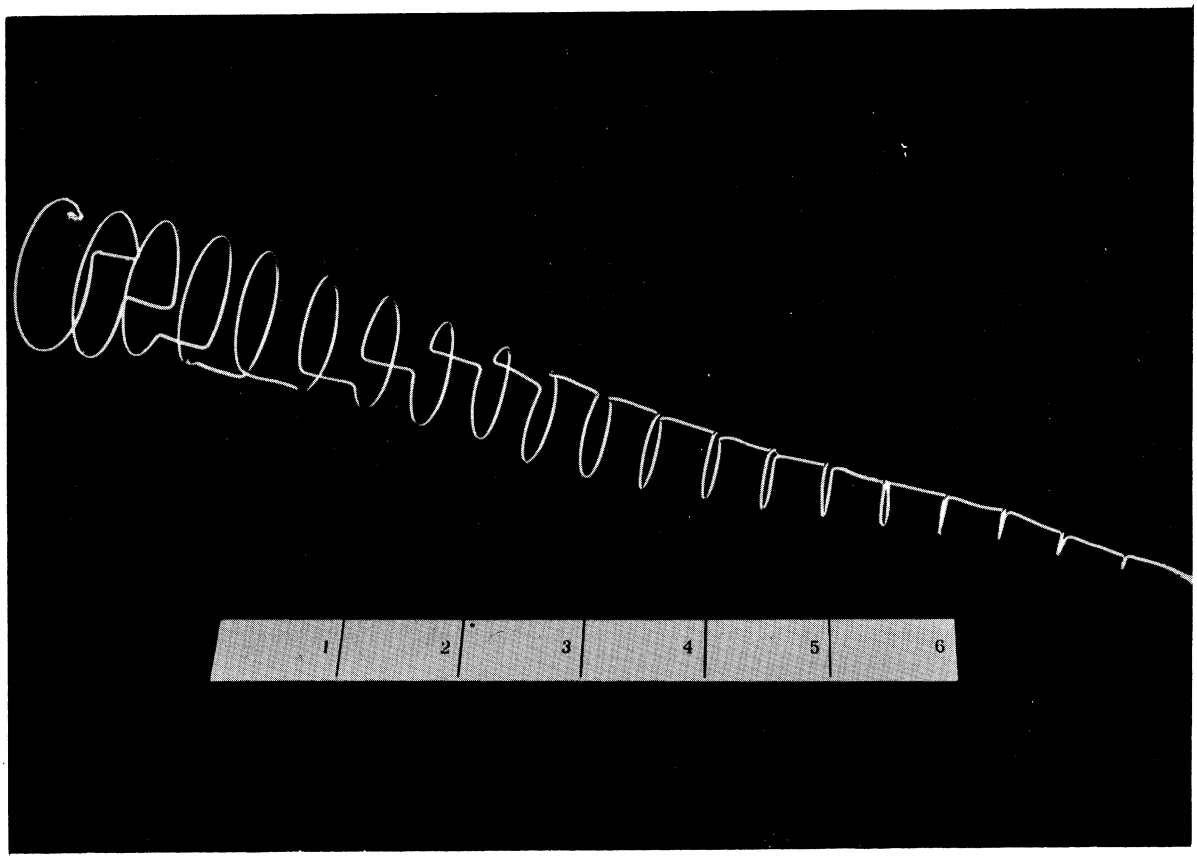

FIG. 4-37: EXPONENTIALLY TAPERED INDUCTIVE ANTENNA

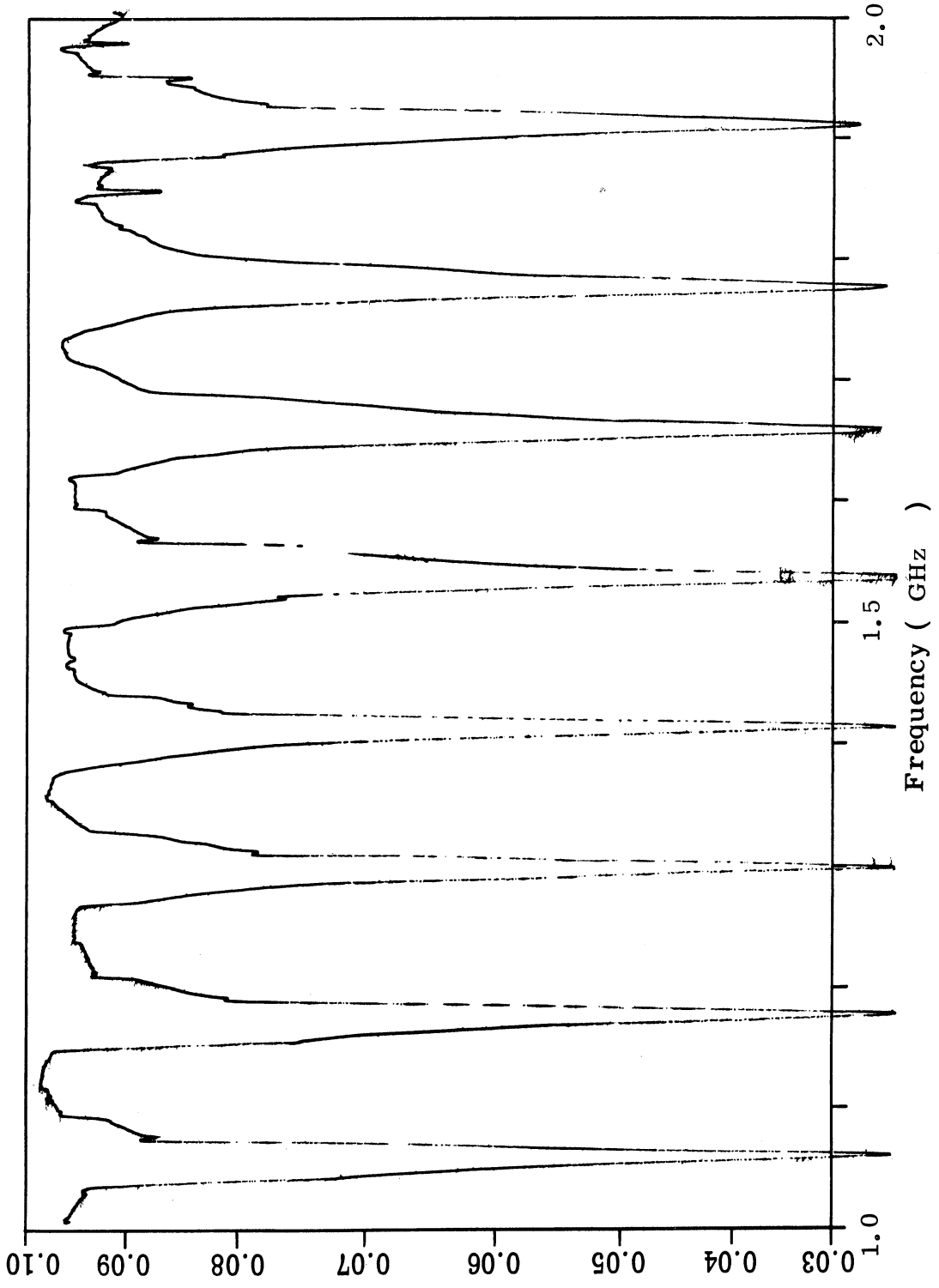

FIG. 4-38: REFLECTION COEFFICIEINT OF EXPONENTIALLY TAPERED INDUCTIVE ANTENNA

typical antennas. The first is called the crossed plate antenna and the second the inductive geometry. The crossed plate antenna used small 1/2 inch diameter crossed plates to increase the effective diameter. When soldered to a thin wire large variations in diameter were obtained. Crossed plates were employed instead of solid cylinders to reduce the shunt capacitance. A series of inductors each shunted by capacitance would not be desirable unless the resonance of each parallel circuit could be controlled to limit the current to various regions of the antenna. As noted in section 4.1, this type of current control is very difficult to achieve for broadband applications. The reflectometer data shown in Fig. 4-41 demonstrates the ineffectiveness of the crossed plates. This antenna is also discussed by Ferris, et al (1967).

The inductive geometry antenna employed several conic sections to reduce the shunt capacitance. The antenna was designed to operate from 300 - 3000 MHz and was $\lambda/4$ (10 inches long) at 300 MHz. The axial length of the cones decreased to produce a variable inductance per unit length of the antenna. The reflectometer data of Fig. 4-42 shows that the antenna's reflection coefficient is similar to a conventional cylindrical monopole of similar dimension (0.5 x 10.0 inches in diameter and length).

From the above discussion it is apparent that antennas with inductive reactance are more difficult to design than antennas employing capacitive reactance. Uniform capacitive reactance improves the broadband impedance performance of a monopole. However, similar improvement employing inductive loading has not been observed at the frequencies considered during this investigation. Possible cause of this may be the lack of a true inductance at frequencies above 100 MHz, e.g., available references generally do not discuss inductance per-se at these frequencies. Langford-Smith, (1953) discusses a few inductances above 100 MHz and notes that the solinoid coil configuration is useful up to 100 MHz, further, it is possible to produce ferromagnetic materials at frequencies in the order of 100 MHz. Ferromagnetic cores have been manufactured which may be used in tuned circuits at 150 MHz, however, air coils are generally used in the 100 - 200 MHz frequency range. Therefore, it is evident that the production of coils above 100 MHz is difficult and the self capacitance of coils tends to reduce the inductance with the added undesirable feature of self resonances. When winding coils such as used on the coil antennas, it is difficult to ascertain whether capacitive or inductive reactance is produced at these frequencies (> 100 MHz) since we cannot talk of a pure inductance. Quite possibly at lower frequencies, say in the 10 - 70 MHz range the inductive antenna could be designed to exhibit broadband impedance characteristics.

A possible method of obtaining inductance may be through the use of ferrite "beads". These "beads" or hollow cylinders, when placed on a wire of proper

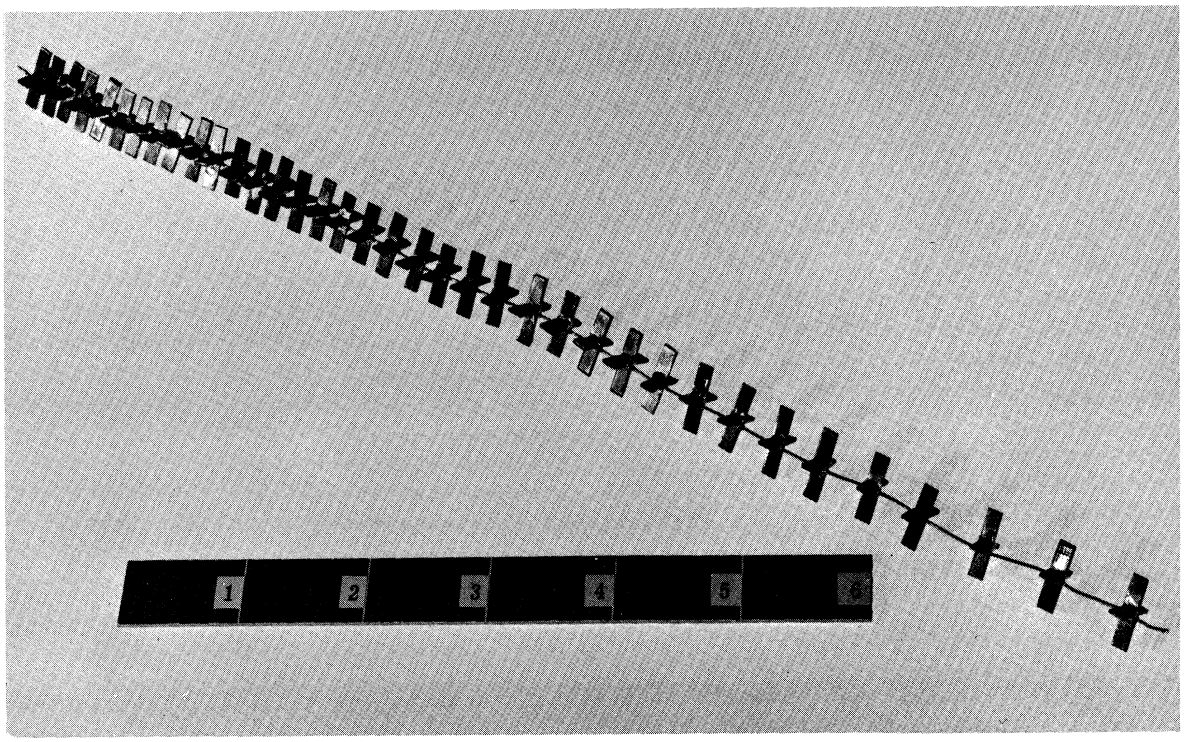

FIG. 4-39: CROSS PLATE INDUCTIVE GEOMETRY

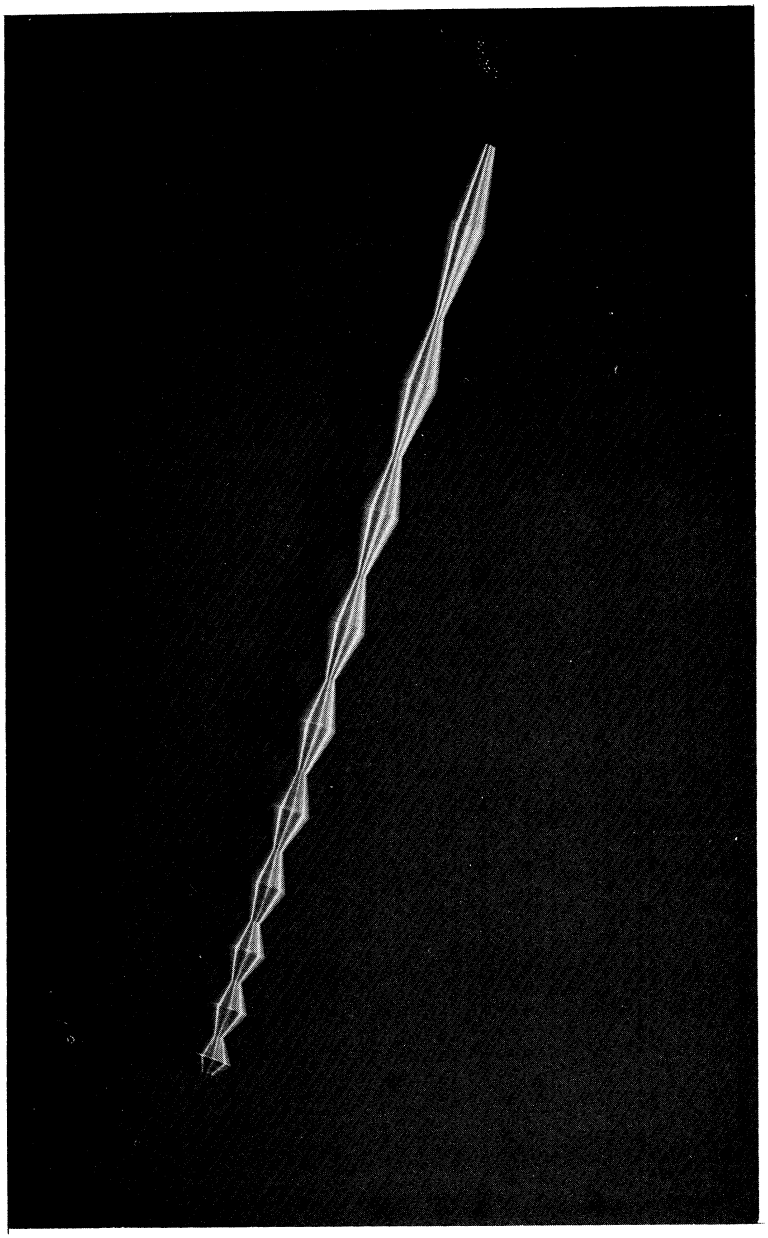

FIG. 4-40: TAPERED INDUCTIVE GEOMETRY ANTENNA

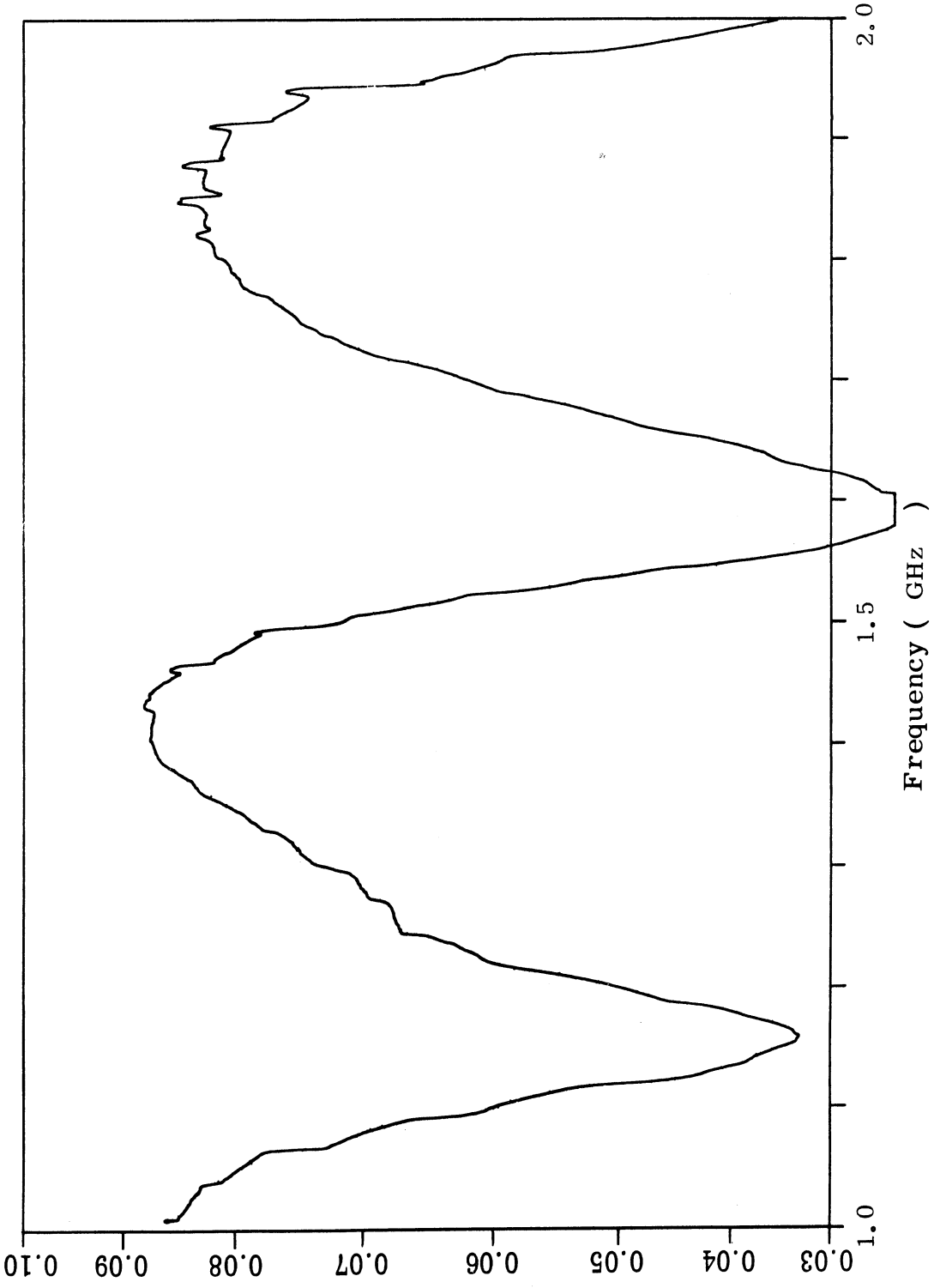

FIG. 4-41: REFLECTION COEFFICIENT OF CROSS PLATE INDUCTIVE GEOMETRY ANTENNA

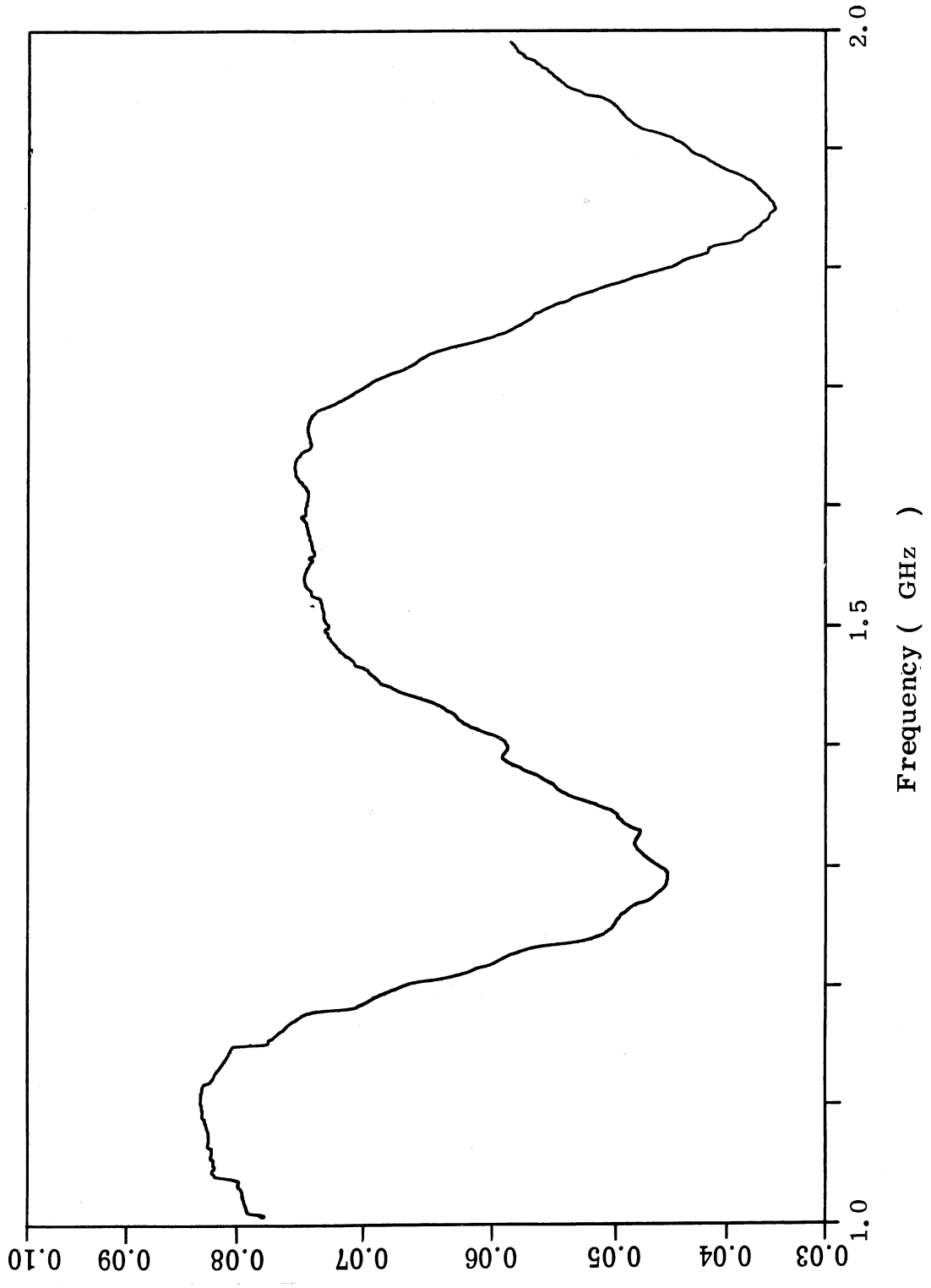

FIG. 4-42: REFLECTION COEFFICIENT OF TAPERED INDUCTIVE GEOMETRY ANTENNA

diameter, are said to appear inductive due to the high permeability of the ferrite. Advertizing brochures suggest these beads can be manufactured to operate in the 10 - 90 MHz and 30 - 300 MHz ranges.

4.6 Recommendations

4.6.1 A Possible Inductively Loaded Antenna Design for 10 - 100 MHz

In the theoretical discussion, it is shown that an antenna loaded with inductive elements is physically smaller than one which is capacitively loaded; in addition it gives the proper current distribution with increase in frequency. For the range of frequencies considered in this report, these advantages could not be realized experimentally due to the difficulty in obtaining pure inductive elements without any side effects. However, it is anticipated that at lower frequency ranges (10 - 100 MHz) where this difficulty is not as severe, an inductive loaded antenna could be designed realizing the above mentioned advantages.

It is recommended that any future studies concentrate in the 10 - 100 MHz range studying ferrite beads and coils as a means of obtaining acceptable inductance. Knowledge gained through this type of program could then be applied to the challenging 100 MHz and above frequency range. At the present time it is felt that insufficient information is known about coils and other forms of inductance at frequencies > 100 MHz to conduct a development program in this frequency range.

4.6.2 Areas to be Investigated

The preliminary theoretical study indicates that it is possible to analyze the reactively loaded antenna for both impedance and radiation characteristics. Using a computer it should not be difficult to analyze the effects of varying the amount of loading and the degree of taper, for both capacitively and inductively loaded antennas. In so doing, it is theoretically possible to determine the loading which best meets the requirements.

Hence, an initial study would include the use of computer techniques in the theoretical determination of the proper loading. Other areas to be investigated include the effects of changing the diameter of the conducting cylinders of the antenna, and the effects of varying the spacing between the reactive elements. An experimental study should accompany the theoretical study and be confined to inductively loaded antennas.

Another area which should be of interest for further study is the traveling wave antennas including V-antennas. Up to now traveling wave antennas have been made either by terminating the antenna end by proper resistive load, or by loading with several resistive elements whose resistance value increases toward the end. Evidently, due to resistive losses, the resulting antennas have very low efficiency. The efficiency of traveling wave antennas could be increased by reactive loading. Traveling wave antennas could be realized by taking a long wire antenna and terminating it with a reactively loaded section.

V

CONCLUSION

The success achieved under Task 1 has been significant as is demonstrated in the results obtained with the exploratory development model of the foreshortened planar log-periodic antenna. During a recent meeting with the contract monitor, the importance of developing an antenna having a significant reduction in the length of the boom as well as the element was emphasized. As a result the effort to obtain such a reduction was intensified. The developmental model of the antenna being delivered to the U.S. Army Electronics Command embodies almost all of the desired features.

It seems likely that these results will influence the design of several tactical antennas of the log planar type.

Considerable time was devoted to Task 2 on the loaded conical helix antenna. It was recognized from the beginning that the requirements for this antenna would be very difficult to meet. In the first years work on this contract an antenna of this general type and for the same range of frequencies was developed, but the resulting model exceeded the specified weight. In the present work on Task 2, specific attempts were made to overcome the weight problem and the approaches used were somewhat radical in nature. Although the weight problem was generally overcome, the methods used had serious drawbacks from the standpoint of meeting the electrical requirements. The tests made with the development model of the loaded conical helix antenna have been informative; its performance can be interpreted as due to specific limitations on the construction used and the manner of winding. The information presented on slow wave structures in general, should be helpful in future work on the design of physically small antennas. The comments on capacitor loading and the possibilities of smaller size with capacitor loading should prove intriguing.

Under Task 3 a thorough investigation has been made of the capacitively loaded reflectionless antenna. This effort has been conducted both from a theoretical and from an experimental approach. Consideration has also been given to inductively loaded reflectionless antenna. The study has shown that it is feasible to design and construct capacitively loaded antenna with reasonable electrical characteristics over a 10:1 frequency band (600 - 6000 MHz). The principal disadvantage associated with the capacitive configuration is that as the frequency increased, the capacitive reactance decreased. As a result the pattern characteristics are not well behaved because the conduction currents are permitted to flow over more than $\lambda/4$ of the antenna at the high frequencies.

Since the inductive reactance is proportional to frequency, a portion of the study was devoted to methods of obtaining an inductance in the 100 - 1000 MHz range. In general the results of this study have shown that the inductive concept should be given further consideration for frequencies below 100 MHz. No satisfactory method was found for building suitable inductors for frequencies above 100 MHz.

It is to be noted that one must be particularly careful when an antenna of this type is operated in a monopole configuration, i.e., the ground plane must be of sufficient size to ensure that it has broadband frequency characteristics. Further, when employing the antenna in a monopole configuration it is recommended that a conical ground plane be employed to ensure pattern coverage on the horizon.

It seems in order to remark that a more thorough investigation of these antennas could have been made had there been no requirement for a deliverable full size exploratory development model. A considerable amount of time and funds was required to design and build the antennas delivered under Task 1 and Task 2. Little or no useful information was gained with these large antennas that could not have been obtained much more easily by working with smaller scale models.

APPENDIX A

ANALYSIS OF DISCRETE COMPONENT LOADING OF HELIX AND CONICAL HELIX ANTENNAS

A.1 Transmission Line Model

From the transmission line equations, it can be readily shown that the phase velocity, v_p, and the characteristic impedance, Z_o, of a transmission line are related to the inductance per unit length, L, and the capacitance per unit length, C, by the expressions,

$$Z_o = \sqrt{L/C} \tag{A.1}$$

$$v_p = 1/\sqrt{LC}\,. \tag{A.2}$$

By manipulation of these expressions, the capacitance and inductance per unit length can be expressed in terms of the characteristic impedance and the phase velocity as follows:

$$C = 1/(Z_o v_p) \tag{A.3}$$

$$L = Z_o/v_p \tag{A.4}$$

Assume that the reduction in size of the antenna is equal to the reduction in the phase velocity and call this reduction factor R. Then assuming that only capacitive loading will be used, the new capacitance per unit length, C', can be expressed as:

$$C' = C/R^2. \tag{A.5}$$

In the series of experiments described in Section 3.3, antenna 228 was used. Antenna 228 is a bifilar 4-7/8 turn helix antenna. It is wound with No. 18 tinned copper wire at a pitch angle of 14 degrees. The diameter of the windings is 9.8 cm. This means that the center of the band of operation is at 800 MHz.

For this antenna, the characteristic impedance was calculated to be 790 Ω by substituting the diameter of No. 18 wire and the diameter of the helix into the formula for the characteristic impedance of a parallel wire transmission line. The capacitance per unit length is calculated to be 4.23 pf./meter by using formula (A.3). For a reduction factor of 0.25, this would require the new capacitance to be 66.2 pf./meter.

However, when originally testing the concept, a characteristic impedance of 150 Ω was used because the value calculated by the transmission line theory appeared unreasonable. For a characteristic impedance of 150 Ω, the capacitance per unit length computed on first trial was 22.2 pf./meter and the capacitance desired for an 0.25 reduction factor is 355 pf./meter. Thus, 333 pf. of discrete capacitors were to be added per meter to obtain a 4 to 1 size reduction. Since capacitors were to be spaced every eighth of a turn, this resulted in every capacitor being 12 pf.

Now, as shown in Pierce's paper (1966), the inductance for a round wire is

$$L = 0.00508h\,(2.303 \log_{10}(4h/d) - 0.75) \text{ microheneries} \qquad (A.6)$$

where "h" is the length of the wire and "d" is the diameter of the wire. There is also an inductance associated with the plates of the capacitor, but this is so small that it can be ignored. These inductances are in series with the capacitor. For the 120 pf. capacitors used in the experiments, the resonant frequency of this series inductance and capacitance is 42.5 MHz. Thus the 120 pf. capacitors used in the experiments were really inductances with an equivalent inductance of 0.117 μh. The 12 pf. capacitors, however, had a resonant frequency of 425 MHz and were thus acting essentially as short circuits.

The problem of the shunt inductively loaded transmission line can be treated in two ways. First, it can be treated as a continuous inductive loading, which for the frequencies at which the patterns were taken on Antenna 228 with 120 pf. capacitor loading in the Type II configuration, is a good assumption. Alternatively the problem can be treated as a periodically shunt inductive loaded transmission line. Both approaches were studied.

A.2 Continuous Inductive Loading

Since the loading is shunt, the susceptance of the loading, and not the inductance, is the parameter to be used. Figure A-1 illustrates the infinitesimal section of the loaded transmission line. By inspecting the rate of change of current i and voltage v with respect to distance, the following differential equations can be written

$$\frac{di}{dz} = C\frac{dV}{dt} + S\int V\,dt \qquad \text{where } S = \frac{1}{L} \qquad (A.7)$$

$$\frac{dV}{dz} = CL\frac{di}{dt}. \qquad (A.8)$$

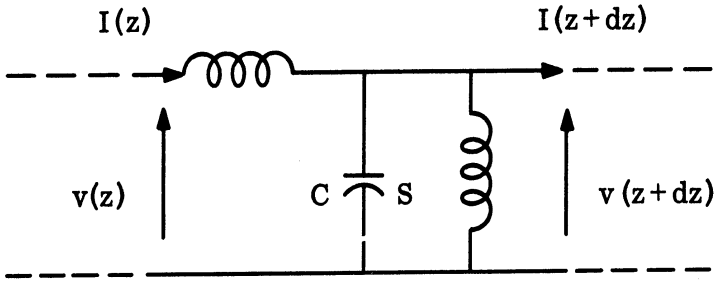

FIG. A-1: AN INFINITESIMAL SECTION OF A CONTINUOUSLY INDUCTIVE LOADED TRANSMISSION LINE.

Differentiating (A.7) with respect to t and (A.8) with respect to z, substituting, and rearranging terms results in

$$\frac{d^2V}{dz^2} = L\frac{d^2V}{dt^2} + SLV. \qquad (A.9)$$

If solutions are assumed that have a form of some arbitrary functions of z times $e^{j\omega t}$, then (A.9) becomes

$$\frac{d^2V}{dz^2} = -\omega^2 LCV + SLV = (SL - \omega^2 LC)V. \qquad (A.10)$$

The solution is

$$V(z) = Ke^{\pm z\sqrt{SL - \omega^2 LC}} \qquad (A.11)$$

where K is an arbitrary constant.

Depending on the sign of the radical, the waves will either propagate or attenuate. If $(SL - \omega^2 LC) \leq 0$, then there will be propagation. However, if $(SL - \omega^2 LC) \geq 0$, there will be only attenuation. The critical frequency, ω_c, occurs when $(SL - \omega^2 LC) = 0$. This occurs when

$$\omega_c = S/C. \qquad (A.12)$$

For Antenna 228 with 120 pf. capacitor loading, the value of the susceptance, S, is 2.22×10^8 meters/henry. This gives a critical frequency of 1155 MHz. Hence, above this frequency, there should be propagation with a phase velocity greater than the speed of light and below this frequency there should be attenuation. This approach predicts both the attenuation and the forward fire radiation, which occurs when the velocity of propagation is greater than the speed of light.

However, the cutoff frequency is about three times that observed. The reason for this is that the value of inductance calculated is too small. The value of inductance given by (A.6) apparently assumes that the current distribution along the capacitor lead is uniform. This is true for lengths that are a small fraction of a wavelength.

However, at 400 MHz, the diameter of the helix is greater than an eighth of a wavelength. Hence, the current is not uniform over the element. The result is that when the equivalent inductance is referred to the terminals, using the value of current at the center of the circuit, the value is too small.

A.3 Periodic Inductance Loading

The analysis of a periodically loaded transmission line follows that of Collin (1960) given in Chapter 9, Sec. 12.5. For inductive loading, the following characteristic equation results:

$$\cos(\beta z_o) = \cos(kz_o) + (B/2)\sin(kz_o) \qquad \text{(A.13)}$$

where k is the free space wave number, β is the wave number for the transmission line, z_o is the spacing between the inductances and B is given by the following formula:

$$B = Z_o/\omega L \qquad \text{(A.14)}$$

where Z_o is the characteristic impedance of the unloaded transmission line and L is the inductance which occurs periodically in the line. Equation (A.13) results in the k-β diagram given in Fig. A-2. Notice that for kz_o between zero and 1.23, there is no solution. Thus, any wave propagating down the transmission line would be rapidly attenuated. The value of $kz_o = 1.23$ corresponds to a frequency of 1520 MHz.

Between kL equal to 1.23 and π, the transmission line maintains a fast wave, a wave whose velocity is greater than the speed of light. This can readily be found from the k-β diagram by noting that the slope of a line drawn from the origin to any point on the characteristic curve corresponds to the ratio of the phase velocity to the speed of light for operation at that particular point. The group velocity at any particular point on the characteristic curves is the slope of the characteristic curve at that point. Fast waves on a helix antenna result in forward fire radiation. Hence this forward fire radiation would occur between kz_o of 1.23 and π, or for frequencies between 1520 MHz and 3900 MHz.

Above $kz_o = \pi$, or above 3900 MHz, the transmission line operates in the backward fire mode. This occurs when the phase velocity is less than the speed of light, but the group velocity is negative, which corresponds to propagation of energy in a direction opposite to that of the phase velocity.

It is interesting to note that the width of the forward fire band is 2.56, based on this theoretical model, while the measured width is 2.3. Thus although the

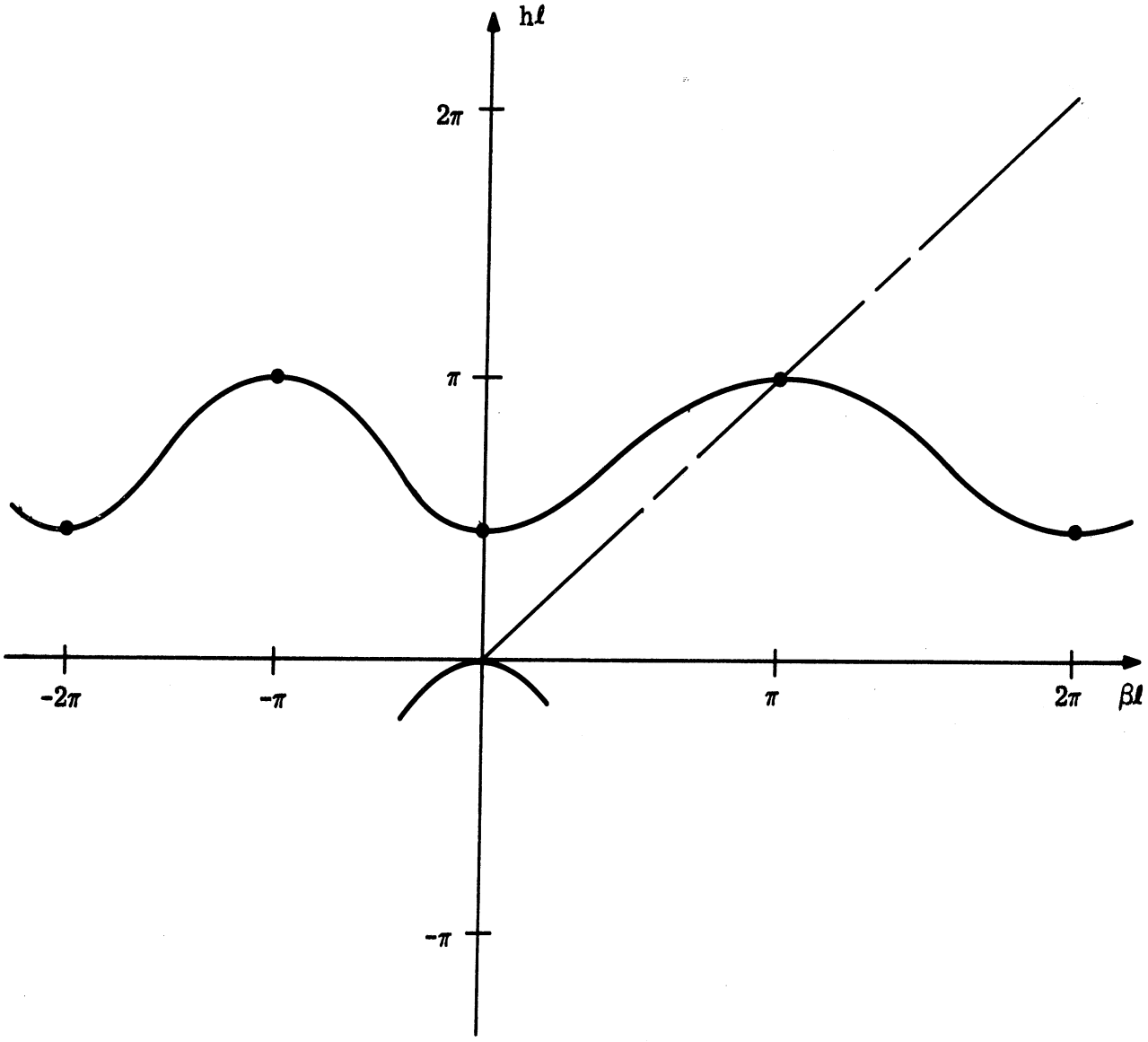

FIG. A-2: A k - β DIAGRAM OF A PERIODICALLY INDUCTANCE LOADED TRANSMISSION LINE.

prediction of the frequencies of operation by the theoretical model appears to be off somewhat, the error in predicting the bandwidth does not appear to be too far off.

A.4 Frequency Limit of Capacitive Loading

Now consider the upper frequency limit on capacitor loading, and assume that a 4:1 size reduction is to be achieved. It is desirable to be at least a factor of ten below the resonant frequency of an individual capacitor C_{dis} to be assured that the value of capacitance is within 99 per cent of the d.c. value. Thus,

$$\omega^2 = \omega_o^2/100 = 1/100\ LC_{dis} \qquad (A.15)$$

where L is the inductance of the lead length.

For a 4 to 1 reduction in the center frequency of a helix antenna, the diameter is approximately $\lambda/4\pi$, since the diameter of a helix antenna is normally λ/π. Thus the diameter, D, of the helix can be expressed as

$$D = C/2\omega \qquad (A.16)$$

where C is the velocity of light in a vacuum.

Now the inductance of the leads can be computed approximately by plugging (A.16) into Pierce's (1966) formula for the inductance of a capacitor lead,

$$L = 0.00508\ D\left[2.303 \log_{10} (fD/d) - 0.75\right] \times 10^{-6} \qquad (A.17)$$

where L is measured in henries and d is the diameter of the wire.

The capacitance per unit length of the unloaded transmission line, C, can be expressed according to the parallel wire transmission line theory and Eq. (A.3)

$$C = 1/Z_o c = 1/\left[276\ c \log_{10} (2D/d)\right] \qquad (A.18)$$

where the diameter of the winding wire of the antenna is assumed to be the same as that of the capacitor leads.

For a 4 to 1 reduction, Δ C, the capacitance per unit length to be added is:

$$\Delta C = 15C = 15/\left[276\ c \log_{10} (2D/d)\right] \qquad (A.19)$$

By noting that the relationship of frequency to wavelength in terms of the velocity of light and that the circumference of a one-quarter size helix is about

one-quarter of a wavelength, the capacitance of an individual capacitor, C_{dis}, can be related to ΔC by the relation:

$$C_{dis} = \frac{c}{2\omega n} \Delta C \qquad (A.20)$$

where n is the number of capacitors used per turn of the helix antenna. Substituting the expressions in (A.20) and (A.17) into (A.15) the following inequality is established:

$$\omega \leq 82.0\ n \times 10^6 \qquad (A.21)$$

or

$$f \leq 13.0\ n \times 10^6. \qquad (A.22)$$

Now, a comparison of the periodically loaded transmission line theory with the experiments indicates that the value of L calculated by (A.17) is too large a factor of three or four. Thus, divide (A.22) by a factor of three or four giving

$$f \leq 4n \times 10^6. \qquad (A.23)$$

Assume that eight capacitors are used per turn, as was the case in the experiments. Then discrete capacitor loading would work below 32 MHz. Thus, in the HF band (3 to 30 MHz) there should be no difficulty in realizing a 4 to 1 size reduction with capacitor loading. Indeed, if more capacitors were used per turn, such an antenna could be realized at somewhat higher frequencies, although the number of capacitors one would be willing to solder on the antenna would be a practical upper limit to the number used.

REFERENCES

Carrel, R.L. (1961), "The Design of Log-Periodic Antenna," IRE Convention Record, pp. 61-75.

Collin, R.E. (1960), Field Theory of Guided Waves, McGraw-Hill Book Company, New York.

Condon, E.U. and H. Odishaw (1958), Handbook of Physics, McGraw-Hill Book Company, New York.

Dyson, J.D. (1965), "The Characteristics and Design of the Conical Log-Spiral Antenna," University of Illinois Technical Report AFAL-TR-65-124.

Ferris, J.E., S. Hong, J.A.M. Lyon, G.G. Rassweiler and W.E. Zimmerman (1965), "Broadband Antenna Techniques Study - Second Quarterly," The University of Michigan Radiation Laboratory Report 7260-2-Q, ECOM-01263-2 (November).

Ferris, J.E., J.A.M. Lyon, G.G. Rassweiler, D.L. Smith, P-R Wu and W.E. Zimmerman (1966a), "Broadband Antenna Techniques Study - Third Quarterly," The University of Michigan Radiation Laboratory Report 7260-3-Q, ECOM 01263-3 (February),

Ferris, J.E., J.A.M. Lyon, G.G. Rassweiler, D.L. Smith, P-R Wu and W.E. Zimmerman (1966b), "Broadband Antenna Techniques Study - Interim Report," The University of Michigan Radiation Laboratory Report 7260-1-T, ECOM-01263-4 (May).

Ferris, J.E., J.A.M. Lyon, G.G. Rassweiler, C.C. Chen, J.C. Parker, D.L. Smith, P-R Wu, W.E. Zimmerman and J.B. Rao, (1967), "Broadband Antenna Techniques Study - Sixth Quarterly," The University of Michigan Radiation Laboratory Report 7260-6-Q, ECOM-01263-7. (February).

Gerst, C.W. and R.A. Worden (1966), "Helical Antennas Take a Turn for the Better," Electronics, Vol. 39, No. 17, pp. 100-110.

Hallen, E., (1962), Electromagnetic Theory, John Wiley and Sons, Inc., New York, pp. 501-504.

Harrington, R.F. (1967), "Matrix Methods for Field Problems," Proc. of IEEE, Vol. 55, No. 2, pp. 136-149.

Hong, S. and G.G. Rassweiler (1966), "Size Reduction of a Conical Log-Spiral Antenna By Loading with a Magneto-Dielectric Material," IEEE Trans., AP-14, No. 5, (September).

IsBell, D.E. (1960), "Log-Periodic Dipole Arrays," IRE Trans., AP-8, No. 3, pp. 260-267.

Jasik, H. (1961), Antenna Engineering Handbook, McGraw-Hill Book Company Inc., New York.

King, R.W.P. (1956), The Theory of Linear Antennas, Harvard University Press.

King, R.W.P. (1965), "The Cylindrical Antennas with Non-Reflecting Resistive Loading," IEEE Trans., AP-13, No. 3, pp. 369-373.

Kraus, J.D. (1950), Antennas, McGraw-Hill Book Company, Inc., New York.

Langford-Smith, F. (1953), Radiotron Designer's Handbook, Radio Corporation of America, Harrison, N.J. Fourth Edition.

Li, T. and R.E. Beam (1957), "Helical Folded Dipoles and Unipoles," Proc. NAECON, Vol. XIII, pp. 89-105.

Neureuther, A.R., P.W. Klock, R. Mittra (1967), "A Study of the Sheath Helix with a Conducting Core and its Application to the Helical Antenna," IEEE Trans. AP-15, No. 2, pp. 203-210.

Okubo, G. (1965), "Helix Frequency Scanning Feed," Microwave J., 8, No. 12, pp. 39-44.

Orr, W.I. (1959), All About Cubical Quad Antennas, Radio Publications, Inc., Wilton, Conn.

Pierce, Robert (1966), "When is a Capacitor an Inductor?" Electronic Products Vol. 12 No. 7, pp. 74-75. (December).

Rassweiler, G.G. (1966), "Helical and Log Conical Helical Antennas Loaded with an Isotropic Material," Dissertation, The University of Michigan Department of Electrical Engineering. Also published as Radiation Laboratory Report 7848-3-Q.

Sensiper, S. (1951), "Electromagnetic Wave Propagation on Helical Conductors," Massachusetts Institute of Technology, Report 194.

Shestopalov, V.P., A.A. Bulgakov and B.M. Bulgakov (1961), "Theoretical and Experimental Investigations of Helix-Dielectric Aerials," Radio Engineering and Electronics, 6, No. 7, pp. 159-172.

Shnitkin, H. and S. Levy (1962), "Getting Maximum Bandwidth with Dipole Antennas," Electronics, 35, pp. 40-42. (31 August 1962).

Smith, C.E. (Ed.) (1966), "Log-Periodic Antenna Design Handbook," Smith Electronics Inc., Cleveland.

Syracuse University (1966), "Electronic Warfare Technology Techniques (U)," Second Quarterly Progress Report, 1 July 1966 to 30 September 1966, Report No. 997, AD378081 (SECRET) (Only unclassified portions referenced).

Tang, C.H. and O.L. McClelland (1962), "Polygonal Spiral Antennas," University of Illinois Antenna Laboratory Report No. 57.

Terman, F.E. (1955), Electronic and Radio Engineering, McGraw-Hill Book Company Inc., New York.

Walter, C.H. (1965), Traveling Wave Antennas, McGraw-Hill Book Company New York. pp. 331-333.

DISTRIBUTION LIST

Director, National Security Agency
Attn: TDL
Ft. Meade, MD 20755 (20)

Naval Ships Systems Command
Attn: Code 6312, Technical Library
Main Navy Building, Rm 1528
Washington DC 20325 (1)

U. S. Naval Research Laboratory
Code 2027
Washington, DC 20390 (1)

Rome Air Development Center
EMTLD, Documents Library
Griffiss AFB, New York 13442 (1)

Electronic Systems Division
Attn: ESTI
L. G. Hanscom Field
Bedford, Mass 01730 (1)

Chief, of Research and Development
Department of the Army
Washington, DC 20315 (1)

U. S. Army Materiel Command
Attn: R and D Directorate
Washington DC 20315 (1)

Commanding Officer
52D USASASOC
Ft. Huachuca, Arizona 85613 (1)

U. S. Army Research Office-Durham
Box CM Duke Station
Durham, NC 27706 (1)

Army Security Agency
Attn: OACofS, Dev. (CDA)
Arlington Hall Station
Arlington, VA 22212 (2)

Harry Diamond Laboratories
Attn: Library
Connecticut Avenue and Van Ness Street
Washington, DC 20438 (1)

U. S. Army Limited War Laboratory
Aberdeen Proving Ground, MD 21005 (1)

Office, Assistant Secretary of Defense
Research and Engineering
Attn: Technical Library, Rm 3E1065
Washington, DC 20301 (1)

Naval Ships Systems Command
Department of the Navy, Code 6454
Washington, DC 20360 (1)

U. S. Navy Electronics Laboratory
Attn: Library
San Diego, California 92101 (1)

Systems Engineering Group
SEPIR
Wright-Patterson AFB, Ohio 45433 (1)

U. S. Air Force Security Service
Attn: ESD
San Antonio, Texas 78241 (1)

Hq, Research and Technology Division
Attn: RTTC
Bolling AFB, DC 20332 (1)

Redstone Scientific Information Center
Attn: Chief, Document Section
USAOMC, Redstone Arsenal, Ala. 35809 (1)

U. S. Army Combat Development Command
Communications-Electronics Agency
Ft. Monmouth, NJ 07703 (1)

U. S. Army Sec. Ag. Combat Dev. Actv.
Arlington Hall Station
Arlington, VA 22212 (1)

Army Security Ag. Processing Ctr.
Attn: IAVAPC-B and D
Vint Hill Farms Station
Warrenton, VA 22186 (1)

A. S. Army Electronic Proving Ground
Attn: Technical Information Center
Fort Huachuca, Ariz. 85613 (1)

Assist. Sec'y of the Army R and D
Attn: Deputy Assist. for Army R and D
Washington, DC 20315 (1)

DISTRIBUTION LIST (continued)

Chief, Mountain View Office
Electronic Warfare Lab., USAECOM
Box 205
Mountain View, Calif.94042 (1)

Chief, Willow Run Office
CSTA Lab., USAECOM,
Box 618, Ann Arbor, MI 48107 (1)

USAECOM Liaison Officer
MIT, Bldg. 26, Rm 131
77 Massachusetts Ave
Cambridge, Mass 02139 (1)

USAECOM Liaison Office
U. S. Army Electronic Proving Ground
Ft. Huachuca, Ariz. 85613 (1)

Chief, Intelligence Materiel Dev. Office
Electronic Warfare Lab., USAECOM
Ft. Holabird, MD 21219 (1)

Chief, Missile Electronic Warfare Tech. Area.
EM Lab, USAECOM
White Sands Missile Range
New Mexico 88002 (1)

USAECOM Liaison Officer
Aeronautical Systems Division
Attn: ASDL-9
Wright-Patterson AFB, Ohio 45433 (1)

Hq, U S Marine Corps
Commandant A02F
Washington, DC 20380 (1)

U. S. Army Electronics Command
Ft. Monmouth, NJ 07730

Attn:	AMSEL-EW	(1)
	AMSEL-10-T	(1)
	AMSEL-RD-MAT	(1)
	AMSEL-RD-MAF	(1) (Record Copy)
	AMSEL-RD-LNA	(1)
	AMSEL-RD-LNR	(1)
	AMSEL-XL-D	(1)
	AMSEL-NL-D	(1)
	AMSEL-HL-CT-D	(3)
	AMSEL-BL-D	(1)
	AMSEL-WL-S	(5)
	AMSEL-PP	(1)

Total Copies 70

UNCLASSIFIED

Security Classification

DOCUMENT CONTROL DATA - R & D

(Security classification of title, body of abstract and indexing annotation must be entered when the overall report is classified)

1. ORIGINATING ACTIVITY (Corporate author)	2a. REPORT SECURITY CLASSIFICATION
The University of Michigan Radiation Laboratory, Dept. of Electrical Engineering, 201 Catherine Street, Ann Arbor, Michigan 48108	UNCLASSIFIED
	2b. GROUP

3. REPORT TITLE

BROADBAND ANTENNA TECHNIQUES STUDY

4. DESCRIPTIVE NOTES (Type of report and inclusive dates)

Final Report April 1965 through May 1967

5. AUTHOR(S) (First name, middle initial, last name)

Joseph E. Ferris, John A. M. Lyon, Chao-Chun Chen, James C. Parker, Boppana L. J. Rao, George G. Rassweiler, Dean L. Smith and Wiley E. Zimmerman

6. REPORT DATE	7a. TOTAL NO. OF PAGES	7b. NO. OF REFS
October 1967	211	32

8a. CONTRACT OR GRANT NO.	9a. ORIGINATOR'S REPORT NUMBER(S)
DA 28-043 AMC-01263(E)	7260-1-F
b. PROJECT NO. 5A6 79191 D902 02 11	
c.	9b. OTHER REPORT NO(S) (Any other numbers that may be assigned this report) ECOM-01263-F
d.	

10. DISTRIBUTION STATEMENT Copies of this report may be obtained from the Dir., National Security Agency, Ft. Meade, MD 20755, Attn: TDL. Each transmittal of this document outside the Dept. of Defense must have the prior approval of CG, U.S. Army Electronics Command, Ft. Monmouth NJ 07703, ATTN AMSEL-WL-S.

11. SUPPLEMENTARY NOTES	12. SPONSORING MILITARY ACTIVITY
	U. S. Army Electronics Command Fort Monmouth, New Jersey 07703

13. ABSTRACT Many of the possibilities of a smaller planar log-periodic antenna have been investigated. Studies on elements included shortening by various methods. Shortening of the boom length was studied. Influences on radiation pattern and VSWR and influence of different phasing lengths of feed line between adjacent elements for a given boom spacing were considered. Experimental array work was done on an adjustable model. Experimental work was then extended to a 1/4 size model of the projected exploratory development design. Later an exploratory development model was built. It showed good radiation performance with adherence to contract specifications except for minor deviations.

Basic studies were made on size-reduced log conical helix antennas. These studies included an investigation of techniques to develop a light weight slow wave winding for a conical helix antenna. The final exploratory development model of the antenna was of square pyramidal shape and utilized coiled windings on air-filled fiber cylinders. No useful size reduction of a log conical helix antenna was realized using this technique. Considerable success was obtained with a cylindrical helix wound with a coiled wire over a plastic tube filled with a ferrite material (see Contract AF33(615)3609). A 4:1 reduction in diameter of a log conical helix can be obtained at the cost of additional weight with this construction.

An extensive study of the exponentially tapered reactive antenna (EXTRA) has been conducted. Typical impedance, pattern and surface current data have been obtained for two EXTRA antenna configurations. These data have shown that this particular antenna configuration satisfied the initial requirements suggested by Hallén. The surface current data demonstrates that the reactive elements caused the current to be attenuated as it propagates toward the tip of the antenna. The impedance data show the antenna to be a broadband device (10:1 frequency band). The pattern data are not as encouraging since there is a tendency for the antenna toward end fire at the higher frequencies. Data are presented for the EXTRA antenna mounted over three gound plane configurations. The deliverable antenna consists of the EXTRA element and the 9" rodded ground plane.

DD FORM 1 NOV 65 1473

UNCLASSIFIED

Security Classification

14. KEY WORDS	LINK A		LINK B		LINK C	
	ROLE	WT	ROLE	WT	ROLE	WT
Broadband						
Omnidirectional						
Size Reduction						
Antennas						
Loaded Helix						
Loaded Conical Helix						
Physically Small Antennas						
Log-Periodic Antenna						
Foreshortened Log-Periodic Antenna						
Hallén Antenna						